Doctoral theses at NTNU, 2020:327

Pål Keim Olsen

Internal Partial Discharges at High DC Voltage and the Effect of Superimposed AC Voltage

Doctoral thesis

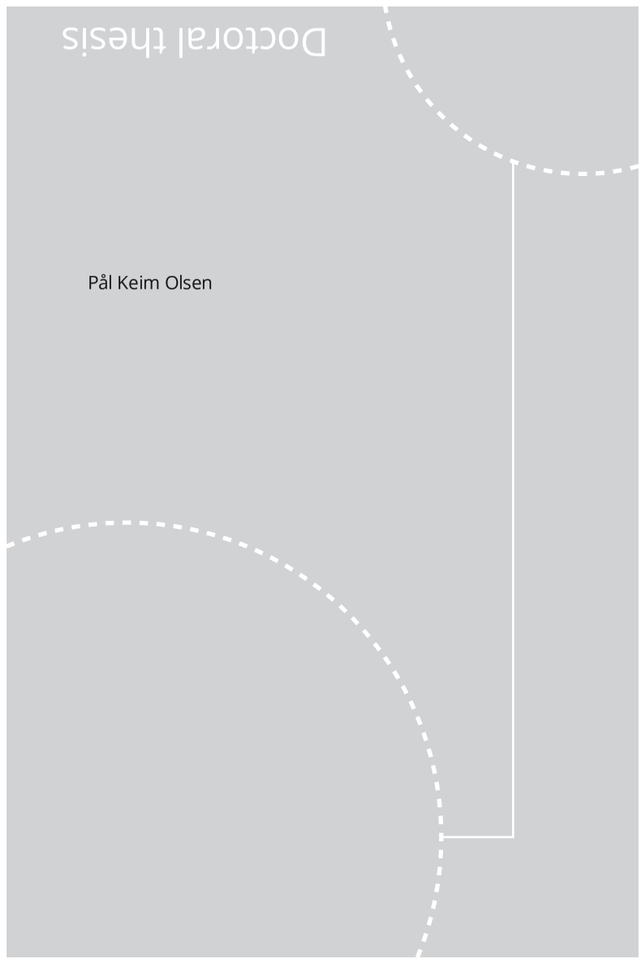

ISBN 978-82-326-5000-2 (printed ver.)
ISBN 978-82-326-5001-9 (electronic ver.)
ISSN 1503-8181

NTNU
Norwegian University of
Science and Technology

NTNU
Norwegian University of Science and Technology
Thesis for the Degree of
Philosophiae Doctor
Faculty of Information Technology and Electrical
Engineering
Department of Electric Power Engineering

Doctoral theses at NTNU, 2020:327

NTNU
Norwegian University of
Science and Technology

Pål Keim Olsen

Internal Partial Discharges at High DC Voltage and the Effect of Superimposed AC Voltage

Thesis for the Degree of Philosophiae Doctor

Trondheim, October 2020

Norwegian University of Science and Technology
Faculty of Information Technology and Electrical Engineering
Department of Electric Power Engineering

NTNU
Norwegian University of
Science and Technology

NTNU
Norwegian University of Science and Technology

Thesis for the Degree of Philosophiae Doctor

Faculty of Information Technology and Electrical Engineering
Department of Electric Power Engineering

ISBN 978-82-326-5000-2 (printed ver.)
ISBN 978-82-326-5001-9 (electronic ver.)
ISSN 1503-8181

Doctoral theses at NTNU, 2020:327

Printed by NTNU Grafisk senter

To all who fight the noise.

Abstract

The power electronic equipment needed in HVDC grids produces an AC ripple voltage with amplitude of around one-hundredth of the main DC voltage. The high voltage can result in partial discharges (PDs), which are a sign of defects and degradation in the insulation material system of the HVDC grid components. The present work aims to simulate and measure how a sinusoidal AC voltage ripple influences the PD process in dielectric bounded cavities.

This thesis describes a new stochastic Monte Carlo model proposed for the PD sequence at DC voltage and at combined DC and AC voltage, and provides statistical tools for a systematic extraction of physical discharge parameters from the PD data. The stochastic variables are the time lag and the phase-of-occurrence. The physical parameters in the model are the Townsend coefficient, the mean statistical waiting time, the capacitance in series with the cavity, and the rate of increase of the voltage over the cavity. The outputs for the Monte Carlo model are the individual discharge magnitude, the separation time, and the phase-of-occurrence. Individual discharges can be filtered out by setting a discharge magnitude detection threshold, emulating the conditions during the measurement of PD. A new statistical estimator is proposed, which performs the extraction of the physical parameters from PD data by the method of moments.

From model prediction and the measured PD data it was found that the main effect of adding a sinusoidal ripple to the DC voltage is a higher discharge magnitude and longer discharge separation time, compared to ideal DC voltage conditions. This was attributed to the increase in the time lag when an AC ripple is superimposed on the DC voltage. The increase in the time lag could be described mathematically using the concept of duty cycle, defined as the fraction of one AC voltage time period in which the cavity voltage is above the critical voltage.

The physical parameters could be estimated using the measured PD data, without resorting to simulations and the trial and error approach. It was found that the presence of a parasitic AC ripple voltage leads to a significant bias in the estimated parameters extracted by DC voltage estimation methods.

Preface

This thesis is submitted in partial fulfillment of the requirements for the degree of Philosophiae Doctor (PhD) at the Norwegian University of Science and Technology (NTNU) in Trondheim, Norway. The PhD work has been carried out at the Department of Electric Power Engineering, between August 2011 and June 2020. Associate Professor Frank Mauseth has been the main supervisor for this work, with Prof. Erling Ildstad as co-supervisor.

The PhD work was part of the Norwegian Renergi R&D project “High Voltage AC and DC Subsea Cables for Offshore Wind Farms and Transmission Grids” funded by the Research Council of Norway and the industrial partners Nexans Norway AS, EDF R&D (France), Equinor ASA, Statnett SF, Statkraft SF, and Borealis.

Acknowledgements

I would like to thank my main supervisor, Frank Mauseth, for the many interesting discussions during the course of the PhD work, and especially for his perseverance and guidance during the final stages of writing this PhD thesis. I am also indebted to my co-supervisor, Erling Ildstad, for trying to make me understand the art of keeping things as simple as possible. I am extremely grateful to Sverre Hvidsten who helped me through the last hurdles; I am not sure how I would have come through without his clear-sightedness. I would also like to thank the Head of Department Ole-Morten Midtgård for a supporting hand on my shoulder, in the form of a well aimed kick in the ass.

A lot of people have contributed to this thesis. Torbjørn Andersen Ve helped me with the conductivity measurements and always had time to show me around the lab. Rasmus Erleman was willing to discuss and guide me through the development of the statistical estimators, although I was a total stranger when I knocked at his door. Dag Linhjell advised me on the many aspects of test setups and measurements, and is also the only one who can operate the beast of an oil purifier we have in the cellar. Hans Helmer Sæternes helped me cast the epoxy for the electrodes, which was not a trivial process. Thank you for always lending your thoughts and hands so willingly.

I am indebted to the many hard working individuals at the Department of Electric Power Engineering. The service lab helped me build various test setups, Bård Almås showed infinite patience with my constant nagging. So did Svein Erling Norum, Vladimir Klubicka and Aksel Hanssen. Computer problems seemed to haunt me all throughout the work, Kurt Salmi and Anders Gytri expertly helped me with all of them. At the workshop I would always get positive and constructive advice from Domimik Häger and Morten Flå; for us less practically minded, your help is invaluable. The administration at our Department often do work behind the scenes, but your efforts are immensely important for us; thank you Bodil Wold, Halsten Aastebøl and Siri Wæhre Lien. Lars Norum and Tore Undeland helped me teach the power electronic courses, so did Inge Nordsteien. Their support and help was essential during the most difficult periods. I am indebted to my other colleagues, as well: Ola Furuhaug for his fresh thinking and compassion, Pål Glimen for his wisdom and care, Robert Nilssen for being a good friend and wise mentor, Vijay Vadlamudi for his undying enthusiasm and psychological support, Arne Nysveen for being so humble on part of his vast competence and goodness, Jonas Nøland for giving good pep talks and being an interesting discussion partner, John Arild Wiggen for always being positive and helping out an stressed individual, and finally Trond Toftevaag for his inspiring approach to teaching. Being part of the EME group is one of the most important reasons I am so happy to go to work each morning.

The work with a PhD thesis has its ups and downs. My son, Sivert, has lived with me through all of them. I hope you will remember the ups best. You are the best son, ever. Cathrine cared for me at the last stage of the PhD work, I am so grateful for your love and patience. I will always try to be *flink* and *snill* to you both.

I am grateful to my mother and father who have always given me so much love and support. My father instilled an undying curiosity in me and my mother taught me that I do not need to follow the path of everybody else. In addition to that, you have been the most fun parents one could hope for. My brother, Jo, has been disproportionally kind to me as long as I can remember and is the finest beer brewer, nature enthusiast and teacher I know.

My friends have seen very little of me the last years, but Kikki Stokstad Haug, Linn Aune, Paal Henrik Sandbu and Karl Magnus Laundal were at my side when I needed them. For all my friends: you are wonderful, I promise to be more social from now on.

Pål Keim Olsen

Trondheim, Norway

June 2020

List of symbols

q_a	Apparent discharge magnitude.
$q_{a,i}$	The i-th apparent discharge magnitude.
$q_{a,i-1}$	Apparent magnitude of previous discharge.
$q_{a,i+1}$	Apparent magnitude of succeeding discharge.
$\bar{q}_a$	Mean apparent discharge magnitude.
t_i	The time-of-occurrence of the discharges.
t_{i-1}	The time-of-occurrence of the previous discharges.
t_{i+1}	The time-of-occurrence of the succeeding discharges.
θ_i	The phase-of-occurrence of the discharges.
θ_{i-1}	The phase-of-occurrence of the previous discharges.
θ_{i+1}	The phase-of-occurrence of the succeeding discharges.
$\Delta t_i, \Delta t_{pre,i}$	Discharge separation time between the i-1th and ith discharge occurrence, $\Delta t_i = \Delta t_{pre,i} = t_i - t_{i-1}$, also termed time to the previous discharge.
$\Delta t_{i+1}, \Delta t_{suc,i}$	Discharge separation time between the ith and i+1th discharge occurrence, $\Delta t_{i+1} = \Delta t_{suc,i} = t_{i+1} - t_i$, also termed time to the succeeding discharge.
$\Delta \bar{t}$	Mean discharge separation time, $\Delta \bar{t} = \Delta \bar{t}_{pre} = \Delta \bar{t}_{suc}$
H	Sample total thickness.
h	Cavity height.
D	Ratio of the total thickness of the series dielectric to the height of the cavity.
σ	Conductivity of material.
ε	Relative permittivity of material.
C_c	Capacitance of cavity.
C_b	Capacitance of dielectric in series with cavity.

R_c	Equivalent resistance of cavity, including volume and surface resistance.
R_b	Resistance of dielectric in series with cavity.
K_{AC}	The capacitive voltage distribution factor, i.e. voltage division factor for AC voltage.
K_{DC}	The resistive voltage distribution factor, i.e. voltage division factor for DC voltage, when $t \to \infty$.
$\hat{V}_{AC}$	The AC voltage amplitude over the electrodes.
V_{DC}	The DC voltage over the electrodes.
$V_{Paschen}$	Breakdown voltage of a gas according to Paschen's law.
v_c	Voltage over the cavity.
$\frac{dv_c}{dt}$	Change in the cavity voltage per time, for DC voltage stress conditions.
$\frac{\widehat{dv_c}}{dt}$	Change in the upper envelope of the cavity voltage per time, for combined DC and AC voltage stress conditions.
V_b	Voltage over the series dielectric.
V_{ign}	Ignition voltage, the voltage over the cavity just before a discharge occurs.
V_{res}	Residual voltage, the voltage over the cavity just after a discharge has occurred.
ΔV_c	The cavity voltage drop due to a discharge.
ΔV_L	The overvoltage or the lag voltage, given as the difference between the ignition voltage and the Paschen voltage.
ΔV_R	Recovery voltage, the difference between the Paschen voltage and residual voltage.
t_L	The time lag is the time required for the cavity voltage to rise to the ignition voltage after having surpassed the critical voltage limit.
t_R	The recovery time is the time required for the cavity voltage to reach the critical voltage limit after a discharge.
τ	Time constant of DC voltage over cavity.
τ_s	The mean waiting time for discharge inception when the critical cavity electric field is above the critical limit.

f_{AC}	Frequency of the AC voltage.
T_{AC}	Period time of AC voltage.
T	Temperature.
r	Geometric radius of the cavity.
A	Geometric area of the cavity.
e	Elementary charge, $e = 1.60217662 \times 10^{-19}\, C$.
k	Boltzman constant, $k = 1.38064852 \times 10^{-23} \frac{m^2\, kg}{s^2 K}$.
ε_0	Permittivity of vacuum, $\varepsilon_0 = 8.854187817\ldots \times 10^{-12} \frac{F}{m}$.
E	Electric field strength.
α	The first Townsend coefficient, also called the gas ionisation coefficient.
Φ	Effective work function.
υ_0	Fundamental phonon frequency.
$\dot{N}_e$	Start electron generation rate.
N_{el}	Mean start electron generation rate, including both surface and volume electron generation mechanisms.
N_{dt}	Number of detrappable electrons on cavity surface.
C_{rad}	Term in the background ionisation law, it characterises the interaction between radiation and gas.
Φ_{rad}	Quantum flux density of the radiation.
p	Gas pressure.
ρ	Density.
Ω_{eff}	Effective gas volume exposed to radiation and electric field.

List of abbreviations

CDF	Cumulative density function
MoM	Method of moments
MSE	Mean squared error
OLS	Ordinary least squares
PD	Partial discharge
PDC	Polarization and depolarization current method
PDF	Probability density function
$PDIV_{AC}$	Partial discharge inception voltage, for applied AC voltage
$PDIV_{DC}$	Partial discharge inception voltage, for applied DC voltage
PE	Polyethylene
PET	Polyethylentereftalate
PRPDA	Phase resolved partial discharge analysis
PSA	Pulse sequence analysis
SEG	Start electron generation
XLPE	Cross linked polyethylene

Contents

1 Introduction

The capability of transporting electric energy over vast distances with low losses has been an essential building block for modern society and technology. It made it possible to consume electrical energy far away from where the actual energy sources were located, giving cities of any size and location the benefits that followed with the development of power systems. The two main types of the electric transmission system are the high voltage AC (HVAC) system and the high voltage DC (HVDC) system. The HVAC system is the predominant technology for electric power transmission, and HVDC systems have traditionally played a minor role. But since the installation of the first commercial HVDC link from the Swedish mainland to Gotland in 1954, the HVDC system has found new applications and gained more commercial interest. The applications of HVDC systems include:

1. Subsea power transmission:
    - between countries
    - to offshore oil platforms
    - from offshore renewable energy resources
    - from mainland to islands
2. Long-distance transmission without intermediate taps.
3. Power transmission and stabilisation between unsynchronized HVAC systems.
4. Facilitating power transmission between regions that use different AC frequencies.
5. Increasing capacity of existing HVAC grid by using the old AC overhead lines for HVDC transmission; presently, there are several ongoing projects in the EU.

Many of the applications of HVDC systems are in offshore grids. Repair and maintenance are costly offshore, and this imposes very high reliability requirements on the electric power components. The insulation material system of these components is one of the main challenges; e.g. the occurrence of partial discharges (PDs) within the cross linked polyethylene (XLPE) power cables rapidly deteriorates the insulation system and must be avoided [1]. A PD is a localised breakdown of solid or liquid insulation that does not bridge the space between two conductors [2]. PDs occur in all high voltage equipment and depend on the types of defect present in the insulation. These defects will be starting points for the following main categories of PD:

1) Internal discharges (also called dielectric bound discharges or dielectric barrier discharges)
2) Surface discharges
3) Corona discharges
4) Treeing discharges

At AC voltage, all the types of discharge can cause damage to the insulation and subsequent failures. At DC voltage, the lifetime effects of PDs are still unknown, but internal discharges are deemed to be the most harmful [3].

Most publications within DC partial discharge, such as [3]–[8], assume an ideal DC voltage, but the DC voltage will have an AC ripple in the HVDC systems used for electric power

transmission, see Fig. 1-1. Moreover, the DC voltage source of the Cockcroft-Walton type used in many high voltage laboratories always has an AC ripple superimposed on the DC voltage. The AC ripple amplitude depends on, among other factors, load current and construction [9].

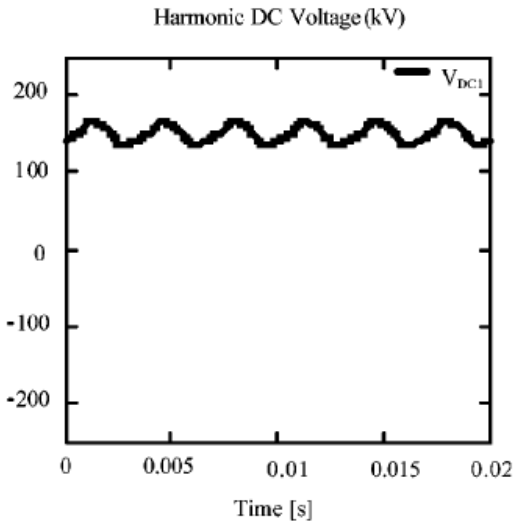

Fig. 1-1 DC voltage with AC voltage harmonics , example with AC voltage amplitude 17% of the DC voltage [10].

The AC ripple voltage on the DC side due to the voltage source converter found in a modern HVDC station can be around 1-15 % of the nominal DC voltage, depending on the size of the filter employed [10]. The harmonic content of the ripple can range up to 30-100 times the switching frequency, with the dominant components close to the switching frequency [10]. The switching frequency is usually around 1 kHz, but can be up to 2 kHz [11].

As AC to DC conversion will result in a high-frequency AC ripple voltage on the DC voltage, it will also affect the partial discharge activity in HVDC insulation [10]. This thesis aims to study the effect of a sinusoidal AC ripple (Fig. 1-1) on the internal discharge behaviour in polymeric insulation. The existing literature on this subject is reviewed in the next section.

1.1 Existing literature on internal discharges at combined DC and AC voltage

A significant amount of research effort has been put into investigating PD at AC voltage, while PD at DC voltage has received much less attention, and PD at combined DC and AC voltage even less still. The existing literature on partial discharges at combined DC and AC voltage can be divided into the following categories: internal discharges [12]–[15], surface discharges [16]–[18], needle-to-plane discharges [19]–[21]. Most of the publications focus on partial discharges in oil-pressboard insulation [14], [15], [22]–[25].

Some publications have addressed the influence of an AC ripple voltage on the mean separation time and magnitude of partial discharges. The mean discharge separation time is the mean time interval between two consecutive discharges, and is the inverse of the discharge repetition rate. Rogers [26] and Densley [27, p. 436] postulate a decrease in discharge separation time when an AC ripple is added to the DC voltage but do not provide experimental evidence for this. Dezenzo [12] and Fard [13] provided empirical support to this postulation. In the model by Rogers and Densley, there is no expected change in discharge magnitude with AC ripple voltage amplitude. The reason is that the model is deterministic; it is assumed that the discharge always occurs at the same critical electric

field strength and the residual electric field strength is the same after the discharge has occurred.

Recent publications after 2010 on internal discharges [28], [29], and the older publications [23], [30], [31] focus on the effect of DC voltage on the partial discharge inception voltage (PDIV) for applied AC voltage. The overall conclusion was that the DC voltage has little or no effect on the PDIV value. These investigations give no information about the PD process at combined voltage. They may be of low relevance to HVDC systems where the AC ripple is in the order of 1-3% of the DC voltage, probably operating far below the PDIV for AC voltage.

Many of the publications are experimental investigations, where the measurement and recognition of partial discharge patterns themselves are of primary interest. Piccin [32] and several other researchers in [14], [15], [22], [25] treat the measurement of PD at DC and AC, but provide no statistical model based on physical parameters for discussing the resulting PD patterns.

A few publications address modelling and physical understanding of the internal discharge process at combined voltage [4], [27]. Still, the PD process is modelled as a deterministic process, ignoring the stochastic nature of the phenomenon [33]–[36]. Furthermore, the discharge separation time and the magnitude are often treated separately [37], or only one of the parameters is considered. A correlation between the separation time and the magnitude should be expected if the PD process is modelled as a PD sequence [38].

1.2 Research gap

The development of measurement methods for PDs has progressed rapidly in the last few decades. However, the analysis and interpretation of the PD data at combined voltages is still a challenge. Some models for PD at DC voltage offer a stochastical, physical model [39], but the parameters are found by trial and error. There is a need for a stochastic, physical model, and tools for analyzing the PD process at combined DC and AC voltage. The model must be able to predict the effect of an AC voltage ripple on the discharge separation time and magnitude. The stochastic model must predict similar PD patterns as the measured data so that the data can be interpreted in the context of the physical parameters. It must also be shown that the statistical tools developed can characterise the physical parameters without resorting to simulations and the trial and error approach.

1.3 Research objectives

The main objective of this thesis is to:

Assess the effect of a sinusoidal AC ripple on stochastic discharge separation time and magnitude in an internal cavity, by theoretical and experimental investigation of the following hypotheses:

H.1: The discharge separation time decreases with increasing AC ripple voltage amplitude.

H.2: The discharge magnitude is constant when the AC ripple voltage amplitude increases.

H.3: The discharge separation time and discharge magnitude are not influenced by the frequency of the AC ripple voltage.

The sub-objectives are:

1) The formulation of a stochastic PD sequence model at DC voltage and combined voltage conditions.
2) The creation of a statistical estimation tool to extract relevant physical parameters from the PD process.

1.4 Scope

The characteristics of a discharge process at combined AC and DC voltage depends on the amplitude of the applied DC and AC voltage [31], compared to the AC and DC partial discharge inception voltage of the test object. Four main conditions can be identified, where the discharge process may have very different characteristics in terms of discharge separation time, magnitude and polarity:

1) Condition A: $|V_{DC}|<|PDIV_{DC}|$ and $V_{AC}<PDIV_{AC}$
2) Condition B: $|V_{DC}|<|PDIV_{DC}|$ and $V_{AC}\geq PDIV_{AC}$
3) Condition C: $|V_{DC}|\geq|PDIV_{DC}|$ and $V_{AC}<PDIV_{AC}$
4) Condition D: $|V_{DC}|\geq|PDIV_{DC}|$ and $V_{AC}\geq PDIV_{AC}$

In Fig. 1-2, conditions are delimited by certain values of $PDIV_{AC}$ and $PDIV_{DC}$, which may change with time, temperature and type of object, as treated in 2.1.1.2. The red box indicates the conditions used in this thesis. In this framework, the AC voltage discharge process can be considered a special case of condition B, where $V_{DC} = 0$. An ideal DC voltage discharge process can be considered a special case of condition C, where $V_{AC} = 0$. The focus in the present work is on how the AC ripple voltage influences the discharge separation time and magnitude of discharges when the AC voltage is below the measured AC inception voltage and the DC voltage is assumed to be above the voltage that would produce repetitive DC discharges, i.e. condition C.

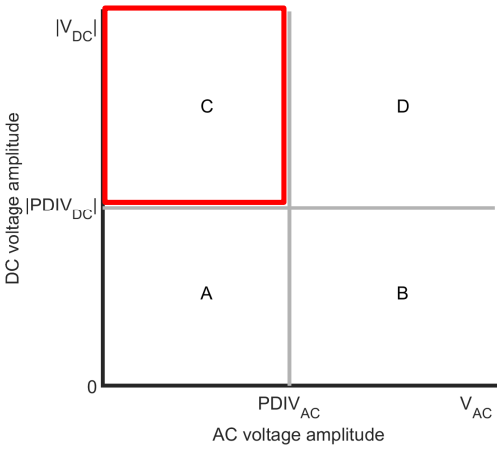

Fig. 1-2 The four main conditions A-D for partial discharge processes at combined DC and AC voltage. The total voltage is the sum of the DC voltage and the AC voltage component.

1.5 Research contributions

The thesis contributes to the body of research within partial discharges with the following items not previously covered in the available literature:

- A stochastical model based on physical parameters, for internal discharges under both DC and combined DC and AC voltage, verified by experimental data.
- A method-of-moments (MoM) estimator to retrieve the physical parameters without simulation.
- An analytical mean model for prediction of discharge magnitude and separation time, as a function of AC voltage amplitude.
- A test setup for combined DC and AC voltage with high noise rejection, high sensitivity and broad discharge magnitude detection range.

1.6 Outline of thesis

Chapter 1 reviews the state-of-the-art and the research objectives for PD at combined voltage. Chapter 2 presents the theoretical foundations necessary to create a stochastic model of the internal partial discharge sequence at DC voltage and combined voltage conditions. A new stochastic model and estimator methods for partial discharges at DC voltage and combined voltage is developed in chapter 3. The experimental techniques and procedures for measuring partial discharges and material parameters are detailed in

chapter 4. Chapter 5 presents the simulated and the experimental data for the PD process at DC voltage and combined voltage, the validity of the proposed model and the results is discussed. Conclusions and further work are found in chapters 6 and 7.

2 Theory

This chapter presents the theoretical foundations necessary to create a stochastic model of the partial discharge sequence at DC voltage and combined voltage conditions, for a cylindrical cavity bounded by insulated surfaces.

An understanding of the partial discharge process at DC voltage serves as a reference for the discharge process at combined voltage conditions; this is given in section 2.1. The scope in section 2.2 is limited to high voltage DC with a superimposed low amplitude AC ripple, i.e. 1-10% of the DC voltage. Section 2.3 treats how to extract physical parameters from the PD process itself using statistical estimation theory.

2.1 Partial discharges at DC voltage

This section presents the main characteristics of the partial discharge process at DC voltage when the AC ripple voltage amplitude is zero. In contrast to PDs at AC voltage stress, the PD process at DC voltage is characterised by:

- Unipolar discharges; the electric field in the cavity always works in one direction.
- Low voltage rise rate over the cavity, governed by the conductivity of the surrounding insulation material.
- Long discharge separation time.
- Low discharge magnitude and high probability for Townsend-like discharges, i.e. a discharge mechanism where free electrons are accelerated by the electric field and freeing new electrons by collision, resulting in avalanche multiplication.

2.1.1 The discharge sequence at DC voltage

Shihab [30], Bartnikas [40] and Fromm [7] describe the partial discharge sequence at DC voltage using the ABC model, including the resistances R_a, R_b and R_c, as well as the capacitances C_a, C_b and C_c, see Fig. 2-1. R_c and C_c are the equivalent resistance and capacitance of the cavity, respectively; the equivalent resistance includes both the surface resistance and the volume resistance. R_b and C_b are the volume resistance and the capacitance of the dielectric in series with the cavity, respectively. C_a and R_a are the volume resistance and capacitance in parallel with the column containing the cavity, respectively.

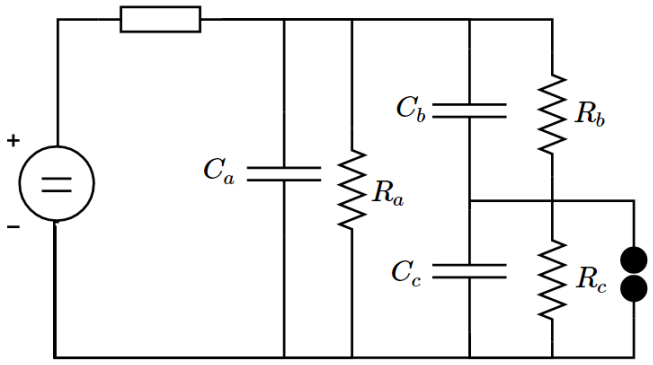

Fig. 2-1 ABC equivalent circuit with material resistances included. The internal impedance of DC voltage source is in series with the ABC circuit.

2.1.1.1 Voltage and electric field strength in a discharge-free cavity

The electric field strength in a flat cavity will be proportional to the cavity voltage assuming that the insulated surfaces at opposite sides of the cavity are at the same potential level. The voltage over the cavity when no discharge occurs can be calculated as [27]:

$$v_c(t) = K_{DC} V_{DC} \cdot \left(1 - e^{-t/\tau}\right) \quad (2.1)$$

where K_{DC} is the resistive distribution factor:

$$K_{DC} = \frac{R_c}{R_c + R_b} \quad (2.2)$$

When the cavity is cylindrical, the ABC-model with *RC* elements is identical to a Maxwell capacitor model [41], so

$$K_{DC} = \left(1 + \frac{H - h}{h}\frac{\sigma_c}{\sigma_b}\right)^{-1} \quad (2.3)$$

where H is the total thickness of the insulation, h is the height of the cavity, σ_c is the equivalent conductivity of the cavity and σ_b is the conductivity of the insulation material in series with the cavity. The time constant of the cavity voltage is [8]:

$$\tau = \frac{\left(C_b + C_c\right)}{\left(\frac{1}{R_b} + \frac{1}{R_c}\right)} \quad (2.4)$$

Or, in terms of the material and geometric parameters:

$$\tau = \frac{\left(\varepsilon_b + \frac{H-h}{h}\varepsilon_c\right)\varepsilon_0}{\sigma_b + \frac{H-h}{h}\sigma_c} \quad (2.5)$$

where ε_b is the relative permittivity of the insulation material and ε_c is the relative permittivity of the gas in the cavity.

The voltage over the cavity will have exponentially converging behaviour, with a time constant τ . This time constant is in the order of minutes to hours when the conductivity of the materials is low. If no discharge occurs, the cavity voltage will reach a value determined by the resistive distribution factor times the applied DC voltage, $K_{DC}V_{DC}$, see Fig. 2-2. If discharges occur, the cavity voltage will vary around the critical voltage, given by Paschen's law, and resemble an irregular saw-tooth-like curve. The criteria for discharges to occur and the resulting cavity voltage are covered in the next two sections.

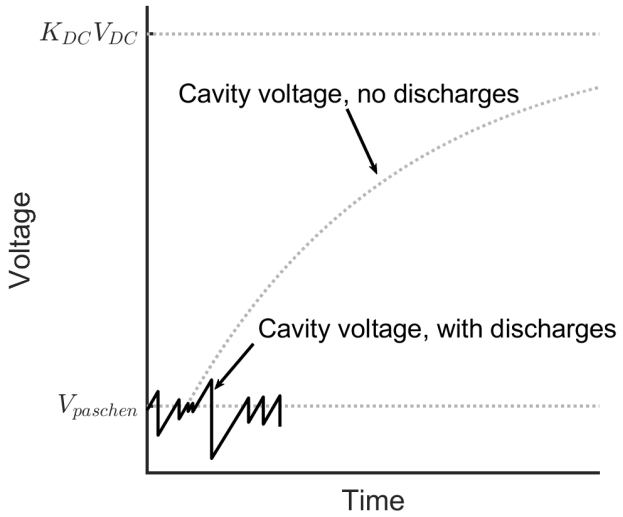

Fig. 2-2 Voltage over a cavity with discharges. Cavity voltage is not to scale.

2.1.1.2 PD inception voltage

Discharges will occur in the cavity when the DC voltage is above the partial discharge inception voltage and if there are free electrons available for starting the avalanche process. For AC, the partial discharge inception voltage (PDIV) is defined as the voltage over the object at which repetitive partial discharges are first observed. The theoretical limit is:

$$PDIV_{AC} = \frac{V_{paschen}}{K_{AC}} \quad (2.6)$$

where K_{AC} is the capacitive distribution factor.

$$K_{AC} = \left(1 + \frac{H-h}{h} \frac{\varepsilon_c}{\varepsilon_b} \right)^{-1} \quad (2.7)$$

In practice, the $PDIV_{AC}$ can be higher or lower than the value given by (2.6). Mason [42] found that the $PDIV_{AC}$ of non-ventilated voids in polyethylene is in fair agreement with the Paschen breakdown voltage between plane parallel metal electrodes, $V_{Paschen}$, but some 10-20% lower. At DC voltage, the PDIV concept is difficult to use, because at the theoretical limit:

$$PDIV_{DC} = \frac{V_{paschen}}{K_{DC}} \quad (2.8)$$

the repetition rate goes to zero, i.e. it is impossible to measure. In practice, it is also difficult to use a certain repetition rate as a threshold for $PDIV_{DC}$, since the repetition rate exhibits a strong temperature and moisture dependence [43]. Varying the temperature and moisture content can change the conductivity considerably and thus the repetition rate, as treated in section 2.2.2. It is clear, however, that the applied DC voltage should be much higher than $PDIV_{DC}$ to produce a sufficiently high repetition rate.

2.1.1.3 Voltage over a discharging cavity – the PD sequence

If discharges occur, the voltage over the cavity is given by [44]:

$$v_{c,i}(t') = K_{DC} V_{DC} - \left(K_{DC} V_{DC} - V_{res,i-1} \right) \exp\left(-\frac{t'}{\tau} \right) \quad (2.9)$$

The change in cavity voltage and the PD sequence can be described as follows, see Fig. 2-3:

1) $t' = 0$ when the cavity voltage has dropped to the residual voltage $V_{res,i-1}$ after the previous discharge. The cavity voltage starts rising again and reaches the critical voltage after a recovery time $t_{R,i-1}$.
2) A start electron will be available within a time lag $t_{L,i}$. When the discharge is ignited $t' = \Delta t_{pre,i}$ and $v_{c,i}(t' = \Delta t_{pre,i}) = V_{ign,i}$. The cavity voltage drops to $V_{res,i}$ and a discharge of apparent magnitude $q_{a,i}$ is registered at time t_i.
3) The discharge process continues from step 1.

The recovery time will depend on the residual voltage from the previous discharge, and the time lag is defined by a stochastic waiting time for start electrons [33]. The time to the previous discharge and the time to the successive discharge is a sum of the corresponding recovery time and the time lag:

$$\Delta t_{pre,i} = t_{R,i-1} + t_{L,i} \quad (2.10)$$

$$\Delta t_{suc,i} = t_{R,i} + t_{L,i+1} \quad (2.11)$$

The term discharge separation time can refer to both these quantities, as a more general notion of the time between discharges.

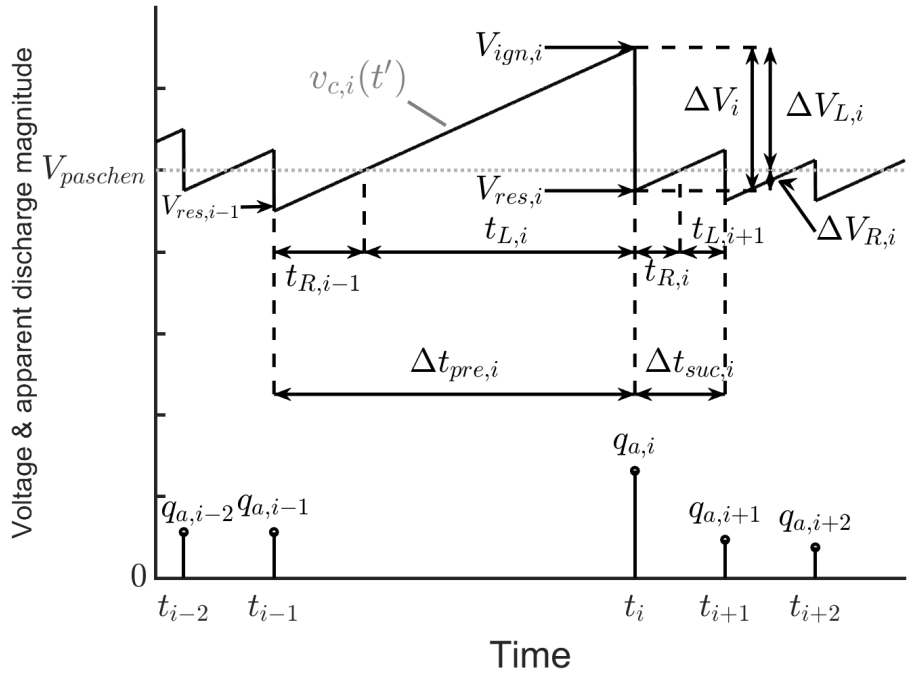

Fig. 2-3 The voltage over a discharging cavity at DC voltage conditions. Shown together with the discharge time of occurrence, t_i (s), and apparent discharge magnitude, $q_{a,i}$ (C). Cavity voltage is not to scale.

2.1.1.4 The measurable quantities at DC voltage

When a discharge occurs, it is possible to detect the apparent discharge at the terminals of the test object, $q_{a,i}$, and the time of the discharge, t_i. The basic pulse sequence data for a DC discharge process are depicted in Fig. 2-4.

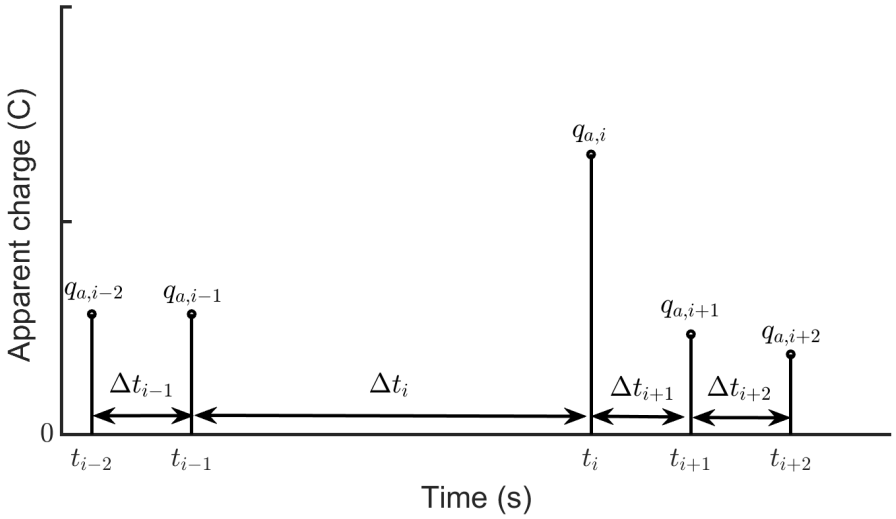

Fig. 2-4 Measurement of discharges occurring at DC voltage as a function of time, t_i , with corresponding time separations and apparent discharge magnitude, $q_{a,i}$.

The measurable quantities from the PD process are the time of the discharge occurrence, t_i , and the apparent discharge magnitude, $q_{a,i}$, giving the following data sets for n discharges:

$$t = \left[t_1, ..., t_i, ..., t_n \right] \quad (2.12)$$

$$q_a = \left[q_{a,1}, ..., q_{a,i}, ..., q_{a,n} \right] \quad (2.13)$$

The measured quantities are the basis for the derived quantities: time to preceding discharge, $\Delta t_{pre,i}$, and time to succeeding discharge, $\Delta t_{suc,i}$:

$$\Delta t_{pre,i} = \Delta t_i = t_i - t_{i-1} \quad (2.14)$$

$$\Delta t_{suc,i} = \Delta t_{i+1} = t_{i+1} - t_i \quad (2.15)$$

Pulse sequence analysis (PSA) is widely used to interpret discharge processes [45]. In PSA, information about the discharge process can be inferred from the correlation between pairs of quantities such as $\left(q_{a,i}, \Delta t_{pre,i} \right)$ and $\left(q_{a,i}, \Delta t_{suc,i} \right)$ [44]. A method to estimate mean time lag and recovery time based on these data pairs is described in section 3.2.4.1.

2.1.2 Mean discharge separation time

Rogers [26] and Bartnikas [40] and found an expression for the mean discharge separation time, $\overline{\Delta t}$, by imposing the following deterministic conditions: the discharge always occurs

at the same ignition voltage V_{ign} and drops to the same residual voltage V_{res} every time. By setting $V_c\ (t' = \overline{\Delta t}) = V_{ign}$ and $V_{res,i-1} = V_{res}$ in (2.9), and solving for $\overline{\Delta t}$:

$$\overline{\Delta t} = -\tau \ln\left(\frac{K_{DC}V_{DC} - V_{ign}}{K_{DC}V_{DC} - V_{res}}\right) \quad (2.16)$$

The mean discharge separation time can be found by assuming a small voltage drop, $\Delta V_c = V_{ign} - V_{res}$, and linearising around the Paschen breakdown voltage:

$$\overline{\Delta t} \cdot \left.\frac{dv_c}{dt}\right|_{v_c = V_{paschen}} = \Delta V_c \quad (2.17)$$

$$\overline{\Delta t} = \tau \frac{\Delta V_c}{K_{DC}V_{DC} - V_{paschen}} \quad (2.18)$$

The maximum discharge separation time can be found by assuming $V_{ign} = V_{paschen}$ and $V_{res} = 0$, and linearising around zero voltage:

$$\overline{\Delta t}_{\max} \cdot \left.\frac{dv_c}{dt}\right|_{v_c = 0} = V_{paschen} \quad (2.19)$$

$$\overline{\Delta t}_{\max} = \tau \frac{V_{paschen}}{K_{DC}V_{DC}} \quad (2.20)$$

The mean discharge separation time at DC voltage conditions can be compared to the separation time at AC voltage as follows:

1) A mean discharge separation time at AC voltage conditions can be estimated [46], [47], based on the assumption of a constant ignition voltage equal to the Paschen breakdown voltage, and zero residual voltage, as:

$$\overline{\Delta t_{AC\max}} = \frac{\tau_{AC}}{4} \frac{V_{Paschen}}{K_{AC}\hat{V}_{AC}} \quad (2.21)$$

   where τ_{AC} is the AC voltage time period, $\hat{V}_{AC}$ is the amplitude and K_{AC} is the capacitive distribution factor.
2) Dividing (2.20) with (2.21) yields:

$$\frac{\overline{\Delta t_{DC\max}}}{\overline{\Delta t_{AC\max}}} = 4 \cdot \frac{\tau}{\tau_{AC}} \cdot \frac{K_{AC}\hat{V}_{AC}}{K_{DC}V_{DC}} \quad (2.22)$$

The time constant at DC conditions, τ, is in the range of minutes to hours. The AC period time, T, is in the range of milliseconds. If $K_{DC}V_{DC} \leq 100 \cdot K_{AC}\hat{V}_{AC}$ it can be concluded that the discharge separation time at DC voltage should be several orders higher than at AC voltage conditions.

Assuming $\sigma_c = 0$ in (2.20) yields:

$$\Delta\bar{t} \propto \frac{\varepsilon_b}{\sigma_b}\frac{1}{V_{DC}} \quad (2.23)$$

Thus, the ABC model predicts that the discharge separation time is proportional to the permittivity of the series dielectric and inversely proportional to the applied DC voltage and the conductivity of the series dielectric. The conductivity of the series dielectric depends strongly on temperature and electric field strength in the series dielectric. The effect of a transient polarization current on the discharge separation time, interpreted as a decrease in the series dielectric conductivity after DC voltage application, is discussed next.

2.1.2.1 Transient discharge separation time due to polarization current

The conductivity of the surrounding medium σ_b shows a non-linear dependence on temperature and electric field strength. Classic conduction mechanisms in polymer materials include bulk, electrode and space charge limited behaviour [48]. The conductivity in polymer materials will display a temporal dependency after voltage application, due to slow polarization phenomena in the material. After voltage application, the initial polarization current exhibits the Curie-von Schweidler power law for a wide range of dielectric materials [49]:

$$i_p = A' \cdot t^{-n} + I_{DC} \quad (2.24)$$

where A', n and I_{DC} depend on bulk material, electrode material, electric field magnitude and temperature. I_{DC} is the conductive, steady-state part of the polarization current i_p. The behaviour in (2.24) has been observed for PET [50] and PE [40]. The polarization current can be interpreted as a function of time-varying conductivity

$$\sigma_b = A'' \cdot t^{-n} + \sigma_{b,DC} \quad (2.25)$$

which is assumed to stabilise to a finite value $\sigma_{b,DC}$ when $t \to \infty$, see Fig. 2-5. The discharge separation time will therefore increase with time of voltage application, according to (2.23). However, the volume conductivity of the dielectric in series with the cavity might not show the same behaviour, due to space charge accumulation on the cavity surfaces and varying voltage over the series dielectric. If the mean voltage drop is small and the space charge effect is negligible, then the bulk conductivity in the insulation material in series with the cavity can be considered constant, after a suitable stabilisation time. The

stabilisation time can be calculated in terms of an allowed maximum deviation from I_{DC}. The deviation is given by the factor $k > 1$:

$$t_{stabilize} = \left(\frac{I_{DC}\left(k-1\right)}{A'} \right)^{-\frac{1}{n}} \quad (2.26)$$

I_{DC}, A' and n can be obtained by the polarization current measurements described in 4.2.1.

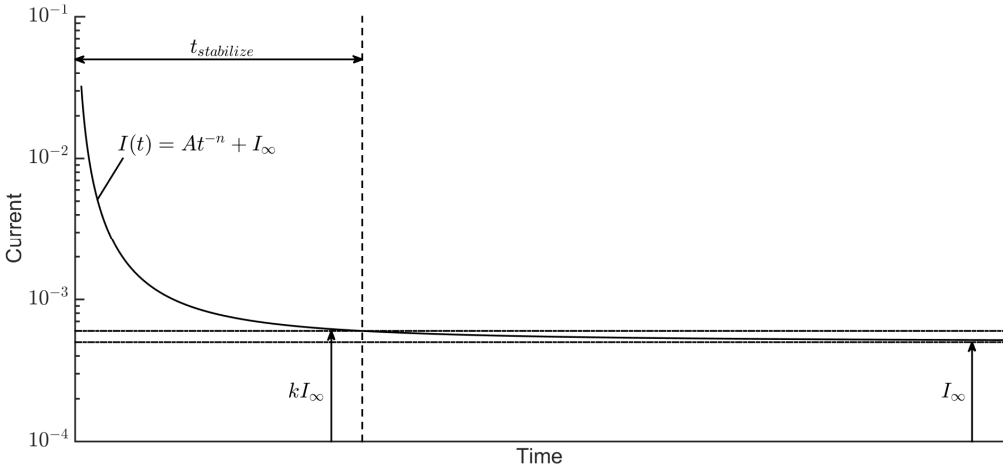

Fig. 2-5 Variation of the current with time of DC voltage application. Arbitrary units on x- and y-axis. $I_\infty = I_{DC}$

2.1.2.2 The distribution of discharge separation time under stationary conditions

After a transient period, as treated in the previous section, the discharge process will reach the stationary stage. It is then possible to measure the distribution of discharge separation times under stationary conditions. In section 2.1.1, the discharge separation time was defined as the sum of the recovery time after preceding discharge and the time lag before the i[th] discharge. Fromm and Kreuger [51] identify the time lag as the main stochastic parameter, and assume that the time lag has an exponential probability density in accordance with experiments with metal gaps by Zuber [52]:

$$pdf_{t_{L,i}}(t_L) = \frac{1}{\tau_s}\exp\left\{-\frac{t_L}{\tau_s}\right\} \quad (2.27)$$

where τ_s is the mean statistical waiting time for discharge inception when the critical cavity electric field is just above the required critical field. The distribution is shown in Fig. 2-6a. Fromm assumed a constant recovery time (2.28) and predicted the distribution for discharge separation time in Fig. 2-6b.

$$\Delta t_{pre,i} = \overline{t_R} + t_{L,i} \quad (2.28)$$

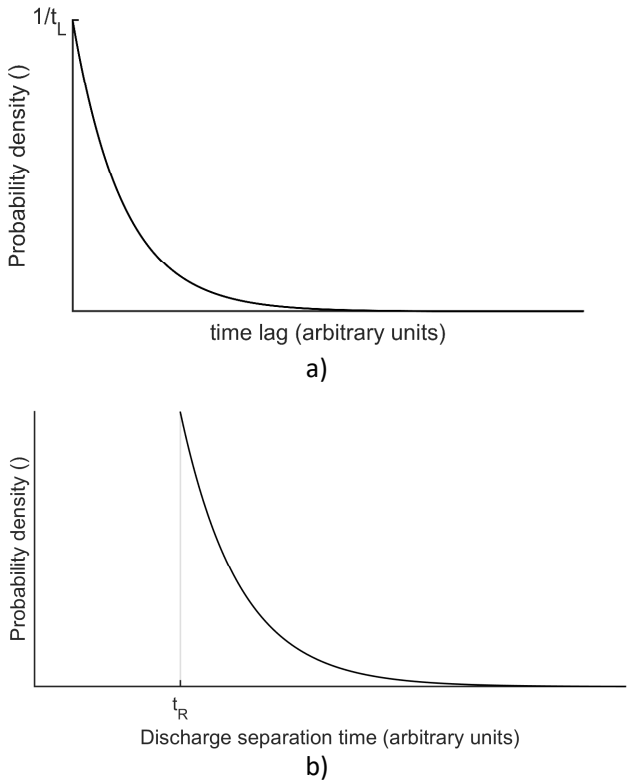

Fig. 2-6 a) Time lag probability density, and b) Discharge separation time, at DC voltage conditions.

2.1.2.3 Mean statistical waiting time and mean start electron generation rate

The PD process may in general be regarded as a life time process with an intensity function[1] equal to the start electron generation (SEG) rate $\dot{N}_e$ [54]. If the SEG rate is constant, i.e. $\dot{N}_e = N_{el}$, and N_{el} is the mean SEG rate, the time lag probability density function will be given by (2.27) with

$$\tau_s = \frac{1}{N_{el}} \quad (2.29)$$

The mean statistical waiting time is known as the scale parameter, and the mean SEG rate is known as the rate parameter. The probability density function may be described either in terms of the scale parameter or the rate parameter.

2.1.2.4 Start electron generation mechanisms

Several SEG mechanisms can be present in any cavity, and depend on temperature, electric field strength, the composition and pressure of the gas in the cavity, and type of material the cavity is embedded in [55]. The SEG mechanisms can be divided into surface- or volume generation. The total SEG rate is a sum of the volume and surface electron generation rates:

$$\dot{N}_e(t) = \dot{N}_{e,volume}(t) + \dot{N}_{e,surface}(t) \quad (2.30)$$

In spherical cavities with a small surface-to-volume ratio, volume ionisation in the gas is the dominating mechanism [56]. In flat cavities, the surface-to-volume ratio is high and surface generation dominates [55]. Experimental data [57],[58] suggest that the surface emission process approximately follows a Richardson-Schottky scaling for both insulating and conducting surfaces [56]:

$$\dot{N}_{e,surface} = \frac{A}{e} S \left(1 - \frac{\eta}{\alpha}\right) \exp\left(-\frac{\Phi}{kT}\right) \exp\left(\frac{e}{kT}\sqrt{\frac{e}{4\pi\varepsilon_0}}\sqrt{E}\right) \quad (2.31)$$

where A is the surface area, e is the elementary charge, k is the Boltzman constant, T is temperature, ε_0 is the permittivity of vacuum and h is the height of the cavity, E is the electric field out of the surface. At insulating surfaces S is given by the amount of detrappable electrons from the surface:

$$S = \upsilon_0 e \frac{N_{dt}}{A} \quad (2.32)$$

where N_{dt} is the number of electrons available in detrappable states, and υ_0 is the fundamental phonon frequency. There is a range of processes that can add or deplete the number of available start electrons from detrappable states [56], [59], [60]:

[1] The intensity function is sometimes called the hazard rate or mortality rate, and in reliability theory it is called the failure rate [53].

a) Deployment of electrons from discharges of opposite polarity, increases N_{dt}
b) Conduction of electrons through series dielectric, increases N_{dt}
c) Conduction along insulation surface walls, decreases N_{dt}
d) Conduction through cavity gas volume, decreases N_{dt}
e) Diffusion into deep traps, decreases N_{dt}

The process in a) holds high importance in bipolar discharge processes, as seen under sinusoidal or other bipolar voltages. The effect is exploited in dielectric barrier discharges (DBD), where the residual charge is used to create a stable and efficient discharge process. By switching the voltage polarity after an appropriate time delay, a back-ignition is achieved [61]. At DC voltage, the residual charge from last discharge will not contribute to the pool of available start electrons, since the voltage polarity is not reversed. At DC voltage, the process in b) may be of higher importance.

Since many of the parameters in (2.31) are often unknown, Forssén [62] proposed a simpler function:

$$\dot{N}_e(t) = N_{e0} \exp\left(\left|\frac{v_c(t)}{V_{cr}}\right|\right) = N_{e0} \exp\left(\left|\frac{E_c(t)}{E_{cr}}\right|\right) \quad (2.33)$$

where v_c is the voltage over the cavity centre, V_{cr} is the critical voltage for discharge and N_{e0} is a constant. The physical process is better understood using (2.31), while (2.33) may be better for modelling purposes. As long as $\dot{N}_e$ is a non-negative function, the probability density function of a discharge occurring after a time lag t_L is [54]:

$$pdf(t_L) = \dot{N}_e \exp\left\{-\int_0^{t_L} \dot{N}_e dt'\right\} \quad (2.34)$$

The corresponding cumulative distribution function is

$$cdf(t_L) = 1 - \exp\left\{-\int_0^{t_L} \dot{N}_e dt'\right\} \quad (2.35)$$

The distribution of the time lag determines the discharge magnitude distribution, as treated in section 2.1.3.3.

2.1.3 Discharge mechanisms and apparent discharge magnitude

The discharge sequence depends on the stochastic time lag, as discussed in the previous section, but will also be influenced by the discharge mechanisms which are active in the

cavity. This section provides a brief overview of the type of mechanisms that may be active in the discharge process, the discharge magnitude, and the importance of the overvoltage.

2.1.3.1 Discharge mechanisms in dielectric bounded cavities

At least two important discharge mechanisms are active in dielectric bounded cavities, according to Devins [63]:

1) The Townsend-like discharge
2) The streamer-like discharge

In the Townsend-like discharge, free electrons are accelerated by the electric field and ionise gas molecules by collision, thus creating new electrons; ionisation repeats itself with new electrons available and causes avalanche multiplication. In the streamer-like discharge space charge distorts the electric field considerably, the high local space charge field creates high energy photons, and successive avalanches are initiated by these photons. Due to the high speed of the photons, the streamer-like discharge propagates faster than the Townsend-like discharge. Townsend-like discharges tend to cover a large area of the cavity, while streamer-like discharges are more localised, but may ignite several parallel streamer channels due to photoionisation feedback [64]. Townsend-like discharges tend to stop when sufficient charge has been dumped at the anode surface to overcome the overvoltage, which results in a higher residual voltage, closer to the critical voltage. Streamer-like discharges tend to discharge the cavity so that the residual voltage is close to zero. This is due to the avalanche-sustaining high field enhancement on the ends of the positive streamers [65].

According to Devins [63] the discharge mechanism is governed by the overvoltage, which is the voltage above the critical voltage before discharge occurrence. A low overvoltage will increase the probability of observing Townsend-like discharges [63], [64]. For a critical overvoltage the discharge mechanism changes, increasing the probability of observing streamer-like discharges [66]. Fromm [44] observed both the Townsend-like and the streamer-like discharge mechanism during the PD process at DC voltage, although the Townsend-like mechanism appeared to dominate. The main properties of Townsend-like and streamer-like discharges are summarised in Table 2-1.

Table 2-1 Properties of Townsend-like and streamer-like discharges [44], [63], [66]

Townsend-like discharges	Streamer-like discharges
1) Low overvoltage 2) Low discharge magnitude 3) Cover a large part of the cavity surface 4) Residual voltage closer to minimal breakdown voltage	1) High overvoltage 2) High discharge magnitude 3) Cover a fraction of the cavity surface 4) Residual voltage is close to zero

2.1.3.2 The discharge magnitude and cavity voltage drop at DC voltage conditions

The magnitude of the discharge itself can be detected indirectly as charge displacement on the terminals of the test object; this is called the apparent discharge magnitude. The classic ABC-equivalent [46] predicts an apparent charge of

$$q_a = C_b \Delta V_c \quad (2.36)$$

where ΔV_c is the cavity voltage drop and C_b is the capacitance in series with the cavity. The ABC model does not include the space charge field due to movement of charged species in the dielectric during breakdown. Several researchers have pointed to this deficiency in the ABC-model [63], [67], [68]. Devins [63] found an expression for the apparent charge for a Townsend discharge, including the effect of the movement of the positive ion space charges during the cavity gas breakdown:

$$q_a = \alpha h \cdot C_b \Delta V_L \quad (2.37)$$

α is the first Townsend ionisation coefficient, h is the height of the cavity and ΔV_L is the overvoltage defined in Fig. 2-3. The first Townsend ionisation coefficient depends on the pressure and the electric field strength in the gas [69], as well as temperature [70], type of gas [71] and humidity [72]. The Townsend coefficient in dry air has been measured for different field strengths and pressures; Kontaratos [69] found that the measured values fits the following equation:

$$\alpha(E_c, p) = p \cdot 0.57 \cdot \exp\left(-\frac{222}{E_c/p}\right) \cdot \left(\frac{\left(E_c/p\right)^{\frac{1}{2}}}{1+4\cdot 10^{-4}\left(E_c/p\right)}\right) \quad (2.38)$$

where E_c is the electric field strength in air in V/cm, and p is the pressure in mmHg. Eq. (2.38) is valid for $\frac{E_c}{p} \in \langle 10,1000 \rangle V/(cm \cdot mmHg)$. The apparent discharge model by Devins predicts a relationship between the overvoltage, ΔV_L, and the recovery voltage, ΔV_R; this was pointed out by Dissado [73]:

$$\frac{\Delta V_R}{\Delta V_L} = \alpha h - 1 \quad (2.39)$$

The total voltage drop is the sum of the overvoltage and the recovery voltage, see Fig. 2-3. By using (2.39), the total voltage drop can be calculated as:

$$\Delta V_c = \Delta V_L + \Delta V_R = \alpha h \Delta V_L \quad (2.40)$$

Thus the apparent discharge magnitude for Townsend discharges can be interpreted as a version of the classic equation in (2.36) with a voltage drop value equal to (2.40).

2.1.3.3 The distribution of the discharge magnitude under stationary conditions

Devins [63, p. 485] argues that the probability density of the discharge magnitude follows the distribution of the time lag. Linearization of the cavity voltage around $v_c = V_{critical}$ yields the following expression for the discharge magnitude as a function of the stochastic time lag:

$$q_{a,i} = \alpha h \cdot C_b \cdot \left(V_{DC} - V_{critical}\right) \frac{t_{L,i}}{\tau} \quad (2.41)$$

valid for $t_{L,i} \ll \tau$. If all the other parameters are constant, the discharge magnitude distribution will be determined by the exponential probability density of the time lag. This seems to be confirmed by measurements from Fromm [74].

2.2 Partial discharges at DC voltage with an AC ripple voltage

In this section, the main characteristics of the partial discharge process at combined DC and AC voltage is presented as described in the existing literature.

2.2.1 The electric field strength in a cavity at combined AC and DC voltage

At combined DC and AC voltage, the same representation of the test object can be used as for DC voltage, see Fig. 2-7. The total electric field in the cavity is then a superposition of a DC- and a sinusoidal AC electric field. The electric field strength in the cavity may be approximated by the voltage over the centre of the cavity divided by the height of the cavity: $E_c(t) = {}^{v_c(t)}\!/_{h}$.

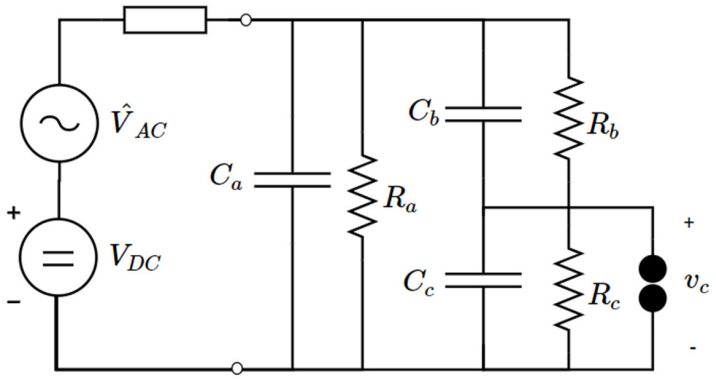

Fig. 2-7 ABC-equivalent at combined DC and AC voltage on the right side of terminals, DC and AC source with internal impedance on the left side.

2.2.2 Discharge separation time and magnitude

Rogers [26] and Densley [27, p. 436] postulate an increase in discharge repetition rate when an AC ripple is added to the DC voltage. Densley represents the test object as in Fig. 2-7, and assumes as in the case of Rogers that:

1) a discharge will occur whenever the cavity voltage reaches the ignition voltage.
2) the cavity voltage is reduced to the same residual voltage after each discharge.
3) the period time of the AC voltage is much lower than the time constant of the DC voltage component.

Under these conditions, it appears as if the cavity DC voltage is offset by the cavity AC voltage. For a discharge to occur, the DC component of the cavity voltage does not have to build up to the full ignition voltage, see Fig. 2-8b.

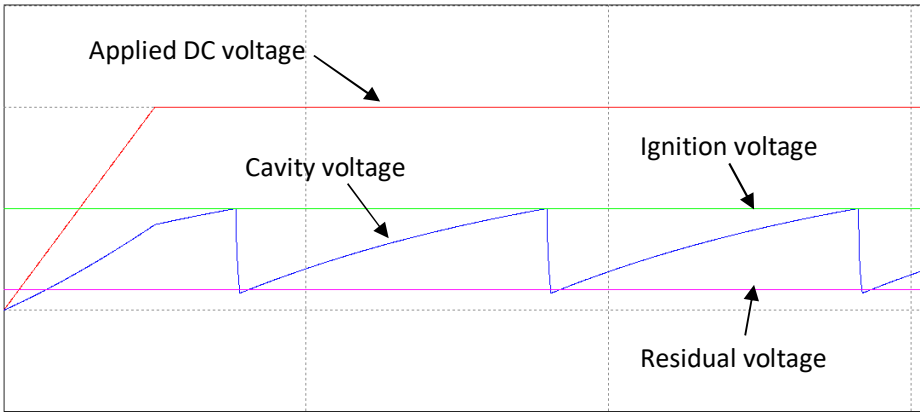

a) DC voltage process

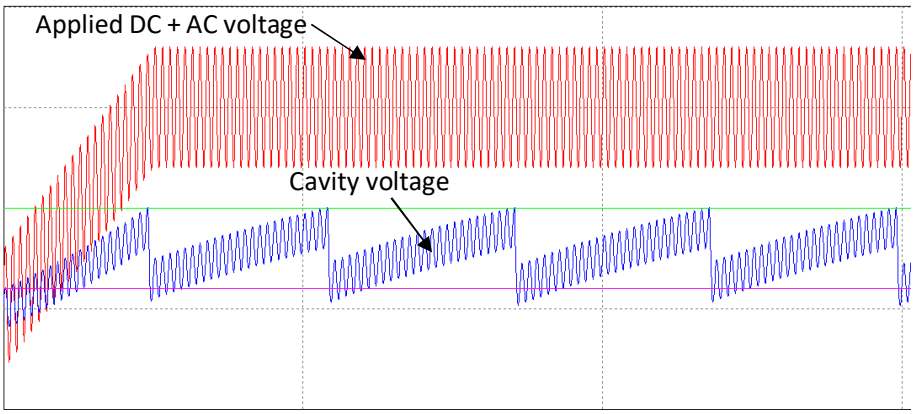

b) Combined DC and sinusoidal AC voltage

Fig. 2-8 Applied voltage (red) and cavity voltage (blue) for a discharging cavity under a) Only DC voltage, and b) Combined DC and AC voltage.

The voltage over a discharging cavity under these conditions is shown in Fig. 2-8. The resulting discharge separation time rate is lower at combined DC and AC voltage, see Fig. 2-8b, compared to pure DC voltage conditions, see Fig. 2-8a.

Under the deterministic conditions assumed by Rogers [26] and Densley [27, p. 436], it is possible to find the discharge separation time by modifying (2.16):

$$\overline{\Delta t} = -\tau \ln\left(\frac{K_{DC}V_{DC} - \left(V_{ign} - K_{AC}\hat{V}_{AC}\right)}{K_{DC}V_{DC} - V_{res}}\right) \quad (2.42)$$

As for DC voltage, the minimum and maximum discharge separation time can be found as:

$$\overline{\Delta t}_{\min} = \tau \frac{\Delta V_c - K_{AC}\hat{V}_{AC}}{K_{DC}V_{DC} - V_{paschen}} \quad (2.43)$$

$$\overline{\Delta t}_{\max} = \tau \frac{V_{paschen} - K_{AC}\hat{V}_{AC}}{K_{DC}V_{DC}} \quad (2.44)$$

The relative change in separation time, from DC to combined DC and AC voltage is found by:

$$\frac{\overline{\Delta t}^{DCAC}}{\overline{\Delta t}^{DC}} = \frac{\overline{\Delta t}_{\max}(V_{AC})}{\overline{\Delta t}_{\max}(V_{AC}=0)} = 1 - \frac{K_{AC}\hat{V}_{AC}}{V_{paschen}} = 1 - \frac{\hat{V}_{AC}}{PDIV_{AC}} \quad (2.45)$$

Based on (2.45) the discharge separation time is predicted to linearly decrease with increasing AC ripple voltage amplitude, see Fig. 2-9a. When the AC voltage approaches the AC inception voltage, the predicted separation time goes to zero, or correspondingly, the repetition rate goes to infinity. There is no expected change in discharge magnitude with AC ripple voltage amplitude, because it is assumed that the discharge always occurs at the same ignition voltage and drops to the same residual voltage.

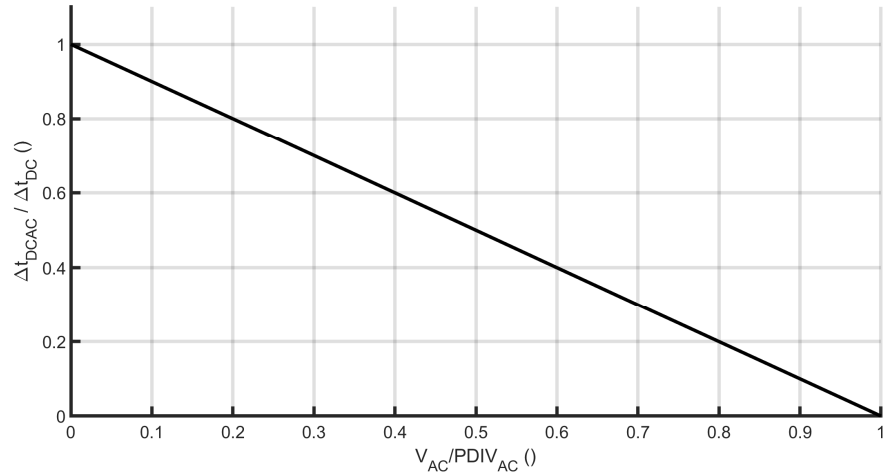

a) Relative change in discharge separation time with AC voltage ripple amplitude

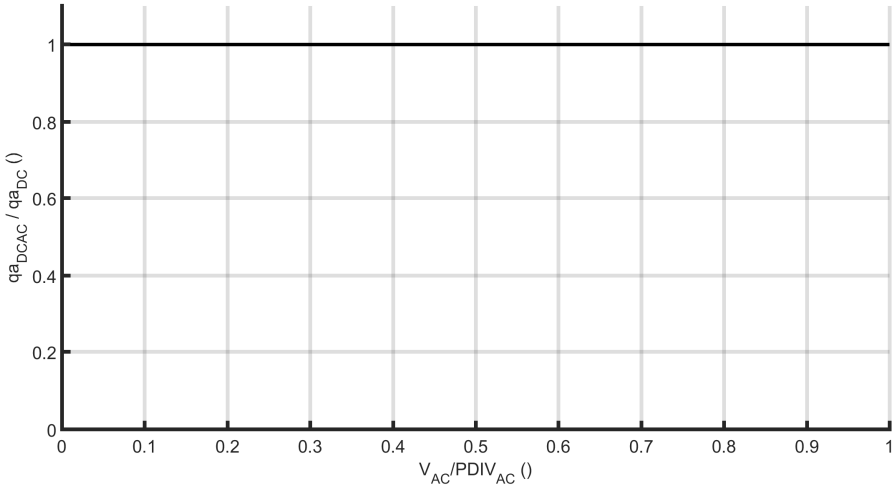

b) Relative change in discharge magnitude with AC voltage ripple amplitude

Fig. 2-9 Relative change in: a) Discharge separation time, and b) Discharge magnitude, as a function of AC ripple voltage amplitude, given as the ratio of the AC amplitude to the AC inception voltage.

2.3 Estimation of PD sequence parameters

This section presents the main properties of estimated PD sequence parameters. Estimated physical parameters provide information about the physical quantities that can be compared to their measured values. Furthermore, the simulation of the PD sequence with the estimated physical parameters can be used to compare the measured probability densities and analyse the validity of the PD sequence model.

2.3.1 Estimation methods

The PD processes in section 2.1 and 2.2 can be described in terms of physical PD sequence parameters and stochastic variables. The physical PD parameters are constant within the simulation time, and the stochastic variables take values corresponding to the probability density of each stochastic variable. Examples of physical PD parameters are the series dielectric capacitance C_b in (2.41) or the mean statistical waiting time τ_s in (2.27) while a stochastic variable would be the time lag for each discharge t_L in (2.27). The values of the physical parameters are found in several ways, including measurement, empirical relationships, and published data. The physical PD parameters can also be found using estimation methods. The estimation methods are statistical tools for a systematic extraction of the physical parameters from PD sequence data itself. In statistics, several methods exist to estimate parameters involved in a stochastic process.

2.3.2 Estimator requirements

The estimated value of the parameter is called the estimator, and the real value of the PD sequence parameter is called the estimand. An estimator is marked with a hat symbol, e.g. $\hat{\tau}_s$. For the estimator to be of value, it must satisfy some requirements [75]:

1) The value of the estimator must be within the known range of the true parameter value.
2) The estimator should approach the estimand when the number of observations n increases, i.e. it should be consistent.
3) The value of the estimator should be at the centre of the estimator distribution, i.e. it should be unbiased.
4) The estimator should have the lowest possible variance, i.e. it should have high efficiency.

Satisfying the requirements above are not a guarantee that the estimator will perform well on measured data, as the real process can deviate from the model assumptions which the estimator is based on. In addition to the requirements 1 to 4, the estimator should also be robust [76]; if the assumptions are only approximately met, the robust estimator will still have a reasonable efficiency and small bias.

A parameter extraction method should not only give an estimated value of the physical parameter but also a confidence interval [36]. This is treated in the next section.

2.3.3 Estimator confidence intervals and performance

The confidence interval for the estimator can be obtained in several ways. One of the most versatile tools is the non-parametric Bootstrap method [77], used by Heitz [36]:

1) The estimator $\hat{\tau}_s$ is calculated using any method on PD data sets $\Delta t_{pre} = \left[\Delta t_{pre,1}, \Delta t_{pre,2}, ..., \Delta t_{pre,n} \right]$ and $q_a = \left[q_{a,1}, q_{a,2}, ..., q_{a,n} \right]$, with size n.
2) A new data set with the same size as the original data set is generated by resampling the data with replacement. The result is the two vectors $\Delta t^*_{pre} = \left[\Delta t^*_{pre,1}, \Delta t^*_{pre,2}, ..., \Delta t^*_{pre,n} \right]$ and $q^*_a = \left[q^*_{a,1}, q^*_{a,2}, ..., q^*_{a,n} \right]$.
3) The estimator $\hat{\tau}^*_s$ is calculated from the data in step 2.
4) Steps 2 and 3 are repeated B times.
5) The distribution the estimator is given by the set $\hat{\tau}^*_{s,1}, \ldots, \hat{\tau}^*_{s,B}$, the 95% confidence interval are found from this set.

$B \in \langle 1000, 10000 \rangle$ to obtain a sufficiently accurate distribution of the estimator [77].

The root mean squared error (RMSE) provides a quantifiable way to evaluate the performance of an estimator, as the RMSE incorporates both its variance and bias [78]. The value can be calculated as the root of the average squared distance between the Bootstrap estimated values to the actual value:

$$RMSE_{\hat{\tau}_s} = \sqrt{\frac{1}{B} \sum_{b=1}^{B} \left(\hat{\tau}^*_{s,b} - \tau_s \right)^2} \qquad (2.46)$$

The RMSE is always non-negative; a good estimator will have an RMSE value close to zero.

3 Model of internal discharges at DC and combined DC and AC voltage

A model for the PD sequence at DC voltage conditions is developed in section 3.2. The model for combined voltage conditions is based on the DC voltage model and is described in section 3.3. The models rely on a stochastic time lag, which is defined by the start electron generation rate. The stochastic time lag produces a stochastic apparent discharge magnitude and separation time at DC voltage conditions. At combined voltage conditions an additional stochastic parameter is required to describe the PD sequence, the stochastic phase-of-occurrence. The value of the AC voltage ripple amplitude influences both the stochastic time lag and phase-of-occurrence, thus changing the expected apparent discharge magnitude and separation time. The main effect of adding a sinusoidal ripple to the DC voltage is the reduction of the effective start electron generation rate, or equivalently, an increase in the effective statistical waiting time. This increases the time lag, discharge magnitude and separation time, compared to DC voltage conditions.

The ordinary least square method and the method of moments are used to estimate physical parameters from the PD process at both DC voltage and combined voltage. The methods utilise the data from the discharge process itself to estimate the physical parameters.

3.1 Assumptions

The following assumptions apply for both the model at DC and the model at combined voltage conditions:

- A.1: All partial discharges are of the Townsend-like type.
- A.2: Equivalent resistance of the cavity surface and volume is much greater than the resistance of the dielectric in series with the cavity, i.e. $K_{DC} \approx 1$.
- A.3: There is no charge decay due to cavity surface conduction, or charge neutralisation by gas ions.
- A.4: The mean separation time is much lower than the time constant of the cavity voltage, $\Delta\bar{t} \ll \tau$.
- A.5: The start electron generation rate is constant, $\dot{N}_e = N_{el} = \frac{1}{\tau_s} = const$.
- A.6: Townsend coefficient is constant, $\alpha = const$.
- A.7: The process is stationary; there is no change of PD parameters during the discharge process.

The following assumption applies only to the model at combined voltage conditions:

- A.8: The AC voltage time period is much lower than the statistical waiting time, $T_{AC} \ll \tau_s$, or equivalently, the start electron generation rate is much lower than the AC ripple frequency, $N_{el} \ll f_{AC}$.

3.2 Internal discharges at DC voltage

This section describes a new stochastic model for the PD sequence at DC voltage for a dielectric bounded, cylindrical cavity. The individual discharge magnitude and separation times are calculated using stochastic variables. The main stochastic variable is the time lag. The mean values, probability densities and pulse correlations are obtained by the Monte Carlo method. The main physical parameters are the Townsend coefficient, the mean statistical waiting time, the capacitance in series with the cavity, and the rate of increase of the voltage over the cavity. Section 3.2.1 describes the PD sequence model and section 3.2.2 the underlying model elements and assumptions. The mean value, probability density, and correlation between the discharge magnitude and the separation time are summarised in section 3.2.3. Section 3.2.4 presents two estimation methods to extract the physical parameters from a measured PD sequence at DC voltage.

3.2.1 PD sequence model

This chapter presents an overview of the PD sequence model for internal discharges at DC voltage. The model elements and assumptions are treated in section 3.2.2.

The simulation time period for one step of the sequence is shown in Fig. 3-1. The simulation time period is divided into three steps:

1) The stochastic time lag interval: the cavity voltage is above the Paschen voltage and increases linearly at a rate of $\frac{dv_c}{dt}$; at a stochastic time lag $t_{L,i}$, the discharge is triggered by a start electron.
2) The discharge: At time instant t_i an apparent discharge magnitude $q_{a,i}$ can be measured at the test object terminals. The cavity voltage is $\Delta V_{L,i}$ above the Paschen voltage just before the discharge and $\Delta V_{R,i}$ under the Paschen voltage just after the discharge.
3) The recovery time interval: The cavity voltage reaches the Paschen voltage after a recovery time $t_{R,i}$.

n discharges are generated by repeating steps 1-3, so the PD sequence is generated using the Monte Carlo method. The time to previous discharge is calculated by summing the recovery time of the previous discharge with the time lag of the ith discharge.

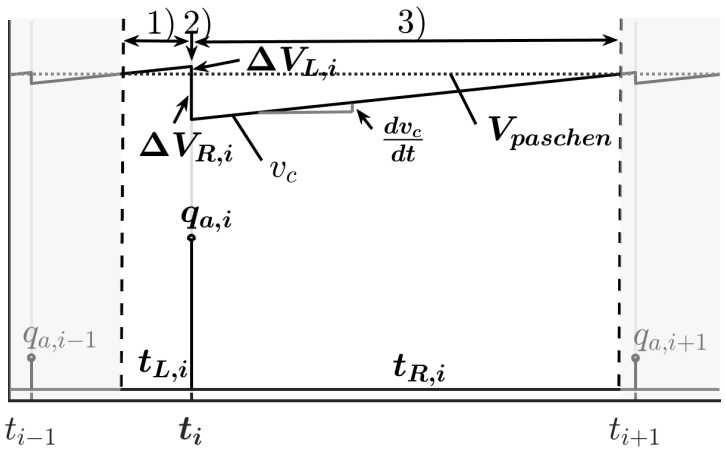

Fig. 3-1 One simulation time period of the PD sequence, for one iteration of the PD sequence model.

The inputs for the model are the PD sequence parameters αh, τ_s, and $C_b \frac{dv_c}{dt}$, as well as the applied DC voltage V_{DC} and the number of discharges n. A flow chart of the PD sequence model is provided in Appendix A. Steps 1 to 3 in Fig. 3-1 are calculated as:

1) Time lag: $t_{L,i} = -\tau_s \ln(1-R)$ where R is a random number in the interval $[0,1)$, model and assumptions as in section 3.2.2.4.
2) The apparent discharge magnitude: $q_{a,i} = \alpha h \cdot C_b \frac{dv_c}{dt} t_{L,i}$, model and assumptions as in section 3.2.2.5.
3) The recovery time: $t_{R,i} = (\alpha h - 1) t_{L,i}$, model and assumptions as in section 3.2.2.6.

The outputs of the model are the measurable quantities, the apparent discharge magnitude, and the discharge separation time, which is assembled from the set t_L, q_a and t_R.

The model can also take into account any detection limit of the apparent discharge magnitude by filtering out any discharges below a magnitude threshold $q_{a,th}$. The filtered or unfiltered output can be postprocessed to obtain mean values, probability densities, and correlations between the measurable quantities, as detailed in section 3.2.3.

3.2.1.1 Calculation of PD sequence parameters

The PD sequence parameters αh, τ_s and $C_b \frac{dv_c}{dt}$ can be found before the experiments as detailed in the following paragraph, or estimated as explained in section 3.2.4.

1) The Townsend coefficient α varies with the electric field strength, E_c, and the pressure p, in the gas. α is assumed constant as argued in section 3.2.2.5, and calculated by (2.38), with $E_c = \frac{V_{paschen}}{h}$ and p equal to atmospheric pressure. $V_{paschen}$ is found by (3.8). Multiplying the Townsend coefficient with the height of the cavity yields the PD sequence parameter αh.
2) The maximum value of the mean waiting time τ_s is given by the radiation ionisation rate, as shown by Niemeyer [33]. In practice the value will be significantly lower due to electron emission from the dielectric surface. Researchers such as Cavallini [79] and Chen [80] treat surface emission from shallow traps but do not estimate the absolute value of the density of detrappable electrons needed to calculate the start electron generation rate and the mean waiting time. Niemeyer concedes that the surface emission mechanism is not well understood, and that a quantitative analysis is difficult. The mean waiting time τ_s and the start electron generation rate are assumed constant, as argued in section 3.2.2.4. Methods to estimate τ_s are outlined in 3.2.4.
3) C_b is approximated by a cylindrical plate capacitor in series with the cavity. C_b is defined by the series dielectric permittivity, ε_b, and the geometric parameters H, the sample thickness, h, the cavity height and r_{cav}, the radius of the cavity:

$$C_b = \varepsilon_b \varepsilon_0 \frac{\pi r_{cav}^2}{H - h} \quad (3.1)$$

4) $\frac{dv_c}{dt}$ is given by (3.6), and is defined by the applied DC voltage V_{DC}, the material parameters ε_b, ε_c and σ_b, and the geometric parameters H and h:

$$\frac{dv_c}{dt} = \frac{V_{DC} - V_{paschen}}{\tau} = \left(V_{DC} - V_{paschen}\right) \frac{\sigma_b}{\left(\varepsilon_b + \frac{H - h}{h}\varepsilon_c\right)\varepsilon_0} \quad (3.2)$$

3.2.2 Model elements and assumptions

The basic elements of the PD sequence model presented in section 3.2.1 are developed in this section. The following aspects are treated:

- The discharge mechanism.
- The electric field strength and voltage over the cavity.
- The critical electrical field strength for PD occurrence.
- The stochastic time lag for PD occurrence.
- The apparent discharge magnitude.
- The recovery time.

3.2.2.1 The discharge mechanism

As mentioned in section 2.1.3, experimental evidence by Fromm [44] suggests that the Townsend-like discharge mechanism dominates during PD at DC voltage. In the model, it will be assumed that all the discharges are Townsend-like, i.e. diffuse discharges which cover most of the insulating surface area of the cavity:

Assumption A.1: All partial discharges are of the Townsend-like type.

When the discharge is Townsend-like:

1) The discharge covers the surface of the cavity: Townsend-like discharges occurring in a cylindrical cavity surrounded by dielectric are diffuse and cover most of the cavity surface area, which is confirmed by simultaneous optical and electrical detection in [64] and [81].
2) The cavity voltage drop during the discharge is proportional to the overvoltage, see section 2.1.3.

3.2.2.2 The electric field strength and voltage over the cavity

Between discharges, the electric field will be homogenous in the cavity, except at the outer radius edge marked by the perpendicular insulation wall. For flat cavities, the radius-to height ratio is high, and the edge effect is negligible. The electric field is also homogeneous just after discharges, as the space charge of the Townsend-like discharge spreads out on the cavity surface [64] .

The electric field strength, between discharges, can be found as a function of the voltage over the cavity, v_c, and the cavity height, h. The voltage v_c can be calculated using the ABC circuit in section 2.1.1, equation (2.9) .

The resistances in the circuit will behave as linear elements when:

1) The DC voltage has been applied for longer than the insulation material conductivity stabilisation time, see section 2.1.2.1.

2) The temperature in the test object is constant.
3) The variation of the electric field strength in the insulation material in series with the cavity is low.

Here, 1) and 2) are ensured by controlling laboratory testing conditions, while 3) holds if the DC voltage variation over the cavity is low, in the order of 10%. This is supported by the observations by Fromm [82]: cavity voltage variation was in the order of 1-10 V at DC voltage conditions.

The capacitances in the circuit will behave as linear elements when:

1) The permittivity and dielectric losses are insensitive to the electric field strength in the material.
2) The temperature is constant

If the materials are not ferroelectric[2], the permittivity of the insulation material should be independent of electric field strength. Insulation materials such as PE and PET are not ferroelectric and show little variation in permittivity and dielectric losses in a broad frequency range, satisfying 1), while 2) is satisfied by controlling laboratory testing conditions.

When the cavity is flat, the ABC-model with linear RC elements is identical to a Maxwell capacitor model [41]. The cavity voltage will then follow an exponentially converging curve with a time constant, τ , determined by the capacitances and resistances of the ABC circuit. In the model, it is assumed that both the bulk- and surface resistance of the cavity are much higher than the resistance of the series dielectric. This assumption is valid because there are far less discharges during PD at DC voltage to generate the conductive layers seen for PD at AC voltage. Morshuis [81] measured significant changes to surface conductivity after around 1 hour of AC discharge activity of the streamer-like type; to generate the same amount of discharges at DC the total measuring time should be 4 orders higher than at AC voltage, i.e. around 10000 hours. The total measuring time for the experiments is well below 500 hours, and the majority of the discharges are of the diffuse Townsend-like type [44].

Assumption A.2: Equivalent resistance of the cavity is much greater than the resistance of series dielectric, i.e.. $R_c \gg R_b$ and $K_{DC} \approx 1$.

The voltage over the cavity after a discharge is:

$$v_{c,i}(t') = V_{DC} - \left(V_{DC} - V_{res,i-1}\right)\exp\left(-\frac{t'}{\tau}\right) \quad (3.3)$$

[2] Examples of ferroelectric insulation materials are PVDF, Barium Titanate and Quartz. PVDF and Barium Titanate are used in low voltage wire insulation and ceramic capacitors. Quartz is used as filler in insulating epoxy resins to improve thermal conductivity.

$t' = 0$ just after a discharge, and

$$\tau = R_b \left(C_b + C_c \right) = \frac{\left(\varepsilon_b + \left(\frac{H-h}{h} \right) \varepsilon_c \right) \varepsilon_0}{\sigma_b} \quad (3.4)$$

3.2.2.2.1 The effect of charge decay in the cavity on the cavity voltage

In (3.3) it is tacitly assumed that there is no surface charge decay in the cavity after the discharge:

Assumption 3 (A.3): There is no charge decay due to cavity surface conduction, or charge neutralisation by gas ions.

This can be justified by the elimination of the known charge decay mechanisms [33], [83]:

1) Conduction from one cavity surface to the opposite surface along cavity walls.
2) Conduction through the insulation in series with the cavity.
3) Charge neutralisation by gas ions.

In the flat cavity, the electric field direction is perpendicular to the top and bottom insulating surfaces, so no lateral conduction can take place at these surfaces. The electric field can have a parallel component at the cavity walls. Still, since the electric field does not change direction during PD at DC voltage, the parallel component will result in a force acting to separate positive and negative charges left after the discharge. Thus, contrary to PDs at AC voltage, there can be no surface conduction like in 1). The charge decay mechanism in 2) is already taken into account in the model, represented by the resistance R_b. The production of ions in the cavity volume will be due to background ionisation, so the charge decay mechanism in 3) is extremely slow; the time constant can be in the order of 1000 minutes [84]. It is concluded that the mechanisms in 1) and 3) do not influence the change in cavity voltage during the PD process.

3.2.2.2.2 Linearisation of cavity voltage

The cavity voltage will fluctuate around the critical voltage if the voltage drop during discharges is small. The cavity voltage can be approximated by linearisation around the critical voltage:

$$v_{c,i}(t') \approx V_{res,i-1} + t' \cdot \left. \frac{dv_c}{dt} \right|_{v_c = V_{critical}} \quad (3.5)$$

where

$$\left. \frac{dv_c}{dt} \right|_{v_c = V_{critical}} = \frac{V_{DC} - V_{critical}}{\tau} \quad (3.6)$$

for $t' \leq \Delta t_i$. The approximation by linearisation will be accurate if the mean discharge separation time is much lower than the time constant of the cavity voltage:

$$\Delta \bar{t} \ll \tau \qquad (3.7)$$

Assumption 4 (A.4): The mean separation time is much lower than the time constant of the cavity voltage, $\Delta \bar{t} \ll \tau$.

3.2.2.3 Critical voltage

For a discharge to occur, the electric field strength must be higher than a critical value. The criterion is fulfilled when the voltage across a uniformly stressed gap reaches the Paschen breakdown voltage. The Paschen voltage law was developed for metallic electrodes, but has been shown to fit well for dielectric bounded cavities [85], suggesting that the breakdown mechanism is similar between metallic electrodes and dielectric electrodes. The Paschen law is applicable for gaps above 4 µm [86], but below this limit quantum tunnelling phenomenon reduces the breakdown voltage considerably. Ritz [87] found the following empirical relationship for the breakdown voltage in short air gaps at atmospheric pressure, which is equal to the critical voltage in the model:

$$V_{Paschen} = 6.7 \cdot h + 24.5 \cdot \sqrt{h} \quad (3.8)$$

where $V_{Paschen}$ is breakdown voltage in kV_{peak} and h is the cavity height in cm.

3.2.2.4 The stochastic time lag

The stochastic time lag is an inherent property of the electron generation processes in the cavity. The mechanisms for generating start electrons were discussed in section 2.1.2.4. The start electron generation rate is a sum of the volume and surface electron generation rates. In flat cavities the surface-to-volume ratio is high, and surface generation can be assumed to dominate. It will be shown that the electron generation rate can be assumed constant when the cavity voltage increases slowly, as characterises PD during DC voltage stress.

Calculations by Fromm [82], based on measured values, indicate that the overvoltage is in the range of a few volts. In this range, the field-dependent start electron generation rate will be constant, by the following argument:

The relative increase in electron generation rate above the Paschen voltage is given, based on (2.33) and (2.31) in section 2.1.2.4, assuming a field-dependent electron generation mechanism. The simple model proposed by Forssén [88] yields:

$$\frac{\dot{N}_e\big|_{V_c \geq V_{paschen}}}{\dot{N}_e\big|_{V_c = V_{paschen}}} = \exp\left(\left|\frac{\Delta V_L}{V_{paschen}}\right|\right) \approx 1 + \left|\frac{\Delta V_L}{V_{paschen}}\right| \quad (3.9)$$

And the Richardson-Schottky surface emission model [56] yields:

$$\frac{\dot{N}_e\big|_{V_c \geq V_{paschen}}}{\dot{N}_e\big|_{V_c = V_{paschen}}} = \exp\left(\frac{e}{kT} \sqrt{\frac{e}{4\pi\varepsilon_0} \cdot \frac{V_{paschen}}{h}} \left(\sqrt{\left(1 + \frac{\Delta V_L}{V_{paschen}} \right)} - 1 \right) \right) \quad (3.10)$$

For a flat, cylindrical void with height 100 µm, the Paschen voltage is 980 V [89]. If the temperature is 60 °C, and the overvoltage is in the range 1-10 V, then (3.9) predicts a 0.1-1.0% increase in electron generation rate, whereas (3.10) predicts a 0.2-2.1% increase in electron generation rate. Thus, for a certain temperature and DC voltage, the electron generation rate can be approximated by a constant rate N_{el}:

$$\dot{N}_e\big|_{V_c \geq V_{paschen}} = N_{el} = \frac{1}{\tau_s} = const \quad (3.11)$$

Assumption 5 (A.5): The start electron generation rate is constant, $\dot{N}_e = N_{el} = \frac{1}{\tau_s} = const$.

The probability density function of a discharge happening after a time lag t_L is calculated from (2.34)

$$pdf(t_{L,i}) = \frac{1}{\tau_s} \exp\left\{ -\frac{t_{L,i}}{\tau_s} \right\} \quad (3.12)$$

The corresponding cumulative distribution function, using (2.35) , is

$$cdf(t_{L,i}) = 1 - \exp\left\{ -\frac{t_{L,i}}{\tau_s} \right\} \quad (3.13)$$

The individual time lags are found by solving (3.13) to find $t_{L,i}$:

$$t_{L,i} = -\tau_s \ln\left(1 - cdf(t_{L,i})\right) \quad (3.14)$$

A value for $t_{L,i}$ is obtained by generating a random number R between 0 and 1 for $cdf(t_{L,i})$:

$$t_{L,i} = -\tau_s \ln\left(1 - R\right) \quad (3.15)$$

The mean time lag is equal to the mean statistical waiting time:

$$\overline{t_L} = \int_0^\infty t_{L,i} \cdot pdf(t_{L,i}) dt_{L,i} = \tau_s \quad (3.16)$$

3.2.2.5 Discharge magnitude

The discharge magnitude of Townsend-like discharge was treated in section 2.1.3. The individual apparent discharge magnitude is

$$q_{a,i} = \alpha h \cdot C_b \Delta V_{L,i} \quad (3.17)$$

The Townsend coefficient will depend on the electric field strength, as in (2.38). For a small expected overvoltage, the electric field strength is approximately constant and thus the Townsend coefficient can be assumed to be constant:

Assumption 6 (A.6): Townsend coefficient is constant, $\alpha = const$

The series dielectric capacitance, C_b, is proportional to the discharged surface area and should be constant for all individual discharges. By using the linearised cavity voltage in (3.5), the overvoltage can be written as a function of the stochastic time lag as

$$\Delta V_{L,i} = \frac{dv_c}{dt} t_{L,i} \quad (3.18)$$

Thus,

$$q_{a,i} = \alpha h \cdot C_b \frac{dv_c}{dt} t_{L,i} \quad (3.19)$$

3.2.2.6 Recovery voltage and recovery time:

Just after the i[th] discharge, the cavity voltage has dropped to a residual voltage which is $\Delta V_{R,i}$ below the Paschen voltage :

$$V_{res,i} = V_{paschen} - \Delta V_{R,i} \quad (3.20)$$

The recovery voltage can be written as a function of the recovery time as:

$$\Delta V_{R,i} = \frac{dv_c}{dt} t_{R,i} \quad (3.21)$$

The recovery voltage can be found as a function of the overvoltage; inserting (3.21) and (3.18) in (2.39) yields a relationship between the recovery time and the time lag:

$$t_{R,i} = (\alpha h - 1) t_{L,i} \quad (3.22)$$

The recovery voltage can be expressed as a function of the time lag:

$$\Delta V_{R,i} = \frac{dv_c}{dt} (\alpha h - 1) t_{L,i} \quad (3.23)$$

3.2.2.7 Stationary process

The derived equations in the previous section are valid for individual discharges, but the model must also be valid for the entire PD sequence to predict mean values, probability densities and correlation between the measurable quantities. This requirement is satisfied if the PD process is stationary, i.e. there is no temporary or permanent change in the PD sequence parameters due to the discharge process itself. The following assumption is made:

Assumption 7 (A.7): The process is stationary; there is no change of PD parameters during the discharge process.

Due to A.7 the model is not valid for the initial stage of the PD process, directly after DC voltage application. In the initial stage, the effective conductivity of the insulation in series with the cavity changes due to polarization phenomena (2.1.2.1), thus changing the resistance R_b, the cavity voltage time constant τ, and the slope of the cavity voltage $\frac{dv_c}{dt}$.

3.2.3 Discharge magnitude and separation time – mean value, probability density and correlation

The individual apparent discharge magnitude is given in section 3.2.2.5 as:

$$q_{a,i} = \alpha h C_b \frac{dv_c}{dt} t_{L,i} \quad (3.24)$$

The individual time to previous discharge is given in section 2.1.1 as:

$$\Delta t_{pre,i} = t_{R,i-1} + t_{L,i} \quad (3.25)$$

By using the relationship developed in section 3.2.2.6, eq. (3.22), the time to previous discharge can be expressed as:

$$\Delta t_{pre,i} = (\alpha h - 1) t_{L,i-1} + t_{L,i} \quad (3.26)$$

Thus, $\Delta t_{pre,i}$ and $q_{a,i}$ only depend on time lag as the stochastic parameter:

$$q_{a,i} = f_1\left(t_{L,i}\right) \quad (3.27)$$

$$\Delta t_{pre,i} = f_2\left(t_{L,i-1}, t_{L,i}\right) \quad (3.28)$$

$t_{L,i}$ and $t_{L,i-1}$ are generated randomly from an exponential distribution, as described in section 3.2.2.4:

$$t_{L,i} = -\tau_s \ln\left(1 - rand(0,1)\right) \quad (3.29)$$

By combining (3.24) with (3.26) the time to previous discharge can be expressed as a function of the physical parameters and the measurable quantities $q_{a,i}$ and $q_{a,i-1}$:

$$\Delta t_{pre,i} = \frac{1}{\alpha h C_b \frac{dv_c}{dt}}\left(\left(\alpha h - 1\right) q_{a,i-1} + q_{a,i}\right) \quad (3.30)$$

This equation describes the pulse sequence correlation between the time to previous discharge and the apparent discharge magnitude. A similar equation can be found for the time to successive discharge:

$$\Delta t_{suc,i} = \frac{1}{\alpha h C_b \frac{dv_c}{dt}}\left(\left(\alpha h - 1\right) q_{a,i} + q_{a,i+1}\right) \quad (3.31)$$

The correlation relationships in (3.30) and (3.31) are used in the estimation of the physical parameters, described in section 3.2.4.

The mean apparent discharge magnitude and separation time can be calculated by the output of the PD sequence model in section 3.2.1:

$$\overline{q}_a = \frac{1}{n}\sum_{i=1}^{n} q_{a,i} \quad (3.32)$$

$$\Delta\overline{t} = \frac{1}{n}\sum_{i=1}^{n} \Delta t_{pre,i} \quad (3.33)$$

The mean values can also be calculated analytically, see Appendix A.1 and A.3 :

$$\overline{q}_a = \alpha h C_b \frac{dv_c}{dt}\tau_s \quad (3.34)$$

$$\Delta\overline{t} = \alpha h \tau_s \quad (3.35)$$

The ratio of the mean apparent discharge magnitude and the separation time only depends on C_b and $\frac{dv_c}{dt}$:

$$\frac{\overline{q}_a}{\Delta\overline{t}} = C_b \frac{dv_c}{dt} \quad (3.36)$$

This relationship predicts that there should be a strong, positive correlation between the mean apparent discharge magnitude and the mean separation time.

The probability density of the apparent discharge magnitude can be obtained directly from the output of the PD sequence model in section 3.2.1. The probability densities are also obtained analytically in Appendix A.2 and A.4 The analytical probability density of the apparent discharge magnitude is:

$$pdf_{q_{a,i}}(q_a) = \frac{1}{\overline{q}_a}\exp\left\{-\frac{q_a}{\overline{q}_a}\right\} \quad (3.37)$$

The analytical probability density of the separation time, for $\alpha h \in \langle 1,2\rangle \cup \langle 2,\infty\rangle$:

$$pdf_{\Delta t_{pre,i}}(\Delta t) = \frac{\alpha h}{(\alpha h-2)\Delta\overline{t}}\left(\exp\left(-\frac{\alpha h}{(\alpha h-1)}\frac{\Delta t}{\Delta\overline{t}}\right)-\exp\left(-\alpha h\frac{\Delta t}{\Delta\overline{t}}\right)\right) \quad (3.38)$$

For $\alpha h = 1$:

$$pdf_{\Delta t_{pre,i}}(\Delta t) = \frac{1}{\Delta\overline{t}}\exp\left(-\frac{\Delta t}{\Delta\overline{t}}\right) \quad (3.39)$$

For $\alpha h = 2$:

$$pdf_{\Delta t_{pre,i}}(\Delta t) = \left(2\frac{1}{\Delta\overline{t}}\right)^2\exp\left(-2\frac{\Delta t}{\Delta\overline{t}}\right)\Delta t \quad (3.40)$$

3.2.4 Estimation of PD sequence parameters

The parameters used in the DC PD sequence model are αh, τ_s, and $C_b\frac{dv_c}{dt}$, see section 3.2.1. It is possible to calculate these parameters before the experiments, as performed in section 3.2.1.1. It is also possible to estimate the parameters with data from the PD experiments. Two methods are outlined which yield estimators for the DC PD sequence parameters in this thesis: the ordinary least square method (OLS) and the method of moments (MoM). The OLS method is based on work by Fromm [44] but extended for the pulse correlation equations found in section 3.2.3; the MoM method is not previously reported in the literature.

3.2.4.1 Ordinary least squares estimation method

The estimates of the mean time lag and the mean recovery time can be found using an OLS regression on the data sets $\left(q_{a,i},\Delta\overline{t}_{pre,i}\right)$ and $\left(q_{a,i},\Delta\overline{t}_{suc,i}\right)$. The model equations developed in section 3.2.3 can be used to describe the functional dependence of $\Delta\overline{t}_{pre,i}$ and $\Delta\overline{t}_{suc,i}$ on $q_{a,i}$, see Appendix C.1 :

$$\Delta\bar{t}_{pre,i}\left(q_{a,i}\right)=\bar{t}_R+\frac{q_{a,i}}{\bar{q}_a}\bar{t}_L \quad (3.41)$$

$$\Delta\bar{t}_{suc,i}\left(q_{a,i}\right)=\bar{t}_L+\frac{q_{a,i}}{\bar{q}_a}\bar{t}_R \quad (3.42)$$

The OLS method to obtain the estimators $\hat{\alpha}h$, $\hat{\tau}_s$, $\widehat{C_b\frac{dv_c}{dt}}$ is detailed in Appendix C.1 and summarised in Table 3-1. For the DC PD model in this thesis, it is not possible to find $\hat{C}_b$ and $\widehat{\frac{dv_c}{dt}}$ directly. However, it is possible to obtain $\widehat{\frac{dv_c}{dt}}$ if $\hat{C}_b$ is assumed to be the same value as calculated in section 3.2.1.1. The confidence intervals of $\hat{\bar{t}}_L, \hat{\bar{t}}_R$, $\hat{\alpha}$ and $\widehat{C_b\frac{dv_c}{dt}}$ are calculated using the non-parametric bootstrap method detailed in section 2.3.3.

Table 3-1 Estimated values obtained from the ordinary least squares method for the DC PD process

Estimator	Expression
$\hat{\tau}_s, \hat{\bar{t}}_L$	An estimator of the mean statistical waiting, or mean time lag, can be found as: $$\hat{\tau}_s = \hat{\bar{t}}_L = \Delta\bar{t}_{suc,i}\left(q_{a,i} \to 0\right) \quad (3.43)$$ which is equivalent to the offset value obtained by OLS regression on the dataset $\left(q_{a,i}, \Delta\bar{t}_{suc,i}\right)$. At DC voltage conditions, the mean time lag should be close to the mean statistical waiting time, provided that the discharge magnitude detection limit is low, i.e. $\hat{\tau}_s = \hat{\bar{t}}_L$.
$\hat{\bar{t}}_R$	An estimator of the mean recovery time can be found as: $$\hat{\bar{t}}_R = \Delta\bar{t}_{pre,i}\left(q_{a,i} \to 0\right) \quad (3.44)$$ which is equivalent to the offset value obtained by OLS regression on the data set $\left(q_{a,i}, \Delta\bar{t}_{pre,i}\right)$.
$\hat{\alpha}h$	The estimator $\hat{\alpha}$ is expressed in terms of the estimators $\hat{\bar{t}}_L$ and $\hat{\bar{t}}_R$ as: $$\hat{\alpha}h = \frac{\hat{\bar{t}}_R}{\hat{\bar{t}}_L} + 1 \quad (3.45)$$
$\widehat{C_b \frac{dv_c}{dt}}$	$$\widehat{C_b \frac{dv_c}{dt}} = \frac{\overline{q_a}}{\overline{\Delta t}} \quad (3.46)$$

3.2.4.2 Method of moments

Due to the explicit formulation of the pulse sequence correlation in (3.30), estimators can also be found using the method of moments (MoM). The moments of a data set are defined as the expected value of powers of the random variable under consideration. An example of the first and second moments of the separation time is:

$$\overline{\Delta t} = E\left[\Delta t_{pre}\right] = \frac{1}{n}\sum_{i=1}^{n}\Delta t_{pre,i} \qquad (3.47)$$

$$\overline{\Delta t^2} = E^2\left[\Delta t_{pre}\right] = \frac{1}{n}\sum_{i=1}^{n}\left(\Delta t_{pre,i}\right)^2 \qquad (3.48)$$

The MoM method to obtain the estimators $\hat{\alpha}h$, $\hat{\tau}_s$, $\widehat{C_b\frac{dv_c}{dt}}$ is detailed in Appendix C.2 and summarised in Table 3-2. Definitions of the moments are given in Appendix C.4 . The method of moments gives two solutions for $\hat{\alpha}h$: one solution is in the interval $\hat{\alpha}_1 h \in \left[1,2\right\rangle$ and one in the interval $\hat{\alpha}_2 h \in \left[2,\infty\right\rangle$; the two $\hat{\alpha}h$ values give two corresponding $\hat{\tau}_s$ values, but $\widehat{C_b\frac{dv_c}{dt}}$ will only have one value. Although there are two mathematically correct answers, the physically plausible value can be assessed under the circumstances of each experiment. The confidence intervals of $\hat{\alpha}h$, $\hat{\tau}_s$ and $\widehat{C_b\frac{dv_c}{dt}}$ are calculated using the non-parametric bootstrap method detailed in 2.3.3.

Table 3-2 Estimated values obtained from method of moments for the DC PD process

Estimator	Expression (function of the measured moments)
$\hat{\alpha}h$	Solve $a\left(\hat{\alpha}h\right)^2+b\hat{\alpha}h+c=0$, where $a=\overline{q_{a,pre}^2}-\left(\overline{q_a}\right)^2\frac{\overline{\Delta t^2}}{\left(\overline{\Delta t}\right)^2}$ (3.49) $b=2\left(\overline{q_a\cdot q_{a,pre}}-\overline{q_{a,pre}^2}\right)$ (3.50) $c=\overline{q_{a,pre}^2}-2\overline{q_a\cdot q_{a,pre}}+\overline{q_a^2}$ (3.51)
$\hat{\tau}_s,\hat{\bar{t}}_L$	The estimated mean time lag can be expressed as a function of the estimated Townsend coefficient product and the mean separation time: $\hat{\tau}_s=\frac{\overline{\Delta t}}{\hat{\alpha}h}$ (3.52) At DC voltage conditions, the mean time lag should be close to the mean statistical waiting time, provided that the discharge magnitude detection limit is low, i.e.. $\hat{\tau}_s=\hat{\bar{t}}_L$.
$\hat{\bar{t}}_R$	The estimated mean recovery time can be expressed as a function of the estimated mean time lag, or the estimated Townsend coefficient product and the mean separation time: $\hat{\bar{t}}_R=\overline{\Delta t}-\hat{\bar{t}}_L=\overline{\Delta t}\left(1-\frac{1}{\hat{\alpha}h}\right)$ (3.53)
$\widehat{C_b\frac{dv_c}{dt}}$	$\widehat{C_b\frac{dv_c}{dt}}=\frac{\overline{q_a}}{\overline{\Delta t}}$ (3.54)

3.3 Internal discharges at combined DC and sinusoidal AC voltage

This section describes a new stochastic model for the PD sequence at combined DC and AC voltage for a dielectric bounded, cylindrical cavity. The individual discharge magnitude, separation time, and phase-of-occurrence are calculated using stochastic variables. The stochastic variables are the time lag and the phase-of-occurrence. The mean values, probability densities and pulse correlations are obtained by the Monte Carlo method. The main physical parameters are the Townsend coefficient, the mean statistical waiting time, the capacitance in series with the cavity, and the rate of increase of the voltage over the cavity.

The main effect of adding a sinusoidal ripple to the DC voltage is the reduction of the effective start electron generation rate, or equivalently, an increase in the effective statistical waiting time. This increases the time lag, the discharge magnitude, and the separation time, compared to DC voltage conditions. The reduction in the effective start electron generation rate is described mathematically using the concept of duty cycle, defined as the fraction of one AC voltage time period in which the cavity voltage is above the critical voltage.

Section 3.3.1 describes the PD sequence model, and section 3.3.2 describes the underlying model elements and assumptions. The mean value, probability density and correlation between the discharge magnitude and separation time are summarised in section 3.3.3. Section 3.3.4 presents an estimation method to extract the physical parameters from a measured PD sequence at combined DC and AC voltage.

3.3.1 PD sequence model

When an AC voltage ripple is added to the DC voltage, the AC voltage and phase-of-occurrence of each discharge can be recorded. All the data representations available for both AC and DC discharge processes can be used. The quantities from the partial discharge process at combined DC and AC voltage, Fig. 3-2, are:

1) The time-of-occurrence, t_i, or the time to previous discharge, Δt_i
2) The apparent discharge magnitude, $q_{a,i}$
3) The discharge phase-of-occurrence, θ_i, the phase position of the AC voltage at the time of the discharge.

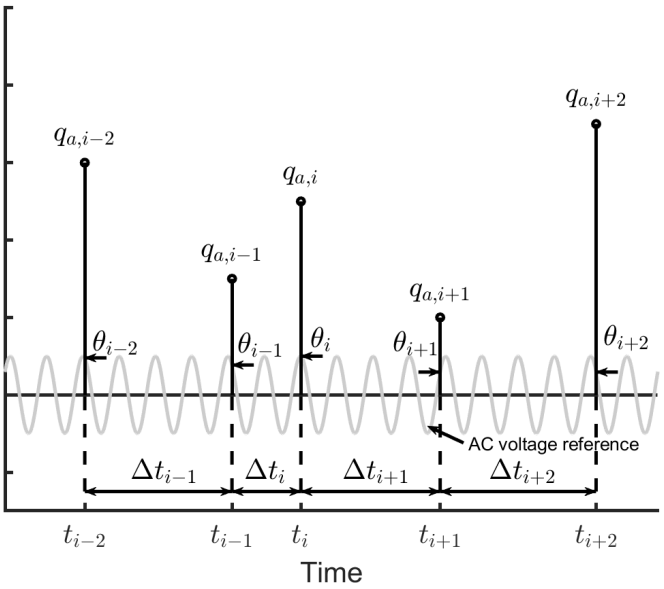

Fig. 3-2 Discharge pulse sequence at combined DC and AC voltage. Measured parameters: time-of-occurrence t_i, discharge magnitude $q_{a,i}$, and phase-of-occurrence θ_i.

In section 3.2.1, the quantities from the partial discharge process at DC voltage were described as a function of the time lag and the recovery time. For combined voltage conditions, the definition of time lag and recovery time must be amended. The time lag and recovery time for combined voltage are related to the envelope of the cavity voltage, denoted as $\widehat{v_c}$ in Fig. 3-3. The definitions are:

- The time lag is the time between the instant the *envelope* of the cavity voltage exceeds the critical voltage and the instant the discharge occurs.
- The recovery time is the time between the instant the discharge occurs and the instant when the *envelope* of the cavity voltage exceeds the critical voltage.

When the time lag and recovery time are mathematically well defined they are comparable under both DC and combined voltage conditions. The definitions of overvoltage and recovery voltage are the same as at DC voltage conditions.

The simulation time period for one step of the sequence is shown in Fig. 3-3. In the same manner as the DC PD sequence model, the simulation time period is divided into three steps:

1) The stochastic time lag interval
2) The discharge
3) The recovery time interval

n discharges are generated by repeating steps 1-3. The main differences from DC PD sequence are: period 1) begins when the envelope of the cavity voltage reaches $V_{paschen}$, after the discharge in 2) the period 3) ends when the cavity voltage reaches $V_{paschen}$ again. The calculation steps are repeated n times in a Monte Carlo simulation, see flow chart of model in Appendix B.

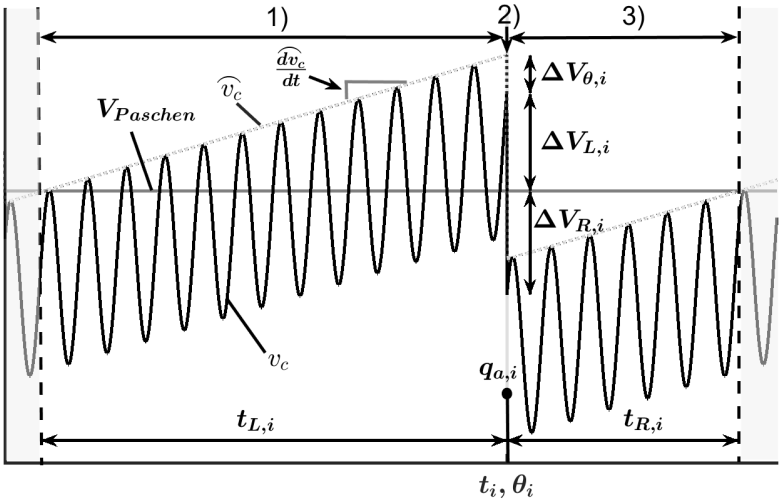

Fig. 3-3 The simulation time period of the PD sequence at combined voltage with voltage over the cavity in the insulation.

The inputs for the model are the physical parameters αh, τ_s, C_b, $\widehat{\frac{dv_c}{dt}}$, as well as the applied DC voltage V_{DC}, the AC cavity voltage amplitude $K_{AC}\hat{V}_{AC}$ and the number of discharges n. The steps 1 to 3 in Fig. 3-3 are calculated as the following:

1) Time lag: $t_{L,i} = D^{-1}\left(-\tau_s \ln\left(1-R\right)\right)$, where R is a random number in the interval $[0,1)$, see model and assumptions as in section 3.3.2.3 .

2) The phase-of-occurrence: $\theta_i = \mathrm{P}\cdot\cos^{-1}\left(1-\frac{\widehat{\frac{dv_c}{dt}}}{K_{AC}\hat{V}_{AC}}t_{L,i}\right)$, where P is a random number in the interval $(-1,1)$, see model and assumptions as in section 3.3.2.4. The apparent discharge magnitude is a function of the time lag and the phase-of-

occurrence: $q_{a,i} = \alpha h \cdot C_b \left(\widehat{\frac{dv_c}{dt}} t_{L,i} - K_{AC} \hat{V}_{AC} \left(1 - \cos\left(\theta_i\right)\right) \right)$, see model and assumptions in section 3.3.2.5.

3) The recovery time: $t_{R,i} = \left(\alpha h - 1\right) t_{L,i} - \alpha h \frac{K_{AC} \hat{V}_{AC}}{\widehat{\frac{dv_c}{dt}}} \left(1 - \cos\theta_i\right)$, model and assumptions in section 3.3.2.6.

The outputs of the model are the measurable quantities Δt_{pre}, q_a and θ. The model implements a detection limit of the apparent discharge magnitude by filtering out any discharges below a certain threshold $q_{a,th}$. The filtered or unfiltered output can be postprocessed to obtain mean values, probability densities, and correlation between the measurable quantities, as detailed in section 3.3.3.

3.3.1.1 Calculation of PD sequence parameters

The PD sequence parameters αh, τ_s and C_b can be found before the experiments as detailed in the DC sequence model section 3.2.1.1, or estimated as explained in section 3.3.4. The value of $\widehat{\frac{dv_c}{dt}}$ at combined voltage differs slightly from its DC counterpart, and is given by (3.61). It is defined by the applied DC voltage V_{DC}, the AC voltage amplitude $\hat{V}_{AC}$, the material parameters ε_b, ε_c and σ_b, and the geometrical parameters H and h:

$$\widehat{\frac{dv_c}{dt}} = \left(V_{DC} + \frac{\hat{V}_{AC}}{\left(\varepsilon_b + \frac{H-h}{h}\varepsilon_c\right)} - V_{paschen} \right) \frac{\sigma_b}{\left(\varepsilon_b + \frac{H-h}{h}\varepsilon_c\right)\varepsilon_0} \quad (3.55)$$

It is assumed that the value of the capacitive distribution factor is known, and can be calculated as

$$K_{AC} = \left(1 + \frac{H-h}{h}\frac{\varepsilon_c}{\varepsilon_b}\right)^{-1} \quad (3.56)$$

3.3.2 Model elements and assumptions

The basic elements of the PD sequence model presented in section 3.3.1 are developed in this section. The following aspects are treated:

- The discharge mechanism.

- The electric field strength and voltage over the cavity.
- The stochastic time lag at PD occurrence.
- The stochastic phase-of-occurrence at PD occurrence.
- The apparent discharge magnitude.
- The recovery time.

3.3.2.1 The discharge mechanism

As at DC voltage conditions it will be assumed that the Townsend-like discharge mechanism dominates, following assumption A.1.

3.3.2.2 The electric field strength and voltage over the cavity

The electric field conditions in the cavity at combined voltage excitation can be described using the same ABC-circuit as for DC voltage and the same assumptions, see section 3.2.2.2. With assumptions A.2 and A.3, the ABC circuit branch in Fig. 3-4 is the result.

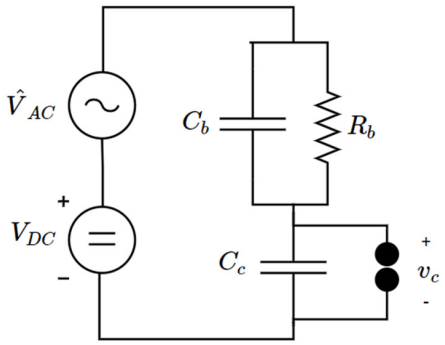

Fig. 3-4 Voltage divider for combined voltage conditions.

The DC offset voltage over the cavity, v_c^{DC}, will follow an exponentially converging curve with a time constant, τ, determined by the capacitances and resistances of the ABC circuit. The AC cavity voltage, v_c^{AC}, is capacitively distributed over the series dielectric and cavity, if the AC frequency is above 50 Hz. The cavity voltage is a superposition of the DC voltage offset and the AC voltage:

$$v_c(t) = v_c^{DC}(t) + v_c^{AC}(t) \quad (3.57)$$

The voltage over the cavity is shown in Fig. 3-5. When no discharges occur in the cavity, the cavity voltage is:

$$v_c(t) = V_{DC} \cdot \left(1 - \exp\left(-\frac{t}{\tau}\right)\right) + K_{AC} \cdot \hat{V}_{AC} \cdot \cos(\omega t) \quad (3.58)$$

where K_{AC} is the capacitive voltage distribution factor and $\omega = 2\pi f_{AC}$. When discharges occur in the cavity, the cavity voltage is:

$$v_{c,i}(t') = V_{DC} - \left(V_{DC} + K_{AC}\hat{V}_{AC} - V_{res,i-1} - \Delta V_{\theta,i-1}\right)\exp\left(-\frac{t'}{\tau}\right) + K_{AC}\hat{V}_{AC}\cos\left(\omega t' + \theta_{i-1}\right) \quad (3.59)$$

Eq. (3.59) is derived in Appendix B.1 , $t' = 0$ just after the previous discharge. θ_{i-1} is the phase-of-occurrence, $V_{res,i-1}$ is the residual voltage, and $\Delta V_{\theta,i-1}$ is the difference between the ignition voltage and the envelope of the cavity voltage, see Fig. 3-3. The envelope of an oscillating signal is a smooth curve outlining its extremes.

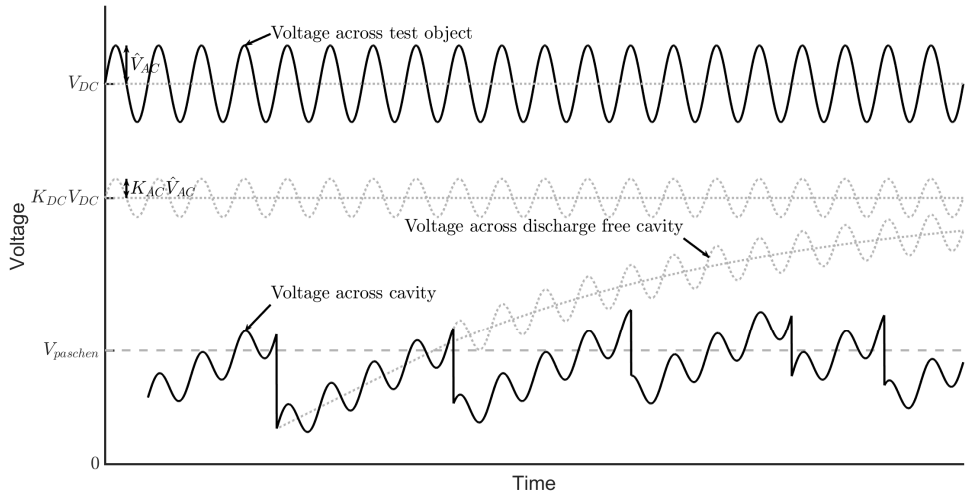

Fig. 3-5 Combined DC and AC voltage across test object and across cavity with discharges. The period time of the AC voltage is exaggerated to display the AC waveform clearly.

The cavity voltage will fluctuate around the critical voltage if the voltage drop during discharges is small. The cavity voltage DC offset can be approximated by linearisation around the Paschen voltage:

$$v_{c,i}^{DC}(t') \approx V_{res,i-1} + \Delta V_{\theta,i-1} + t' \cdot \left.\frac{\widehat{dv_c}}{dt}\right|_{\widehat{v_c} = V_{paschen}} \quad (3.60)$$

where

$$\left.\frac{\widehat{dv_c}}{dt}\right|_{\widehat{v_c}=V_{paschen}} = \frac{V_{DC} + K_{AC}\hat{V}_{AC} - V_{Paschen}}{\tau} \quad (3.61)$$

for $0 \le t' \le \Delta t_{pre,i}$. The phase shift θ_{i-1} can be ignored because the resulting time shift is extremely small compared to the separation time. the cavity voltage is then:

$$v_{c,i}(t') = \underbrace{V_{res,i-1} + \Delta V_{\theta,i-1} + \left(V_{DC} + K_{AC}\hat{V}_{AC} - V_{paschen}\right)\frac{t'}{\tau}}_{v_c^{DC}} + \underbrace{K_{AC}\hat{V}_{AC}\cos(\omega t')}_{v_c^{AC}} \quad (3.62)$$

The approximation by linearisation will be accurate if the mean discharge separation time is much lower than the time constant of the cavity voltage, as in assumption A.4.

If the conductivity of the cavity surface and volume is included, the cavity voltage slope can be expressed as:

$$\left.\frac{\widehat{dv_c}}{dt}\right|_{\widehat{v_c}=V_{paschen}} = \frac{K_{DC}V_{DC} + K_{AC}\hat{V}_{AC} - V_{Paschen}}{\tau} \quad (3.63)$$

3.3.2.3 The stochastic time lag

At DC voltage conditions, the electron generation rate was assumed constant when the increase in cavity voltage is very slow. It will be shown that applying an AC ripple to the DC voltage will lead to a duty cycle effect which effectively decreases the electron generation rate and increases the time lag. This has not been previously described in the literature.

Effective start electron generation rate at combined voltage conditions – introduction of the duty cycle concept

At DC voltage conditions, there will be a mean statistical waiting time, τ_s, which is the average time to produce a discharge when the cavity voltage is above the Paschen voltage, see section 3.2.2.4. At DC conditions the cavity voltage increases monotonically, while at combined DC and AC conditions the cavity voltage will increase while oscillating, i.e. a sinusoidal waveform with an increasing DC offset. The cavity voltage will be above the Paschen voltage for just a fraction of each AC voltage time period, thus decreasing the probability for a randomly produced start electron to result in a discharge within an AC voltage time period. In Fig. 3-6 the time lag at DC and combined voltage conditions is compared. The accumulated time when the cavity voltage is above the Paschen voltage is the same, i.e. $\sum_{i=1}^{6} t_i = t_L^{DC}$, which in this case leads to a time lag at the combined voltage condition that is almost 3 times larger.

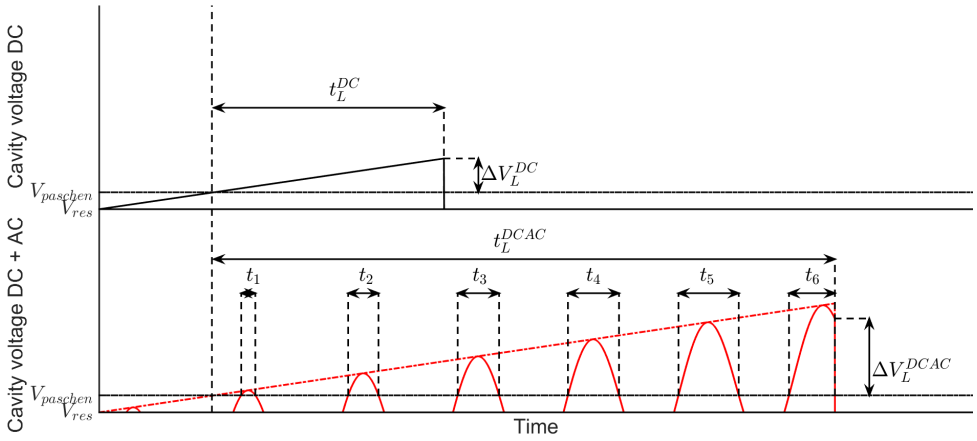

Fig. 3-6 The time lag at DC and combined voltage conditions; the AC ripple voltage decreases the time the cavity voltage is above the Paschen voltage, and thus increases the stochastic time lag.

This behaviour can be described using the concept of duty cycle. A duty cycle is the fraction of one period in which a signal or system is active. In this thesis "duty cycle" is defined as the fraction of one AC voltage time period in which the cavity voltage is above the critical voltage. The duty cycle, d , will be less than or equal to 1, and depends on the amplitude of the AC ripple voltage and the time lag. For a sinusoidal AC ripple voltage, the duty cycle can be calculated as (Appendix B.3):

$$d = \frac{\Delta\hat{\theta}}{\pi} = \frac{1}{\pi}\cos^{-1}\left(1 - \frac{\Delta\hat{V}_L}{K_{AC}\hat{V}_{AC}}\right) \quad (3.64)$$

The relationship in (3.64) is valid under the following assumption:

A.8: The AC voltage time period is much lower than the statistical waiting time, $\tau_{AC} \ll \tau_s$, or equivalently $N_{el} \ll f_{AC}$.

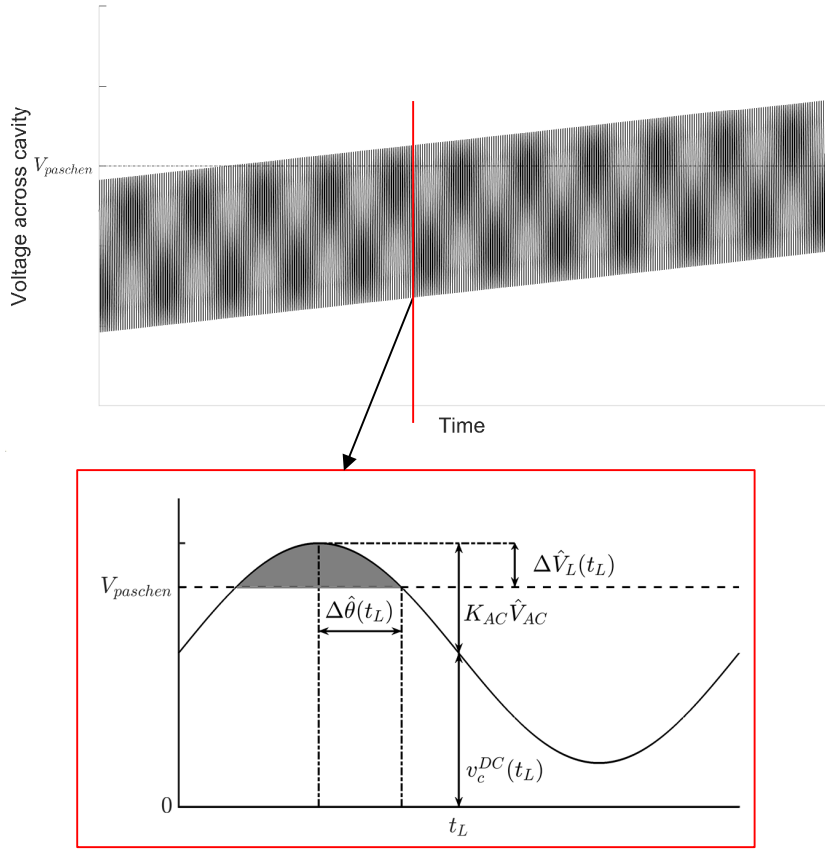

Fig. 3-7 Calculation of duty cycle. The offset voltage is assumed to be constant within one cycle of the AC voltage. A discharge is only possible when the cavity voltage is above the Paschen voltage, marked by the grey area.

$\Delta\hat{\theta}$ is the maximum possible phase-of-occurrence, measured from the peak of the cavity voltage, for a time lag t_L. $\Delta\hat{V}_L = \widehat{\frac{dv_c}{dt}} t_L$ is the maximum overvoltage at t_L, and $K_{AC}\hat{V}_{AC}$ is the peak AC cavity voltage amplitude, see Fig. 3-7 . The duty cycle effect introduced by the AC ripple voltage will reduce the efficient start electron generation rate, compared to DC voltage conditions. The start electron generation rate at combined voltage conditions can be approximated by a constant electron generation rate N_{el} times the duty cycle:

$$\dot{N}_e\Big|_{V_c \geq V_{paschen}} = N_{el} \cdot d \quad (3.65)$$

$N_{el} = const$ by assumption A.5, and (3.65) is valid when:

$$\tau_{AC} \ll \tau_s \quad (3.66)$$

where τ_{AC} is the AC voltage period time.

Assumption A.8: The AC voltage time period is much lower than the statistical waiting time, $T_{AC} \ll \tau_s$, or equivalently $N_{el} \ll f_{AC}$.

The effective electron generation rate and the duty cycle will be zero when the time lag is zero. The effective electron generation rate increases with longer time lag. The effective electron generation rate will reach N_{el} when

$$t_L^{d=1} = \frac{2K_{AC}\hat{V}_{AC}}{\widehat{\frac{dv_c}{dt}}} \quad (3.67)$$

After $t_L = t_L^{d=1}$ the combined DC and AC cavity voltage is always above the Paschen voltage. This behaviour can be contrasted with the situation for DC voltage conditions, where the electron generation rate will be zero when the cavity voltage is under the Paschen voltage and will be N_{el} the instant the cavity voltage is equal to the Paschen voltage. The application of an AC ripple will result in a much longer time transition to the full start electron generation rate N_{el}.

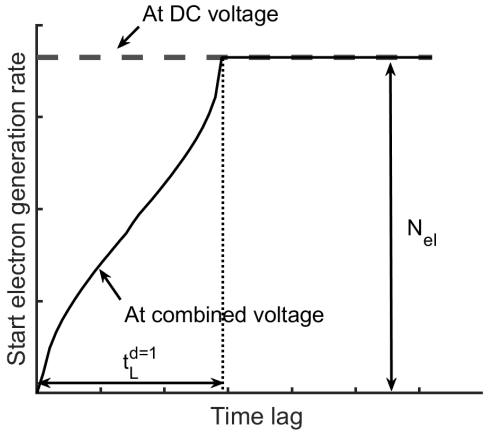

Fig. 3-8 The AC ripple effect on average start electron generation rate, according to eq. (3.65).

Distribution of the time lag at combined voltage conditions

The probability density function of a discharge happening after a time lag $t_{L,i} \geq 0$ is calculated in Appendix B.4 :

$$pdf_{t_{L,i}}(t_L) = \frac{1}{\tau_s} d \cdot \exp\left(-\frac{1}{\tau_s} D\right) \quad (3.68)$$

where

$$d = \frac{1}{\pi}\cos^{-1}\left(1 - Kt_L\right) \quad (3.69)$$

and

$$D = -\frac{1}{K\pi}\left(\left(1-Kt_L\right)\cos^{-1}\left(1-Kt_L\right)-\sqrt{1-\left(1-Kt_L\right)^2}\right) \quad (3.70)$$

with

$$K = \frac{\widehat{\frac{dv_c}{dt}}}{K_{AC}\hat{V}_{AC}} \quad (3.71)$$

The cumulative probability is:

$$cdf_{t_{L,i}}\left(t_L\right) = 1-\exp\left(-\frac{1}{\tau_s}D\right) \quad (3.72)$$

The individual time lag can be found by generating a random number R between 0 and 1, set $cdf_{t_{L,i}}\left(t_L\right) = R$, and solving (3.72) numerically.

$$t_{L,i} = D^{-1}\left(-\tau_s \ln\left(1-R\right)\right) \quad (3.73)$$

3.3.2.3.1 Mean time lag

The mean time lag at combined voltage conditions can be calculated by numerically solving the integral, see Appendix B.5 :

$$\overline{t_L} = \int_0^\infty \exp\left(-\frac{1}{\tau_s}D\left(t_L\right)\right)dt_L \quad (3.74)$$

The numerical integration can be represented by the function F_1 which depends on the PD sequence parameters $\widehat{\frac{dv_c}{dt}}$, $K_{AC}\hat{V}_{AC}$ and τ_s:

$$\overline{t_L} = F_1\left(\widehat{\frac{dv_c}{dt}}, K_{AC}\hat{V}_{AC}, \tau_s\right) \quad (3.75)$$

In terms of physical parameters, the mean time lag will be a function of:

$$\overline{t_L} = F_1\left(V_{DC}, \hat{V}_{AC}, V_{paschen}\left(h,p\right), \sigma_b, \sigma_c, \varepsilon_b, \varepsilon_c, H, h, \tau_s\right)$$

Under stationary conditions all parameters except the control variable $\hat{V}_{AC}$ are constant. So,

$$\overline{t_L} = F_1\left(\hat{V}_{AC}\right)$$

In conclusion, the time lag at combined voltage conditions should depend on AC ripple voltage amplitude. The time lag at combined voltage conditions relative to the time lag at DC conditions can be calculated by dividing (3.74) by τ_s.

$$\frac{\overline{t}_L^{DCAC}}{\overline{t}_L^{DC}} = \frac{1}{\tau_s}\int_0^{\infty} \exp\left(-\frac{1}{\tau_s} D\left(t_L\right)\right) dt_L \quad (3.76)$$

$\frac{\overline{t}_L^{DCAC}}{\overline{t}_L^{DC}} \geq 1$ and $\frac{\overline{t}_L^{DCAC}}{\overline{t}_L^{DC}}$ will be a function of the dimensionless parameters $\frac{K_{AC}\hat{V}_{AC}}{V_{paschen}}$, $\frac{K_{DC}V_{DC}}{V_{paschen}}$ and $\frac{\tau_s}{\tau}$. The main interest of this thesis is how the AC voltage ripple influences the discharge process. If (3.76) is solved for appropriate choice of dimensionless variables, then it is predicted that increasing the AC ripple amplitude, $\hat{V}_{AC}$, will increase the mean time lag, independent of AC ripple frequency f_{AC}. The increase in time lag is also reflected in the distribution of the time lag, a small AC ripple leads to a wider and flatter distribution, see Fig. 3-9. If the mean time lag increases, the discharge separation time and apparent charge are expected to increase.

It can also be noted that if $\frac{K_{DC}V_{DC}}{V_{paschen}}$ or $\frac{\tau_s}{\tau}$ increases, then $\frac{\overline{t}_L^{DCAC}}{\overline{t}_L^{DC}}$ decreases.

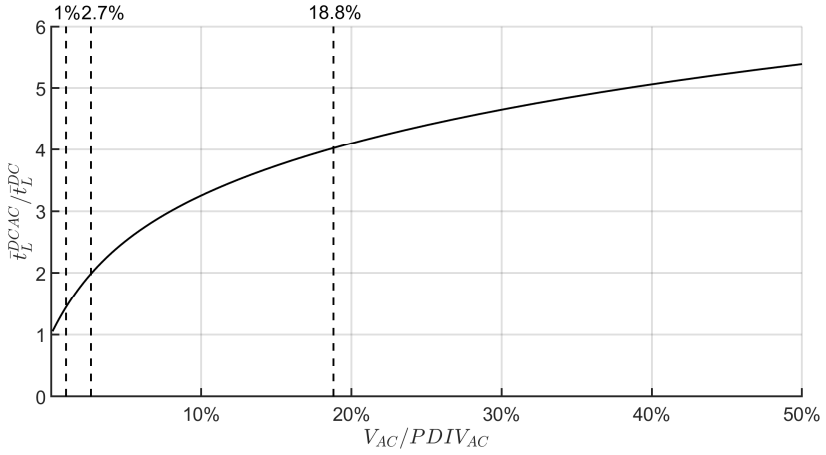

a) Change in time lag with AC ripple amplitude

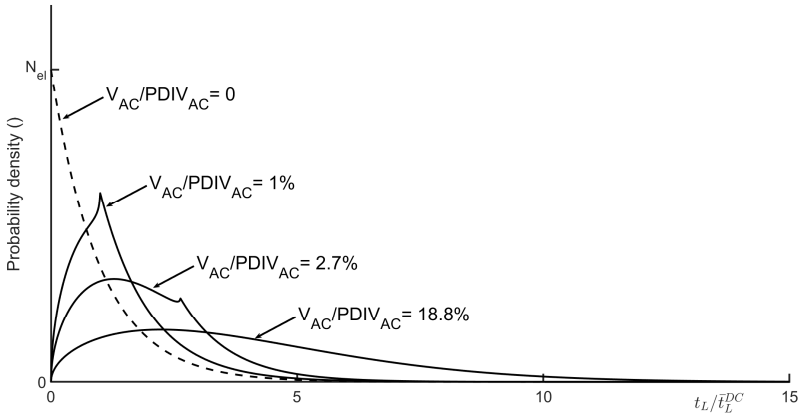

b) Change in time lag distribution with AC ripple amplitude. PDF shown for

$$\frac{V_{AC}}{PDIV_{AC}} = \frac{K_{AC}\hat{V}_{AC}}{V_{paschen}} = 1\%, 2.7\%, 18.8\%$$

Fig. 3-9 Calculated relative mean time lag (a)) and time lag distribution (b)) for $\frac{\tau_s}{\tau} = 10^{-2}$,

$$\frac{K_{DC}V_{DC}}{V_{paschen}} = 3 \ .$$

3.3.2.4 The stochastic phase-of-occurrence

Since the timescale of the AC period time is much lower than the timescale of mean time lag (A.8), the probability of a discharge within a certain AC period can be regarded as constant. The time lag appears with the probability density discussed in the previous section, and the phase-of-occurrence θ_i will then be a random value in the interval $\left[-\Delta\hat{\theta}_i, \Delta\hat{\theta}_i\right]$; the maximum phase-of-occurrence, $\Delta\hat{\theta}_i$, is defined by each $t_{L,i}$ as:

$$\Delta\hat{\theta}_i = \cos^{-1}\left(1 - \frac{\widehat{\frac{dv_c}{dt}}}{K_{AC}\hat{V}_{AC}} t_{L,i}\right) \quad (3.77)$$

Thus, the phase-of-occurrence is:

$$\theta_i = \mathrm{P} \cdot \Delta\hat{\theta}_i \quad (3.78)$$

where P is a random number in the interval $(-1,1)$. The phase-of-occurrence is a stochastic parameter, depending on the stochastic time lag. The distribution and the phase-of-occurrence can be generated by the Monte Carlo method. The distribution will be symmetric around the peak of the AC voltage. In Fig. 3-10, increasing the AC voltage amplitude and holding all other parameters constant will lead to a higher and more narrow distribution of the discharge phase-of-occurrence.

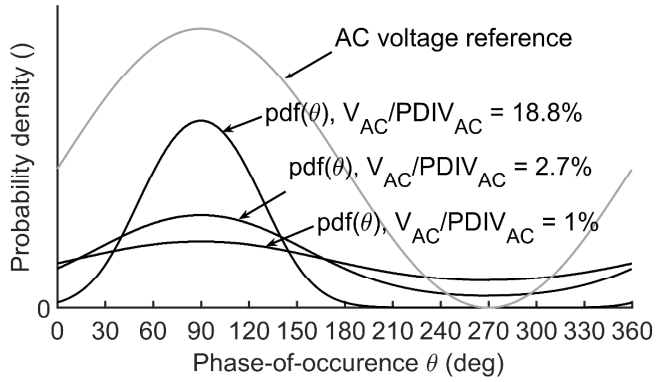

Fig. 3-10 A Calculated discharge phase-of-occurrence distribution for three different AC voltage ripple amplitudes in terms of percentage of the PDIV at AC voltage. $\frac{\tau_s}{\tau} = 10^{-2}$ **and** $\frac{K_{DC}V_{DC}}{V_{paschen}} = 3$.

It is possible to approximate $\overline{\cos\theta}$, which is needed to calculate the mean discharge separation time and magnitude. The mean of the cosine to the phase-of-occurrence is found when the time lag is at its mean value $\overline{t_L}$ given by (3.74):

$$\overline{\cos\theta} = F_2\left(\widehat{\frac{dv_c}{dt}}, K_{AC}\hat{V}_{AC}, \tau_s\right) = \frac{\sqrt{1-\left(1-\frac{\widehat{\frac{dv_c}{dt}}}{K_{AC}\hat{V}_{AC}}\overline{t_L}\right)^2}}{\cos^{-1}\left(1-\frac{\widehat{\frac{dv_c}{dt}}}{K_{AC}\hat{V}_{AC}}\overline{t_L}\right)} \quad (3.79)$$

3.3.2.5 Discharge magnitude

The discharge magnitude of Townsend-like discharge was treated in section 2.1.3. The individual apparent discharge magnitude is

$$q_{a,i} = \alpha h \cdot C_b \Delta V_{L,i} \quad (3.80)$$

$\alpha = const$ under assumption A.6. The overvoltage $\Delta V_{L,i}$ depends on the time lag $t_{L,i}$ and the phase-of-occurrence θ_i, and is given by :

$$\Delta V_{L,i} = \Delta\hat{V}_{L,i} - \Delta V_{\theta,i} \quad (3.81)$$

$\Delta\hat{V}_{L,i}$ is the upper envelope of the cavity voltage, and $\Delta V_{\theta,i}$ is the difference between the ignition voltage and the envelope of the cavity voltage when the i^{th} discharge occurs, see Fig. 3-11. $\Delta\hat{V}_{L,i}$ and $\Delta V_{\theta,i}$ are derived in Appendix B.2 :

$$\Delta\hat{V}_{L,i} = \widehat{\frac{dv_c}{dt}} t_{L,i} \quad (3.82)$$

$$\Delta V_{\theta,i} = K_{AC}\hat{V}_{AC}\left(1-\cos\theta_i\right) \quad (3.83)$$

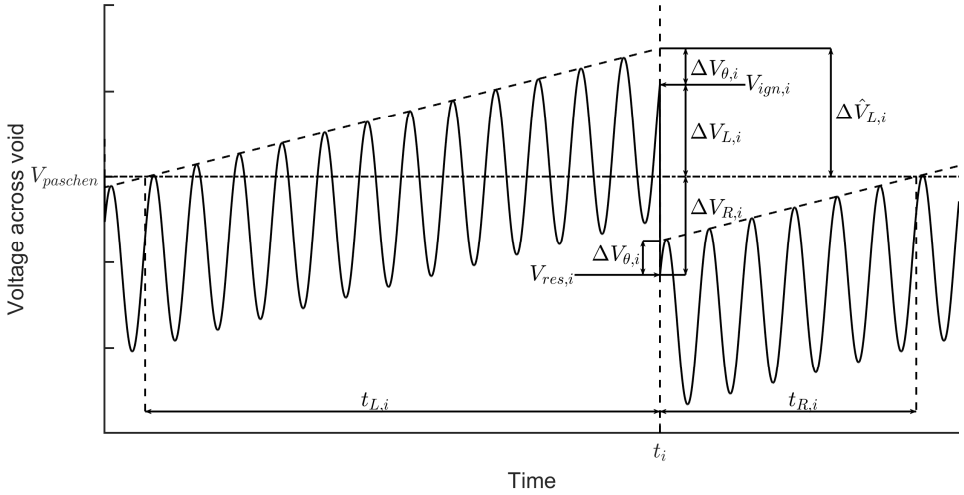

Fig. 3-11 A discharge at combined DC and AC voltage, resulting in a voltage drop in the cavity voltage. $\Delta V_{L,i} = \Delta V_L(t_{L,i}, \theta_i)$, $\Delta \hat{V}_{L,i} = \Delta \hat{V}_L(t_{L,i})$, $\Delta V_{\theta,i} = \Delta V_\theta(\theta_i)$.

The apparent discharge magnitude can be written as a function of the stochastic time lag and the stochastic phase-of-occurrence:

$$q_{a,i} = \alpha h \cdot C_b \left(\widehat{\frac{dv_c}{dt}} t_{L,i} - K_{AC} \hat{V}_{AC} \left(1 - \cos(\theta_i)\right) \right) \quad (3.84)$$

3.3.2.6 Recovery voltage and recovery time

The recovery voltage can be found as a function of the overvoltage, from (2.39):

$$\frac{\Delta V_{R,i}}{\Delta V_{L,i}} = \alpha h - 1 \quad (3.85)$$

To find the recovery time $t_{R,i}$, consider that the envelope of the voltage must increase by $\Delta \hat{V}_{R,i}$ within the recovery time $t_{R,i}$, see Fig. 3-11.

$$\Delta \hat{V}_{R,i} = \Delta V_{R,i} - \Delta V_{\theta,i} \quad (3.86)$$

Using linearisation of the upper envelope of the cavity voltage, $t_{R,i}$ can be found by:

$$\Delta \hat{V}_{R,i} = t_{R,i} \cdot \widehat{\frac{dv_c}{dt}} \quad (3.87)$$

Solving for $t_{R,i}$ and inserting (3.86) yields

$$t_{R,i} = \frac{\Delta V_{R,i} - \Delta V_{\theta,i}}{\widehat{\frac{dv_c}{dt}}} \quad (3.88)$$

By using (3.85), (3.81), (3.82) and (3.83), the recovery time can be expressed as a function of the stochastic time lag $t_{L,i}$ and the stochastic phase-of-occurrence θ_i as:

$$t_{R,i} = (\alpha h - 1) t_{L,i} - \alpha h \frac{K_{AC} \hat{V}_{AC}}{\widehat{\frac{dv_c}{dt}}} (1 - \cos\theta_i) \quad (3.89)$$

Observe that this function may give a negative recovery time $t_{R,i}$; this is the case when $\Delta V_{R,i} < \Delta V_{\theta,i}$ in eq. (3.88), or when

$$(\alpha h - 1) t_{L,i} < \alpha h \frac{K_{AC} \hat{V}_{AC}}{\widehat{\frac{dv_c}{dt}}} (1 - \cos\theta_i) \quad (3.90)$$

When $\Delta V_{R,i} < \Delta V_{\theta,i}$ occurs, the cavity voltage will be above the critical voltage within an AC time period, i.e. the envelope of the cavity voltage is above $V_{Paschen}$ just after the discharge; an example is shown in Fig. 3-12. This phenomenon is termed the rapid recovery effect, referring to the possibility that the cavity voltage can be higher than the critical voltage within an AC time period after a small discharge has occurred.

In the PD sequence model, the rapid recovery effect is taken into account by setting $t_{R,i} = 0$ when $\Delta V_{R,i} < \Delta V_{\theta,i}$, assuming that the AC time period is much shorter than the mean statistical waiting time, i.e.. $\tau_{AC} \ll \tau_s$.

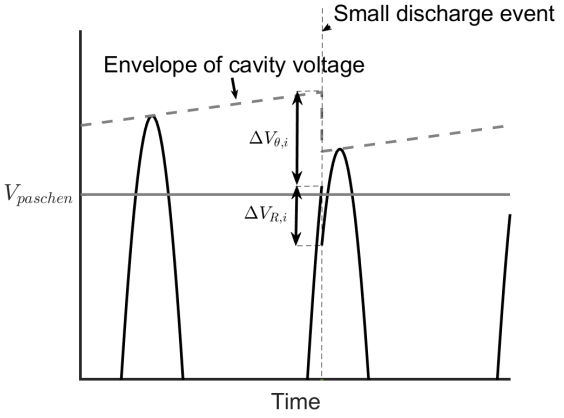

Fig. 3-12 A discharge at combined DC and AC voltage, where $\Delta V_{R,i} < \Delta V_{\theta,i}$.

3.3.3 Discharge magnitude and separation time – mean value, probability density and correlation

The i[th] apparent discharge magnitude is given in section 3.3.2.5 as:

$$q_{a,i} = \alpha h \cdot C_b \left(\widehat{\frac{dv_c}{dt}} t_{L,i} - K_{AC} \hat{V}_{AC} \left(1 - \cos\left(\theta_i\right)\right) \right) \quad (3.91)$$

The i[th] time to previous discharge is given in section 2.1.1 as

$$\Delta t_{pre,i} = t_{R,i-1} + t_{L,i} \quad (3.92)$$

By inserting $t_{R,i-1}$ from (3.89) into (3.92), the time to previous discharge can be expressed as :

$$\Delta t_{pre,i} = \left(\alpha h - 1\right) t_{L,i-1} + t_{L,i} - \alpha h \frac{K_{AC} \hat{V}_{AC}}{\widehat{\frac{dv_c}{dt}}} \left(1 - \cos\left(\theta_{i-1}\right)\right) \quad (3.93)$$

Thus $\Delta t_{pre,i}$ and $q_{a,i}$ depend on time lag and the phase-of-occurrence as the stochastic parameter:

$$q_{a,i} = f_1\left(t_{L,i}, \theta_i\right) \quad (3.94)$$

$$\Delta t_{pre,i} = f_2\left(t_{L,i-1}, t_{L,i}, \theta_{i-1}\right) \quad (3.95)$$

$t_{L,i}$ and $t_{L,i-1}$ are generated randomly from the same distribution, as described in section 3.3.2.3:

$$t_{L,i} = D^{-1}\left(-\tau_s \ln\left(1 - R\right)\right) \quad (3.96)$$

where R is a random number in the interval $[0,1)$.

θ_i and θ_{i-1} are generated randomly from the same distribution, as described in section 3.3.2.4:

$$\theta_i = \mathrm{P} \cdot \cos^{-1}\left(1 - \frac{\widehat{\frac{dv_c}{dt}}}{K_{AC} \hat{V}_{AC}} t_{L,i}\right) \quad (3.97)$$

where P is a random number in the interval $(-1,1)$.

By combining (3.91) with (3.93), the time to previous discharge can be expressed as a function of the physical parameters and the measurable quantities $q_{a,i}$, $q_{a,i-1}$, θ_i and θ_{i-1} :

$$\Delta t_{pre,i} = \frac{1}{\alpha h C_b \widehat{\frac{dv_c}{dt}}}\left((\alpha h - 1) q_{a,i-1} + q_{a,i}\right) + \frac{K_{AC}\hat{V}_{AC}}{\widehat{\frac{dv_c}{dt}}}\left(\cos\theta_{i-1} - \cos\theta_i\right) \quad (3.98)$$

This equation describes the pulse sequence correlation between the time to previous discharge and the apparent discharge magnitude and is used in the MoM estimation method described in section 3.3.4.

The probability density of the apparent discharge magnitude can be obtained directly from the output of the PD sequence model in section 3.2.1. The mean values can be calculated by:

$$\overline{q}_a = \frac{1}{n}\sum_{i=1}^{n} q_{a,i} \quad (3.99)$$

$$\overline{\Delta t} = \frac{1}{n}\sum_{i=1}^{n} \Delta t_{pre,i} \quad (3.100)$$

The mean values can also be calculated analytically, see Appendix B.7 and B.8 :

$$\overline{q}_a = \alpha h C_b \left(\widehat{\frac{dv_c}{dt}} \cdot \overline{t}_L - K_{AC}\hat{V}_{AC}\left(1 - \overline{\cos\theta}\right) \right) \quad (3.101)$$

$$\overline{\Delta t} = \alpha h \left(\overline{t}_L - \frac{K_{AC}\hat{V}_{AC}}{\widehat{\frac{dv_c}{dt}}}\left(1 - \overline{\cos\theta}\right) \right) \quad (3.102)$$

As shown in section 3.3.2.3 and section 3.3.2.4, the $\overline{t}_L$ and $\overline{\cos\theta}$ depends on $\widehat{\frac{dv_c}{dt}}$, $K_{AC}\hat{V}_{AC}$ and τ_s :

$$\overline{t}_L = F_1\left(\widehat{\frac{dv_c}{dt}}, K_{AC}\hat{V}_{AC}, \tau_s \right) \quad (3.103)$$

$$\overline{\cos\theta} = F_2\left(\widehat{\frac{dv_c}{dt}}, K_{AC}\hat{V}_{AC}, \tau_s \right) \quad (3.104)$$

The ratio of the mean apparent discharge magnitude and the mean separation time depends on C_b and $\frac{\widehat{dv_c}}{dt}$. Dividing (3.101) by (3.102), we get:

$$\frac{\overline{q}_a}{\Delta\overline{t}} = C_b \frac{\widehat{dv_c}}{dt} \quad (3.105)$$

This relationship predicts a positive correlation between the mean apparent discharge magnitude and the mean separation time, as was observed for PD at DC voltage, in (3.36). The cavity voltage slope at combined voltage is greater than the slope at DC voltage, i.e. $\frac{\widehat{dv_c}}{dt} > \frac{dv_c}{dt}$.

3.3.3.1 Relative change in mean values from DC to combined voltage conditions

The relative change in the mean separation time is obtained by dividing (3.102) by (3.35):

$$\frac{\Delta\overline{t}^{DCAC}}{\Delta\overline{t}^{DC}} = \frac{\overline{t}_L^{DCAC}}{\overline{t}_L^{DC}} \left(1 - \frac{K_{AC}\hat{V}_{AC}\left(1-\overline{\cos\theta}\right)}{\frac{\widehat{dv_c}}{dt}\overline{t}_L^{DCAC}} \right) \quad (3.106)$$

The relative change in the mean discharge magnitude is obtained by dividing (3.101) by (3.34); the relative increase in discharge magnitude is higher than the relative increase in mean separation time:

$$\frac{\overline{q}_a^{DCAC}}{\overline{q}_a^{DC}} = \left(1 + \frac{\frac{K_{AC}\hat{V}_{AC}}{V_{paschen}}}{\left(\frac{K_{DC}V_{DC}}{V_{paschen}} - 1\right)} \right) \frac{\Delta\overline{t}^{DCAC}}{\Delta\overline{t}^{DC}} \quad (3.107)$$

3.3.4 Estimation of PD sequence parameters

The parameters used in the combined voltage PD sequence model are αh, τ_s, C_b and $\widehat{\frac{dv_c}{dt}}$, see section 3.2.1. It is possible to calculate these parameters before the experiments, as performed in section 3.3.1.1. It is also possible to estimate the parameters after the experiments by utilizing the information in the measurable quantities Δt_{pre}, q_a and θ. The estimators $\hat{\alpha}\hat{h}, \hat{C}_b, \widehat{\frac{dv_c}{dt}}$ and $\hat{\tau}_s$ can be obtained by the method of moments as described in Appendix C.3 , when $K_{AC}\hat{V}_{AC}$ are assumed known. The mean recovery time, $\hat{\bar{t}}_R^{DCAC}$, and mean time lag, $\hat{\bar{t}}_L^{DCAC}$, at combined voltage can also be estimated.

The confidence intervals of the estimators are calculated using the non-parametric bootstrap method detailed in section 2.3.3. At DC conditions, it was only possible to estimate the product $C_b \frac{dv_c}{dt}$. At combined voltage conditions C_b and $\widehat{\frac{dv_c}{dt}}$ can be estimated explicitly.

Table 3-3 Estimated values obtained from method of moments for the combined voltage PD process

Estimator	Expression (function of the measured moments)
$\hat{\alpha}h$ and $\hat{C}_b$	A solution for $\hat{\alpha}h$ and $\hat{C}_b$ exists which satisfies $\frac{\widehat{\widehat{dv_c}}}{dt}_1 = \frac{\widehat{\widehat{dv_c}}}{dt}_2 = \frac{\widehat{\widehat{dv_c}}}{dt}_3$ (equations on p. 187) Find the intersecting contour line L1 (i.e. the set of $\hat{\alpha}h$ and $\hat{C}_b$) that satisfies $\frac{\widehat{\widehat{dv_c}}}{dt}_1 = \frac{\widehat{\widehat{dv_c}}}{dt}_2$. Find the intersecting contour line L2 (i.e. the set of $\hat{\alpha}h$ and $\hat{C}_b$) that satisfies $\frac{\widehat{\widehat{dv_c}}}{dt}_1 = \frac{\widehat{\widehat{dv_c}}}{dt}_3$. The intersection points of the contour lines L1 and L2 give a solution for $\hat{\alpha}h$ and $\hat{C}_b$ where $\frac{\widehat{\widehat{dv_c}}}{dt}_1 = \frac{\widehat{\widehat{dv_c}}}{dt}_2 = \frac{\widehat{\widehat{dv_c}}}{dt}_3$.
$\frac{\widehat{\widehat{dv_c}}}{dt}$	$\frac{\widehat{\widehat{dv_c}}}{dt}$ is found by inserting the solution for $\hat{\alpha}h$ and $\hat{C}_b$ into eq. (0.171) on p. 187.
$\hat{\bar{t}}_L^{DCAC}$	$$\hat{\bar{t}}_L^{DCAC} = \frac{\Delta\bar{t}}{\hat{\alpha}h} + \frac{K_{AC}\hat{V}_{AC}}{\frac{\widehat{\widehat{dv_c}}}{dt}}\left(1-\overline{\cos\theta}\right) \quad (4.1)$$ $\Delta\bar{t}$ is measured from the PD process, $\overline{\cos\theta}$ is calculated from measured phase-of-occurrence.
$\hat{\bar{t}}_R^{DCAC}$	$$\hat{\bar{t}}_R^{DCAC} = \Delta\bar{t} \; - \hat{\bar{t}}_L^{DCAC} \quad (4.2)$$
$\hat{\tau}_s$	Using (3.75), find the $\hat{\tau}_s$ that satisfies $$\hat{\bar{t}}_L^{DCAC} = F_1\left(\frac{\widehat{\widehat{dv_c}}}{dt}, K_{AC}\hat{V}_{AC}, \hat{\tau}_s\right) \quad (4.3)$$

4 Experimental techniques and test procedures

This chapter describes the experimental techniques that are used to obtain data at combined DC and AC voltage. The dominating voltage is DC and the AC voltage is kept below the AC PD inception voltage. The PD repetition rate in a DC voltage dominated process is several orders below the repetition rate under an AC voltage dominated processes. The discharge magnitude is also extremely low. The low repetition rate and discharge magnitude make the PD measurements vulnerable to intermittent noise, and thus efficient methods to suppress such noise are paramount to obtain valid data.

Section 4.1 reviews some of the challenges involved in designing and building an experimental setup for the measurement of partial discharge at combined DC and AC voltage. A design of a modular test cell is presented, as well as all parameters relevant to the proper control of the experimental conditions. The test procedures for measurement of discharges at DC voltage and combined voltage are described in section 4.1.8.

Section 4.2 describes methods to measure the permittivity and conductivity of the insulation material. The measurements are used to calculate PD process input parameters, as detailed in section 3.2.1.1 and section 3.3.1.1. Test setups and procedures are described in section 4.2.1 and section 4.2.1.4.

4.1 Experimental technique for measuring partial discharges at combined voltage

This section describes the design of an experimental test setup for measuring partial discharges at combined DC and sinusoidal AC voltage, with temperature control. The experimental setup described is capable of stressing the test sample with sinusoidal AC voltage up to 2 kV_{rms} for frequencies up to 5 kHz, and DC voltage up to 15 kV. The experimental setup measures discharges spanning 3 orders of magnitude, using two detectors at different gain levels. No parasitic partial discharges or noise are detected above 0.5 pC during measurement intervals spanning 24 hours.

4.1.1 Test circuit

The test circuit is shown in Fig. 4-1, and can be divided into three main functions:

1) AC generation, a suitable circuit for producing high amplitude, high frequency sinusoidal voltage.
2) DC generation, a suitable circuit for producing highly stabilised HVDC voltage.
3) PD measurement, PD signal path.

The PD measurement circuit is decoupled from the AC and DC generating circuits by a large transformer inductance in the AC branch and a large resistor in the DC source branch. The PD detectors are placed in the coupling capacitor branch and the test object branch. The PD detectors measure within the same frequency band, but on different gain levels. The measurement sensitivity in the test object branch is higher than in the coupling capacitor

branch. The high gain unit, the detector for low amplitude discharges, was therefore placed in the test object branch.

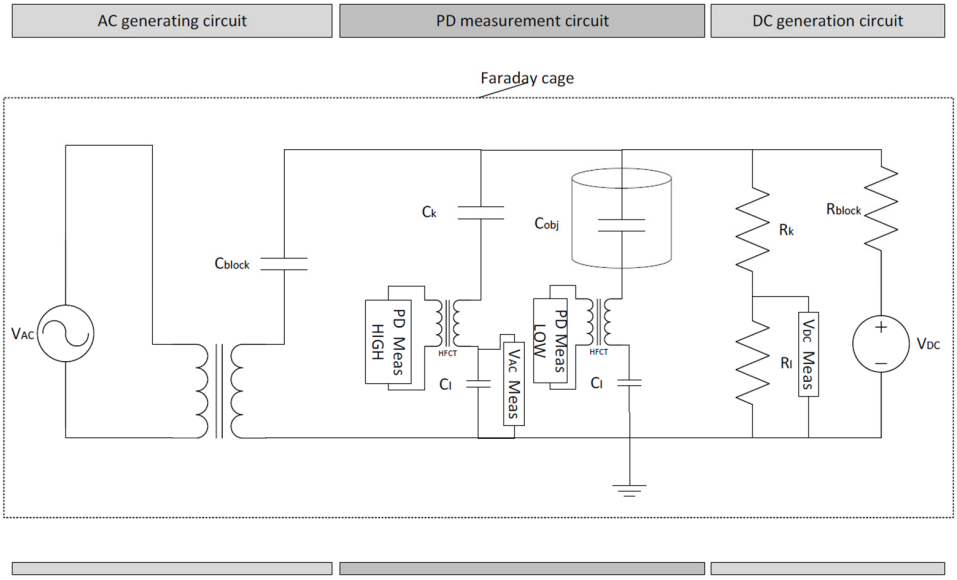

Fig. 4-1 Electric circuit for measurement of PD at combined DC and AC voltage.

The high frequency AC voltage is generated by a high voltage oscillator and stepped up using a voltage transformer. A capacitor, C_{block}, is connected in series to block any DC current from entering the transformer's secondary side. The blocking capacitor is large compared to the coupling capacitor, C_k, and the capacitance of the test object, so that most of the AC voltage drop is over the test object. The high inductance of the voltage transformer makes the AC generation branch a high impedance path for the discharge current. A highly stabilised HVDC source (AC ripple amplitude of 10-100 mV) supplies the DC voltage through a resistor, R_{block}. The resistor blocks the AC current injection into the DC source, attenuates noise coming from the DC source, and makes the DC branch a high impedance path for the discharge currents. The blocking resistor is quite smaller than the coupling resistor, R_k, so most of the DC voltage drop is over the test object. The low arm components, C_l and R_l, enable direct AC and DC voltage measurement, and their impedance values are smaller compared to the other components. The realisation of the test circuit is shown in Fig. 4-2.

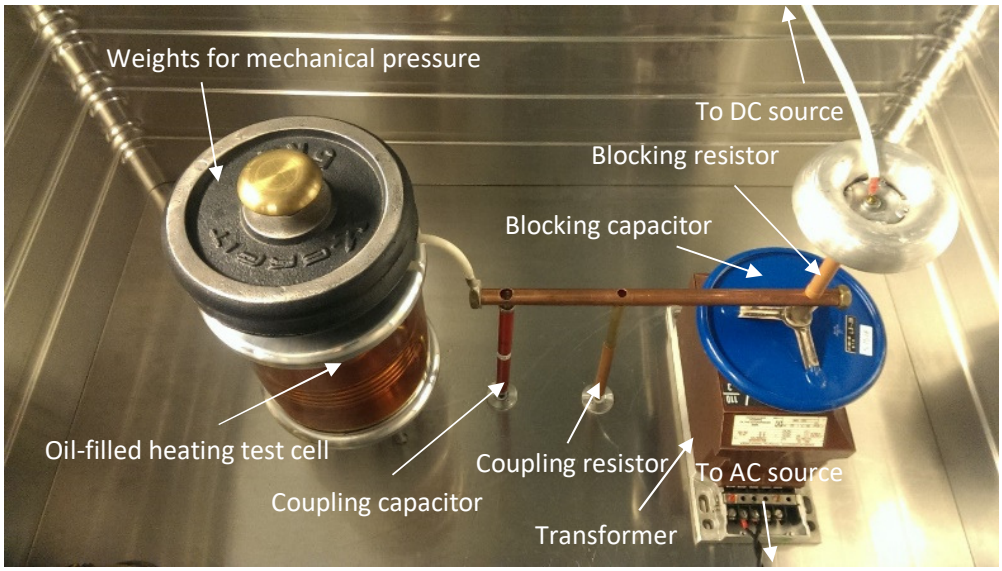

Fig. 4-2 Realised test setup for measurement of PD at combined DC and AC voltage.

4.1.2 Determination of test circuit components

The voltage over the test object is given by

$$V_{obj} = V_{obj,DC} + V_{obj,AC} \quad (4.4)$$

where

$$V_{obj,DC} = \frac{R_k}{R_k + R_{block}} \cdot V_{DC} = \frac{1}{1 + \frac{R_{block}}{R_k}} \cdot V_{DC} \quad (4.5)$$

$$V_{obj,AC} = \frac{C_{block}}{C_{block} + \left(C_k + C_{obj}\right)} \cdot V_{AC} = \frac{1}{1 + \frac{\left(C_k + C_{obj}\right)}{C_{block}}} \cdot V_{AC} \quad (4.6)$$

The influence of C_l is ignored, as $C_l \gg C_k, C_{obj}$. The resistance of the test object is ignored because it is much higher than R_k , in the order of 100 GΩ, even for the highest measurement temperature. Three aspects must be considered when designing the generation circuit:

The first aspect is the voltage over the blocking impedances, which should be minimised, in order to fully utilise the voltage rating of the voltage sources. This is especially important for the AC source, due to the reduced voltage step up in the transformer at higher frequencies. The following two criteria should be satisfied:

$$\frac{\left(C_k + C_{obj}\right)}{C_{block}} \ll 1 \quad (4.7)$$

$$\frac{R_{block}}{R_k} \ll 1 \quad (4.8)$$

The following design equations have been employed:

$$C_{block} \geq 10\left(C_k + C_{obj}\right) \quad (4.9)$$

$$R_k \geq 5R_{block} \quad (4.10)$$

The second aspect is the rated current of the voltage sources. The two following criteria must be satisfied to ensure continuous operation (assuming (4.7) and (4.8) are satisfied):

$$\left(C_{obj} + C_k\right) \leq \frac{I_{rated,AC}}{\max\left\{U_{obj,AC}\right\}\max\left\{\omega\right\}} \quad (4.11)$$

$$R_k \geq \frac{\max\left\{U_{obj,DC}\right\}}{I_{rated,DC}} \quad (4.12)$$

The third aspect is the residual voltage safety time. There will be a residual DC voltage over the total capacitance of the circuit $C_{tot} = C_k + C_{obj} + C_{block}$. The stored energy in the capacitors must be discharged through R_k. The voltage should be below 50 V within approximately 10 seconds, and this is satisfied for

$$5\tau_{dis} \approx 10\,\mathrm{sec} \quad (4.13)$$

$$\tau_{dis} = R_k\left(C_{tot} = C_k + C_{obj} + C_{block}\right) \leq 2\,\mathrm{sec} \quad (4.14)$$

Based upon these simplified considerations and the estimated capacitance of the test object and the coupling capacitor, the following values as shown in Table 4-1 were found.

Table 4-1 Calculation of circuit element values

INPUT		OUTPUT			
Voltage requirements		Max/min values		Chosen circuit element values	
$V_{obj,AC,\max}$	2 kV	$R_{k,\min}$	10 MΩ	R_k	500 MΩ
$V_{obj,DC,\max}$	20 kV			R_{block}	100 MΩ
$f_{AC,\max}$	5 kHZ			C_k	200 pF
$I_{rated,AC}$	20 mA	$\max\left(C_{obj}+C_k\right)$	318 pF	$\max(C_{obj})$	100 pF
				$\min(C_{block})$	3000 pF
$I_{rated,DC}$	2 mA			τ_{dis}	2.16 s

The selection of resistors and capacitors depends on the value and PD free voltage rating of the components. The sensitivity of the PD measurement depends on C_k and will be treated in section 4.1.3.1. The maximum capacitance of the test object provides input for designing the size of the electrodes, see section 4.1.4.1 . With the circuit element values in Table 4-1, approximately 83% of the DC source voltage and 91% of the AC source voltage will reach the test object terminals.

Adding a high frequency AC voltage source adds noise to the setup. Noise detection must be assessed for each AC voltage frequency, and careful selection of the detection frequency band is necessary to cope with the higher level of disturbance. The circuit elements, especially the impedance and voltage ratio of the voltage transformer, change when increasing the frequency. Resonance may occur in the circuit on the secondary side of the transformer, due to the broad frequency range of the AC voltage. Capacitor values must be selected with care to avoid any resonance.

4.1.3 Measuring circuit

The measurement circuit in Fig. 4-1 is the standard straight circuit for PD detection [2]. A coupling capacitor C_k provides a low impedance path for the detection of the discharge currents, and forms part of a capacitive divider together with a low arm capacitor C_l to measure the AC voltage component. The resistor, R_k, provides a way of automatically discharging the capacitances after a measurement, and forms a resistive divider together with a low arm resistor R_l to measure the DC voltage. The measuring impedance is the internal quadripole of an Omicron MPD 600 amplifier and digitiser, which consists of a HF current transformer and the low arm capacitor with $C_l = 1\mu F$. The gain level is set as high

as possible at the MPD in the test object branch, detecting discharges of magnitudes 0.5 to 700 pC. In a previous setup by the author of this thesis [90], two detectors were connected to the same measuring impedance, but this effectively halved the signal-to-noise ratio. The present setup allows a better signal-to-noise ratio.

4.1.3.1 Sensitivity

The detector will register a fraction of the apparent charge, called the measurable charge Q_m, as the integral of the current in the coupling capacitor branch. The ratio between measurable and apparent charge is:

$$\frac{Q_m}{q_a} = \frac{C_k}{C_k + C_t} \quad (4.15)$$

assuming that the stray capacitance C_{stray} is negligible compared to the coupling capacitor, and $C_l \gg C_k$. There is a trade-off between the required sensitivity and the power rating of the AC source; a large coupling capacitor will draw a high current from the transformer when the AC test frequency is high. C_k must be chosen so that it is as large as possible without drawing too large a current from the transformer at high frequencies, and the test object capacitance should be as low as possible. The latter requirement restricts the diameter of the electrodes. For the setup used in this thesis, $C_k = 200\,pF$; $C_t < 100\,pF$, and thus $\frac{Q_m}{q_a} > 0.667$, see Fig. 4-3.

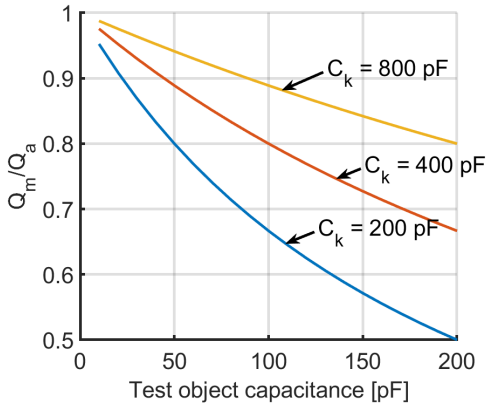

Fig. 4-3 The sensitivity of the detector as a function of test object and coupling capacitance, according to eq. (4.15).

However, the sensitivity is given by the relation between the discharge magnitude in the cavity Q_{dis} and the measured discharge Q_m:

$$\frac{Q_m}{Q_{dis}} \approx \frac{C_k}{C_k + C_t} \cdot \frac{C_b}{C_c} \quad (4.16)$$

Larger coupling capacitance gives better sensitivity, but draws a higher current from the AC source. For the setup and test object used in this thesis:

$$\frac{Q_m}{Q_{dis}} > 0.667 \cdot 1.65 = 1.10 \quad (4.17)$$

The test setup is therefore capable of detecting very small discharges in the cavity, well below 1 pC. In practice, the lower detection limit depends on the noise level.

4.1.3.2 Analogue and digital bandwidth of measuring system

The partial discharge that takes place in the cavity usually lasts a couple of microseconds, but it is not possible to measure the charge displacement process directly. Instead, the resulting charge transport in the external circuit is measured. The externally measured PD pulse waveform depends on the circuit used to measure the PD pulses. To minimize inductance and noise in the signal path, the setup was made as small as possible and the leads to the measuring device as short as possible. The data are transferred through optical cables. In the current work, the PD pulse was measured with PD acquisition system MPD 600 from Omicron. The system was chosen due to its excellent noise suppression features, and versatility in data acquisition and storage.

The PD pulse is measured with a wide band high frequency transformer (HFCT) as shown in Fig. 4-1, which in this case is the attenuator. The complete signal flow is shown in Fig. 4-4.

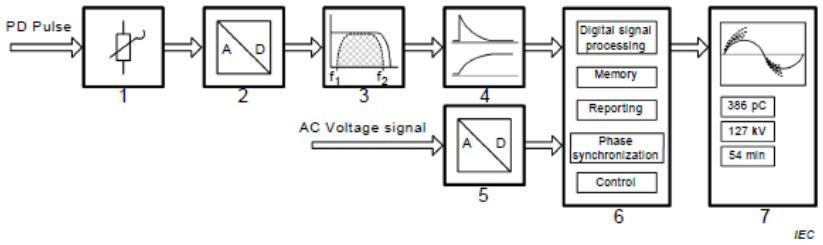

Fig. 4-4 Analogue and digital signal flow, according to IEC 60270 [2]**. Direct A/D conversion of the input PD pulses. 1 - Attenuator; 2 - A/D converter for PD pulses voltage; 3 - Digital band-pass filter; 4 - Numerical integrator; 5 - A/D converter for AC voltage; 6 - Acquisition unit; 7 - Evaluation and visualization unit**

The attenuator has a lower cut-off frequency at 30 kHz and upper cut-off frequency around 20 MHz. To measure the apparent charge, the conventional quasi-integration technique is used. The general rule is that for sufficiently low frequencies, the spectrum of any PD pulse contains the complete information needed for determining the time integral, i.e. the apparent charge. The principle is shown in Fig. 4-5.

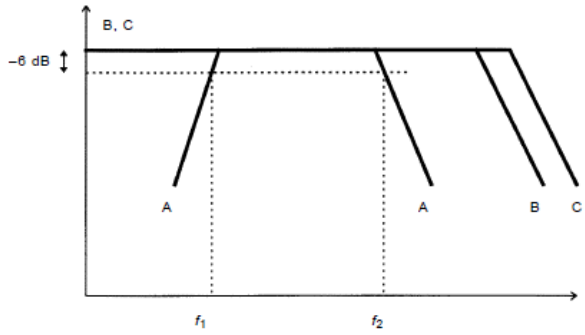

Fig. 4-5 Correct relationship between amplitude and frequency to minimize integration errors for a wide band system, from [2]**. A: Bandpass of the measuring system. B: Amplitude frequency spectrum of the PD pulse. C: Amplitude frequency spectrum of calibration pulse.**

The integration bandwidth and upper cut-off frequency are set digitally from the software interface. The choice of bandwidth determines the minimum pulse resolution time (the time between two consecutive recognized pulses), and influences the noise level and correct polarity detection. In the measurements in this thesis work, the integration bandwidth was set to 300 kHz and the centre frequency to 700 kHz. A high centre frequency was chosen due to noise in the band below 100 kHz from the AC source. At a bandwidth of 300 kHz the pulse resolution time is 3.33 µs, the inverse of the bandwidth. The noise level is around 0.3 pC for the present setup, but threshold was set to 0.5 pC.

4.1.3.3 Calibration

The two PD detectors were calibrated at different levels. The low PD amplitude detector in series with the test object was calibrated at 5 pC, and the high PD amplitude detector in the coupling capacitor branch was calibrated at 50 pC. The calibration pulse was injected at the test object terminals.

It is important that the capacitance of the calibrator is smaller compared to the test object capacitance, since the calibrator is removed after calibration. The calibrator capacitance was less than 1 pF.

4.1.3.4 Electric noise suppression

The following measures were taken to reduce constant and intermittent noise:

- Complete setup placed inside Faraday cage, and all power provided through filtered mains.
- No switch mode power supplies for measurement instruments.
- Twisting of AC voltage low voltage cables.
- Control and data over optical cables, to avoid any antenna effects.
- Star point ground, no ground loops.
- Clean lab environment, high voltage circuit in dust-proof metal box.
- Ferrite cores on all USB and signal leads in and out of control box described in section 4.1.6.

4.1.4 Test cell

A modular test cell designed for the setup is shown in Fig. 4-6. The test cell in this work uses a brass ground electrode, and an epoxy encapsulated high voltage electrode, described in section 4.1.4.1. Mechanical pressure is controlled by weights on the top electrode, temperature is controlled by the electric heat coil, oil is used as a thermal conductor and for suppressing discharges at the edges of the electrodes. O-rings were used to ensure the cell is oil-, vacuum- and airtight. PT 100 elements measure the temperature inside the bottom brass electrode, and in the oil.

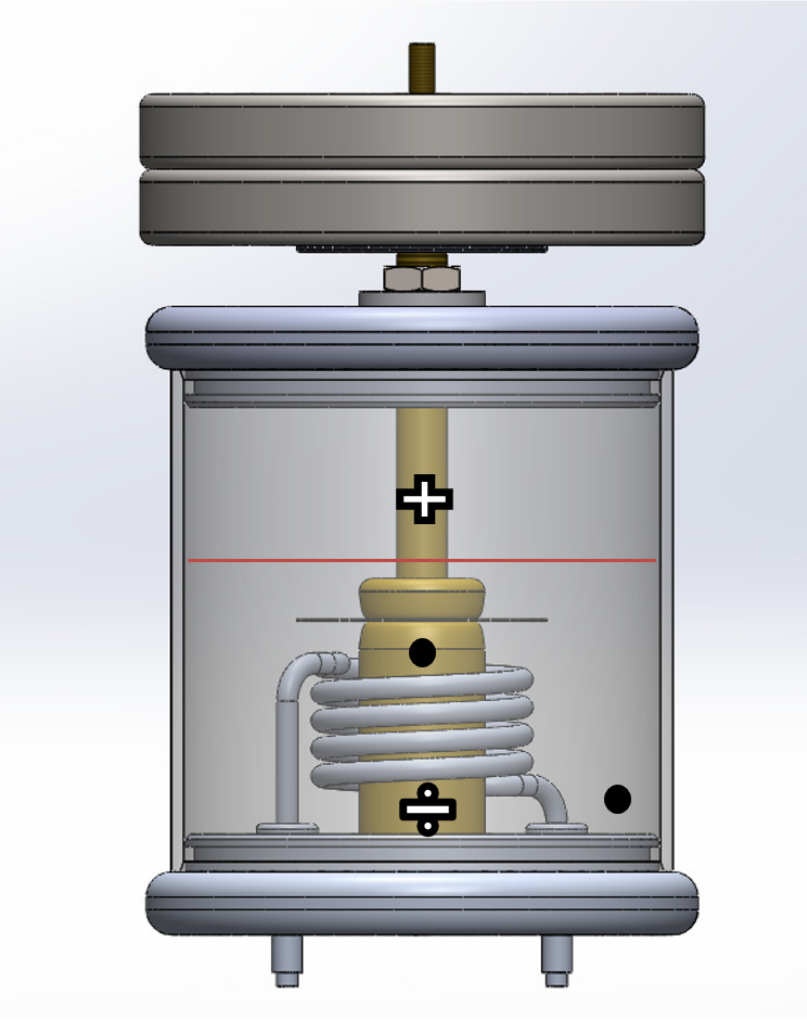

Fig. 4-6 Test cell. Resistive heating coil (grey spiral) heats oil and sample, red line marks oil. Brass electrodes in beige, + sign marks top electrode, ÷ sign marks bottom electrode, black dots mark temperature sensors.

4.1.4.1 Electrodes

The risk of parasitic PD increases with higher voltage, especially at the edges of the electrodes and at sharp protrusions in the external high voltage circuit. Furthermore, lack of pressure outside the electrode periphery may allow small pockets of air in the interface between the films. To mitigate external discharges, the high voltage electrode must be cast in epoxy. PD at the edge of the electrode is then mitigated and there will be sufficient pressure on the films, even outside the electrode radius. The DC electric field is graded using a linear slope, see electrode design drawing in Fig. 4-7a. The design was first used by Kreuger [91], but the slope was made steeper to restrict the electrode diameter and the capacitance of the test object.

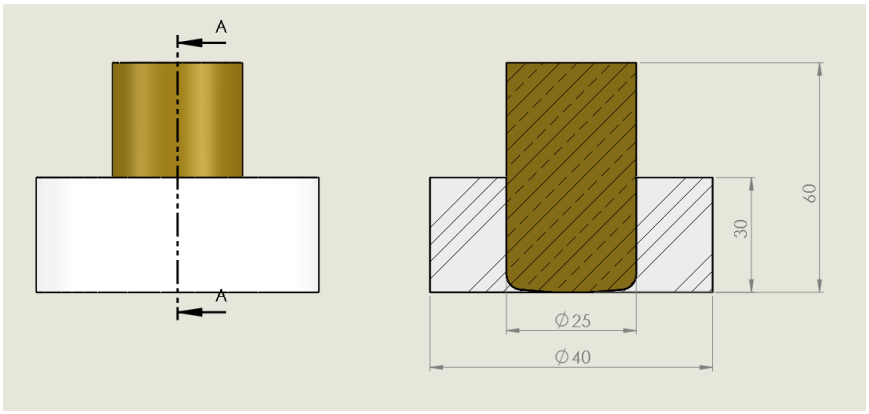

a)

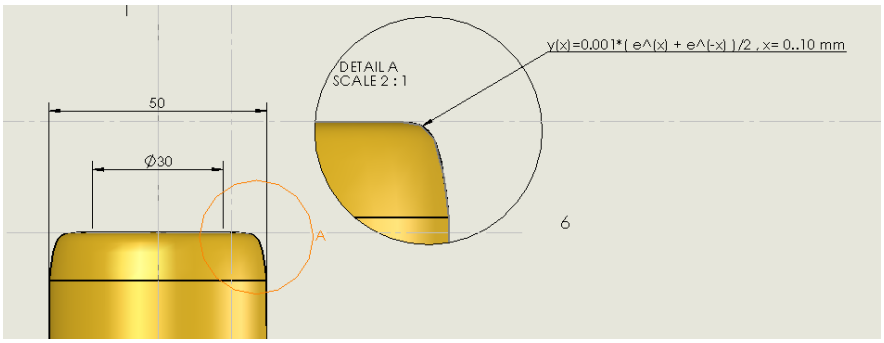

b)

Fig. 4-7 The high voltage electrode with diameter 25 mm shown in a). The slope outside the centre plateau (diameter 1 cm) is 1:12, and the radius of the egde is 4 mm. The ground electrode with Rogowski profile shown in b).

The ground electrode was rounded with a Rogowski profile at the edges, see Fig. 4-7a. The electrodes were submerged in mineral oil up to 3-4 cm above the test object. A picture of the electrode assembly is shown in Fig. 4-8.

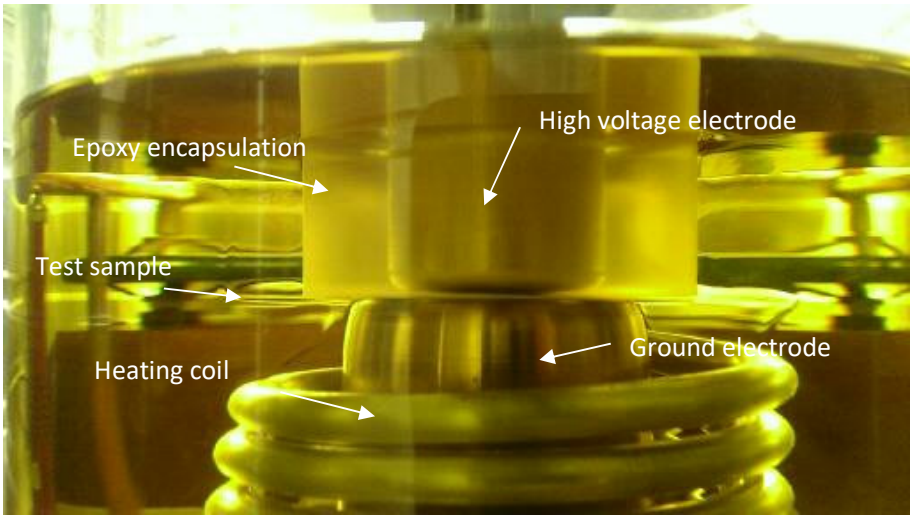

Fig. 4-8 Epoxy encapsulated high voltage electrode, final assembly.

4.1.5 Test sample

It is preferable to choose a material that is used in electrical apparatus, and where there is substantial scientific literature on the conductivity and permittivity of the material. A layered sample with a cylindrical cavity facilitates an easy and repeatable preparation of samples. For such reasons, a biaxially oriented PET film was chosen. The test samples in this thesis are made from sheets of Hostaphan RN 50-350 from Mitsubishi Polyester Film GmbH. The film can be supplied in thicknesses from 50 to 350 µm.

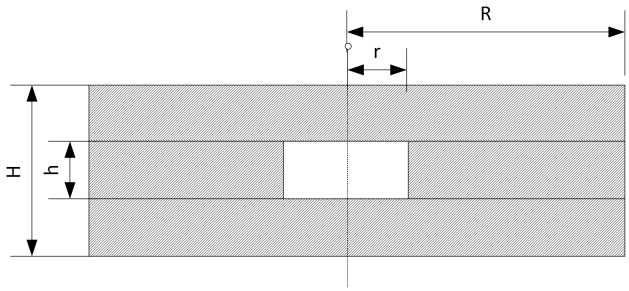

Fig. 4-9 Structure of test object, three layers of PET film with cylindrical hole in the middle layer.

The cavity size choice was influenced by two aspects:

- The high voltage which is necessary to generate a sufficiently high PD repetition rate at DC causes an increased probability of occurrence of discharges in the external circuit, and thus a thin film is preferable. This reduces the DC voltage needed to start discharges in the sample.
- The cavity diameter should not be too small due to non-homogeneity of the field inside the cavity and not too large due to the danger of deformation of the cavity due to electrostatic forces on the cavity surface [91].

For the experiments, a cavity with 2 mm in diameter was chosen, and the film thickness was 75 µm. The films were pressed together and glued at the outer edge to avoid ingress of oil into the cavity. The capacitance of the test object with the electrodes in section 4.1.4.1 is approximately 64 pF and is lower than the 100 pF limit given in section 4.1.3.1.

4.1.6 Control of test setup

All data and control signals were transferred via optical cables. NI USB 6216 was used to measure temperature and control the resistive heating element. The NI USB 6216 also controlled voltage output of the AC and DC sources, and AC frequency. The voltage sequence output and temperature controller were implemented using LabVIEW.

4.1.7 Verification of setup

A systematic approach is vital for acquiring confidence in the final test results. The test setup is comprised of many sub-systems; the DC and AC generating branches, PD measurement system, temperature control, voltage control, test cell, etc. The lab environment will also influence the setup. A test procedure of the setup was used, which was intended to reduce the complexity, and work its way from component level to full assembly of the test setup:

1. Sub-system test: verification of function and noise level of separate components.
2. System test: verification of function of assembled components and noise level.
3. Main test: PD detection in the PET test objects.

In steps 1 and 2, the following tools were used:

- High bandwidth oscilloscope measurements of voltage waveforms.
- FFT, to identify frequency band with lowest noise levels.
- 24-hour PD measurement to check for intermittent noise.
- 24-hour temperature measurement.
- 24-hour voltage stability measurement.

In step 3, the following procedure was followed:

1. 24-hour PD measurement on solid PET sample with thickness 250 µm at the highest DC and AC voltages planned for the final experiments. Temperature of 75 °C.
2. 24-hour PD measurement on 3 sheets of PET, without cavity, at the highest DC and AC voltages planned for the final experiments. Temperature of 75 °C. Various values of mechanical pressure.
3. PD Measurements on samples with cylindrical cavity, see test procedure in the next section.

During step 2, it was found that a mechanical pressure of 2 kg/cm^2 yielded no discharges above 0.5 pC for 24 hours, thus confirming that the test setup was robust against continuous and intermittent noise.

4.1.8 Test procedure

The PD test programme on samples with cylindrical cavity consists of three test series with variable AC voltage:

- Test series 1: DC + variable AC ripple amplitude
- Test series 2: DC with no AC ripple
- Test series 3: DC + variable AC frequency

For test series 1 and 3, the individual apparent discharge magnitude, time-of-occurrence, and phase-of-occurrence are registered. For test series 2, only the apparent discharge magnitude and the time-of-occurrence is registered. The test sample used is described in section 4.1.5. The temperature and DC voltage were the same for all three test series: The temperature was controlled to 75±1 °C, and the DC voltage over the test sample was 10 kV. The AC voltage varied between 0 to 500 V_{rms} and the AC frequency between 50 to 1000 Hz.

One test series is divided into five test sequences, and each test sequence is divided into seven stages, see Fig. 4-10. For the test sequences:

- A test sequence lasts 42 hours.
- A test sequence always starts with applying DC voltage, the DC voltage is ramped up at approximately 30 V/s, to 10 kV. The DC voltage is kept at this level throughout the test sequence and ramped down at the end.

- The sample is grounded for 48 hours between each test sequence to investigate the effect of grounding on the PD process.
- A PDIV test at AC voltage was performed just before the second test sequence to investigate the effect of an AC PDIV test on the subsequent PD process. Care was taken to limit the number of discharges in this test between 30 000 to 40 000, to avoid any permanent changes to the cavity.

For the test stages:

- Each stage is 6 hours.
- The first stage (0) of a test sequence is the transient stage, where the polarisation current in the sample stabilises.
- In the next stages (1-6), which are of primary interest, the PD process is in the steady state condition.
- In stages 0, 1 and 6, labelled DC0, DC1 and DC2, respectively, no AC ripple is superimposed on the DC voltage.
- AC voltage is superimposed on the DC voltage in stages 2, 3, 4, and 5, labelled AC1, AC2, AC3, and AC4, respectively.
- Stage DC1 is the reference for DC2, Stage AC1 is the reference for AC4, the use of reference stages makes it possible to track any of the PD process on the PD sequence parameters.

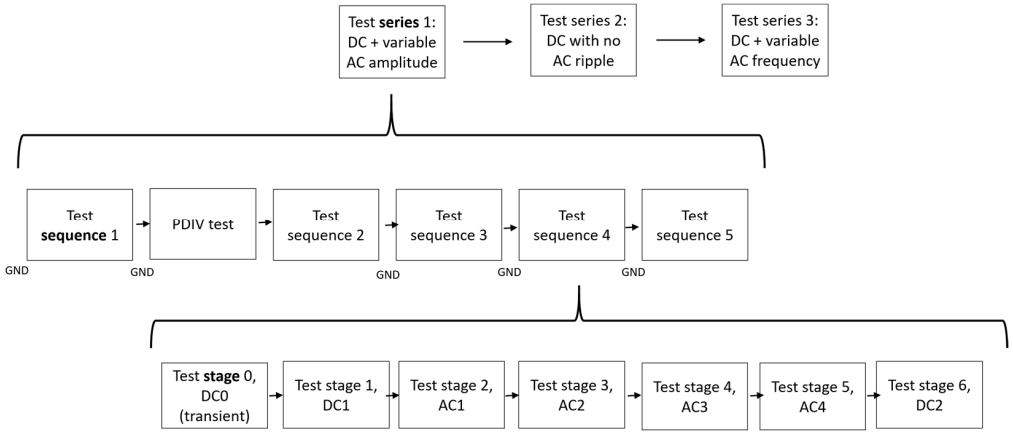

Fig. 4-10 General overview of the partial discharge test programme.

A test sequence for DC with variable AC voltage amplitude is shown in Fig. 4-11. The AC voltage ripple with constant frequency was applied with a logarithmic increase in amplitude through stages AC1 to AC3. In stage AC4 the amplitude was reduced to the same level as AC1, for reference. AC voltage is ramped up or down at a rate of 30 V/s.

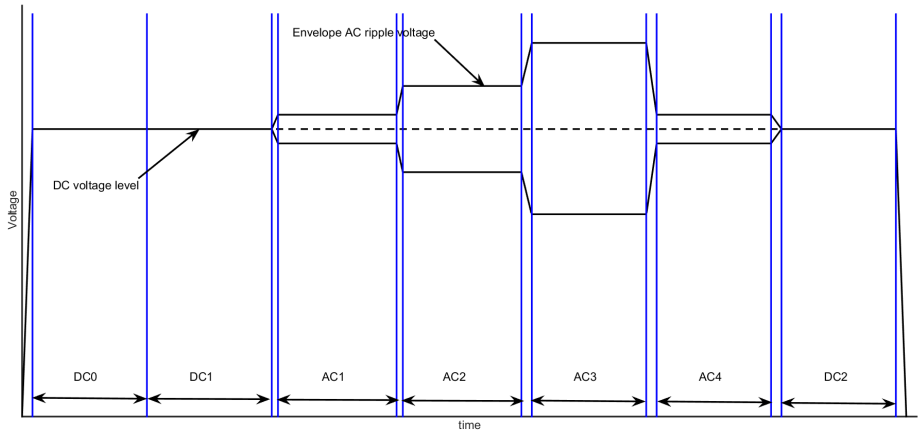

Fig. 4-11 The different stages of voltage application during a test sequence with DC + variable AC amplitude, see values in Table 4-2.

The AC voltage ripple with constant amplitude was applied with a logarithmic increase in frequency through stages AC1 to AC3. In stage AC4, the frequency was reduced to the same level as AC1, for reference. The applied DC and AC voltage for all test series is given in Table 4-2. During test series with DC variable AC ripple amplitude and frequency, the AC voltage is never higher than around 60% of the theoretical AC PDIV value: $PDIV_{AC} = 1234 V_{peak}$, given in section 5.2.1.

The DC electric field in the series dielectric of the PD test sample can be estimated by assuming that the voltage over the cavity is close to the Paschen voltage. The total voltage over the series dielectric is:

$$V_b = V_{DC} - V_{paschen} \quad (4.18)$$

The electric field strength is found by dividing the total voltage over the series dielectric by the total thickness of the series dielectric:

$$E_b = \frac{V_b}{H - h} \quad (4.19)$$

h=75 µm, H = 225 µm and $V_{DC} = 10$ kV, and $V_{paschen} = 765 V_{peak}$ for atmospheric pressure, so $E_b \approx 61.5$ kV/mm.

Table 4-2 Overview measurement programme, voltage stress under different test sequences. Each stage is 6 hours. Each test sequence is performed 5 times.

Stage number	Stage label	Time interval (hour)	DC series (VAC ≈ 0)	DC + variable AC amplitude test series			DC + variable AC frequency test series		
			kVDC	kVDC	VAC (rms)	Hz	kVDC	VAC (rms)	Hz
0	DC0	0-6	10	10	0	0	10	0	0
1	DC1	6-12	10	10	0	0	10	0	0
2	AC1	12-18	10	10	**44**	50	10	44	**50**
3	AC2	18-24	10	10	**176**	50	10	44	**500**
4	AC3	24-30	10	10	**500**	50	10	44	**1000**
5	AC4	30-36	10	10	**44**	50	10	44	**50**
6	DC2	36-42	10	10	0	0	10	0	0

A series of measurements was carried out at the same DC voltage and temperature level as in the DC test series reported in section 5.2, but an AC ripple voltage 100 V_{rms} below the theoretical AC partial discharge inception voltage was superimposed on the DC voltage after 12 hours. The applied voltage for the entire test sequence is given in Table 4-3. The test series consisted of 2 repeated test sequences. An AC PDIV test was performed just before the second test sequence.

Table 4-3 Test sequence with constant DC voltage and an high AC ripple voltage. Each test sequence consisted of 4 stages, the length of one stage was 6 hours.

Stage number	Stage label	DC + high AC voltage test sequence		
		VDC (kV)	VAC (Vrms)	fAC (Hz)
0	DC0	10	0	0
1	DC1	10	0	0
2	AC	10	760	50
3	DC2	10	0	0

4.2 Experimental technique for measuring material parameters

The conductivity and permittivity must be measured to determine the PD sequence parameters C_b and $\frac{dv_c}{dt}$, as detailed in sections 3.2.1.1 and 3.3.1.1. Section 4.2.1 describes the Pol/Depol method used to obtain the conductivity for electric field strength between 22-44 kV/mm. Section 4.2.1.4 describes the AC dielectric response method to obtain the permittivity in the frequency range 1-5000 Hz. All measurements are performed on sheets of biaxially oriented PET with thickness 75 µm, in the temperature range 40-80 °C.

4.2.1 Conductivity

The conductivity of the PET film was measured with a guarded electrode setup in a temperature-humidity chamber. The electric field strength (V_{DC}/h), was 22, 33, and 44 kV/mm. The measurements were made at 40, 60, and 80 °C, at room relative humidity (i.e. 30-50%). The humidity in the samples was not controlled, because the partial discharge measurements were performed at uncontrolled room relative humidity. The design of the test setup is the same as in [92].

4.2.1.1 Method and test setup

The polarisation and depolarisation current method (PDC) is used to measure the conductivity. The details of this method can be found in a paper by Zaengl [93]. In short, the conductive current I_{DC} (described in section 2.1.2.1) through a dielectric material can be found by the sum of the polarisation current i_p and the depolarisation current i_d:

$$I_{DC} = i_p(t) + i_d(t) \quad (4.20)$$

The depolarisation current will be opposite in sign to the polarization current. The conductivity of the sample is calculated based on the measured quantities as [92],[94]:

$$\sigma = \frac{\varepsilon_r}{C}\frac{\left(i_p(t)+i_d(t)\right)}{V_{DC}} \quad (4.21)$$

where ε_r and C are the relative permittivity and the capacitance of the sample at or near power frequency, respectively, and V_{DC} is the applied DC voltage during the polarisation stage.

The experimental setup is shown in Fig. 4-12. The test cell with the test sample is placed in a temperature-humidity chamber which controls the temperature to $\pm 0.1\,^{\circ}C$; the humidity was not controlled during the experiments. The low ripple HVDC voltage source is connected to the sample through two resistors and a high voltage (HV) relay. A picoammeter measures the current through the sample, a grounded guard electrode is used to eliminate surface leakage current. The polarisation stage starts by switching the HV relay from low to high position. After a polarisation time of 1 hour, the HV relay switches

to the low position and grounds the test sample for a depolarisation time of 10 hours. This longer depolarisation time is necessary to remove any remaining space charge in the sample between each test. The picoammeter is protected by a low voltage (LV) relay during switching of the HV relay, grounding the terminals of the picoammeter.

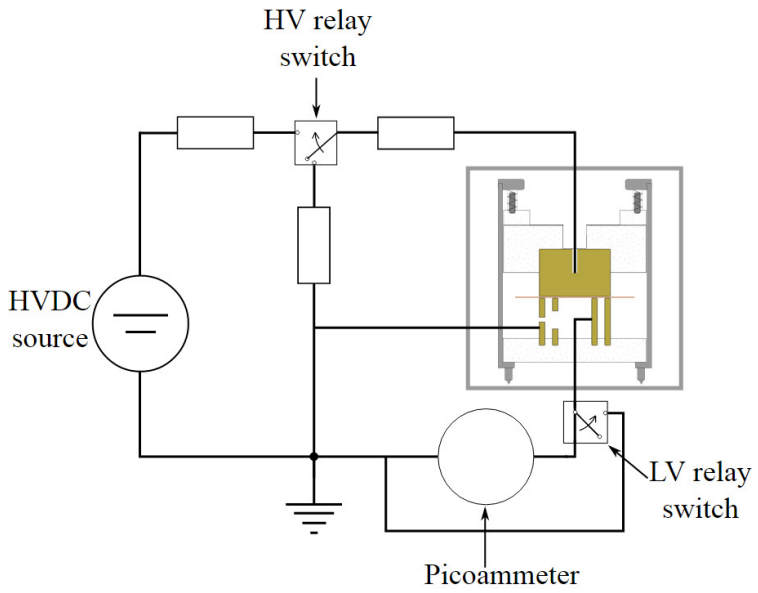

Fig. 4-12 Test cell and setup for PDC conductivity measurement, from [92]**.**

4.2.1.2 Test sample

The test sample is 75 µm thick PET film with aluminium electrodes as shown in Fig. 4-13. A 3-electrode system is used, comprising a high voltage electrode on one side and a guard and sense electrode on the other side. The diameter of the sense electrode is 40 mm, the thickness of all electrodes was below 1 µm. The aluminium electrodes were made using a vacuum evaporation technique.

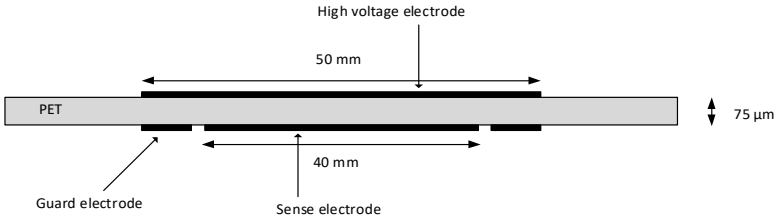

Fig. 4-13 Test sample with vacuum evaporated guard aluminium electrodes, thickness of electrodes is <1 µm.

The test samples were prepared as follows:

1. Cleaning of samples with Isopropanol.
2. Drying in vacuum oven at 80 °C for 48 hours.
3. Vacuum deposition of aluminium on both sides of the sample.

4.2.1.3 Test procedure

The tests were performed in the order shown in Table 4-4, by the following procedure:

1. Insert test sample in test cell.
2. Set temperature. Humidity is not controlled and is the same inside the chamber as in the laboratory.
3. Allow stabilisation of test cell and sample temperature for 24 hours.
4. Measure capacitance and permittivity of sample, using RLC meter.
5. Connect cables for conductivity measurement, wait minimum 12 hours for relaxation of any triboelectric effects in the connected cables. Measure polarisation and depolarisation currents at each voltage (1.65 kV, 2.5 kV and 3.3 kV) with 1-hour polarisation time and 10-hour depolarisation time.
6. Set next temperature, start from step 2 again.

Table 4-4 Order of the conductivity measurements

	Test voltage		
Temperature	1.65 kV (11 kV/mm)	2.5 kV (22 kV/mm)	3.3 kV (44 kV/mm)
40 °C @ Room RH	Measurement no. 1	Measurement no. 2	Measurement no. 3
60 °C @ Room RH	Measurement no. 4	Measurement no. 5	Measurement no. 6
80 °C @ Room RH	Measurement no. 7	Measurement no. 8	Measurement no. 9

4.2.1.4 Fitting of conductivity data

Das Gupta and Joyner [95] found that the temperature dependence of conductivity in PET was consistent with the Arrhenius equation in the temperature range 273 ≤ *T* ≤ 450 K:

$$\sigma(T) = \sigma_0 \exp\left(-\frac{E_A}{kT}\right) \quad (4.22)$$

A strong field dependence was observed in PET by Inuishi and Powers [96]:

$$\sigma(E) = \sigma_0 \exp(\alpha E) \quad (4.23)$$

Based on the above observed empirical relationships and Lawson [97], it will be assumed that the combined temperature and electric stress dependence can be represented by

$$\sigma(E,T) = \sigma_0 \exp\left(-\frac{E_A}{kT}\right)\exp\left(\frac{bE}{kT}\right) \quad (4.24)$$

The data obtained by measurement as described in section 4.2.1.3 can be fitted by (4.24) to find conductivity at values of temperature and electric field strength other than those directly measured.

4.2.2 Permittivity

The permittivity of the PET film was measured using AC dielectric response method in the frequency range 1-5000 Hz. The measurements were made at 40, 60, and 80 °C, and at room relative humidity (i.e. 30-50%). The test setup used is the same as in [98].

4.2.2.1 Method and test setup

The dielectric response method [99] is used to find the permittivity. The measurements were performed using a Novocontrol Alpha A analyser with ZG4 4-wire impedance interface and a heating oven capable of regulating the temperature within $\pm 1^{\circ}C$. The test circuit is shown in Fig. 4-14. The AC voltage was 3 V_{rms} and the frequency varied between 1-5000 Hz in steps of 250 Hz. There was no guard electrode on the test samples, and the effect of stray capacitance and conduction around the edges was not compensated for.

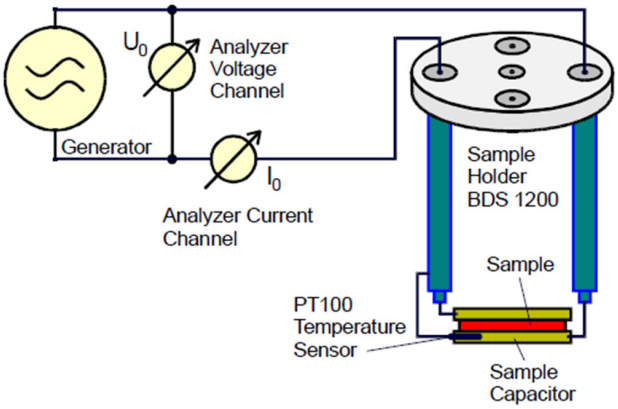

Fig. 4-14 Test circuit for measurement of permittivity as function of frequency, the Novocontrol Alpha A.

4.2.2.2 Test sample

The test sample and preparation is similar to the one described in section 4.2.1.2 for the conductivity measurements, with the exception that there is no guard electrode and the diameter of the top and bottom electrodes is 40 mm each.

4.2.2.3 Test procedure

The tests were performed in sequence at 40, 60, and 80 °C by the following procedure:

1. Insert test sample in test cell.
2. Set temperature, lowest first. Humidity is not controlled and is the same inside the chamber as in the laboratory.
3. Allow stabilisation of test cell and sample temperature for 24 hours.
4. Measure capacitance and permittivity of sample, from 1 to 5000 Hz in steps of 250 Hz.
5. Set next temperature, start from step 2 again.

5 Results and discussion

This chapter presents the simulated and experimental data for the PD process at DC voltage and combined DC and AC voltage. The validity of the results and that of the proposed model is discussed. The structure of the chapter is given in Fig. 5-1: In section 5.1, the measurement of the material parameters - conductivity and permittivity, is presented. The measured values are used to calculate the PD sequence input parameters for the simulation model in section 5.2. In section 5.3, the results of the experimental investigation of PD at DC voltage are discussed. In section 5.4, the results of the experimental investigation of PD at combined DC and AC voltage are discussed.

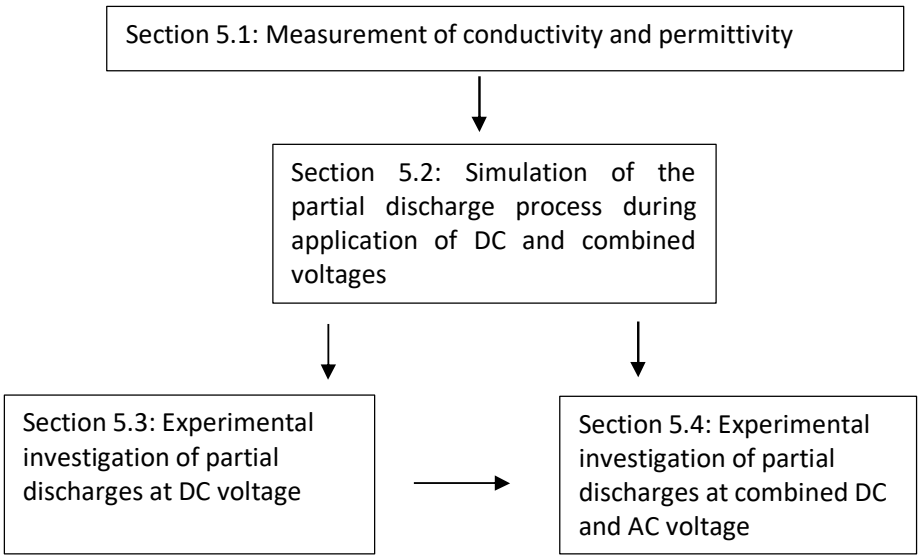

Fig. 5-1 Structure of chapter 5: Results and discussion

5.1 Measurement of conductivity and permittivity

The results and discussion for the material parameters - conductivity and permittivity, are presented in the following sections. The measured values are used to calculate the PD sequence input parameters for the simulation model in section 5.2.

5.1.1 Conductivity

The conductivity of a single PET film was measured at 40, 60, and 80 °C, using the PDC method, see Table 5-1 and Fig. 5-2. It is noted that the conductivity of biaxially oriented PET is extremely low compared to other insulation materials used in power cables. XLPE has a conductivity of around 3E-15 S/m at 19.1 kV/mm and 60°C [92], which is almost 30 times higher than the conductivity of PET at 22 kV/mm for the same temperature.

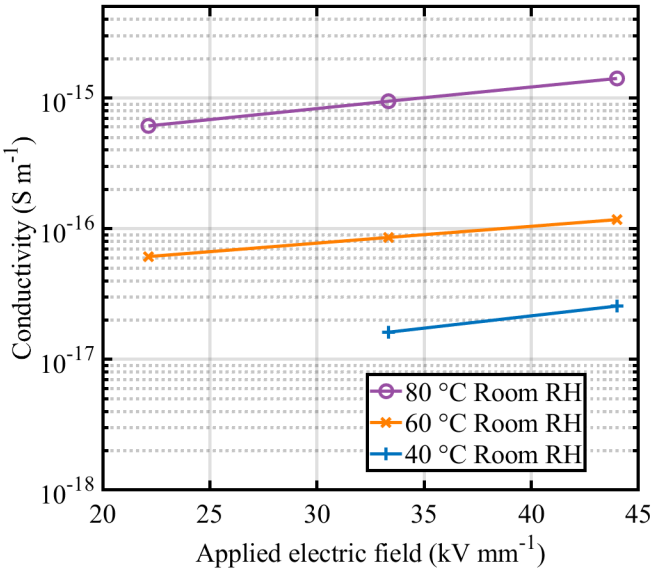

Fig. 5-2 Conductivity of PET 40 °C, 60 °C and 80 °C at 22 kV/mm, 33 kV/mm and 44 kV/mm. Thickness of PET film: 75 µm.

In the measurement at 40 °C and 22 kV/mm, the current measurement was close to the noise current band; this may explain the apparent drop in conductivity. This measurement is considered not valid.

Table 5-1 Measured conductivity in 75 µm PET film (S/m)

	DC Voltage (bulk electric field)		
Temperature	**1650 V (22 kV/mm)**	**2500 V (33 kV/mm)**	**3300 V (44 kV/mm)**
40 °C	-	1.61E-17	2.56E-17
60 °C	6.16E-17	8.58E-17	1.17E-16
80 °C	6.16E-16	9.45E-16	1.41E-15

The measured conductivity is close to the values obtained from Lilly and McDowell [100] for PET film with aluminium electrodes; they report 7.2e-16 S/m at 21 kV/mm and 78 °C, and the measured value at 22 kV/mm and 80 °C is 17% lower. Extrapolation of data from Lilly and McDowell to higher electric field strength is shown in Table 5-2. Overall, the measured values are lower, but close to the extrapolated values. Since the extrapolated values are obtained at a 2 °C lower temperature, it can be expected that the discrepancy is even higher. However, considering the large effect of inconsistent conditioning of the PET samples [101] and the uncontrolled humidity, the measurements are in good agreement with previously reported results at 80 °C. It is not possible to evaluate the values measured for lower temperatures, as no studies were found for biaxially oriented PET in the range of 40 to 60 °C and electric field strength between 22-44 kV/mm.

Table 5-2 Measured conductivity (S/m) at 80 °C versus published data

	DC Voltage (bulk electric field)		
Temperature	**1650 V (22 kV/mm)**	**2500 V (33 kV/mm)**	**3300 V (44 kV/mm)**
80 °C (measured)	6.16E-16	9.45E-16	1.41E-15
78 °C (extrapolated data, Lilly and McDowell [100])	7.57e-16 (+22.9%)	1.12e-15 (+18.5%)	1.42e-15 (+0.7%)

The difference in conductivity from 60-80 °C is consistently higher than from 40-60 °C in Fig. 5-2. This jump in the measured conductivity is supported by Neagu *et al*. [101] who observed a change in the conductivity mechanism and activation energy in the glass temperature region of PET. According to [102], the glass temperature, T_g, is 67 °C for amorphous PET and 81 °C for crystalline PET. Separate mechanical tests showed that T_g was in the region of 75-80 °C for the PET film used in this thesis, confirming that a change in activation mechanism indeed influenced the conductivity at 80 °C.

In the PD tests in sections 5.2.6.2.2 and 5.3.6, the mean electric field strength in the PET film is approximately 61.5 kV/mm at 75 °C, using (4.19). The conductivity is estimated by fitting the measured data to (4.24), and extrapolating as described in section 4.2.1.4. The change in activation energy close to the glass temperature (75-80 °C) [101] makes it difficult to fit to the entire temperature region. An alternative approach is to estimate the conductivity by fitting for the data T≤60 °C and T≥60 °C; the two estimated values of σ_b represent the lower and the upper bound. According to Table 5-3, $\sigma_b(75°C, 61.5kV/mm) \in \langle 6.1e-16, 13.5e-16 \rangle$ (S/m). Due to the lack of accurate data in this temperature region, the conductivity is estimated to $(9.8 \pm 3.7)e-16$ (S/m). Extrapolation of data from Lilly and McDowell [100] to 61.5 kV/mm at 78 °C yields a conductivity of 1.8e-15 S/m, which is in good agreement with the estimated value considering the accuracy of extrapolation and the higher temperature. The estimated value is used as input to the PD sequence parameter calculation in section 5.2.

Table 5-3 Estimation of the conductivity for E= 61.5 kV/mm and T= 75 °C.

Data points used ->		all T, all E	T<= 60 °C, all E	T>= 60 °C, all E
Fitted parameters	σ_0 (S/m)	0.0802	8.8114e-06	205.0871
	E_A (eV)	1.02	0.76	1.25
	b (eVmV^-1)	1.86e-28	1.48e-28	1.60e-28
Calculated value	**σ_b (S/m) @ 75 °C, 61.5 kV/mm**	***15.0e-16***	***6.1e-16***	***13.5e-16***

5.1.2 Permittivity

The relative permittivity was measured between 1 to 5000 Hz at 40, 60, and 80 °C, see Fig. 5-3. The permittivity varies very little with temperature in this frequency range; the value is between 3.15 and 3.2 for all measurements.

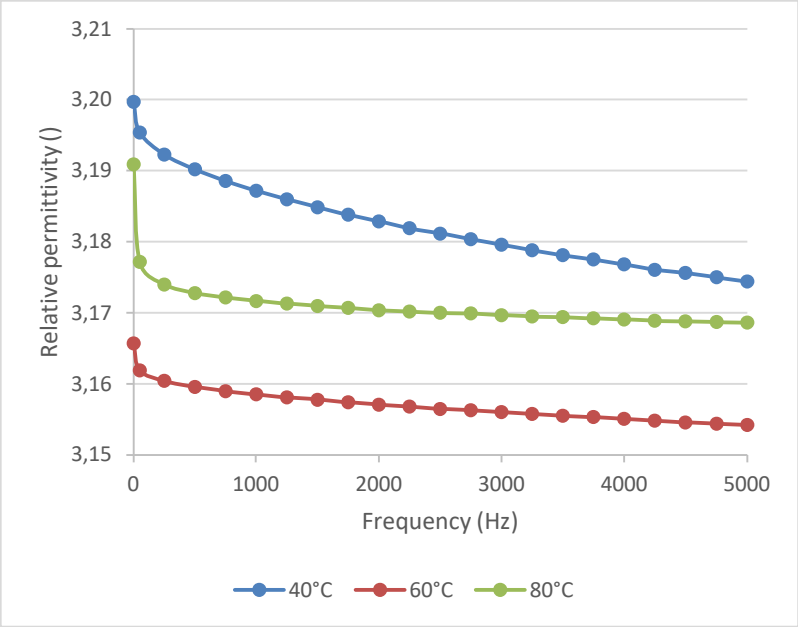

Fig. 5-3 Measurement permittivity of PET, at 40, 60, 80 °C and 1-5000 Hz. AC voltage amplitude: 3 V_{rms}. Thickness of sample: 75 µm, diameter: 40 mm.

The measured permittivity is in the range 3.15-3.2, which is somewhat lower than the value of 3.3 given in the data sheet (Hostaphan RN 50-350, measured at 23 °C for 50 and 1000 Hz). Neagu *et al*. [103] measure a relative permittivity between 3.3 and 3.4 in the same frequency and temperature range. The reason for this discrepancy is not clear, but the AC

current measurement accuracy is lower for the measurements performed on 75 µm film in this work compared to the ones on 6 µm film by Neagu *et al*. [103]. A value of 3.3 will be used as input to the PD sequence parameter calculation in section 5.2. It can be safely assumed that this value will not change significantly with temperature and AC voltage frequency. Furthermore, the permittivity of PET does not change with DC voltage as it is not a ferroelectric material, which is confirmed by experimental data from Hami *et al*. [104].

5.2 Simulation of the partial discharge process during application of DC and combined voltage

In this section, the PD process is simulated for both DC voltage and combined DC and AC voltage conditions. The structure of this section is shown in Fig. 5-4. The calculation of the input parameters is done in section 5.2.1. The theoretical effect of the AC voltage ripple on the PD sequence and the mean values are evaluated in sections 5.2.2 to 5.2.4. In section 5.2.5, the hypotheses in section 1.3 are evaluated by comparison with the simulation results. Finally, the performance and robustness of the estimators are assessed in section 5.2.6.

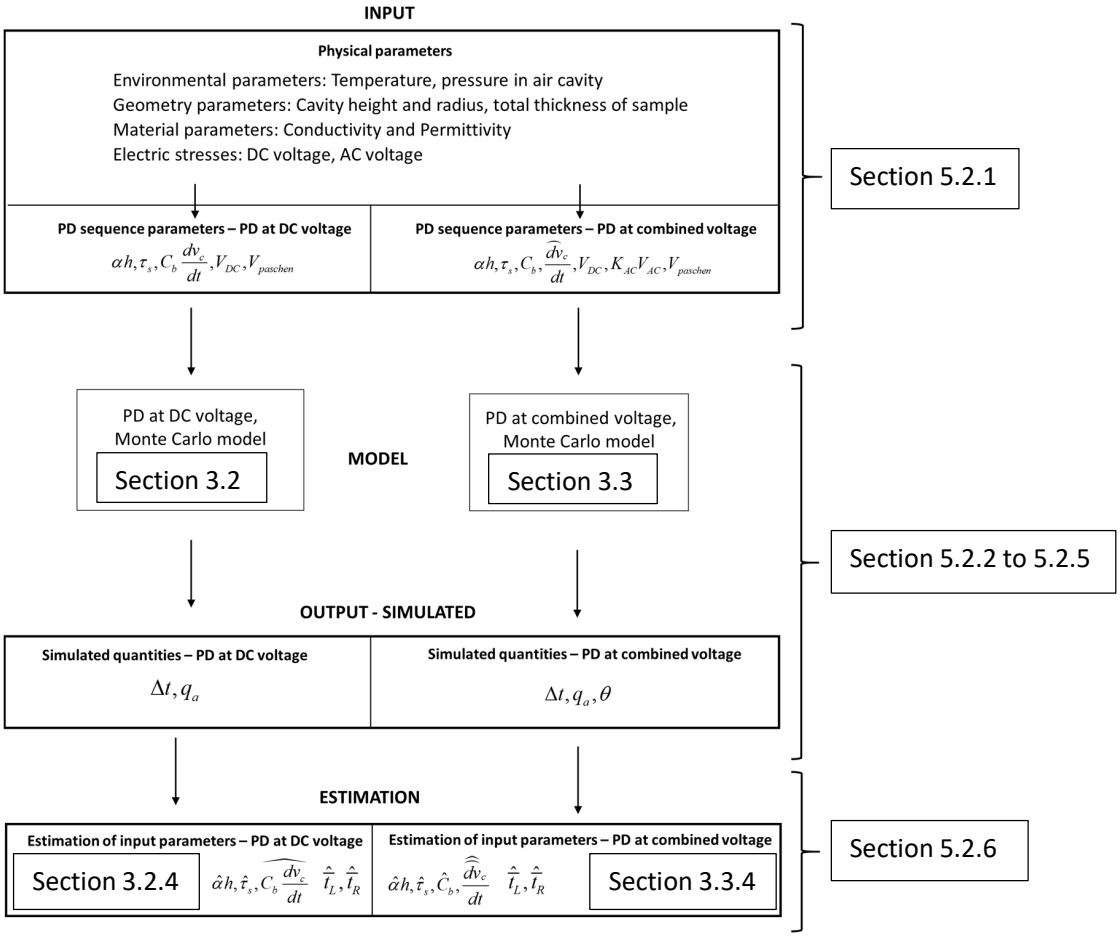

Fig. 5-4 Structure of section 5.2.

5.2.1 PD sequence parameters

In chapter 3, the PD process was characterised by the PD sequence parameters, which are calculated for DC and combined voltages using the physical parameters, see section 3.2.1.1 and section 3.3.1.1.

The conductivity and relative permittivity used in the PD models are 9.8e-16 S/m and 3.3 respectively, at 61.5 kV/mm and 75 °C. The DC voltage is 10 kV, and the AC voltage ripple amplitude is 62.2 V. The physical values are summarised in Table 5-4, while the PD sequence parameters are summarised in Table 5-5, calculated as follows:

1) $K_{AC} = 0.62$, from (3.56) using permittivity from section 5.1.2.
2) The ignition voltage in the cavity is 765 V_{peak} at 75 µm cavity depth and atmospheric pressure according to the empirical equation of Ritz [87], which is close to 790 V_{peak} found by interpolation in the tables of Dakin [89]. Thus, the PDIV value for AC is:

$$PDIV_{AC} = \frac{V_{paschen}}{K_{AC}} = \frac{765}{0.62} = 1234 V_{peak} \quad (5.1)$$

3) $\alpha h \approx 7$ for cavity height h = 75 µm, atmospheric pressure and critical electric field strength 10 kV/mm, $V_{paschen}/h$, with (2.38) from Kontaratos [69].
4) A value of $\tau_s = 5\ s$ is chosen. The mean time for detrapping of electrons in HVDC cables during service conditions (20 kV/mm, 76 °C) is in the order of seconds, according to Serra *et al*. [105]. The mean statistical waiting time for a discharge to be initiated will be probably higher, as not all detrapped electrons will cause a discharge.
5) $C_b = 0.61 pF$, from (3.1) using permittivity from section 5.1.2.
6) $\frac{dv_c}{dt} \approx \frac{\widehat{dv_c}}{dt} = 0.19\ \ V/s$, from (3.2) and (3.55), using conductivity from section 5.1.1 and permittivity from section 5.1.2.

Table 5-4 Material properties, geometry and voltages

Parameter	Value	Parameter	Value
Electrode separation, H	225 µm	Tau, τ	47 885 s
Cavity height, h	75 µm	DC voltage, V_{DC}	10 000 V
Cavity radius, r_{cav}	1 mm	AC voltage amplitude, $\hat{V}_{AC}$	62.2 V_{peak} (44 V_{rms})
Permittivity of series dielectric, ε_b	3.3	Frequency AC voltage, f_{AC}	>50 Hz
Permittivity of air in cavity, ε_c	1	Paschen voltage, and AC PD inception voltage	$V_{paschen}$ = 765 V_{peak} $PDIV_{AC} = 1234V_{peak}$ $PDIV_{AC} = 873V_{rms}$
Conductivity of series dielectric, σ_b	9.8e-16 S/m	Equivalent conductivity of cavity, including surface and gas conductivity, σ_c	0 S/m

Table 5-5 PD sequence parameters, model input

Parameter	Value	Parameter	Values
Townsend coefficient product, αh	7	Capacitance of dielectric in series with cavity, C_b	0.61 pF
Mean statistical waiting time, τ_s	5 s	Slope of cavity voltage, $\frac{dv_c}{dt} \approx \widehat{\frac{dv_c}{dt}}$	0.19 V per second

5.2.2 The PD sequence

Data are simulated for the PD sequence both at DC voltage and at combined voltage, to evaluate the effect of the AC ripple on the discharge magnitude and the separation time. The Monte Carlo PD models described in section 3.2 and section 3.3. are used, with input parameters from Table 5-5.

The simulated PD sequence for a 12-hour window is shown in Fig. 5-5, under steady-state conditions. The superimposed AC voltage ripple with amplitude 62.2 V results in longer separation times (Fig. 5-5d), higher discharge magnitude (Fig. 5-5b), as well as larger scatter and stronger fluctuation of their moving average value.

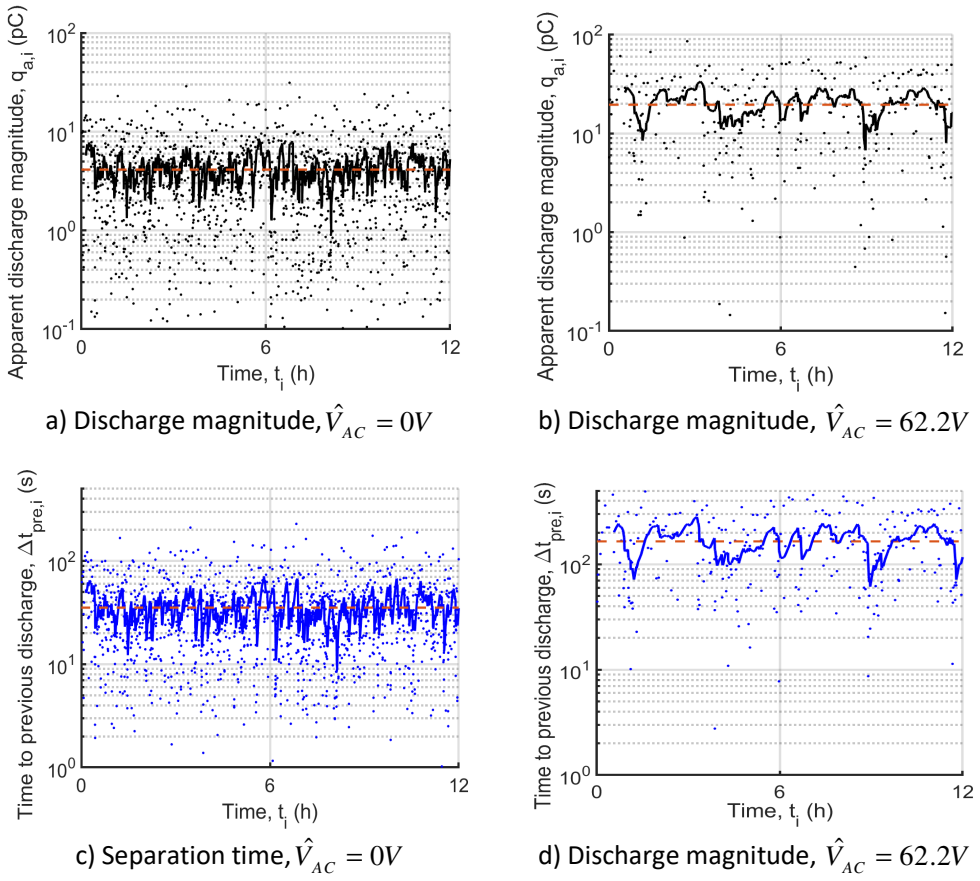

a) Discharge magnitude, $\hat{V}_{AC} = 0V$

b) Discharge magnitude, $\hat{V}_{AC} = 62.2V$

c) Separation time, $\hat{V}_{AC} = 0V$

d) Discharge magnitude, $\hat{V}_{AC} = 62.2V$

Fig. 5-5 Data from the PD sequence models at DC conditions a), c), V_{DC} = 10 kV, and combined voltage b), d), V_{DC} = 10 kV and V_{AC} = 62.2 V. Dots = individual magnitude or time to previous discharge, dashed line = population mean, line = moving average (last 10 values).

The behaviour can be explained in terms of the model presented in section 3.3. The mean statistical waiting time for start electrons is the same during DC voltage and combined voltage application. For DC conditions, the cavity voltage increases monotonically and will stay above the critical voltage until a start electron arrives to initiate a discharge, and thus

the mean time lag will be equal to the mean statistical waiting time. For combined voltage, however, the cavity voltage is above the critical voltage for only a short interval of the AC period time, which decreases the probability for a discharge to occur per time. The arrival of a start electron can occur at any time during the AC voltage period but does not cause a discharge unless it arrives in the short time interval when the cavity voltage is above the critical value. This causes a higher mean time lag than the mean statistical waiting time, and higher discharge magnitude and separation time.

The classic model of Rogers [26] and Densley [27, p. 436] predicts a decrease in separation time when an AC ripple is added to the DC voltage, which is contrary to the prediction of the model presented in this thesis. The main difference between the model presented in section 3.3 compared to the classic model is the use of a stochastic time lag. The stochastic time lag causes discharges to occur at variable ignition voltage, which results in a variable discharge magnitude and separation time. The classic model, however, assumes that discharges occur as the cavity voltage reaches a predetermined ignition voltage.

When an AC ripple is applied, the classic model states that a discharge will occur when the sum of the peak of the AC voltage and the DC voltage over the cavity reaches the ignition voltage. If the DC offset of the cavity voltage always starts at the same residual voltage, the DC offset needs to increase by $\Delta V_c - K_{AC}\hat{V}_{AC}$, thus reducing the separation time, according to (2.43). There are at least two challenges with the validity of the classic model:

1) The DC offset of the cavity voltage does not always start at the residual voltage. If the discharge occurs close to the peak of the AC voltage, then the voltage drops to the residual voltage and the DC offset is $K_{AC}\hat{V}_{AC}$ below the residual voltage. The discharge separation time should then follow (2.18), and not (2.43). The result would be that the discharge separation time does not change significantly compared to DC voltage conditions, contradicting the prediction of the classic model.
2) Physically, the time lag determines the ignition voltage, and not vice versa. In the classic model approach, the ignition voltage determines the time lag. This can be regarded as an artificial relationship which does not represent the causality of the underlying process.

The stochastic time lag describes the PD process in a way that conserves the causality and seems to explain the effect of an AC ripple both theoretically and experimentally, as will be discussed in section 5.3.6.

A strong correlation between the moving average of the discharge magnitude and the separation time can be observed for DC conditions, Fig. 5-6, and combined voltage conditions, Fig. 5-5b and Fig. 5-5d. This positive correlation is described by the pulse correlation equation in (3.30) at DC voltage, and (3.98) at combined voltage. It is also reflected in the predicted ratio of the mean discharge magnitude by separation time in (3.36) at DC voltage, and (3.98) at combined voltage.

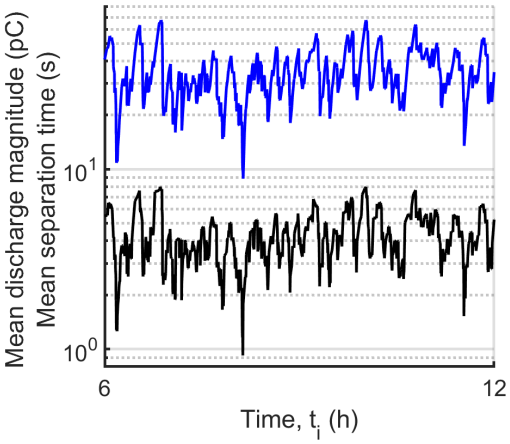

Fig. 5-6 Discharge magnitude and separation time moving average for last 10 discharges between 6 to 12 hours, simulated data for PD at DC voltage.

5.2.3 Phase resolved partial discharge analysis for combined voltage conditions

Partial discharges at AC voltage are often analysed using phase resolved partial discharge (PRPD) diagrams. At DC voltage, there is no information about phase-of-occurrence, so registering discharges with the AC power frequency voltage as reference gives no correlation, see Fig. 5-7a. For combined voltage, however, it is possible to register the phase-of-occurrence and analyse the correlation between phase position and discharge occurrence, see Fig. 5-7b. The model predicts that the discharges occur close to the peak of the AC voltage; this has been observed experimentally by Dezenzo [12]. When the stochastic waiting time is much higher than the AC period time, the probability of a discharge occurring before the peak of the AC voltage is the same as that after the peak, and the discharge pattern is therefore symmetrical around the peak.

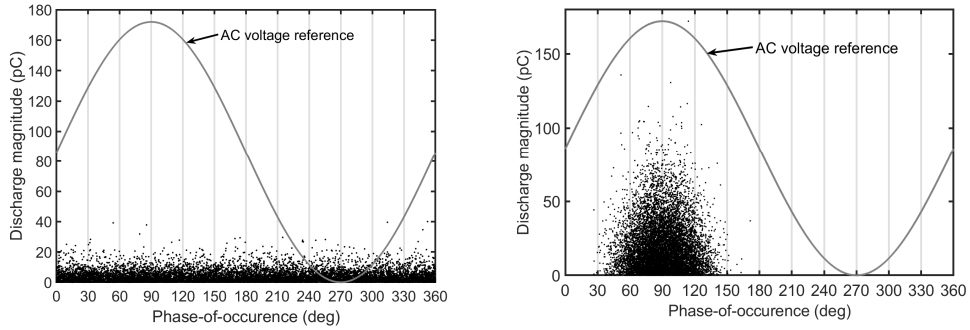

a) PRPD, $\hat{V}_{AC} = 0V$

b) PRPD, $\hat{V}_{AC} = 62.2V$

Fig. 5-7 PRPD diagrams for PD at a) DC voltage, and b) Combined voltage.

5.2.4 Mean separation time and magnitude

The predicted mean discharge magnitude and separation time increases by a factor of almost 5 by superimposing the AC voltage, compared to DC voltage conditions, see Table 5-6. The expected increase is substantial, even when the AC ripple amplitude is only 5 % of the AC PD inception voltage. However, the ratio of discharge magnitude and separation time does not change appreciably. This is also expected since $\frac{dv_c}{dt} \approx \frac{\widehat{dv_c}}{dt}$ when $K_{AC}\hat{V}_{AC} \ll V_{DC}$, then $\left(\frac{\overline{q_a}}{\Delta\overline{t}}\right)^{DC} \approx \left(\frac{\overline{q_a}}{\Delta\overline{t}}\right)^{DCAC}$ according to (3.36).

The values from the analytical model are very close to the Monte Carlo model at DC voltage, but are slightly lower at combined voltage. The PD sequence model sets the recovery time to zero whenever a rapid recovery of the cavity voltage occurs, as mentioned in section 3.3.2.6. The analytical model, however, accepts a negative recovery time which on average leads to a slightly lower discharge magnitude and separation time. Despite the apparent unphysical notion of a negative recovery time, the two models correspond well, essentially predicting the same mean values. However, the causality of the PD process is represented better in the PD sequence model.

Table 5-6 Output for Vac = 0 V (DC) and Vac = 62.2 V (DC +AC), comparison analytical and Monte Carlo models.

	DC analytical	DC Monte Carlo, $n = 10000$	DC + AC analytical	DC + AC Monte Carlo, $n = 10000$
$\overline{\Delta t}$ (s)	35.0	35.4	158.4	165.2
$\overline{t_L}$ (s)	5.0	5.1	34.1	34.4
$\overline{t_R}$ (s)	30.0	30.3	124.4	130.8
$\frac{\overline{t_R}}{\overline{t_L}}$	6	5.9	3.6	3.8
$\overline{q_a}$ (pC)	4.1	4.2	18.8	19.5
$\frac{\overline{q_a}}{\Delta\overline{t}}$ (pC/s)	0.12	0.12	0.12	0.12

It is noted that the ratio of the mean recovery time to the mean time lag decreases with AC ripple voltage amplitude. The reduction of the recovery time relative to the time lag can

be explained as follows: the recovery time decreases for discharges that do not occur at the peak of the AC voltage. The recovery time can even be zero, as described in section 3.2.2.6, referred to as the rapid recovery effect. The time lag is not affected by the phase-of-occurrence, so there is an effective reduction in the recovery time relative to the time lag.

5.2.4.1 Effect of detection threshold

In an experimental setup there will always be a magnitude detection limit which affects the measured mean discharge magnitude and separation time. The output data of the PD sequence model in section 5.2.2 was digitally filtered by a detection threshold value between 0-12 pC. The calculated mean values are shown as a function of the detection threshold value in Fig. 5-8.

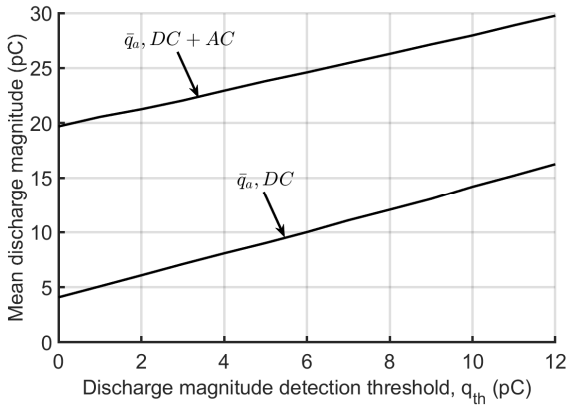

a)

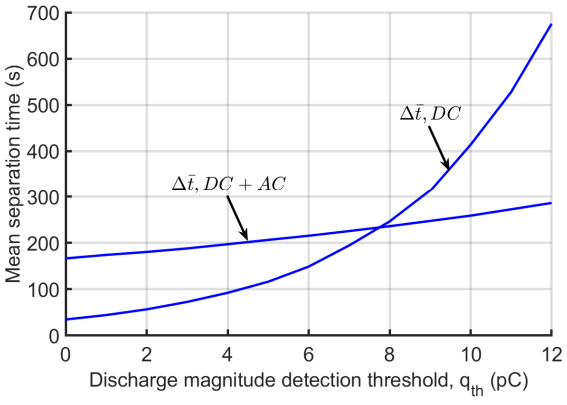

b)

Fig. 5-8 a) Simulated mean discharge magnitude and b) Mean discharge separation time, as a function of the detection threshold value.

The mean discharge magnitude increases linearly with the detection threshold value for PD at DC and combined voltage. The discharge magnitude is always higher at combined voltage, compared to DC voltage. The mean separation time increases with a higher detection threshold; a detection threshold of over 8 pC results in a mean separation time that is higher for DC voltage than for combined voltage. This effect may be explained by the discharge magnitude distributions in Fig. 5-9; when the detection threshold increases, a larger fraction of the discharges at DC voltage is filtered out, compared to the discharges at combined voltage. The mean separation time increases more at DC voltage, as the detection threshold value increases. Thus, from a theoretical point of view, it is important to keep the detection threshold as low as possible, as a high detection threshold value may erroneously indicate that the separation time is higher at DC voltage.

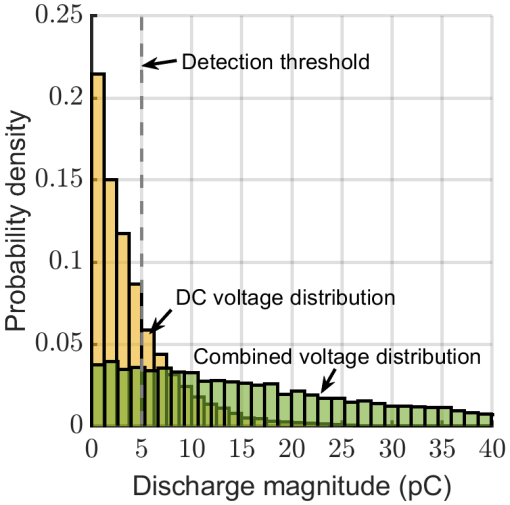

Fig. 5-9 Simulated discharge magnitude probability density for DC and combined voltage. There is a larger fraction of discharges under the detection threshold at DC voltage.

5.2.5 Evaluation of hypotheses by simulation result

The predicted relative change in separation time and discharge magnitude, from DC voltage conditions to combined voltage conditions, are shown in Fig. 5-10. The expressions for the relative change in mean values are given in section 3.3.3.1. Both the analytical model and the PD sequence model predict an increase in the mean separation time, thus contradicting hypothesis H.1: The discharge separation time decreases with increasing AC ripple voltage amplitude. The main reason for this prediction is the reduction of the start electron generation rate, or equivalently, an increase in the effective mean time lag, described in section 3.3.2.3. In section 5.2.4.1, it was found that the discharge separation time may be lower at combined voltage conditions, but only if the discharge detection threshold value is too high.

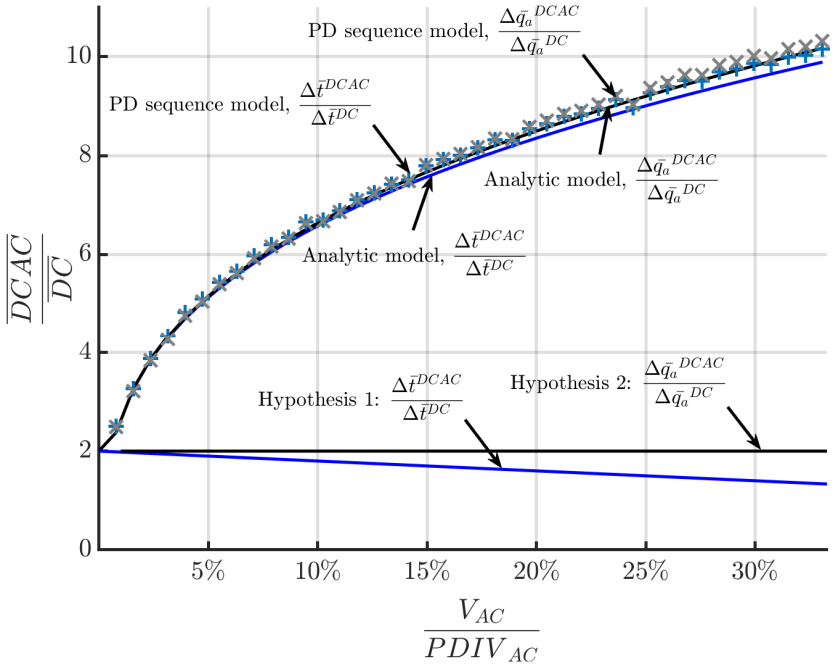

Fig. 5-10 Simulated relative increase in mean discharge separation time and apparent magnitude for an AC ripple amplitude between 0 to 33 % of $PDIV_{AC}$. n = 10 000 number of discharges simulated in PD sequence model.

The model predicts a relative increase in discharge magnitude with increasing AC ripple magnitude, contradicting hypothesis H.2: The discharge magnitude is constant when the AC ripple voltage amplitude increases.

A higher AC frequency will not change the total time the cavity voltage is above the critical voltage, and will not change the effective time lag. This statement is only valid when the AC time period is significantly shorter than the mean statistical waiting time. The model is in line with hypothesis H.3: The discharge separation time and discharge magnitude are not influenced by the frequency of the AC ripple voltage.

The hypotheses are evaluated based on the experimental results in section 5.3.6.

5.2.6 Evaluation of estimator performance

For the estimators to be of value, they must satisfy the requirements stated in section 2.3.2. The input data to the estimation methods is generated by the Monte Carlo PD models with PD sequence parameters from Table 5-5, see Fig. 5-11. The consistency and performance of the proposed estimators in sections 3.2.4 and 3.3.4 are evaluated in section 5.2.6.1. The robustness of the estimators is evaluated in section 5.2.6.2.

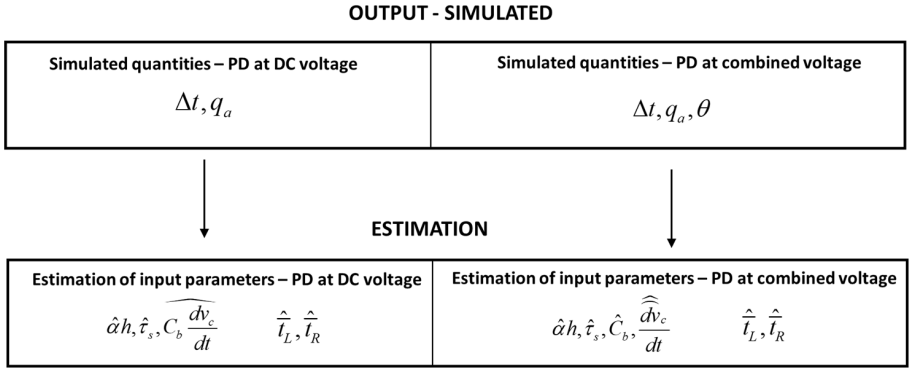

Fig. 5-11 Estimation of PD sequence parameters from simulated data.

5.2.6.1 Consistency and performance

An estimator is consistent if it approaches the real value when the number of observations n increases. This means that the bias and confidence intervals should be smaller when the number of observations increases. The root mean squared error (RMSE), defined in section 2.3.3, is used to evaluate the performance of the estimators. The RMSE value is a sum of the bias and the variance, and the closer the value is to zero, the better.

The PD sequence parameters are estimated based on the unfiltered simulated quantities, i.e. the discharge magnitude detection threshold is zero. This represents an ideal condition, were all the information is available. The DC voltage is 10 kV and the AC ripple amplitude is 62.2 V. Fig. 5-12 shows the estimated mean time lag and mean recovery time at DC voltage and combined voltage, presented as a ratio of their real values as given in Table 5-6. The estimated value and the confidence interval refer to the left y-axis and the corresponding RMSE value refers to the right y-axis. All the estimators can be said to be consistent as more data is available; the confidence intervals narrow, and the estimated values approach the real values. The MoM estimator at combined voltage performs better than the estimators at DC voltage, as the confidence interval is smaller for the same number of simulated discharges. At DC voltage, the OLS estimator performs better than the MoM method, i.e. the RMSE value is lower for the OLS estimator at the same number of simulated discharges.

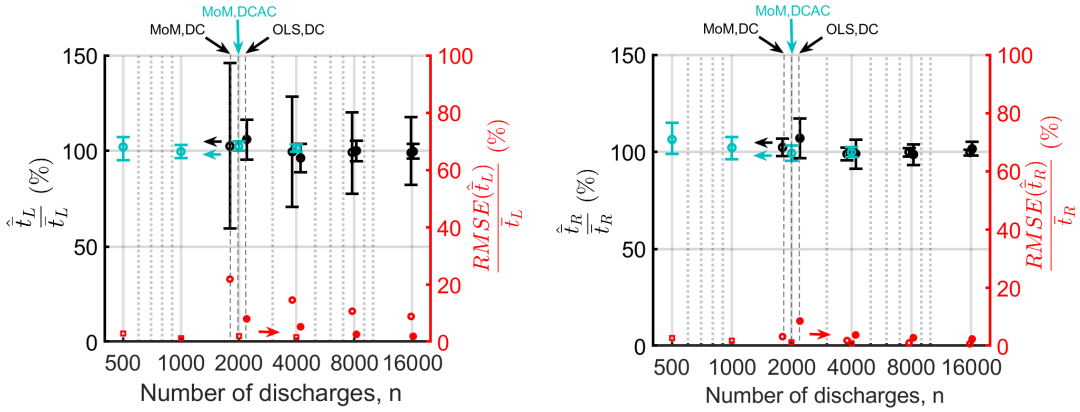

Fig. 5-12 Estimation of PD sequence parameters from simulated data at DC and combined voltage, as a function of the number of discharges. Whiskers: 95% confidence interval. a) Estimated mean time lag. b) Estimated mean recovery time.

The observations above indicate that proposed estimators satisfy the requirements, and are valid from a theoretical point of view. In the next section, some aspects of the robustness of the estimators are evaluated.

5.2.6.2 Robustness

The robustness of an estimator is its ability to estimate the real PD sequence parameters with satisfactory accuracy even under data loss or small departures from model assumptions. During PD tests, there can be considerable data loss due to the discharge magnitude detection threshold for the test setup. The effect of a detection threshold on the estimators at DC and combined voltages is evaluated in sections 5.2.6.2.1 and 5.2.6.2.2.

The DC voltage sources used in DC PD test setups may have an AC ripple, as is common for the Cockcroft-Walton DC sources used in many high voltage laboratories. The AC ripple represents a departure from model assumptions for the DC estimation methods; the robustness of the estimators for this type of deviation is evaluated in section 5.2.6.2.3.

5.2.6.2.1 Detection threshold effect on DC estimation methods

In this section, the PD data is generated from the DC voltage model. The simulated discharges are filtered by the discharge detection threshold. Since the discharge magnitude is so low during PD tests at DC voltage, the detection threshold has a significant effect on the amount of data that can be used for estimation. The threshold already leads to data loss at a detection threshold of 3 pC, and the estimated values deviate considerably from the real values, see Fig. 5-13. This indicates that test setups used for DC voltage PD detection should have a very low detection threshold to conserve information in the PD

data. The test setup used for this thesis has a threshold of 0.5 pC, which would lead to a small bias in the estimators, but probably at a tolerable level, within ±25% of the real value.

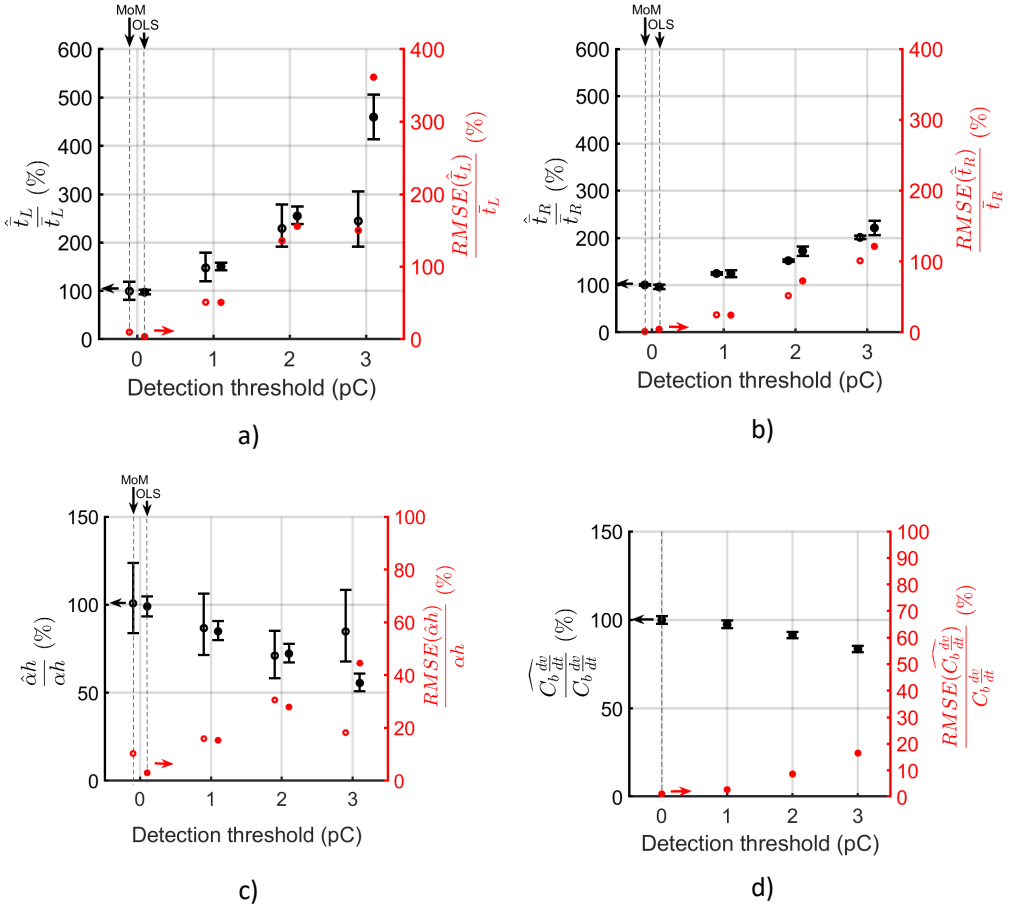

Fig. 5-13 Estimation of PD sequence parameters from simulated data at DC voltage, as a function of the discharge magnitude detection threshold value. n = 10 000. a) The mean time lag, b) The mean recovery time, c) The Townsend coefficient product, d) The product $C_b \frac{dv}{dt}$.

The overall observations of estimation on simulated PD data with a detection threshold are as follows:

- The detection threshold can lead to considerable overestimation of mean time lag and recovery time, see Fig. 5-13a and Fig. 5-13b. At 2 pC detection threshold the estimated time lag are 2.5 times the real value, and the mean recovery time is around 1.7 times the real value. The mean time lag estimation is more sensitive to the data loss than the recovery time estimation.

- The OLS estimated Townsend coefficient value decreases as a function of the detection threshold, whereas the value from the MoM estimator decreases first and then increases again. The confidence interval of the OLS estimator is smaller and the bias is more predictable, so the OLS estimator is considered more robust for the Townsend coefficient.
- The $\widehat{C_b \frac{dv_c}{dt}}$ estimator is the most robust, the value of which is underestimated by 20% at 3 pC detection threshold, see Fig. 5-13d.

5.2.6.2.2 Detection threshold effect on the MoM combined voltage estimation method

In this section, PD data is generated from the combined voltage model with an AC ripple of 62.2 V amplitude. The simulated discharges are filtered by the discharge detection threshold. The MoM combined voltage estimation performs well for the mean time lag and the mean recovery time, even at high detection thresholds, see Fig. 5-14. The was also observed for the other PD sequence parameters, the RMSE value was lower than 15% for all values. The main reason is that the data loss is less severe for a certain detection threshold, since the mean discharge magnitude is significantly higher at combined voltage.

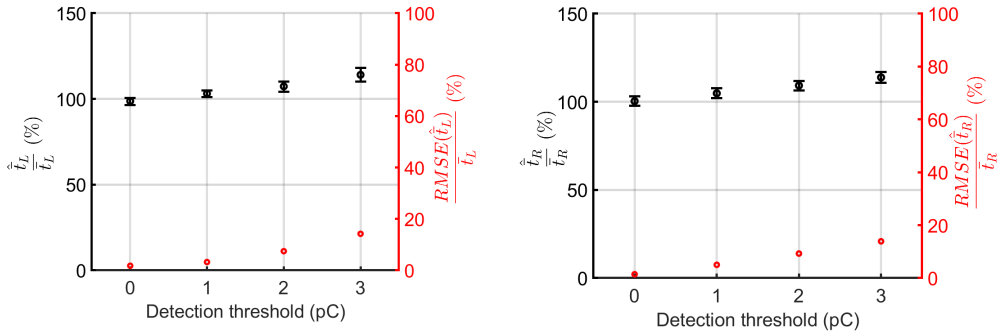

Fig. 5-14 Estimation of PD sequence parameters from simulated data at combined voltage, as a function of the discharge magnitude detection threshold value. V_{AC} = 62.2 V, n = 10 000. a) The mean time lag, b) The mean recovery time.

5.2.6.2.3 DC estimation methods on combined voltage PD process data

In this section, the PD sequence parameters are estimated by the DC estimators, but the PD data is generated from the combined voltage model with an AC ripple of 10 V amplitude. The use of the DC MoM and OLS estimation method on data generated from a combined voltage PD process leads to severe overestimation of time lag and recovery time, see Fig. 5-15a and Fig. 5-15b. The MoM estimator performs better for the mean time lag and the

recovery time; the RMSE value is lower due to the lower bias. If an accurate estimation of the time lag and recovery time is needed, then the DC voltage supply should be of a low AC ripple design. However, the $\hat{\alpha}h$ OLS estimator and the $\widehat{C_b \frac{dv_c}{dt}}$ estimator are robust for an AC ripple voltage, giving estimated values wihtin 10% of the real value and narrow confidence intervals if the detection threshold is below 3 pC. The MoM estimator of $\hat{\alpha}h$ is less robust than the OLS estimator on data generated from a combined voltage PD process.

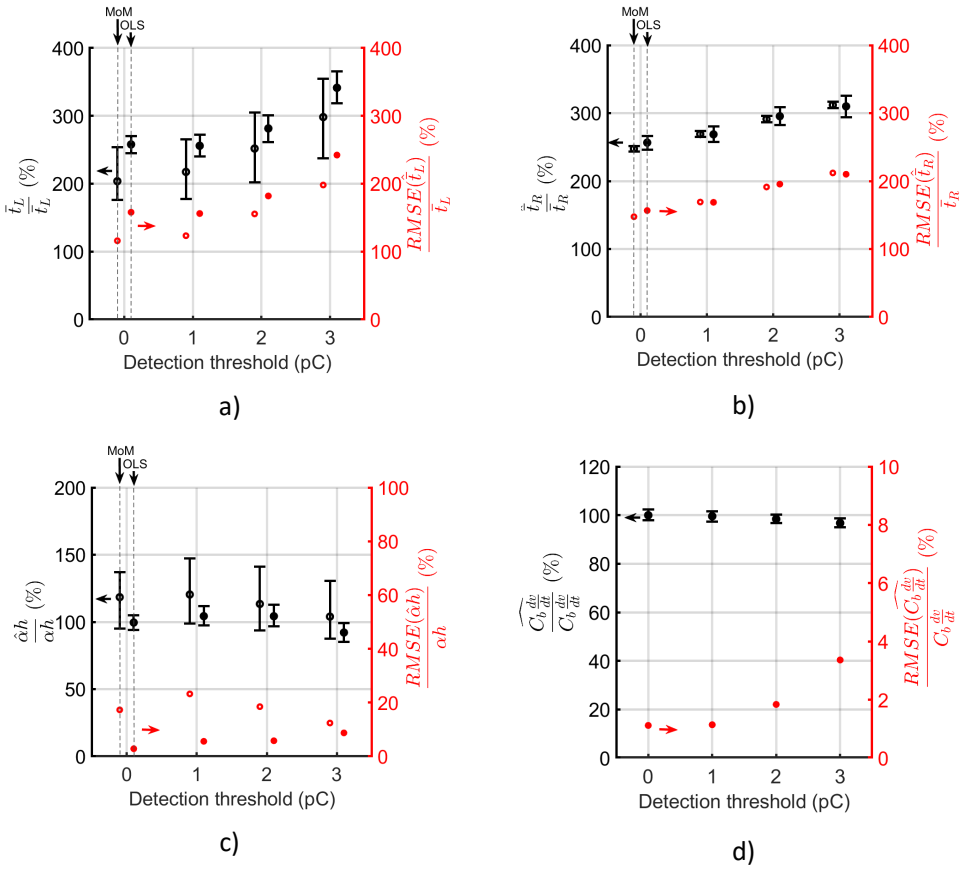

Fig. 5-15 DC estimation methods on simulated data at combined voltage, values plotted as a function of the discharge magnitude detection threshold value. V_{AC} = 10 V, n = 10 000. a) The mean time lag, b) The mean recovery time, c) The Townsend coefficient product, d) The product $C_b \frac{dv}{dt}$.

5.2.7 Summary

The main observations from the simulated discharge magnitude and the separation time at DC voltage and combined DC and AC voltage are as follows:

- Application of an AC voltage ripple results in longer separation times, higher discharge magnitude, as well as larger scatter and stronger fluctuation of their moving average value. The predicted mean discharge magnitude and separation time increases by a factor of almost 5 at an AC voltage ripple with amplitude 62.2 V, compared to DC voltage conditions. The proposed model contradicts hypotheses H.1 and H.2.
- A high detection threshold value may erroneously indicate that the mean separation time is higher at DC voltage.
- The value of the mean separation time and discharge magnitude at combined voltage is frequency independent, in line with hypothesis H.3.
- The model predicts that discharges occur close to the peak of the AC voltage, shown as a symmetrical pattern in a PRPD diagram.
- The mean discharge magnitude per separation time does not change appreciably with the application of an AC voltage ripple, if $K_{AC}\hat{V}_{AC} \ll V_{DC}$.

The observations for the proposed estimators are as follows:

- All estimators, at DC and combined voltages, are consistent and have a low RMSE value under ideal conditions.
- The DC estimators are most sensitive to the discharge detection threshold; the estimated values deviate considerably from the real values at a detection threshold of 3 pC. This indicates that test setups used for DC voltage PD detection should have a very low detection threshold to conserve information in the PD data.
- The MoM estimator at combined voltage is less sensitive to the detection threshold because less discharges, and less information, are filtered out at combined voltage.
- The mean time lag and the mean recovery time are overestimated if extracted using a DC estimator on data from a combined voltage PD process.
- The DC OLS estimated value $\hat{\alpha}h$ is close to the real value even if extracted using data from a combined voltage PD process.
- The estimated value of $\widehat{C_b \frac{dv_c}{dt}}$ is close to the real value even if extracted using data from a combined voltage PD process.

5.3 Experimental investigation of partial discharges at DC voltage

In this section, partial discharges are measured during the application of DC voltage, and compared to the predictions of the DC PD model developed in section 3.2. The PD sequence parameters are estimated using the methods developed in section 3.2.4.

5.3.1 The PD sequence

The measured discharge data for the DC test sequence is shown in Fig. 5-16. The DC test voltage was 10 kV and the temperature 75 °C during all measurements. The test sequence data is divided into stages of 6 hours each, and the total measuring time is 42 hours. It was not possible to verify the unipolarity of the discharges at DC voltage. All discharges above approximately 10 pC were of one polarity; smaller discharges were registered at both polarities. The frequency band measurement distorts the original PD current signal, resulting in an oscillating signal which makes it difficult to discern the polarity at small PD current amplitudes. For clarity of presentation, the apparent discharge magnitude is always given by its absolute value, i.e. positive polarity.

During the first 6 hours the mean separation time increases from 10 seconds to around 30 seconds, and the mean separation time is constant for the remaining test time. The transient behaviour during the first 6 hours is consistent with the decreasing polarisation current after DC voltage application, before the conductivity of the material can be considered constant, as mentioned in section 2.1.2.1. The same pattern is mirrored for the discharge magnitude, starting at around 3 pC and then plateauing at around 15 pC within the first 6 hours, reaching a steady-state condition. Some of the discharges are close to the detection threshold of 0.5 pC; discharges probably occurred in the cavity below the detection threshold as well.

During the DC test series, the AC source was connected to the circuit, but the AC voltage was set to zero. The AC source introduced a small ripple during the PD tests, even if the AC voltage was set to zero. The ripple amplitude was measured to be 10 V, with AC period time around 20 ms, see Appendix D.2 . It is plausible that the ripple caused higher discharges and longer separation times than what would have been measured at DC voltage without any AC voltage ripple, as predicted by model simulations in section 5.2.2 and measurements in section 5.4.1.

A rule of thumb is that the diameter of a streamer-like discharge channel is approximately equal to the cavity height [106], which is supported by optical observation [81]. It would be possible to have multiple discharge sites in the 2 mm diameter cavity, as a streamer-like discharge will have channel diameter in the order of 0.1 mm. Indication of multiple discharge sites in an internal cavity is the occurrence of several discharge bands in the $t - q_a$ graphs [8, p. 85]. However, in Fig. 5-16a, the discharges are concentrated within one discharge band, which indicates that there is only one discharge site. Furthermore, in Fig. 5-17, a strong correlation between the apparent discharge magnitude and the separation time is observed, corresponding well to the simulated results in section 5.2.2. Beyer [8, p. 78] observes a loss of this correlation for a cavity with multiple discharging sites. The

observed correlation between $t - q_a$ and $t - \Delta t$, and only one discharge band in $t - q_a$ is a strong indication that the registered discharges originate from Townsend-like discharges that cover the surface of the cavity. This is also in line with the observations of Fromm [44, p. 38] for a test sample with a cavity of similar dimensions and the same applied DC voltage.

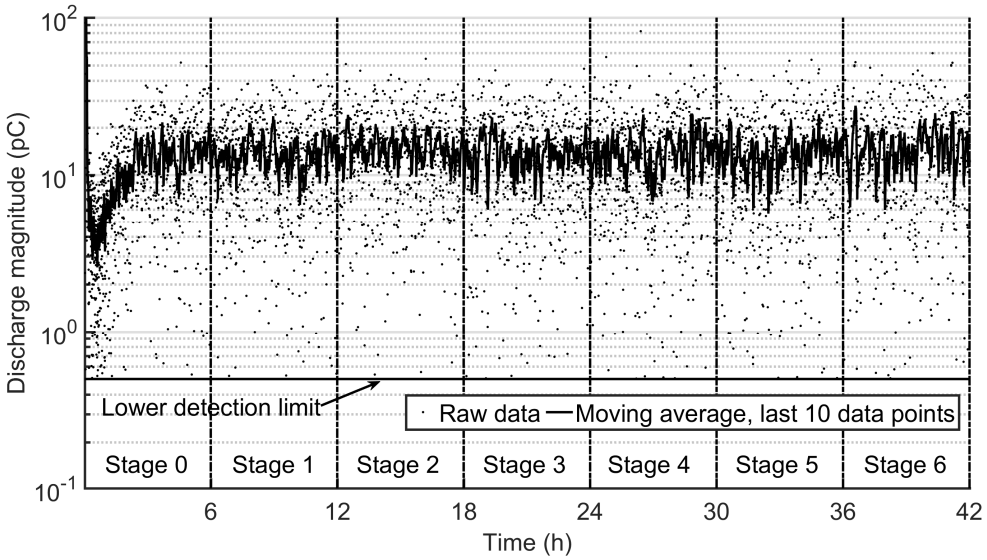

a)

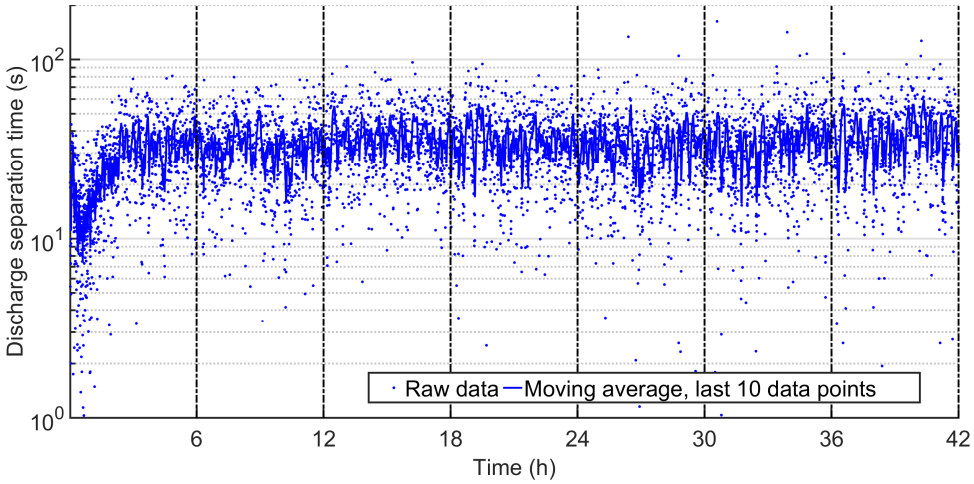

b)

Fig. 5-16 Measured PD sequence data for DC voltage; a) Apparent discharge magnitude, b) Discharge separation time. Test sequence 4, DC test series.

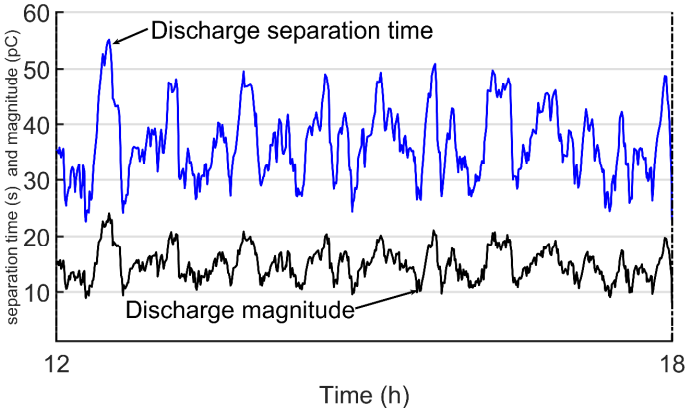

Fig. 5-17 Moving average for last 10 discharges between 12 to 18 hours, stage 2. Measurement from test sequence 4, DC test series.

5.3.2 Mean separation time and magnitude

The mean and median values for the complete DC test series are given in Fig. 5-18. The measured mean discharge separation time is between 13 and 54 seconds, for the whole DC test series. The measured mean discharge magnitude is between 4.5 to 18.5 pC. Using the model with input as in section 5.2.1 it is estimated that the unwanted AC ripple caused a doubling of the mean discharge magnitude and separation time.

In the PDIV test performed just before test sequence 2, the AC inception voltage was measured at 1 kV_{rms}, which is 15% higher than the predicted value in section 5.2.1. Around 30 000 discharges occurred during the PDIV test, and the apparent discharge magnitude was between 600 and 800 pC. The measurements at DC voltage show 4-5 orders higher mean discharge separation time and 2-3 orders lower mean discharge magnitude, compared to AC discharges measured under PDIV tests. Beg and Salvage observed the same for similar cavity dimensions, in [107] and [108].

The PDIV test resulted in a decrease of the mean discharge magnitude and separation time by almost 75% from sequence 1 to sequence 2. Steinberg and Salvage [109] have observed the same effect. The discharge process under the AC PDIV test may deposit charges on both cavity surfaces, and the charge decay through the dielectric is very slow due to the extremely high resistivity of biaxial oriented PET. Thus, the PDIV test may cause higher availability of start electrons and lowers the statistical time lag, reducing the subsequent discharge separation time and magnitude. The effect is temporary, and the measured discharge magnitude and the separation time in sequence 5 are close to the values measured in sequence 1, before the PDIV test.

After sequence 2, the discharge separation time increases; this may be attributed to depletion of available start electrons in shallow traps deposited during the PDIV test. Whenever a discharge occurs due to surface emission, the number of start electrons that

are available from shallow traps at the cavity surface decreases, thus increasing the stochastic waiting time. Grounding can have a similar effect, by moving electrons from shallow traps at the surface into deeper traps within the bulk of the dielectric. Grounding seems to have a minor effect; the increase in the separation time can be larger within a test sequence than before and after the grounding period. The decrease of start electrons in shallow traps will lead to larger discharges and longer discharge separation times. Eventually, a stabilisation of discharge separation time may occur. It is not possible to conclude that the PD process has stabilised in the last test sequence, but the values are close to the ones measured in the first test sequence.

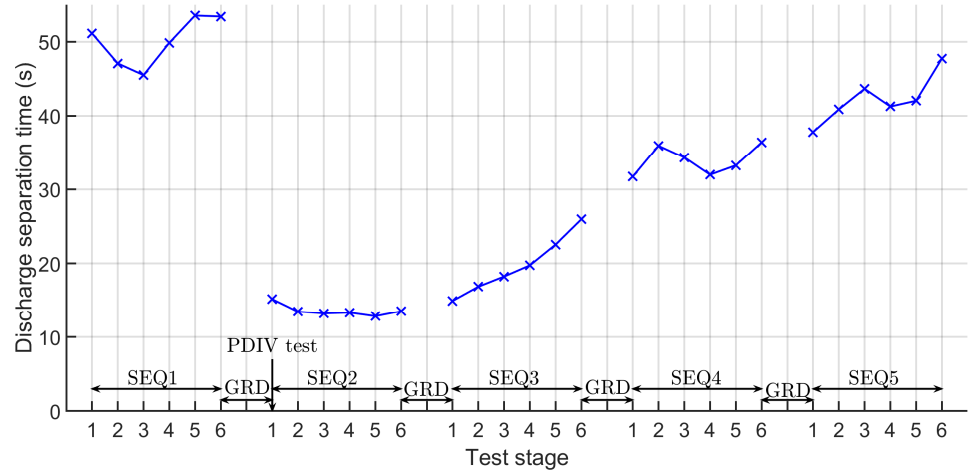

a)

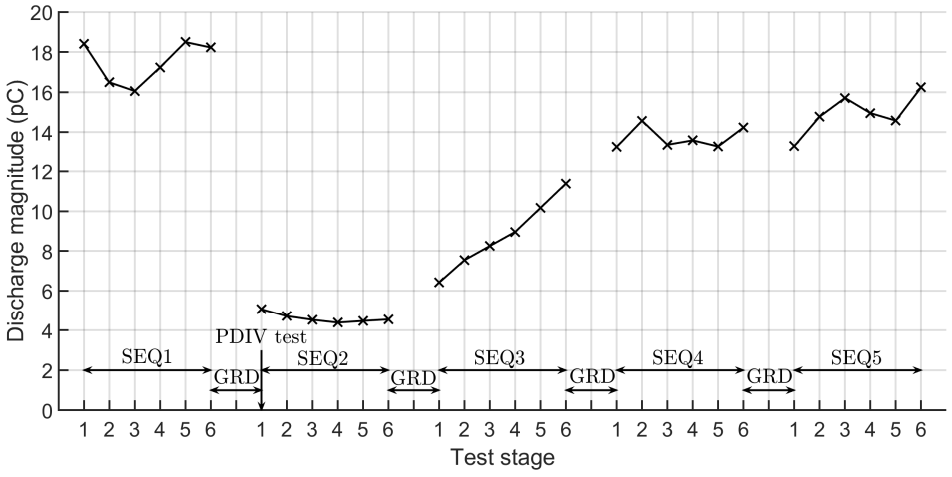

b)

Fig. 5-18 The mean values for the DC test series. a) Mean discharge separation time, b) Mean discharge magnitude

5.3.3 Mean discharge magnitude per separation time

The strong correlation between discharge magnitude and separation time was seen in the PD sequence data in Fig. 5-17. In Fig. 5-19, the mean discharge magnitude per separation time varies between 0.39 and 0.42 pC/s, deviating 3-5% from its mean value of 0.41 pC/s.

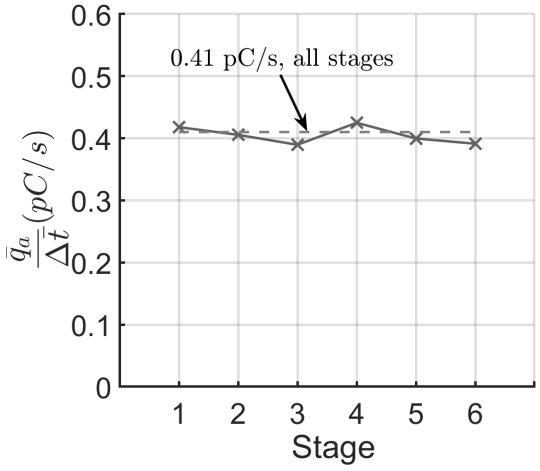

Fig. 5-19 Mean apparent discharge magnitude per separation time by test stage PD data from test sequence 4.

The mean discharge magnitude per separation time is predicted to be constant and will depend on the series dielectric capacitance and cavity voltage slope, $\frac{\bar{q}_a}{\Delta t} = C_b \frac{dv_c}{dt}$, see section 3.2.3. In section 5.2.4, the predicted value was 0.12 pC/s, and the measured value is over 3 times higher. The value of the series dielectric capacitance is probably not the reason for this discrepancy; it is not plausible that more than 100% of the cavity surface is involved in the discharge. This points to the cavity voltage slope, which must then be higher than its predicted value. If the conductivity of the cavity surface and volume is included, and it is assumed that a parasitic AC ripple is present, the cavity voltage slope is expressed as in (3.63). It is only a decrease in the time constant of the cavity voltage that can increase the value of the cavity voltage slope and the mean discharge magnitude per separation time:

- If the walls of the cavity or the gas are conductive, the resistive distribution factor K_{DC} decreases, and the cavity voltage slope decreases instead of increasing.
- The AC ripple voltage stress over the cavity, $K_{AC}\hat{V}_{AC}$, is 1/1000 of the DC voltage stress: $K_{AC}\hat{V}_{AC} \ll K_{DC}V_{DC}$. The parasitic AC ripple cannot affect the cavity voltage slope by more than 0.1%.
- $V_{paschen} \ll K_{DC}V_{DC}$, and thus the cavity voltage slope is not sensitive to variation in the Paschen breakdown voltage.

The time constant of the cavity voltage depends on the permittivity and conductivity of PET, the height of the cavity, and the total thickness of the sample. The conductivity of PET, σ_b, is the most sensitive of all these parameters; the uncertainty in the measurement of this parameter was discussed in 5.1.1. If the conductivity is higher in the PD experiments than the measured value, the result is a proportional increase in the cavity voltage slope, according to (3.2). The estimated uncertainty in the PET conductivity was ±38%, which does not explain the 3.4-factor increase in the cavity voltage slope. Data from Lilly and McDowell

[100] yields a conductivity of 1.8e-15 S/m, thus increasing the predicted cavity voltage slope by a factor of 1.8, which still does not explain the discrepancy completely. This indicates that there are other sources of error than the measurement uncertainty of PET conductivity. During the PD tests, the PET sample is submerged in mineral oil with uncontrolled water content. The relative humidity in the laboratory was between 40-60%. Both the oil and the water in the mineral oil can diffuse into the PET sample and increase the conductivity. The conductivity of XLPE increases by a factor of 1.8-3.4 with water content [92]. XLPE absorbs water up to 0.04 wt% [110], PET can absorb 0.5 wt% according to the data sheet (Hostaphan RN 50-350), i.e. 100 times more than XLPE. The diffusion of water into PET takes long time, but the sample had been in the oil for more than 48 hours before voltage application to allow stabilisation of the temperature in the test cell. It is thus possible that water content in the oil contributed to the high PET conductivity, and may explain the higher than predicted cavity voltage slope and mean discharge magnitude per separation time. However, further investigation is needed to determine the effect of oil and the water content in the oil on the conductivity of PET.

5.3.4 Measured distributions

In Fig. 5-20, the measured distributions of the discharge magnitude and the separation time are compared to the simulated distributions at DC voltage, using the PD sequence parameters in Table 5-5. In Fig. 5-20a, the measured discharges have the highest probability of occurrence at low discharge magnitude. The measured probability density decreases with higher discharge magnitude, but not in an exponential manner. There is no indication of multiple discharge sites as may have been visible by multiple peaks in the discharge magnitude distribution [8, p. 85]. The measured distribution of separation times has the same shape as predicted for PD at DC voltage, but the peak probability is shifted to higher separation times, see Fig. 5-20b.

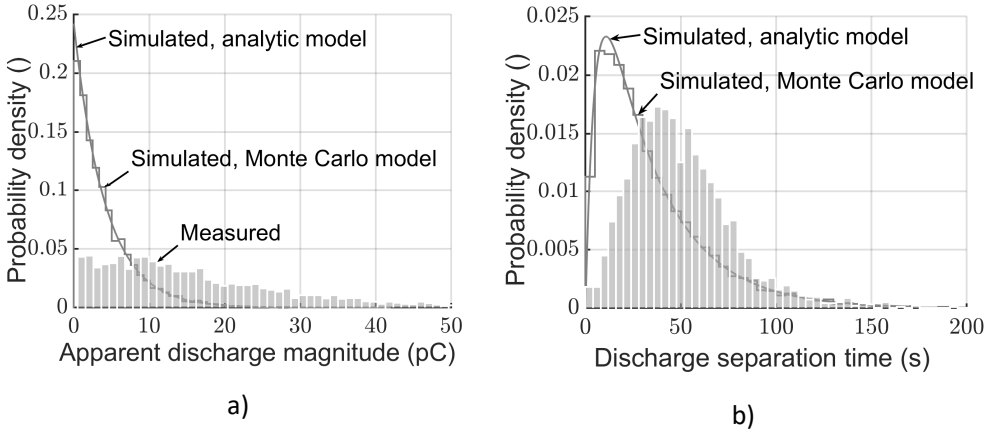

Fig. 5-20 Measured and simulated distributions of a) Apparent discharge magnitude and b) Separation time. Measured data from test sequence 1, DC test series.

The PD sequence model and the analytical models yield the same probability densities at DC voltage. The apparent discrepancy between the measured and the calculated distributions can be attributed to the effect the small AC ripple during the measurement. See Fig. 5-21 for comparison with a simulated distribution with the same parameters, but with a superimposed AC ripple with V_{AC} = 10 V.

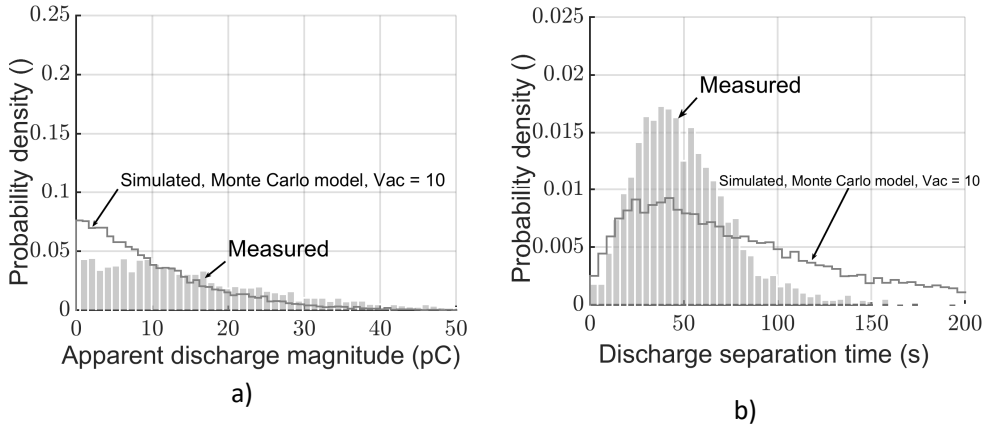

Fig. 5-21 Comparison between measured and calculated distributions with Vac = 10 V, PD sequence parameters as in Table 5-5. a) Distribution of discharge magnitude, and b) Separation time. Measured data are from test sequence 1.

The predicted distributions and the measured distributions are very close to each other if the corrected estimated PD sequence parameters found in section 5.3.5 are used as model input, see Fig. 5-22. The consistency between measurements and the PD model predicted values is very good considering that the parasitic AC ripple contains multiple frequency harmonics.

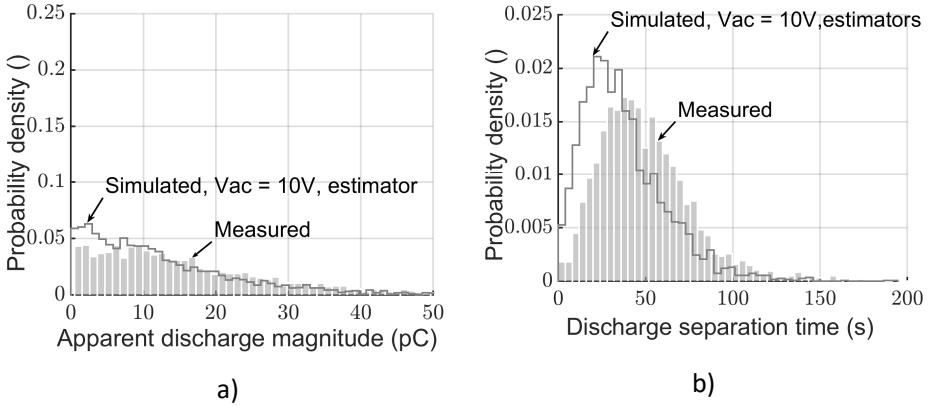

Fig. 5-22 Comparison between measured and calculated distributions with Vac = 10 V and PD sequence parameters obtained by estimation: a) Distribution of discharge magnitude, b) Separation time. Measured data are from test sequence 1.

5.3.5 Estimation of PD sequence parameters

In this section, the estimated values of the PD sequence parameters from the measured PD data at DC voltage are presented and compared with their expected values. The Townsend coefficient product is estimated in section 5.3.5.1, and the mean time lag and recovery time are estimated in section 5.3.5.2. The product $C_b \frac{dv_c}{dt}$ has been treated in section 5.3.3; its estimator is given by $\widehat{C_b \frac{dv_c}{dt}} = \frac{\overline{q_a}}{\Delta t}$, and will not be treated further in this section.

5.3.5.1 Townsend coefficient product

The estimated values for the Townsend coefficient product are given in Fig. 5-23. The estimated values are lower than the expected values, $\alpha h \approx 7$. The DC MoM estimator yields values up to 5, and the DC OLS estimator yields values between 2 to 3. It is expected that the DC estimators give biased values when the input data stems from a combined voltage PD process, as shown in section 5.2.6. The MoM estimator yields a value that is more overestimated. The DC OLS estimation method was shown to be more robust, closer to the real value, for an AC ripple of 10 V.

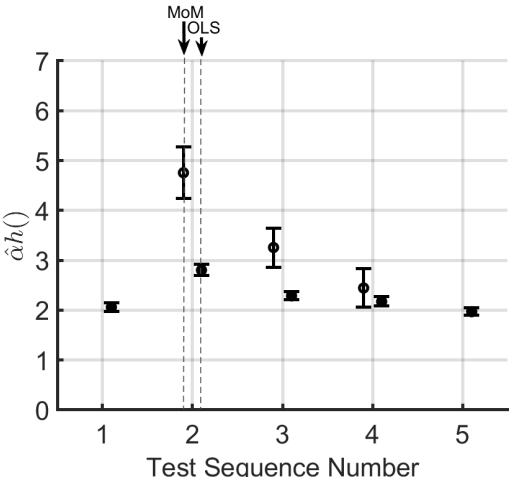

Fig. 5-23 Estimated Townsend coefficient product, αh , for all test sequences in the DC test series.

The MoM estimator yielded a complex value for test sequences 1 and 5, which have less discharge data. All complex values were discarded, as the Townsend coefficient product is a real value. In general, the MoM method is less robust than the OLS method and requires more data to give real valued estimates. Therefore, it is concluded that the estimated value is in the range between 2 and 3, given by the DC OLS estimator. This is confirmed by Devins [63, p. 485] who estimates the value to 3.2, based on experimental data and a different parameter extraction method. The estimated values are then significantly lower than the predicted values. Devins attributed the estimated low value to the slow formation of the discharge avalanche at low overvoltages. There may be other reasons for the low values, as given below:

1) Air laboratory room conditions with relative humidity of 59% give a Townsend coefficient that is 40% lower than for dry air according to measurements by Dutton [72] . A similar reduction will give an expected value of αh = 4.2.

2) The Townsend coefficient is measured with metallic electrodes; the dielectric surfaces of the cavity may influence the ionisation process considerably and limit the value of αh .

In this thesis, the ratio of overvoltage to recovery voltage is assumed constant and is a function of the Townsend coefficient, but can also just be regarded as a general proportionality constant, as K in $\Delta V_{R,i} = K \cdot \Delta V_{L,i}$. The recovery voltage can be a non-linear function of the overvoltage, given by the temporal growth of the discharge current. The exact relationship is probably very complex, but could be obtained from detailed discharge current models such as the ones described in [81], [111] and [112]. Ultimately, the estimated Townsend coefficient may be far from the real value. However, comparison between measured and simulated PD data in section 5.4.2.1 indicates that the PD process at combined voltage can be described by assuming that the overvoltage is proportional to the recovery voltage, $\Delta V_{R,i} = K \cdot \Delta V_{L,i}$.

5.3.5.2 Time lag and recovery time

As noted in section 5.2.6.2.3, the DC OLS estimators are sensitive to the input data. If data from a combined voltage discharge process are used as input to the DC OLS estimator, the result is overestimation of the time lag and the recovery time. This is confirmed by comparing the sum of the estimated mean time lag and recovery time with the measured mean discharge separation time, see Fig. 5-24. The sum is larger than the actual discharge separation time, which indicates that the mean time lag and recovery time indeed are overestimated. The same can be concluded from data provided by Fromm in [82], who also reported the presence of a parasitic AC ripple voltage. The DC MoM estimator gives perfect correspondence with the measured mean separation time. This does not mean that the estimated mean time lag and recovery time are correct for the MoM estimator; the parasitic AC ripple probably increased the mean separation time and thereby the estimated mean time lag and recovery time.

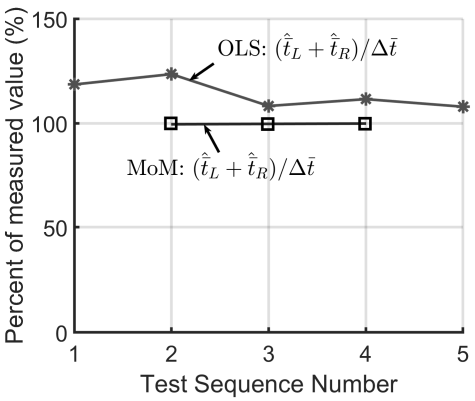

Fig. 5-24 Sum of estimated mean time lag and recovery time over measured mean discharge separation time, for DC test series.

An estimate of the mean time lag and recovery time at DC voltage can be obtained by correcting for the parasitic AC ripple 10 V. The uncorrected and corrected estimated values of the mean time lag and recovery time are plotted in Fig. 5-25. The MoM estimator yielded a complex value for test sequences 1 and 5, which have less discharge data. All complex values were discarded. The corrected values were obtained by the following procedure:

- Using the estimated Townsend coefficient product from the OLS DC estimation method in the previous section, as its value should be robust with respect to data from a combined voltage PD process. This is supported by the theoretical investigation in section 5.2.6.2.3.
- Assume that C_b is equal to its calculated value in section 5.2.1, thus obtaining $\frac{dv_c}{dt}$ as in section 3.2.3.
- Now only $\hat{\tau}_s = \hat{\bar{t}}_L^{DC}$ needs to be found. This is done by setting the AC ripple voltage amplitude to 10 V and calculating the mean separation time at combined voltage for a range of $\hat{\tau}_s$, using the Monte Carlo model in section 3.3.1. The value of $\hat{\tau}_s$ that gives mean separation time closest to the measured mean separation time is thereby found.
- The corrected estimate of the mean recovery time at DC voltage is calculated with (3.22) as $\hat{\bar{t}}_R^{DC} = (\hat{\alpha}h - 1)\hat{\bar{t}}_L^{DC}$.

The DC MoM estimator yields a value of the mean time lag closer to the corrected value, compared to the DC OLS estimator. Both estimators yield similar values for the mean recovery time. The estimated mean time lag is around 28 seconds in test sequence 1, before the PDIV test. The corrected value indicates a mean time lag at DC voltage of around 20 seconds. Since $\hat{\tau}_s = \hat{\bar{t}}_L^{DC}$, the assumption A.8 that the mean statistical waiting time is much larger than the AC period time is satisfied, i.e. $T_{AC} \ll \tau_s$. The estimated mean recovery time is around 30 seconds, the corrected value indicates a mean recovery time at DC voltage of around 22 seconds. Although the estimated mean recovery time is slightly higher than the mean time lag, it can be concluded that the mean recovery time is approxamitely equal to the mean time lag at DC voltage conditions, i.e. $\hat{\bar{t}}_R^{DC} \approx \hat{\bar{t}}_L^{DC}$.

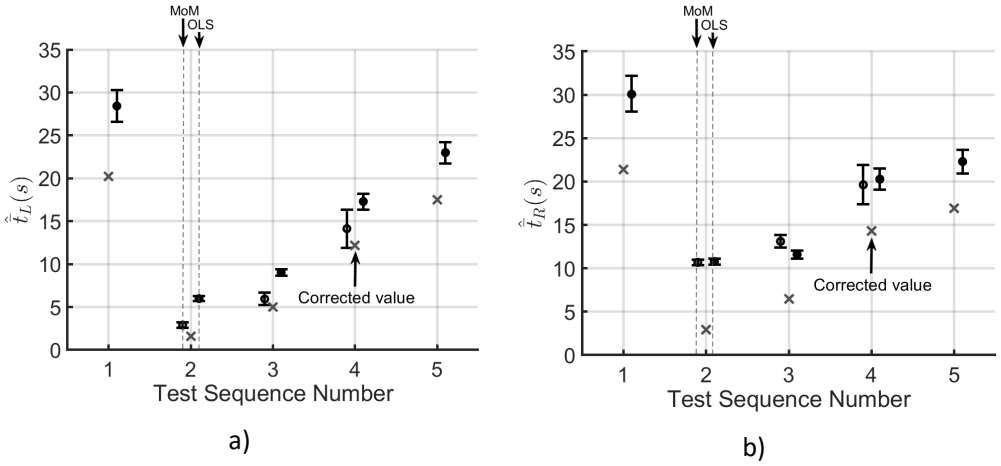

Fig. 5-25 a) Mean time lag and, b) Recovery time. Estimated with measured PD data from DC test series.

5.3.6 Summary

The main observations from the measured discharge magnitude and separation time at DC voltage are as follows:

- There is a positive correlation between the measured moving average of the apparent discharge magnitude and the separation time as a function of time. The observed correlation is consistent with one discharge band visible in the PD sequence plot and is a strong indication that the registered discharges originate from Townsend-like discharges that cover the surface of the cavity.
- The measured mean discharge magnitude per separation time is essentially constant during a test sequence, and is around 0.41 pC/s, while the predicted value was 0.12 pC/s. The measured value is over 3 times higher; this was attributed to a higher conductivity in the PET film during the PD experiments than expected. The two main reasons for this discrepancy were uncertainty in the measurement of the conductivity and the water content in the oil that may have increased the conductivity during the PD experiments.
- Some of the discharges are close to the discharge detection magnitude threshold of 0.5 pC; discharges probably occurred in the cavity below the detection threshold.
- The AC source introduced a ripple of around 10 V during the PD tests at DC voltage, even if the AC voltage was set to zero. It is plausible that the ripple caused higher discharges and longer separation times than what would have been measured at DC voltage without any AC voltage ripple.
- The measured distribution of the separation times has the same shape as predicted for PD at DC voltage, but the peak probability is shifted to higher separation times. The measured probability density of the discharge magnitude does not follow the predicted exponential distribution, although the smallest discharge magnitude has the highest probability and then decreasing probabilities for higher discharge magnitudes. The predicted distributions and the measured distributions are very close to each other, if the PD sequence parameters are estimated and corrected for an AC ripple of 10 V.

The observations for the proposed estimators on measured PD data are as follows:

- The estimated value of the Townsend coefficient product, $\hat{\alpha}h$, is in the range between 2 and 3, given by the DC OLS estimator. The estimated values are then significantly lower than the predicted value of around 7 for dry air. Two reasons were given for this discrepancy: Firstly, the humiditiy in the cavity may decrease the Townsend coefficient by as much as 40%, compared to dry air conditions. Secondly, the dielectric surfaces of the cavity may influence the ionisation process considerably and limit the value of αh .
- The MoM estimator yielded a complex value for the Townsend coefficient in some of the test sequences. It was found that the MoM method is less robust than the

OLS method for the Townsend coefficient and requires more data to give real valued estimates; this was also confirmed by the simulation performed in section 5.2.6.2.3.

- The estimated mean time lag is between 20 and 28 seconds, and so the assumption A.8 that the mean statistical waiting time is much larger than the AC period time is satisfied, i.e. $T_{AC} \ll \tau_s$. The estimated mean recovery time is between 22 and 30 seconds, and so the mean recovery time is approxamitely equal to the mean time lag at DC voltage conditions, i.e. $\hat{\bar{t}}_R^{DC} \approx \hat{\bar{t}}_L^{DC}$.
- The DC MoM estimator yields a value of the mean time lag closer to the corrected value, compared to the DC OLS estimator. Both estimators yield similar values for the mean recovery time. This is in line with the simulation performed in section 5.2.6.2.3.

5.4 Experimental investigation of partial discharges at combined DC and AC voltage

In this section, the main hypotheses are evaluated based on the experimental data, and compared to the predictions of the model for internal discharges at combined DC and AC voltage. Section 5.4.1 investigates the effect of AC ripple frequency in the range of 50-1000 Hz. Section 5.4.2 investigates the effect of an AC ripple with voltage amplitude between 4 and 50% of the AC partial discharge inception voltage. Section 5.4.3 describes the effect of increasing the AC ripple amplitude above 50% of the AC partial discharge inception voltage.

5.4.1 Variable AC ripple frequency and constant voltage amplitude

The observed discharge separation time and magnitude did not change appreciably when the AC ripple amplitude at 44 V_{rms} was held constant and the frequency was applied from stages 2 to 4 in the steps 50, 500, 1000 and 50 Hz, see Fig. 5-26. The same behaviour was observed in all the measurements. The explanation given for this observation is that the AC ripple frequency does not change the time the cavity voltage exceeds the critical voltage per time. That is to say, the duty cycle does not change with frequency, so the effective time lag, separation time and discharge magnitude stay the same. The experimental data and the model simulation results thus confirm the hypothesis that the discharge separation time and discharge magnitude are not influenced by the frequency of the AC ripple voltage (H.3).

A marked increase in discharge separation times and discharge magnitude is observed when going from stage 1 with AC voltage ripple set to zero to stage 2 with AC ripple amplitude of 44 V_{rms}, which was predicted in section 5.2.2. This point is elaborated in section 5.4.2, where the AC ripple amplitude was increased up to 500 V_{rms}.

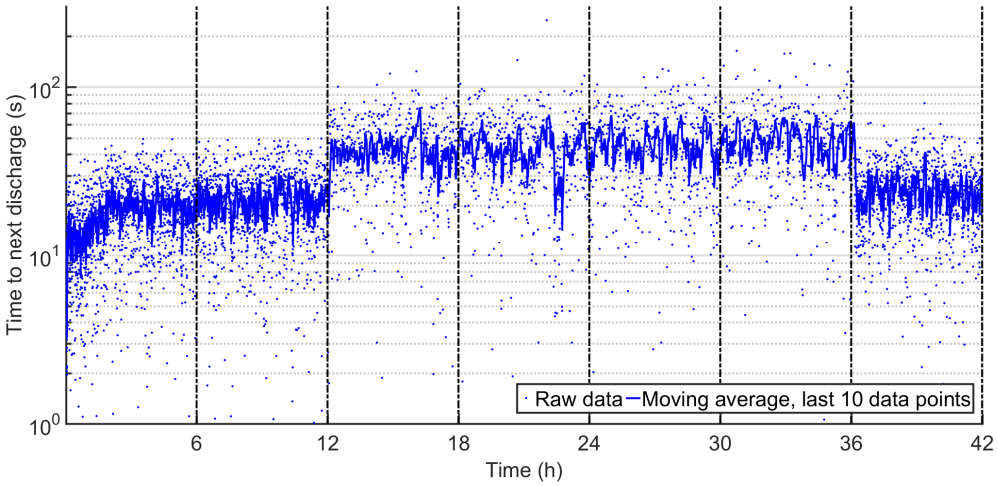

a)

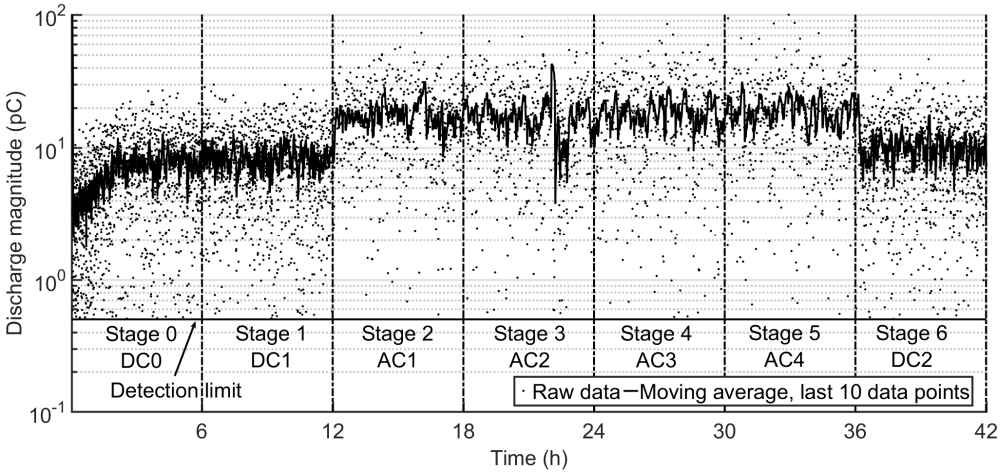

b)

Fig. 5-26 Measured PD data from test sequence 3 at DC + variable AC frequency. a) Separation time, b) Discharge magnitude (absolute value), versus time of occurrence. The AC voltage amplitude is 44 Vrms (62.2 Vpeak) in stage 2 to 5. The AC applied frequencies are AC1: 50 Hz, AC2: 500 Hz, AC3: 1000 Hz, AC4: 50 Hz.

5.4.2 Variable AC ripple voltage amplitude and constant frequency

The data in the previous section show a clear increase in discharge separation time and discharge magnitude with the AC ripple amplitude, independent of the AC ripple frequency. In this section, the effect of the AC ripple voltage is shown in greater detail and compared with model predictions.

5.4.2.1 The measured PD sequence

The measured PD sequence is shown in Fig. 5-27. The increasing AC voltage ripple results in a longer mean separation time and higher discharge magnitude, as well as larger scatter and stronger fluctuation of their moving average value.

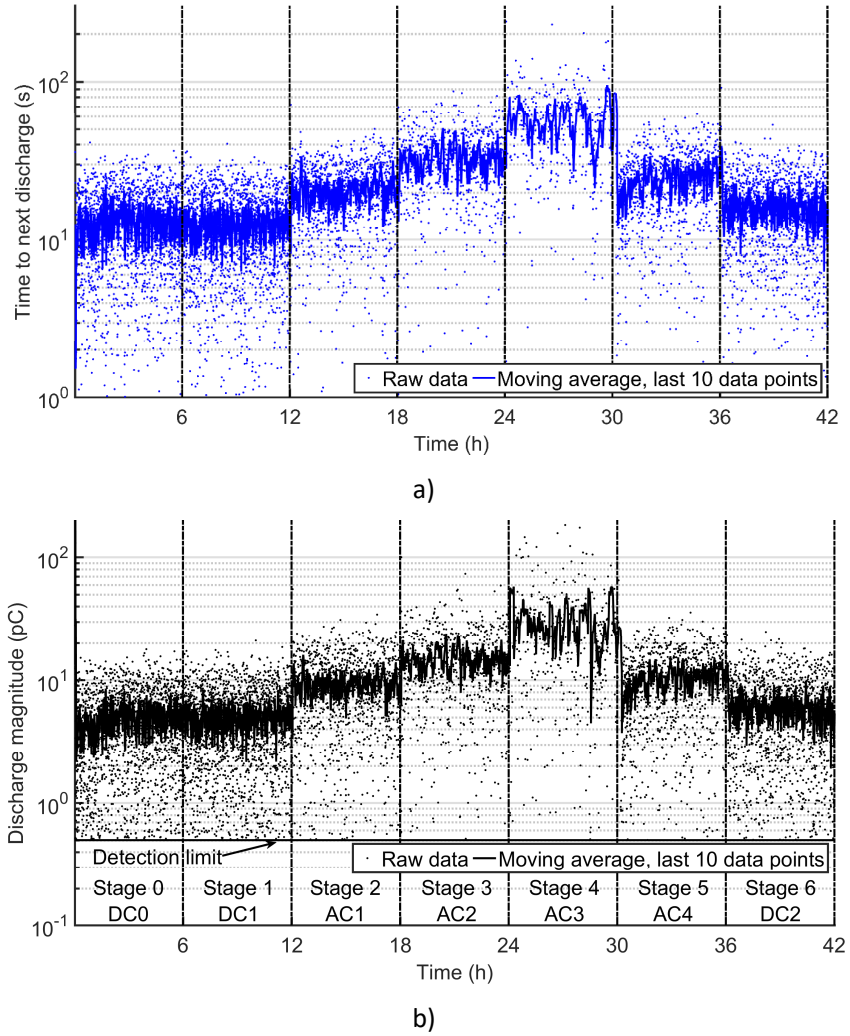

Fig. 5-27 Measured PD sequence at variable AC ripple voltage amplitude, data from test sequence 4. a) Separation time, b) Discharge magnitude (absolute value), versus time of occurrence. AC1: V_{AC} = 44 V_{rms}, AC2: V_{AC} = 176 V_{rms}, AC3: V_{AC} = 500 V_{rms}, AC4: V_{AC} = 44V_{rms}.

The PD sequence parameters were estimated at stage AC1 (44 V_{rms}) using the MoM method for combined voltage in section 3.3.4, see Table 5-7. The values in parenthesis are the 95% confidence intervals. The estimated values were used as input to the PD model for combined voltage, and the predicted and measured mean values are plotted as a function of the AC ripple voltage in Fig. 5-28. It can be observed that the predicted values are close to the measured values at all AC ripple amplitudes, not only at the 44 V_{rms} from which data the PD sequence parameters were estimated. The prediction for zero AC ripple amplitude is below the measured values, and is attributed to the parasitic AC ripple voltage present during the DC measurement stage; the parasitic AC ripple caused higher discharge magnitude and separation time.

Based on the experimental evidence and the stochastic PD model, it can be concluded that both the discharge magnitude and the discharge separation time increase when an AC ripple is superimposed on the DC voltage. Thus, the two main hypotheses must be rejected under the assumptions given in section 3.1:

- The discharge separation time decreases with increasing AC ripple voltage amplitude (H.1).
- The discharge magnitude is constant when the AC ripple voltage amplitude increases (H.2)

Table 5-7 Estimated PD parameters by the MoM combined voltage estimation method, PD data from stage AC1 (44Vrms) in test sequence 4. 95% confidence intervals in parenthesis.

Estimated PD parameter	$\hat{\alpha}h$	$\hat{C}_b$ (pF)	$\widehat{\frac{dv_c}{dt}}$ (V/s)	$\hat{\hat{t}}_L^{DCAC}$ (s)	$\hat{\hat{t}}_R^{DCAC}$ (s)	$\hat{\tau}_s = \hat{\hat{t}}_L^{DC}$ (s)	$\hat{\hat{t}}_R^{DC}$ (s)
Estimated value	**2.3** (1.6,2.8)	**0.39** (0.12,0.47)	**1.1** (0.9,3.3)	**20.4** (15.6,26.6)	**18.7** (13.3,23.7)	**6.6**	**8.5**

The estimated PD sequence values were discussed in section 5.3.5 for PD at DC voltage. For the MoM estimator at combined voltage, the following are noted:

- The value of $\hat{\alpha}h$ is in the same range as estimated for the DC test series, the significant difference between the estimated and predicted values is discussed in section 5.3.5.1.
- The predicted value of the series dielectric capacitance is C_b = 0.61 pC. The estimated value is 36% lower than predicted. The discharge can be estimated to cover around 64% of the cavity surface area, corresponding to a cavity radius of 0.8 mm. This is close to the real radius of 1 mm.
- The estimated cavity voltage slope is 5 times the predicted value of 0.19 V per sec, calculated in Table 5-5. The discrepancy is thus higher than for the estimated value discussed in section 5.3.3 for PD at DC voltage. In both cases, the reason for the

higher cavity slope may be the mismatch between the measured conductivity of PET and the actual conductivity during the PD tests.

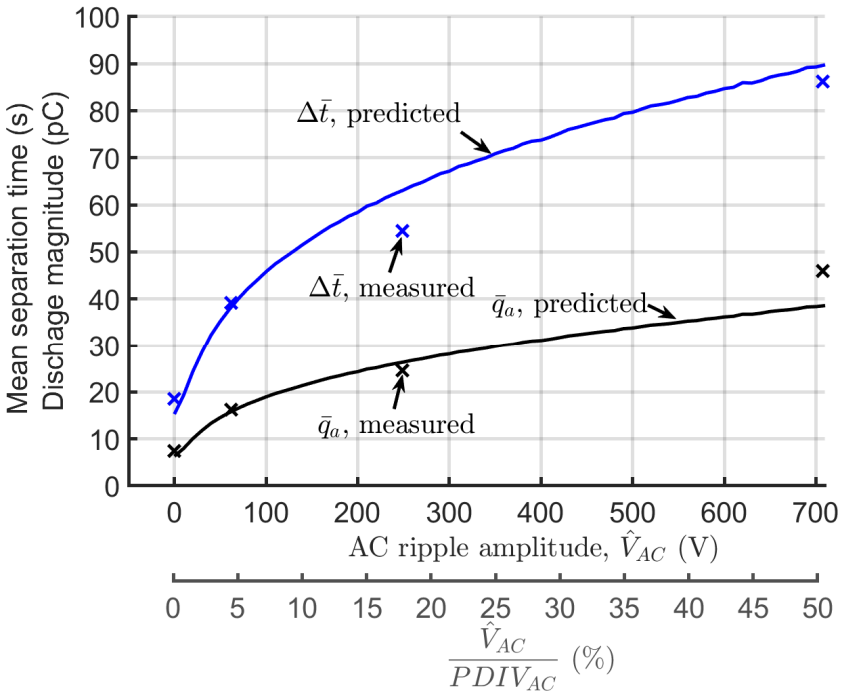

Fig. 5-28 Comparison of predicted and measured mean in sequence 4, at 10 kVDC + 44 V_{rms} (62.2V_{peak}), 176 V_{rms} (248.9 V_{peak}) and 500 V_{rms} (707.1 V_{peak}) at 50 Hz. Based on estimated PD sequence parameters at 44 V_{rms} (AC1).

5.4.2.2 Mean discharge separation time and magnitude

The correlation between the mean discharge separation time and discharge magnitude is very high, see Fig. 5-29. Essentially, the same behaviour is observed for the two parameters – they increase with applied AC voltage amplitude. The increase of the mean discharge separation time is much more pronounced during the variable AC ripple amplitude test series, compared to the DC test series and the variable frequency test series. The PDIV test influences the PD process in the same manner for all the test series, decreasing the stochastic time lag and thus decreasing the separation time and magnitude. The discharge magnitude and separation time is almost the same for all the test series in stages 1 and 6 at test sequence 1, before the PDIV test.

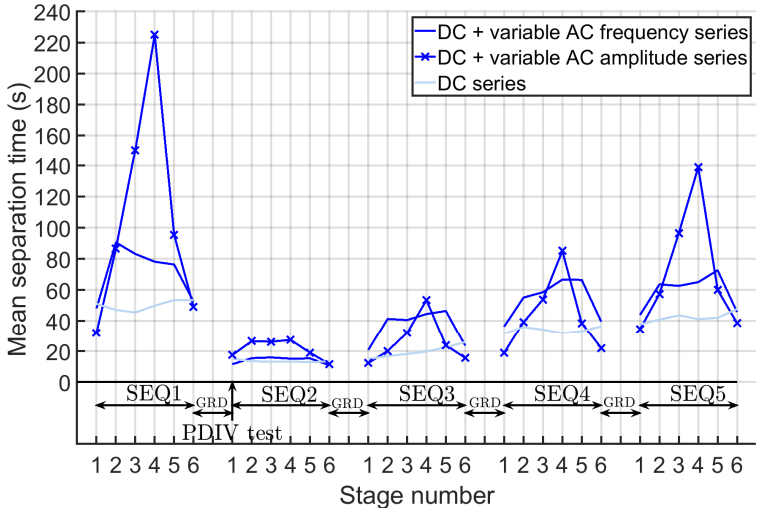

a)

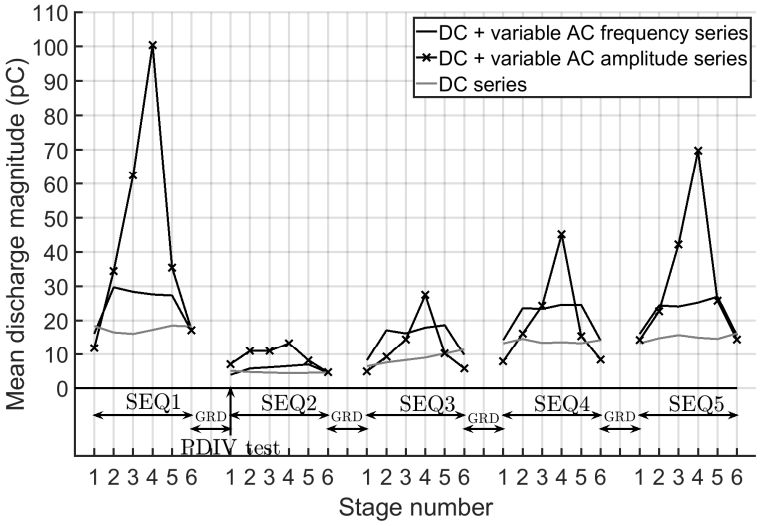

b)

Fig. 5-29 . a) The measured mean separation time, for all test series. b) The measured mean discharge magnitude, for all test series.

5.4.2.3 Phase resolved partial discharge analysis

In section 5.2.3 it was predicted that the discharges occur close to the peak of the AC voltage, shown as a symmetrical pattern in a PRPD diagram; this is also observed in the measurements, see a), c) and e) in Fig. 5-30. Predicted values are from the combined voltage PD model with PD sequence parametres as given in Table 5-7. Both the measured and the predicted PD phase distribution narrows and heightens when the AC ripple amplitude increases, see b), d) and f) in Fig. 5-30. This is in line with the duty cycle effect described in section 3.3.2.3. A higher AC ripple amplitude decreases the time that the cavity voltage is above the critical voltage, which narrows the available range of phase-of-occurrence for a given time lag.

The predicted phase distributions are consistently wider than the measured distributions, which may indicate that the estimated PD sequence parameters deviate somewhat from the real values. One reason for this may be that the precision of the estimated values is low, as indicated by the wide confidence intervals in Table 5-7, when there are few PD data points available – the estimators are extracted from a data set of 519 discharges. Another reason may be that the MoM estimation method itself is inaccurate, i.e. it is biased, and there may be other methods, like the Maximum Likelihood Estimation method [113], that can give more accurate estimates. But, currently the only estimation method available for PD at combined voltage is the MoM estimator proposed in this thesis. Considering that the estimated PD sequence parameters are extracted from a small data set, the predicted values are close to the measured values. The increasingly narrow phase distribution with increasing AC ripple amplitude is predicted by the proposed model.

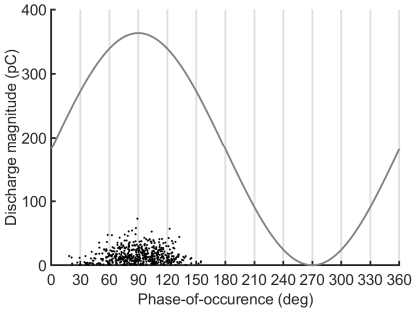

a) Measured PRPDA, V_{AC} = 44 V_{rms}

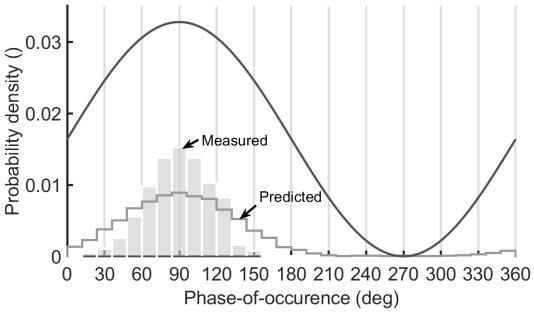

c) Measured and predicted phase distribution, V_{AC} = 44 V_{rms}

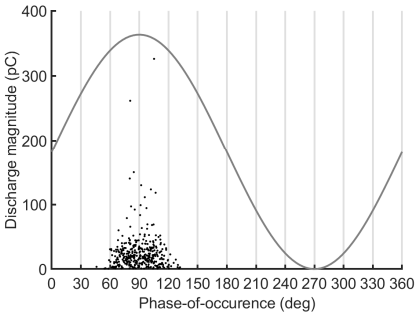

c) Measured PRPDA, V_{AC} = 176 V_{rms}

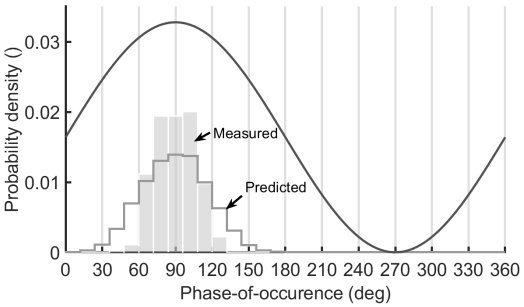

d) Measured and predicted phase distribution, V_{AC} = 176 V_{rms}

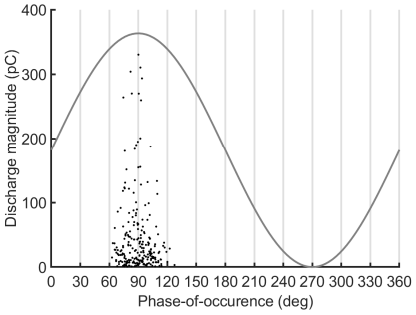

d) Measured PRPDA, V_{AC} = 500 V_{rms}

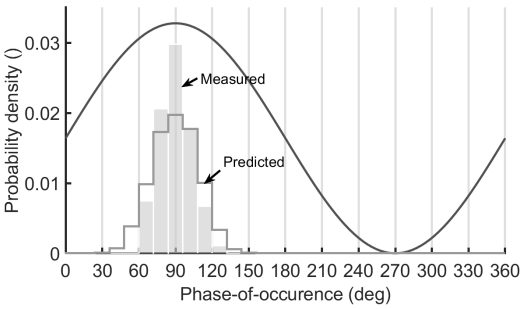

f) Measured and predicted phase distribution, V_{AC} = 500 V_{rms}

Fig. 5-30 Measured discharge magnitude versus phase-of-occurrence in a), c) and e). Measured and predicted phase distributions shown in b), d) and f). PD data are from test sequence 4, AC variable amplitude test series.

5.4.2.4 Measured discharge separation time and magnitude distributions

In Fig. 5-31 a), c) and e) the measured and predicted discharge magnitude distribution is plotted for 44, 176 and 500 Vrms AC ripple superimposed on 10 kV DC. The measured data are from test sequence 4. Predicted values are from the combined voltage PD model with PD sequence parametres in given in Table 5-7. The discharge magnitude probability distribution is drawn out when the AC ripple amplitude increases. There are fewer discharges close to the discharge magnitude detection threshold, and the probability for large discharges increases with higher AC ripple amplitude. The measured and predicted discharge separation time distributions in Fig. 5-31 b), d) and f) are shifted to higher separation time, and flatten with increasing AC ripple amplitude; this is in line with the increased mean discharge separation observed in Fig. 5-28. The proposed model predicts the discharge magnitude and separation time distributions with good accuracy for all AC ripple amplitudes, below 50 % of the AC partial discharge inception voltage.

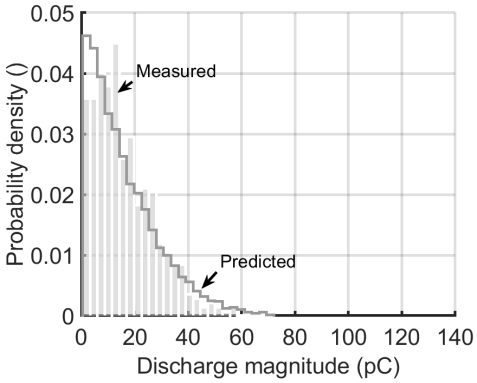

a) q_a -distribution, V_{AC} = 44 V_{rms}

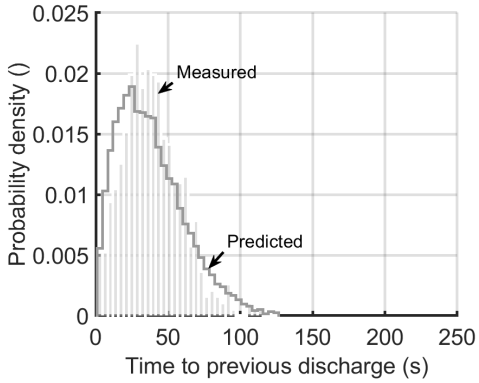

b) Δt -distribution, V_{AC} = 44 V_{rms}

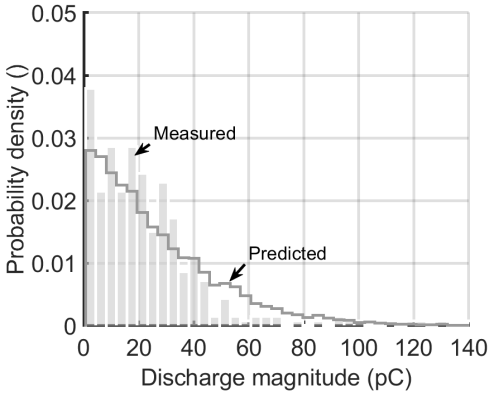

c) q_a -distribution, V_{AC} = 176 V_{rms}

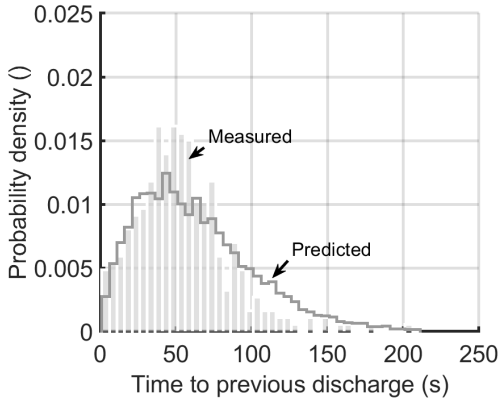

d) Δt -distribution, V_{AC} = 176 V_{rms}

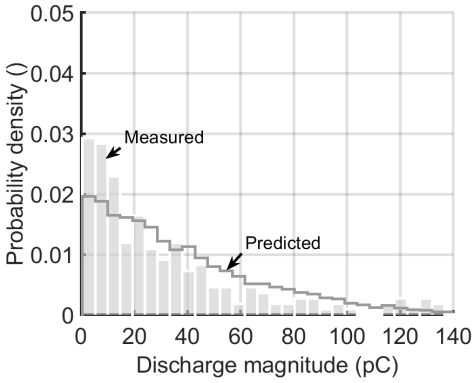

e) q_a -distribution, V_{AC} = 500 V_{rms}

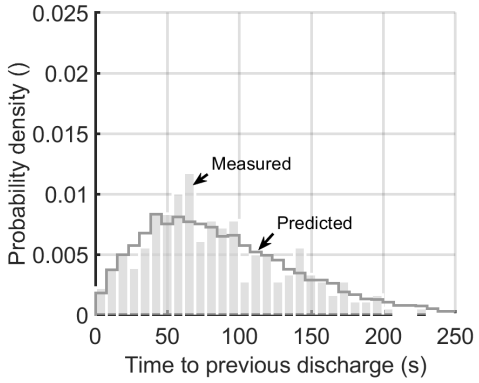

f) Δt -distribution, V_{AC} = 500 V_{rms}

Fig. 5-31 Measured and predicted discharge magnitude distributions shown in a), c) and e). Measured and predicted separation time distributions shown in b), d) and f).

5.4.3 High AC ripple voltage amplitude

A series of measurements was carried out at the same DC voltage and temperature level, but an AC ripple voltage of 760 V_{rms}, which is 100 V_{rms} below the predicted AC partial discharge inception voltage, was superimposed on the DC voltage after 12 hours. The applied voltage for the entire test sequence is given in Table 4-3. The test series consisted of 2 repeated test sequences. An AC PDIV test was performed just before the second test sequence; the measured $PDIV_{AC}$ value was 1 kV_{rms}.

In the test sequence before the PDIV test, no high repetition rate discharges are observed, see Fig. 5-32. There is an increase in discharge separation time and magnitude in the combined DC and AC voltage stage, in the same manner as observed in the measurements where the AC ripple voltage was below the 50% of the PDIV value, see section 5.4.2. In the test sequence after the PDIV test, an alternation between high and low repetition rates is observed. The clusters of discharges with short discharge separation times, termed bursts, are characterised as follows:

- Discharges are of negative and positive polarity during the bursts.
- The discharge magnitude is higher during the bursts, than between the bursts.
- The discharge separation times are in the same order, and one order lower, as the AC ripple period time during the bursts, see Fig. 5-32a.

In the interval between the discharge bursts, the discharge separation time can be up to 4 orders higher, see Fig. 5-32a. The discharge magnitude does not vary to the same extent, but shows a marked decrease in discharge magnitude between the bursts, see Fig. 5-32b. It should be noted that the behaviour could not be observed without a PDIV test before the test sequence. This can be explained by the deposition of start electrons on both cavity surfaces during the PDIV test, increasing the probability for discharges at both AC voltage polarities in the subsequent test sequence.

The combination of long and short discharge separation times can be explained as follows: If a small discharge is triggered at the positive half-period, there is a lower probability for discharges occurring on the negative AC voltage half period; this is so because the voltage on the negative AC cycle may never reach the negative Paschen voltage, see Fig. 5-33. This leads to the probability of long separation times after a discharge burst, which may be caused by a small discharge in the positive half-period.

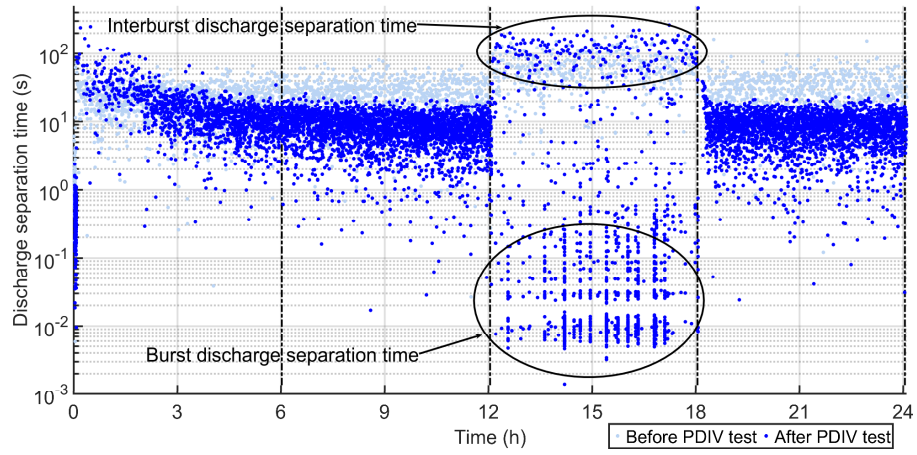

a)

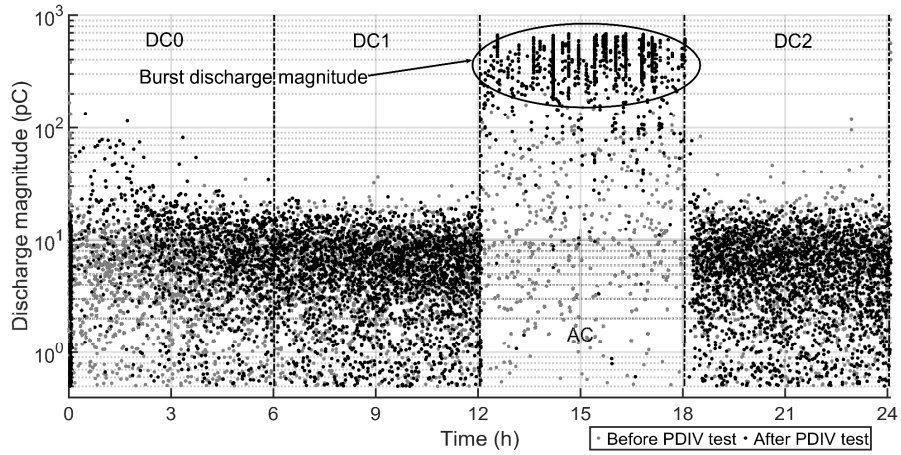

b)

Fig. 5-32 Separation time, a), and discharge magnitude (absolute value), b), versus time of occurrence. Data from the preceding test sequence, before PDIV test, shown in lighter colour. V_{AC} = 760 Vrms, 76 % of the measured $PDIV_{AC}$ value.

It is concluded that an AC ripple voltage with amplitude between 50% and 100% of the PDIV value can provoke high frequency, bipolar PD bursts separated by large time intervals. This limits the scope of the model presented in section 3.3; the AC voltage ripple amplitude must be below 50% of the $PDIV_{AC}$ value for the model to be strictly valid. The mean discharge separation time can be influenced by the frequency of the AC ripple voltage, although this was not investigated here.

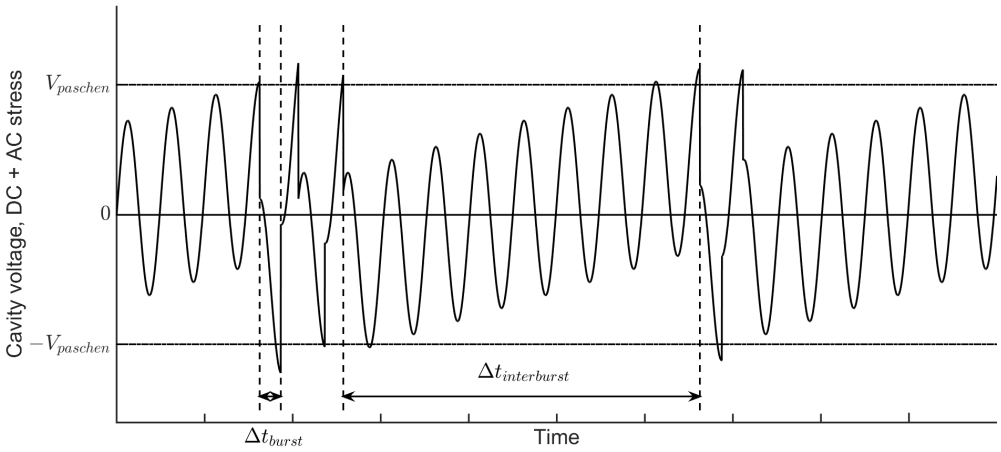

Fig. 5-33 Theoretical voltage across a discharging cavity at combined DC and AC voltage. AC voltage between 50 and 100% of $PDIV_{AC}$.

5.4.4 Summary

The main observations from the measured PD data at combined voltage are as follows:

- The observed discharge separation time and magnitude did not change appreciably when the AC ripple amplitude was held constant and the frequency varied from 50 to 1000 Hz. The experimental data and the model simulation results thus confirm the hypothesis that the discharge separation time and discharge magnitude are not influenced by the frequency of the AC ripple voltage (H.3).
- Increasing AC voltage ripple results in a longer mean separation time and higher discharge magnitude, as well as larger scatter and stronger fluctuation of the moving average value in a PD sequence plot.
- Based on the experimental evidence and the stochastic PD model, it could be concluded that both the discharge magnitude and the discharge separation time increase when an AC ripple is superimposed on the DC voltage. The predicted mean discharge magnitude and separation time are close to the measured values for an AC ripple amplitude between 44 V_{rms} and 500 V_{rms}, corresponding to 4.4-50% of the measured $PDIV_{AC}$ value. Thus, the two main hypotheses H.1 and H.2 were rejected under the assumptions given in section 3.1.
- The discharges at combined voltage occur close to the peak of the AC voltage, shown as a symmetrical pattern in a PRPD diagram.
- Both the measured and the predicted PD phase distributions narrow and heighten when the AC ripple amplitude increases. A higher AC ripple amplitude decreases the time that the cavity voltage is above the critical voltage, which narrows the available range of phase-of-occurrence for a given time lag.
- The discharge magnitude probability distribution is drawn out when the AC ripple amplitude increases. There are fewer discharges close to the discharge magnitude detection threshold, and the probability for large discharges increases with higher AC ripple amplitude. The measured and predicted discharge separation time probability densities are shifted to higher separation time and flatten with increasing AC ripple amplitude.
- The proposed model predicts the discharge magnitude and separation time distributions with good accuracy for all AC ripple amplitudes, below 50% of the AC partial discharge inception voltage.
- An AC ripple voltage with amplitude between the 50% and 100% of the PDIV value can provoke high frequency, bipolar PD bursts separated by large time intervals. The PD bursts are clusters of discharges with short discharge separation times. The discharge magnitude is higher during the bursts, than between the bursts. The discharge separation times are in the same order, and one order lower, as the AC ripple period time during the bursts.

The observations for the proposed MoM estimator at combined voltage on measured PD data are as follows:

- The estimated value for $\hat{\alpha}h$ of around 2.3 is in same range as estimated for the DC test series.

- The predicted value of the series dielectric capacitance is C_b = 0.61 pC; the estimated value is 0.39 pC, 36% lower than predicted. The estimated discharge radius is 0.8 mm, which is close to the 1 mm cavity radius.
- The estimated cavity voltage slope is 5 times the predicted value of 0.19 V per sec. The discrepancy is thus higher than for the estimated value for PD at DC voltage. In both cases, the reason for the higher cavity slope may be the mismatch between the measured conductivity of PET and the actual conductivity during the PD tests.

6 Conclusion

Partial discharges have previously been studied at AC voltage or DC voltage separately, but very little is known about partial discharges at combined DC and AC voltage. The present study was motivated by this knowledge gap and the fact that modern and future HVDC systems always will have an AC ripple voltage superimposed on the DC voltage.

The present work describes theoretical and experimental investigations of how a sinusoidal AC voltage ripple influences the PD process in dielectric bounded cavities. A new stochastic Monte Carlo model for the PD process at DC voltage and combined DC and AC voltage has been developed. The stochastic variables are the time lag and the phase-of-occurrence. The main physical parameters in the model are the Townsend coefficient product, αh, the mean statistical waiting time, τ_s, the capacitance in series with the cavity, C_b, and the rate of increase of the voltage over the cavity, $\frac{dv_c}{dt}$. The physical parameters could be extracted from statistical estimation methods using the measured PD data.

For PD at combined voltage, under the condition that the AC ripple voltage is lower than 50% of the AC partial discharge inception voltage, the following conclusions could be drawn:

- The discharge magnitude and the discharge separation time increase when an AC ripple is superimposed on the DC voltage. The predicted mean discharge magnitude and separation time are close to the measured values for AC ripple amplitudes corresponding to 4.4-50% of the measured $PDIV_{AC}$ value. The main effect of adding a sinusoidal ripple to the DC voltage is the increase in the effective time lag for starting electrons to trigger a discharge. The increase in the time lag could be described mathematically using the concept of duty cycle, defined as the fraction of one AC voltage time period in which the cavity voltage is above the critical voltage.
- The discharge separation time and discharge magnitude are not influenced by the AC ripple frequency if the AC ripple period time is shorter than the statistical waiting time.
- The discharge separation time distribution and apparent magnitude distribution widen and flatten with higher AC ripple amplitude.
- The discharge phase-of-occurrence distribution is symmetrical around the peak of the AC voltage and heightens and narrows with higher AC ripple amplitude.
- The estimated mean statistical waiting time from PD data is around 6 seconds, which is of the order of 1 second, as expected.
- The estimated value for the Townsend coefficient product is around 2.3. The estimated values from PD data are significantly lower than the predicted value of around 7 for dry air. The humidity in the cavity may decrease the Townsend coefficient by as much as 40%, compared to dry air conditions. The dielectric surfaces of the cavity may also influence the ionisation process considerably and decrease the value of the Townsend coefficient product.

- The predicted value of the series dielectric capacitance is C_b = 0.61 pC; the estimated value from measured PD data is 0.39 pC, 36% lower than predicted. The estimated discharge radius is 0.8 mm, which is close to the 1 mm cavity radius.
- The estimated cavity voltage slope is 5 times the predicted value of 0.19 V per sec. This may be explained by a mismatch between the measured conductivity of PET and the actual conductivity during the PD tests.

For PD at combined voltage, under the condition that the AC ripple voltage is higher than the 50% of measured AC partial discharge inception voltage, the following conclusions could be drawn:

- Clusters of discharges with short separation times can be observed if sufficient amount of start electrons are available on both cavity surfaces. The clusters are separated by long time periods.
- The clusters of discharges are termed bursts and are characterised by:
    - Discharges of negative and positive polarity.
    - The discharge magnitude is higher during the bursts, than between the bursts.
    - The discharge separation times are in the same order, and one order lower, as the AC ripple period time during the bursts.

For PD at DC voltage, the following conclusions can be drawn:

- There is a positive correlation between the measured moving average of the apparent discharge magnitude and the separation time as a function of time.
- The measured mean discharge magnitude per separation time is essentially constant during a test sequence, as predicted by the model. The predicted value is lower than the measured value, which may be explained by a higher conductivity of the PET film than expected during the PD experiments.
- By simulation of PD at DC voltage, it was shown that the DC OLS and MoM estimators are sensitive to the discharge detection threshold. The estimated values are expected to deviate considerably from the real values if the detection threshold is higher than 3 pC. Test setups used for DC voltage PD detection should have a very low detection threshold to conserve information in the PD data.
- The AC source introduced a ripple of around 10 V during the PD tests at DC voltage, even if the AC voltage was set to zero. It is plausible that the ripple caused higher discharges and longer separation times than what would have been measured at DC voltage without any AC voltage ripple.
- It was shown by simulation that the mean time lag and the mean recovery time are overestimated for both the DC OLS and DC MoM estimators on PD data from a combined voltage PD process. The estimated mean recovery time from PD data is approxamitely equal to the estimated mean time lag from PD data, at DC voltage conditions.
- The Townsend coefficient product can be estimated with reasonable accuracy by the DC OLS estimator on PD data from a combined voltage PD process. The

estimated value of the Townsend coefficient product from the measured PD data is in the range between 2 to 3, given by the DC OLS estimator.

7 Further work

Suggestions for further work are:

1. The effect of other waveforms should be studied: AC ripple waveform from Cockroft-Walton DC sources used in laboratories, waveforms with higher harmonics, and waveforms from HVDC stations with voltage source converter and current source converter technology.
2. The effect of an AC ripple should be studied for other materials, such as XLPE and mass-impregnated paper, for various cavity diameters and sample thicknesses.
3. A PD test setup with the ability to measure time-resolved PD currents together with a camera for visual inspection of the PDs can better distinguish between Townsend-like and streamer-like discharges and could be constructed to further evaluate the validity of the proposed model.
4. The ageing of PD under combined voltage should be studied for two regimes: AC ripple below 50% of the PDIVAC value and above 50% of the PDIVAC value. It is suspected that the occurrence of bursts will accelerate ageing of the insulation for the latter regime due to the higher discharge magnitude and repetition.
5. The pulse sequence analysis for PD at combined voltage can be improved, with application of the proposed model for the interpretation of $q_{a,i} - \Delta t_{pre,i}$ and $q_{a,i} - \Delta t_{suc,i}$ diagrams.

References

[1] R. Vogelsang, B. Cables, O. Sekula, H. Nyffenegger, W. Weissenberg, and B. Cables, "Long-term experiences with XLPE cable systems up to 550 kV," 2009. /paper/Long-term-experiences-with-XLPE-cable-systems-up-to-Vogelsang-Cables/eb7edd69a2baa7705061a53173f2398402432840 (accessed Jun. 05, 2020).

[2] I. E. C. Standard, "High-voltage test techniques: partial discharge measurements," *IEC-60270*, 2000.

[3] P. H. F. Morshuis and J. J. Smit, "Partial discharges at DC voltage: their mechanism, detection and analysis," *Dielectr. Electr. Insul. IEEE Trans. On*, vol. 12, pp. 328–340, 2005.

[4] E. C. Rogers and D. J. Skipper, "Gaseous discharge phenomena in high-voltage dc cable dielectrics," *Proc. IEE-Part Power Eng.*, vol. 107, no. 33, pp. 241–251, 1960.

[5] S. Beg and B. Salvage, "Discharge repetition in an air-filled cavity in polythene under high direct electric stresses at elevated temperatures," *Electron. Lett.*, vol. 5, no. 6, pp. 118–120, 1969.

[6] J. C. Devins, "The 1984 J. B. Whitehead Memorial Lecture the Physics of Partial Discharges in Solid Dielectrics," *IEEE Trans. Electr. Insul.,* vol. EI-19, pp. 475–495, 1984, doi: 10.1109/TEI.1984.298770.

[7] U. Fromm, "Interpretation of partial discharges at dc voltages," *Dielectr. Electr. Insul. IEEE Trans. On*, vol. 2, pp. 761–770, 1995, doi: 10.1109/94.469972.

[8] J. Beyer, *Space charge and partial discharge phenomena in high voltage DC devices*. TU Delft, Delft University of Technology, 2002.

[9] R. E. Jones and R. T. Waters, "Factors controlling the performance of cascade rectifier circuits," *Proc. Inst. Electr. Eng.*, vol. 111, no. 5, pp. 1059–1067, May 1964, doi: 10.1049/piee.1964.0163.

[10] C. H. Chien and R. W. G. Bucknall, "Analysis of harmonics in subsea power transmission cables used in VSC-HVDC transmission systems operating under steady-state conditions," *IEEE Trans. Power Deliv.*, vol. 22, pp. 2489–2497, 2007, doi: 10.1109/tpwrd.2007.905277.

[11] M. Barnes and A. Beddard, "Voltage Source Converter HVDC Links – The State of the Art and Issues Going Forward," *Energy Procedia*, vol. 24, pp. 108–122, 2012, doi: http://dx.doi.org/10.1016/j.egypro.2012.06.092.

[12] T. Dezenzo, T. Betz, and A. Schwarzbacher, "Transfer and evaluation of the AC PRPD representation for internal PD at DC voltage," in *2016 IEEE International Conference on Dielectrics (ICD)*, Jul. 2016, vol. 1, pp. 528–531, doi: 10.1109/ICD.2016.7547658.

[13] M. A. Fard, A. J. Reid, and D. M. Hepburn, "Analysis of HVDC superimposed harmonic voltage effects on partial discharge behavior in solid dielectric media," *IEEE Trans. Dielectr. Electr. Insul.*, vol. 24, no. 1, pp. 7–16, Feb. 2017, doi: 10.1109/TDEI.2016.005934.

[14] Y. Sha, Y. Zhou, J. Li, and J. Wang, "Partial discharge characteristics in oil-paper insulation under combined AC-DC voltage," *IEEE Trans. Dielectr. Electr. Insul.*, vol. 21, no. 4, pp. 1529–1539, Aug. 2014, doi: 10.1109/TDEI.2014.004273.

[15] B. Qi, Z. Wei, C. Li, Y. Gao, and X. Zhang, "Influences of Different Ratios of AC-DC Combined Voltage on Internal Gas Cavity Discharge in Oil-Pressboard Insulation,"

IEEE Trans. Power Deliv., vol. 31, no. 3, pp. 1026–1033, Jun. 2016, doi: 10.1109/TPWRD.2015.2431275.

[16] F. Seifert and C. Leu, "Characterization of surface discharges at high DC voltage superimposed by a medium frequency high voltage," in *VDE High Voltage Technology 2018; ETG-Symposium*, Nov. 2018, pp. 1–6.

[17] Y. X. Zhou *et al.*, "Effects of thermal aging on creepage discharge in oil- impregnated pressboard under combined AC-DC voltage," *IEEE Trans. Dielectr. Electr. Insul.*, vol. 22, no. 5, pp. 2737–2746, Oct. 2015, doi: 10.1109/TDEI.2015.005023.

[18] F. Jin, Y. Zhou, B. Liang, Z. Zhou, and L. Zhang, "Effects of temperature on creepage discharge characteristics in oil-impregnated pressboard insulation under combined AC-DC voltage," *Plasma Sci. Technol.*, vol. 21, no. 5, 2019, doi: 10.1088/2058-6272/aaff01.

[19] S. Li, W. Si, and Q. Li, "Partition and recognition of partial discharge development stages in oil-pressboard insulation with needle-plate electrodes under combined AC-DC voltage stress," *IEEE Trans. Dielectr. Electr. Insul.*, vol. 24, no. 3, pp. 1781–1793, Jun. 2017, doi: 10.1109/TDEI.2017.006361.

[20] S. Li, Q. Li, W. Si, and J. Yao, "An image-oriented recognition method for PD development stage in oil-pressboard insulation with needle-plate model under AC-DC mixed voltage," in *2017 1st International Conference on Electrical Materials and Power Equipment (ICEMPE)*, May 2017, pp. 275–282, doi: 10.1109/ICEMPE.2017.7982084.

[21] T. Dezenzo, T. Betz, and A. Schwarzbacher, "An equivalent circuit for corona discharges caused by a point to plane arrangement at ac, dc and combined voltages," in *2017 IEEE Conference on Electrical Insulation and Dielectric Phenomenon (CEIDP)*, Oct. 2017, pp. 315–318, doi: 10.1109/CEIDP.2017.8257456.

[22] K. Helal, R. A. A. El-Aal, S. S. Dessouky, K. Backhaus, J. Speck, and S. Grossmann, "Partial discharge characteristics of a gas void embedded between oil impregnated papers under the effect of AC and DC voltage," in *2018 IEEE 2nd International Conference on Dielectrics (ICD)*, Jul. 2018, pp. 1–4, doi: 10.1109/ICD.2018.8514667.

[23] E. Takahashi, Y. Tsutsumi, K. Okuyama, and F. Ogata, "Partial discharge characteristics of oil-immersed insulation systems under DC, combined AC-DC and DC reversed polarity voltage," *IEEE Trans. Power Appar. Syst.*, vol. 95, no. 1, pp. 411–420, 1976.

[24] W. Si, S. Li, H. Xiao, and Q. Li, "PD characteristics and development degree assessment of oil-pressboard insulation with ball-plate model under 1:1 combined AC-DC voltage," *IEEE Trans. Dielectr. Electr. Insul.*, vol. 24, no. 6, pp. 3677–3686, Dec. 2017, doi: 10.1109/TDEI.2017.006737.

[25] J. Li, X. Han, Z. Liu, X. Yao, and Y. Li, "PD characteristics of oil-pressboard insulation under AC and DC mixed voltage," *IEEE Trans. Dielectr. Electr. Insul.*, vol. 23, no. 1, pp. 444–450, Feb. 2016, doi: 10.1109/TDEI.2015.004650.

[26] E. C. Rogers and D. J. Skipper, "Gaseous discharge phenomena in high-voltage dc cable dielectrics," *Proc. IEE-Part Power Eng.*, vol. 107, no. 33, pp. 241–251, 1960.

[27] E. J. M. R. Bartnikas, *Corona measurement and interpretation*, vol. 1, 6 vols. American society for testing and materials, 1979.

[28] H. Saadati, J. Seifert, P. Werle, and E. Gockenbach, “Investigation on the partial discharge behaviour in GFRP under AC and combined AC/DC field stress,” in *VDE High Voltage Technology 2016; ETG-Symposium*, Nov. 2016, pp. 1–5.
[29] T. Kawashima, K. Inoue, K. Yokomi, Y. Murakami, T. Ishida, and M. Nagao, “Influence of surface charge on DC or AC partial discharge inception voltage in insulation-air gap composite system,” *IEEJ Trans. Fundam. Mater.*, vol. 135, no. 4, pp. 235–240, 2015, doi: 10.1541/ieejfms.135.235.
[30] Samir Shihab, “Teilentladungen in Hohlräumen von polymeren Isolierstoffen bei hoher Gleichspannung,” Braunschweig, Techn. Univ., Fak. f. Maschinenbau u. Elektrotechnik, 1972.
[31] H. Feibus, “Corona in Solid-Insulation Systems,” *IEEE Trans. Electr. Insul.*, vol. EI-5, no. 3, pp. 72–78, Sep. 1970, doi: 10.1109/TEI.1970.299099.
[32] R. Piccin, A. R. Mor, P. Morshuis, A. Girodet, and J. Smit, “Partial discharge analysis of gas insulated systems at high voltage AC and DC,” *IEEE Trans. Dielectr. Electr. Insul.*, vol. 22, no. 1, pp. 218–228, Feb. 2015, doi: 10.1109/TDEI.2014.004711.
[33] L. Niemeyer, “A generalized approach to partial discharge modeling,” *IEEE Trans. Dielectr. Electr. Insul.*, vol. 2, pp. 510–528, 1995.
[34] P. von Glahn and R. J. V. Brunt, “Continuous recording and stochastic analysis of PD,” *IEEE Trans. Dielectr. Electr. Insul.*, vol. 2, no. 4, pp. 590–601, Aug. 1995, doi: 10.1109/94.407024.
[35] C. Heitz, “A generalized model for partial discharge processes based on a stochastic process approach,” *J. Phys. Appl. Phys.*, vol. 32, no. 9, p. 1012, 1999, doi: 10.1088/0022-3727/32/9/312.
[36] R. Altenburger, C. Heitz, and J. Timmer, “Analysis of phase-resolved partial discharge patterns of voids based on a stochastic process approach,” *J. Phys. Appl. Phys.*, vol. 35, no. 11, p. 1149, 2002, doi: 10.1088/0022-3727/35/11/309.
[37] P. Morshuis, M. Jeroense, and J. Beyer, “Partial discharge. Part XXIV: The analysis of PD in HVDC equipment,” *IEEE Electr. Insul. Mag.*, vol. 13, no. 2, pp. 6–16, Mar. 1997, doi: 10.1109/57.583421.
[38] R. J. van Brunt and P. von Glahn, “Improved Monte-Carlo simulator of partial discharge,” in *Proceedings of Conference on Electrical Insulation and Dielectric Phenomena - CEIDP ’96*, Oct. 1996, vol. 2, pp. 504–509 vol.2, doi: 10.1109/CEIDP.1996.564520.
[39] C. Pan *et al.*, “Investigation of cavity PD physical processes at DC voltage by simulation,” *IEEJ Trans. Electr. Electron. Eng.*, vol. 13, no. 10, pp. 1376–1383, 2018, doi: 10.1002/tee.22704.
[40] E. J. M. R. Bartnikas, *Corona measurement and interpretation*, vol. 1, 6 vols. American society for testing and materials, 1979.
[41] H. A. Haus and J. R. Melcher, *Electromagnetic fields and energy*. Prentice Hall, 1989.
[42] J. H. Mason, “The deterioration and breakdown of dielectrics resulting from internal discharges,” *Proc. IEE - Part Gen.*, vol. 98, no. 109, pp. 44–59, Jan. 1951, doi: 10.1049/pi-1.1951.0019.
[43] M. Budde and M. Kurrat, “Partial Discharge Diagnostics of Micro Cavities in Epoxy Insulating Materials and their Modelling,” in *Conference Record of the 2008 IEEE*

International Symposium on Electrical Insulation, Jun. 2008, pp. 369–372, doi: 10.1109/ELINSL.2008.4570351.
[44] Udo Fromm, "Partial Discharge and Breakdown Testing at High DC Voltage," Monograph, Delft University of Technology, 1995.
[45] R. Patsch and F. Berton, "Pulse Sequence Analysis - a diagnostic tool based on the physics behind partial discharges," *J. Phys. Appl. Phys.*, vol. 35, no. 1, p. 25, 2002, doi: 10.1088/0022-3727/35/1/306.
[46] W. Böning, "Luftgehalt und Luftspaltverteilung geschichteter Dielektrika I. Untersuchung der Entladungen in einzelnen Luftspalten bei äußerem Wechselfeld," *Arch. Für Elektrotechnik*, vol. 48, no. 1, pp. 7–22, Jan. 1963, doi: 10.1007/BF01580156.
[47] D. R. Bartnikas, "Discharge rate and energy loss in helium at low frequencies," *Arch. Für Elektrotechnik*, vol. 52, no. 6, pp. 348–359, Nov. 1969, doi: 10.1007/BF01573780.
[48] K. C. Kao, *Dielectric phenomena in solids*. Academic press, 2004.
[49] A. K. Jonscher, "Dielectric relaxation in solids," *J. Phys. Appl. Phys.*, vol. 32, no. 14, p. R57, 1999, doi: 10.1088/0022-3727/32/14/201.
[50] D. M. Taylor and T. J. Lewis, "Electrical conduction in polyethylene terephthalate and polyethylene films," *J. Phys. Appl. Phys.*, vol. 4, no. 9, p. 1346, 1971.
[51] F. H. Kreuger and U. Fromm, "Partial Discharges in Gaseous Voids for DC Voltage," *Jpn. J. Appl. Phys.*, vol. 33, no. Part 1, No. 2, pp. 1079–1084, Feb. 1994, doi: 10.1143/JJAP.33.1079.
[52] K. Zuber, "Über die Verzögerungszeit bei der Funkenentladung," *Ann. Phys.*, vol. 381, no. 2–3, pp. 231–260, 1925, doi: 10.1002/andp.19253810208.
[53] M. Rausand and A. Høyland, *System Reliability Theory: Models and Statistical Methods*. Hoboken, UNITED STATES: John Wiley & Sons, Incorporated, 1994.
[54] C. Forssén, "Modelling of cavity partial discharges at variable applied frequency," KTH, 2008.
[55] K. Temmen, "Evaluation of surface changes in flat cavities due to ageing by means of phase-angle resolved partial discharge measurement," *J. Phys. Appl. Phys.*, vol. 33, no. 6, p. 603, 2000, doi: 10.1088/0022-3727/33/6/303.
[56] L. Niemeyer, "A generalized approach to partial discharge modeling," *IEEE Trans. Dielectr. Electr. Insul.*, vol. 2, pp. 510–528, 1995.
[57] D. B. Hibbert and A. J. B. Robertson, "The emission of electrons from glass induced by a strong electric field and the mechanism of the silent electric discharge," *Proc R Soc Lond A*, vol. 349, no. 1656, pp. 63–79, Apr. 1976, doi: 10.1098/rspa.1976.0060.
[58] D. B. Hibbert, T. M. Roberts, and S. H. Bhote, "A model of field induced electron emission from ionically-conducting glasses," *J. Phys. Appl. Phys.*, vol. 18, no. 9, p. 1833, 1985, doi: 10.1088/0022-3727/18/9/014.
[59] R. Patsch, F. Berton, and J. Jung, "Space charge, local electric field and partial discharges," in *Dielectric Materials, Measurements and Applications, 2000. Eighth International Conference on (IEE Conf. Publ. No. 473)*, 2000, pp. 519–522, doi: 10.1049/cp:20000563.
[60] R. J. V. Brunt, E. W. Cernyar, and P. von Glahn, "Importance of unraveling memory propagation effects in interpreting data on partial discharge statistics," *IEEE Trans. Electr. Insul.*, vol. 28, no. 6, pp. 905–916, Dec. 1993, doi: 10.1109/14.249364.

[61] M. Meißer, “Resonant Behaviour of Pulse Generators for the Efficient Drive of Optical Radiation Sources Based on Dielectric Barrier Discharges,” Karlsruher Instituts für Technologie (KIT), 2013.
[62] C. Forssen and H. Edin, “Partial discharges in a cavity at variable applied frequency part 2: measurements and modeling,” *IEEE Trans. Dielectr. Electr. Insul.*, vol. 15, pp. 1610–1616, 2008.
[63] J. C. Devins, “The 1984 J. B. Whitehead Memorial Lecture the Physics of Partial Discharges in Solid Dielectrics,” *IEEE Trans. Electr. Insul.*, vol. EI-19, no. 5, pp. 475–495, Oct. 1984, doi: 10.1109/TEI.1984.298770.
[64] P. Morshuis and L. Niemeyer, “Measurement and simulation of discharge induced ageing processes in voids,” Oct. 1996, vol. 2, pp. 520–524 vol.2, doi: 10.1109/ceidp.1996.564524.
[65] L. A. Dissado and J. C. Fothergill, *Electrical degradation and breakdown in polymers*. London: P. Peregrinus, 1992.
[66] P. H. F. Morshuis, “Partial discharge mechanisms: mechanisms leading to breakdown, analyzed by fast electrical and optical measurements,” Delft University Press, Delft, 1993.
[67] A. Pedersen, G. C. Crichton, and I. W. McAllister, “The theory and measurement of partial discharge transients,” *IEEE Trans. Electr. Insul.*, vol. 26, no. 3, pp. 487–497, Jun. 1991, doi: 10.1109/14.85121.
[68] J. B. Luezynski, “Partial Discharges in Artificial Gas-Filled Cavities in Solid High-Voltage Insulation,” Ph. D. Thesis, Electric Power Engineering Dept., Technical University of Denmark, Lyngby, 1979.
[69] A. N. Kontaratos, “On the functional dependence of Townsend’s first ionization coefficient,” *Appl. Sci. Res. Sect. A*, vol. 12, no. 1, pp. 27–32, Jan. 1965, doi: 10.1007/BF00382104.
[70] W. S. Zaengl, S. Yimvuthikul, and G. Friedrich, “The temperature dependence of homogeneous field breakdown in synthetic air,” *IEEE Trans. Electr. Insul.*, vol. 26, no. 3, pp. 380–390, Jun. 1991, doi: 10.1109/14.85107.
[71] “Measurement of the First Townsend’s Ionization Coefficients in Helium, Air, and Nitrogen at Atmospheric Pressure,” *J. Phys. Soc. Jpn.*, vol. 83, no. 7, p. 074503, Jun. 2014, doi: 10.7566/JPSJ.83.074503.
[72] J. Dutton, F. M. Harris, and F. L. Jones, “The Determination of Attachment and Ionization Coefficients in Air,” *Proc. Phys. Soc.*, vol. 81, no. 1, p. 52, 1963, doi: 10.1088/0370-1328/81/1/311.
[73] L. A. Dissado and J. C. Fothergill, *Electrical degradation and breakdown in polymers*. London: P. Peregrinus, 1992.
[74] U. Fromm and E. Gulski, “Statistical behaviour of internal partial discharges at DC voltage,” in *, Proceedings of the 4th International Conference on Properties and Applications of Dielectric Materials, 1994*, Jul. 1994, vol. 2, pp. 670–673 vol.2, doi: 10.1109/ICPADM.1994.414099.
[75] A. Høyland, *Sannsynlighetsregning og statistisk metodelære: 2 : Statistisk metodelære*, 3. utg., vol. 2. Trondheim: Tapir, 1983.
[76] *Introduction to Robust Estimation and Hypothesis Testing*. Elsevier, 2012.

[77] B. Efron and R. J. Tibshirani, *An Introduction to the Bootstrap*. CRC Press, 1994.
[78] "Mean squared error," *Wikipedia*. Apr. 15, 2020, Accessed: May 27, 2020. [Online]. Available: https://en.wikipedia.org/w/index.php?title=Mean_squared_error&oldid=951189167.
[79] A. Cavallini, R. Ciani, M. Conti, P. F. H. Morshuis, and G. C. Montanari, "Modeling memory phenomena for partial discharge processes in insulation cavities," in *Conference on Electrical Insulation and Dielectric Phenomena, 2003. Annual Report*, Oct. 2003, pp. 723–727, doi: 10.1109/CEIDP.2003.1254956.
[80] G. Chen and Z. Xu, "Charge trapping and detrapping in polymeric materials," *J. Appl. Phys.*, vol. 106, no. 12, p. 123707, Dec. 2009, doi: 10.1063/1.3273491.
[81] P. H. F. Morshuis, "Partial discharge mechanisms: mechanisms leading to breakdown, analyzed by fast electrical and optical measurements," Delft University Press, Delft, 1993.
[82] U. Fromm and F. H. Kreuger, "Statistical Behaviour of Internal Partial Discharges at DC Voltage," *Jpn. J. Appl. Phys.*, vol. 33, no. 12R, p. 6708, Dec. 1994, doi: 10.1143/JJAP.33.6708.
[83] J. Kindersberger and C. Lederle, "Surface charge decay on insulators in air and sulfurhexafluorid - part II: measurements," *IEEE Trans. Dielectr. Electr. Insul.*, vol. 15, no. 4, pp. 949–957, Aug. 2008, doi: 10.1109/TDEI.2008.4591215.
[84] J. Kindersberger and C. Lederle, "Surface charge decay on insulators in air and sulfurhexafluorid - part I: simulation," *IEEE Trans. Dielectr. Electr. Insul.*, vol. 15, no. 4, pp. 941–948, Aug. 2008, doi: 10.1109/TDEI.2008.4591214.
[85] H. C. Hall and R. M. Russek, "Discharge inception and extinction in dielectric voids," *Proc. IEE-Part II Power Eng.*, vol. 101, no. 79, pp. 47–55, 1954.
[86] R. S. Dhariwal, J. M. Torres, and M. P. Y. Desmulliez, "Electric field breakdown at micrometre separations in air and nitrogen at atmospheric pressure," *IEE Proc. - Sci. Meas. Technol.*, vol. 147, no. 5, pp. 261–265, Sep. 2000, doi: 10.1040/ip-smt:20000506.
[87] H. Ritz, "Durchschlagfeldstärke des homogenen Feldes in Luft," *Arch. Für Elektrotechnik*, vol. 26, no. 4, pp. 219–232, Apr. 1932, doi: 10.1007/BF01657189.
[88] C. Forssén, "Modelling of cavity partial discharges at variable applied frequency," KTH, 2008.
[89] T. W. Dakin, G. Luxa, G. Oppermann, J. Vigreux, G. Wind, and H. Winkelnkemper, "Breakdown of gases in uniform fields. Paschen curves for nitrogen, air and sulfur hexafluoride," *Electra*, vol. 32, pp. 61–82, 1974.
[90] P. K. Olsen, F. Mauseth, and E. Ildstad, "The effect of DC superimposed AC voltage on partial discharges in dielectric bounded cavities," Sep. 2014, pp. 1–4, doi: 10.1109/ICHVE.2014.7035408.
[91] F. H. Kreuger, "Determination of the Internal Discharge Resistance of Dielectric Materials," *IEEE Trans. Electr. Insul.*, vol. EI-3, pp. 106–114, 1968, doi: 10.1109/TEI.1968.299039.
[92] T. A. Ve, F. Mauseth, and E. Ildstad, "Effect of water content on the conductivity of XLPE insulation," in *2012 Annual Report Conference on Electrical Insulation and*

Dielectric Phenomena (CEIDP), Oct. 2012, pp. 649–653, doi: 10.1109/CEIDP.2012.6378864.

[93] W. S. Zaengl, "Dielectric spectroscopy in time and frequency domain for HV power equipment. I. Theoretical considerations," *IEEE Electr. Insul. Mag.*, vol. 19, no. 5, pp. 5–19, Sep. 2003, doi: 10.1109/MEI.2003.1238713.

[94] T. K. Saha and P. Purkait, "Investigation of polarization and depolarization current measurements for the assessment of oil-paper insulation of aged transformers," *IEEE Trans. Dielectr. Electr. Insul.*, vol. 11, no. 1, pp. 144–154, Feb. 2004, doi: 10.1109/TDEI.2004.1266329.

[95] D. K. D. Gupta and K. Joyner, "On the nature of absorption currents in polyethyleneterephthalate (PET)," *J. Phys. Appl. Phys.*, vol. 9, no. 5, p. 829, 1976, doi: 10.1088/0022-3727/9/5/016.

[96] Y. Inuishi and D. A. Powers, "Electric Breakdown and Conduction through Mylar Films," *J. Appl. Phys.*, vol. 28, no. 9, pp. 1017–1022, Sep. 1957, doi: 10.1063/1.1722899.

[97] W. G. Lawson, "High-field conduction and breakdown in polythene," *Br. J. Appl. Phys.*, vol. 16, no. 12, p. 1805, 1965, doi: 10.1088/0508-3443/16/12/304.

[98] L. E. Lundgaard, D. Linhjell, O. L. Hestad, and J.-T. Borlaug, "High frequency dielectric response of paper/oil insulation," in *2008 IEEE International Conference on Dielectric Liquids*, Jun. 2008, pp. 1–4, doi: 10.1109/ICDL.2008.4622461.

[99] A. K. Jonscher, "Dielectric relaxation in solids," *J. Phys. Appl. Phys.*, vol. 32, no. 14, p. R57, 1999, doi: 10.1088/0022-3727/32/14/201.

[100] A. C. Lilly and J. R. McDowell, "High-Field Conduction in Films of Mylar and Teflon," *J. Appl. Phys.*, vol. 39, no. 1, pp. 141–147, Jan. 1968, doi: 10.1063/1.1655720.

[101] E. Neagu, P. Pissis, and L. Apekis, "Electrical conductivity effects in polyethylene terephthalate films," *J. Appl. Phys.*, vol. 87, pp. 2914–2922, 2000.

[102] B. Demirel, A. Yaraş, and H. Elçiçek, "Crystallization behavior of PET materials," *Balıkesir Üniversitesi Fen Bilim. Enstitüsü Derg.*, vol. 13, no. 1, pp. 26–35, 2016.

[103] E. Neagu, P. Pissis, L. Apekis, and J. L. G. Ribelles, "Dielectric relaxation spectroscopy of polyethylene terephthalate (PET) films," *J. Phys. Appl. Phys.*, vol. 30, no. 11, p. 1551, 1997, doi: 10.1088/0022-3727/30/11/003.

[104] F. Hami, H. Boulzazen, F. Duval, and M. Kadi, "Wideband impedance characterization and modeling of power electronic capacitors under high bias voltage variation," in *2014 International Symposium on Electromagnetic Compatibility*, Sep. 2014, pp. 928–933, doi: 10.1109/EMCEurope.2014.6931036.

[105] S. Serra, G. C. Montanari, and G. Mazzanti, "Theory of inception mechanism and growth of defect-induced damage in polyethylene cable insulation," *J. Appl. Phys.*, vol. 98, no. 3, p. 034102, Aug. 2005, doi: 10.1063/1.1978986.

[106] J. H. Mason, "Dielectric breakdown in solid insulation," *Prog. Dielectr.*, vol. 1, pp. 1–58, 1959.

[107] S. Beg and B. Salvage, "Discharge repetition in an air-filled cavity in polythene under high direct electric stresses at elevated temperatures," *Electron. Lett.*, vol. 5, no. 6, pp. 118–120, 1969.

[108] S. Beg and B. Salvage, “Discharge repetition in an air-filled cavity in polythene under high direct electric stresses at elevated temperatures,” *Electron. Lett.*, vol. 5, pp. 118–120, 1969, doi: 10.1049/el:19690089.
[109] B. Salvage and N. R. Steinberg, “Discharge repetition in an air-filled cavity in a solid dielectric under direct-voltage conditions,” *Electron. Lett.*, vol. 2, no. 11, pp. 432–433, Nov. 1966, doi: 10.1049/el:19660362.
[110] L. Hui, L. S. Schadler, and J. K. Nelson, “The influence of moisture on the electrical properties of crosslinked polyethylene/silica nanocomposites,” *IEEE Trans. Dielectr. Electr. Insul.*, vol. 20, no. 2, pp. 641–653, Apr. 2013, doi: 10.1109/TDEI.2013.6508768.
[111] A. A. Ganjovi, N. Gupta, and G. R. Govinda Raju, “A kinetic model of a PD pulse within voids of sub-millimeter dimensions,” *IEEE Trans. Dielectr. Electr. Insul.*, vol. 16, no. 6, pp. 1743–1754, Dec. 2009, doi: 10.1109/TDEI.2009.5361598.
[112] R. Bartnikas and J. P. Novak, “Effect of overvoltage on the risetime and amplitude of PD pulses,” *IEEE Trans. Dielectr. Electr. Insul.*, vol. 2, no. 4, pp. 557–566, Aug. 1995, doi: 10.1109/94.407021.
[113] “Maximum likelihood estimation,” *Wikipedia*. Mar. 04, 2020, Accessed: Mar. 19, 2020. [Online]. Available: https://en.wikipedia.org/w/index.php?title=Maximum_likelihood_estimation&oldid=943960597.
[114] “Probability density function,” *Wikipedia*. Jun. 23, 2020, Accessed: Jun. 28, 2020. [Online]. Available: https://en.wikipedia.org/w/index.php?title=Probability_density_function&oldid=964115520.
[115] “Probability density function,” *Wikipedia*. May 20, 2020, Accessed: May 28, 2020. [Online]. Available: https://en.wikipedia.org/w/index.php?title=Probability_density_function&oldid=957864017.
[116] “Expected value,” *Wikipedia*. Nov. 23, 2019, Accessed: Nov. 26, 2019. [Online]. Available: https://en.wikipedia.org/w/index.php?title=Expected_value&oldid=927523456.
[117] J. K. Blitzstein and J. Hwang, *Introduction to Probability*, 2nd ed. CRC Press, Chapman & Hall, 2019.
[118] P. Morshuis, M. Jeroense, and J. Beyer, “Partial discharge. Part XXIV: The analysis of PD in HVDC equipment,” *IEEE Electr. Insul. Mag.*, vol. 13, no. 2, pp. 6–16, Mar. 1997, doi: 10.1109/57.583421.
[119] “Ordinary least squares,” *Wikipedia*. Feb. 06, 2020, Accessed: Mar. 19, 2020. [Online]. Available: https://en.wikipedia.org/w/index.php?title=Ordinary_least_squares&oldid=939371901.

Appendix A Model of the PD sequence at DC voltage

A flow chart of the PD sequence model at DC voltage is shown in Fig. 0-1. The input for the model is the physical parameters αh , τ_s , C_b , $\frac{dv_c}{dt}$, as well as the applied DC voltage V_{DC} and the number of discharges n . The model produces the sets:

$$t_L = \left[t_{L,1}, ..., t_{L,i}, ..., t_{L,n} \right] \quad (0.1)$$

$$q_a = \left[q_{a,1}, ..., q_{a,i}, ..., q_{a,n} \right] \quad (0.2)$$

$$t_R = \left[t_{R,1}, ..., t_{R,i}, ..., t_{R,n} \right] \quad (0.3)$$

The output of the model are the measurable quantities the apparent discharge magnitude and the discharge separation time, which is assembled from the sets t_L, q_a and t_R :

$$q_a = \left[q_{a,2}, ..., q_{a,i}, ..., q_{a,n-1} \right] \quad (0.4)$$

$$\Delta t_{pre} = \left[\left(t_{R,1} + t_{L,2} \right), ..., \left(t_{R,n-2} + t_{L,n-1} \right) \right] \quad (0.5)$$

$$\Delta t_{suc} = \left[\left(t_{R,2} + t_{L,3} \right), ..., \left(t_{R,n-1} + t_{L,n} \right) \right] \quad (0.6)$$

Although n discharges is generated in the Monte Carlo simulation, the output is $n-2$ discharges because the first and last discharge must be discarded. If a threshold is set the discharge separation time is recalculated as follows:

1) The set of time-of-occurrence before filtering, for k elements in, is:

$$t = \left[\Delta t_{pre,1}, \left(\Delta t_{pre,1} + \Delta t_{pre,2} \right), ..., \sum_{j=1}^{k} \Delta t_{pre,j} \right] \quad (0.7)$$

2) The set of time-of-occurrence after filtering, t^*, is found by deleting all elements in (0.7) corresponding to $q_{a,i} < q_{a,threshold}$, resulting in m elements in t^* .

3) The filtered time to previous discharge and to successive discharge is calculated as:

$$\Delta t^*_{pre} = \left[t^*_1, \left(t^*_2 - t^*_1 \right), ..., \left(t^*_{m-1} - t^*_{m-2} \right) \right] \quad (0.8)$$

$$\Delta t^*_{suc} = \left[\left(t^*_2 - t^*_1 \right), \left(t^*_3 - t^*_2 \right), ..., \left(t^*_m - t^*_{m-1} \right) \right] \quad (0.9)$$

4) The corresponding filtered discharge magnitudes are found by

$$q^*_a = q_a \left(t^* \right) \quad (0.10)$$

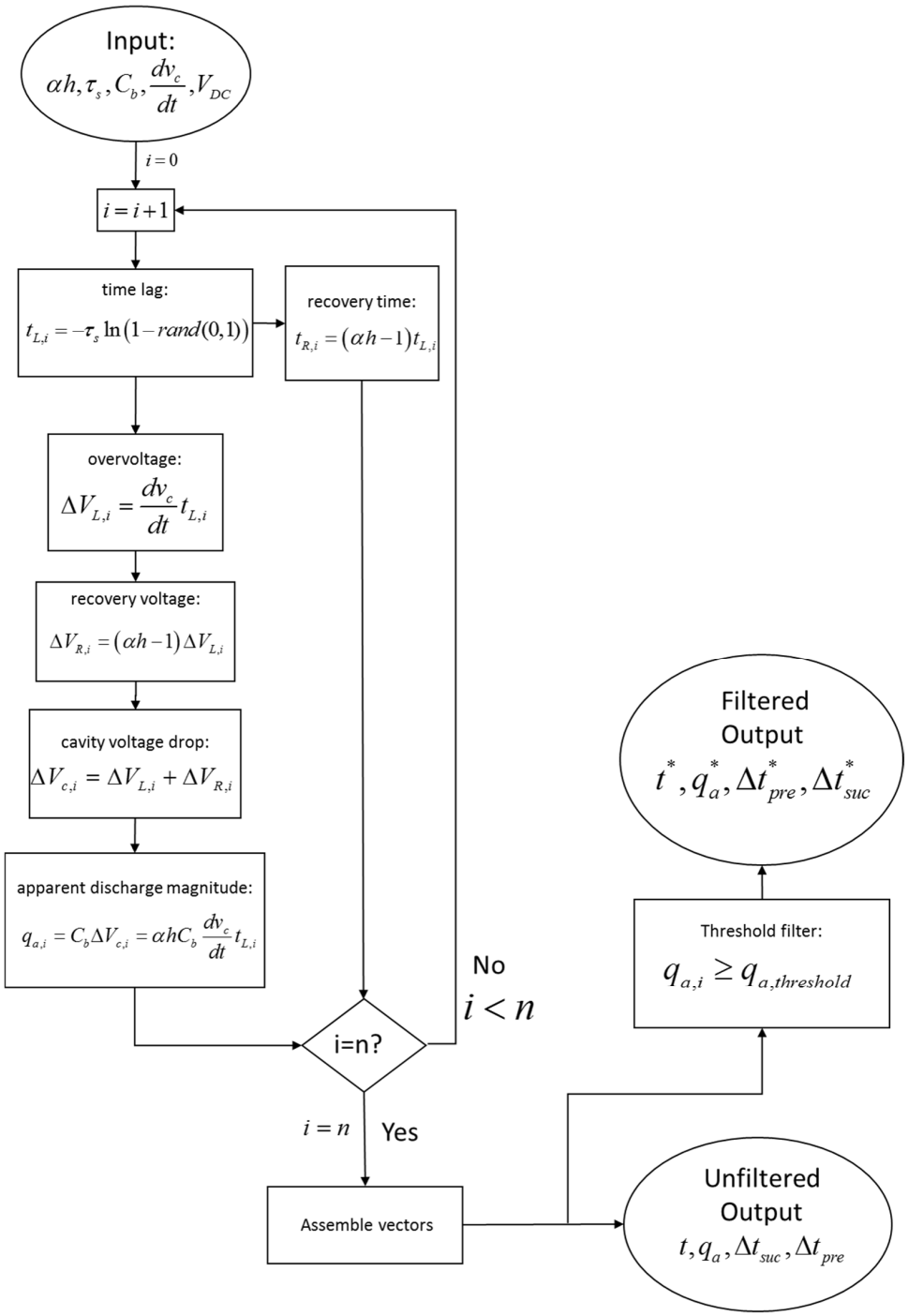

Fig. 0-1 Pulse sequence Monte Carlo model for partial discharges at DC voltage with no AC ripple voltage

A.1 Analytic expression for mean discharge magnitude

By using the relationship developed in 3.2.2.5, eq. (3.19), the apparent discharge magnitude of the i-th discharge can be expressed as:

$$q_{a,i} = \alpha h C_b \frac{dv_c}{dt} t_{L,i} \quad (0.11)$$

The analytic expression for the mean discharge magnitude can be obtained as follows:

1) Take the sum on both sides of (0.11), from $i = 1$ to $i = n$:

$$\sum_{i=1}^{n} q_{a,i} = \sum_{i=1}^{n} \alpha h C_b \frac{dv_c}{dt} t_{L,i} \quad (0.12)$$

$$\sum_{i=1}^{n} q_{a,i} = \alpha h C_b \frac{dv_c}{dt} \sum_{i=1}^{n} t_{L,i} \quad (0.13)$$

2) Divide by n on each side

$$\frac{1}{n}\sum_{i=1}^{n} q_{a,i} = \alpha h C_b \frac{dv_c}{dt} \frac{1}{n}\sum_{i=1}^{n} t_{L,i} \quad (0.14)$$

3) By the definition of the mean quantities given in C.4 , we obtain:

$$\overline{q}_a = \alpha h C_b \frac{dv_c}{dt} \overline{t}_L \quad (0.15)$$

4) For large number of discharges $n \to \infty$ and $\overline{t}_L \to \tau_s$, the mean apparent discharge magnitude is then:

$$\overline{q}_a = \alpha h C_b \frac{dv_c}{dt} \tau_s \quad (0.16)$$

A.2 Analytic expression for discharge density function

The apparent discharge magnitude is given by:

$$q_{a,i} = \alpha h C_b \frac{dv_c}{dt} t_{L,i} \quad (0.17)$$

The distribution of the apparent discharge magnitude , $q_{a,i}$, can be found by transformation of the probability density of $t_{L,i}$:

$$pdf_{t_{L,i}}(t_L) = \frac{1}{\tau_s} \exp\left\{-\frac{1}{\tau_s} t_L\right\} \quad (0.18)$$

Now, by denoting:

$$f_Y(y) = pdf_{q_{a,i}}(q_a) \quad (0.19)$$

and

$$f_X(x) = pdf_{t_{L,i}}(t_L) \quad (0.20)$$

So, $Y = q_{a,i}$, $y = q_a$, $X = t_{L,i}$, and $x = t_L$. $y = g(x)$, corresponding to $q_a = g(t_L) = \alpha h C_b \frac{dv_c}{dt} t_L$. Then the distribution of the apparent discharge magnitude can be found by change of variables [114]:

$$f_Y(y) = f_X\left(g^{-1}(y)\right)\left|\frac{d}{dy} g^{-1}(y)\right| \quad (0.21)$$

Inserting into (0.38) yields :

$$pdf_{q_{a,i}}(q_a) = pdf_{t_{L,i}}\left(g^{-1}(q_a)\right)\left|\frac{d}{dq_a} g^{-1}(q_a)\right| \quad (0.22)$$

where

$$g^{-1}(q_a) = \frac{1}{\alpha h C_b \frac{dv_c}{dt}} q_a \quad (0.23)$$

and

$$\left|\frac{d}{dq_a} g^{-1}(q_a)\right| = \frac{1}{\alpha h C_b \frac{dv_c}{dt}} \quad (0.24)$$

Using eq. (0.18) we obtain

$$pdf_{q_{a,i}}(q_a) = \frac{1}{a h C_b \frac{dv_c}{dt} \tau_s} \exp\left\{-\frac{1}{a h C_b \frac{dv_c}{dt} \tau_s} q_a\right\} \quad (0.25)$$

Recognizing that $\bar{q}_a = \alpha h C_b \frac{dv_c}{dt} \tau_s$, eq. (0.16), the probability density of the apparent discharge magnitude can be expressed in terms of the mean apparent discharge magnitude:

$$pdf_{q_{a,i}}(q_a) = \frac{1}{\bar{q}_a} \exp\left\{-\frac{q_a}{\bar{q}_a}\right\} \quad (0.26)$$

A.3 Analytic expression for mean discharge separation time

By using the relationship developed in 3.2.2.6, eq. (3.22) , the i-th time to previous discharge can be expressed as:

$$\Delta t_{pre,i} = (\alpha h - 1) t_{L,i-1} + t_{L,i} \quad (0.27)$$

The mean discharge separation time can be obtained by the following steps:

1) Take the sum on both sides of (0.27), from $i = 1$ to $i = n$:

$$\sum_{i=1}^{n} \Delta t_{pre,i} = \sum_{i=1}^{n} (\alpha h - 1) t_{L,i-1} + t_{L,i} \quad (0.28)$$

$$\sum_{i=1}^{n} \Delta t_{pre,i} = (\alpha h - 1) \sum_{i=1}^{n} t_{L,i-1} + \sum_{i=1}^{n} t_{L,i} \quad (0.29)$$

2) Divide by n on each side

$$\frac{1}{n} \sum_{i=1}^{n} \Delta t_{pre,i} = (\alpha h - 1) \frac{1}{n} \sum_{i=1}^{n} t_{L,i-1} + \frac{1}{n} \sum_{i=1}^{n} t_{L,i} \quad (0.30)$$

3) By the definition of the mean quantities given in C.4 , we obtain:

$$\overline{\Delta t} = (\alpha h - 1) \overline{t}_{L,pre} + \overline{t}_L \quad (0.31)$$

4) For a large number of discharges $n \to \infty$, $\overline{t}_{L,pre} = \overline{t}_L$ and $\overline{t}_L \to \tau_s$. So:

$$\overline{\Delta t} = \alpha h \tau_s \quad (0.32)$$

A.4 Analytic expression for discharge separation time probability density function

The i-th time to previous discharge can be expressed as, see 2.1.1.3:

$$\Delta t_{pre,i} = t_{R,i-1} + t_{L,i} \quad (0.33)$$

The probability density of the time to previous discharge is the combined probability density of the two independent random variables $t_{R,i-1}$ and $t_{L,i}$, which may be found by convolution of the two corresponding probability densities [115]. The probability density for the discharge separation time is obtained by the three steps below.

Step 1:

Find $pdf_{t_{L,i}}(t_L)$; the probability density function of a discharge happening after a time lag $t_{L,i}$ is

$$pdf_{t_{L,i}}(t_L) = \frac{1}{\tau_s}\exp\left\{-\frac{1}{\tau_s}t_L\right\} \quad (0.34)$$

Step 2:

Find $pdf_{t_{R,i-1}}(t_L)$; the distribution of the previous recovery time, $t_{R,i-1}$, can be found by transformation of the probability density of $t_{L,i-1}$. The time lag of previous discharge, $t_{L,i-1}$, is independent from the time lag of the present discharge, $t_{L,i}$, and has the same probability density:

$$pdf_{t_{L,i-1}}(t_L) = \frac{1}{\tau_s}\exp\left\{-\frac{1}{\tau_s}t_L\right\} \quad (0.35)$$

Now, by denoting:

$$f_Y(y) = pdf_{t_{R,i-1}}(t_R) \quad (0.36)$$

and

$$f_X(x) = pdf_{t_{L,i-1}}(t_L) \quad (0.37)$$

So, $Y = t_{R,i-1}$, $y = t_R$, $X = t_{L,i-1}$, and $x = t_L$. A function can be defined so that us $y = g(x)$, corresponding to $t_R = g(t_L) = (\alpha h - 1)t_L$, see 3.2.2.6. Then the distribution of the previous recovery time, $t_{R,i-1}$, can be found by change of variables [114]:

$$f_Y(y) = f_X\left(g^{-1}(y)\right)\left|\frac{d}{dy}g^{-1}(y)\right| \quad (0.38)$$

Inserting into (0.38) yields :

$$pdf_{t_{R,i-1}}(t_R) = pdf_{t_{L,i-1}}\left(g^{-1}(t_R)\right)\left|\frac{d}{dt_R}g^{-1}(t_R)\right| \quad (0.39)$$

where

$$g^{-1}(t_R) = \frac{1}{(\alpha h - 1)}t_R \quad (0.40)$$

and

$$\left|\frac{d}{dt_R}g^{-1}(t_R)\right| = \frac{1}{(\alpha h - 1)} \quad (0.41)$$

Using eq. (0.35) we obtain

$$pdf_{t_{R,i-1}}(t_R) = \frac{1}{(\alpha h - 1)} \frac{1}{\tau_s} \exp\left\{ -\frac{1}{(\alpha h - 1)} \frac{1}{\tau_s} t_R \right\} \quad (0.42)$$

Step 3:

Now we can find the distribution of the time between discharges. The time between discharges is a sum of two exponentially distributed random variables, $t_{R,i-1}$ and $t_{L,i}$. The sum of two independent stochastic variables corresponds to the convolution the probability distributions [115]:

$$pdf_{\Delta t_{pre,i}}(\Delta t) = \int_0^{\Delta t} pdf_{t_{L,i}}(t_L)\, pdf_{t_{R,i-1}}(\Delta t - t_L) dt_L \quad (0.43)$$

$t_{L,i}$ has the distribution:

$$pdf_{t_{L,i}}(t_L) = \lambda_1 \exp\{-\lambda_1 t_L\} \quad (0.44)$$

with $\lambda_1 = \frac{1}{\tau_s}$. $t_{R,i-1}$ has the distribution:

$$pdf_{t_{R,i-1}}(t_R) = \lambda_2 \exp\{-\lambda_2 t_R\} \quad (0.45)$$

with $\lambda_2 = \frac{1}{(\alpha h - 1)} \frac{1}{\tau_s}$. The distribution of the time between discharges is

$$pdf_{\Delta t_{pre,i}}(\Delta t) = \frac{\lambda_1 \lambda_2}{\lambda_2 - \lambda_1} \left(\exp\{-\lambda_1 \Delta t\} - \exp\{-\lambda_2 \Delta t\} \right) \quad (0.46)$$

which is

$$pdf_{\Delta t_{pre,i}}(\Delta t) = \frac{1}{(\alpha h - 2)} \frac{1}{\tau_s} \left(\exp\left\{ -\frac{1}{(\alpha h - 1)} \frac{1}{\tau_s} \Delta t \right\} - \exp\left\{ -\frac{1}{\tau_s} \Delta t \right\} \right) \quad (0.47)$$

(0.47) is valid for $\alpha h \in \langle 1, 2 \rangle \cup \langle 2, \infty \rangle$. When $\alpha h = 1$, the integral in (0.43) becomes:

$$pdf_{\Delta t_{pre,i}}(\Delta t) = \frac{1}{\tau_s} \exp\left\{ -\frac{1}{\tau_s} \Delta t \right\} \quad (0.48)$$

When $\alpha h = 2$, the integral in (0.43) becomes:

$$pdf_{\Delta t_{pre,i}}(\Delta t) = \left(\frac{1}{\tau_s} \right)^2 \exp\left\{ -\frac{1}{\tau_s} \Delta t \right\} \Delta t \quad (0.49)$$

By using (0.32), τ_s can expressed in terms of the mean separation time as:

$$\tau_s = \frac{\Delta\overline{t}}{\alpha h} \quad (0.50)$$

The probability density of the separation time can the be expressed in terms of the mean separation time and the Townsend coefficient, for $\alpha h \in \langle 1,2 \rangle \cup \langle 2,\infty \rangle$:

$$pdf_{\Delta t_{pre,i}}(\Delta t) = \frac{\alpha h}{(\alpha h - 2)\Delta\overline{t}} \left(\exp\left(-\frac{\alpha h}{(\alpha h - 1)} \frac{\Delta t}{\Delta\overline{t}} \right) - \exp\left(-\alpha h \frac{\Delta t}{\Delta\overline{t}} \right) \right) \quad (0.51)$$

For $\alpha h = 1$:

$$pdf_{\Delta t_{pre,i}}(\Delta t) = \frac{1}{\Delta\overline{t}} \exp\left(-\frac{\Delta t}{\Delta\overline{t}} \right) \quad (0.52)$$

For $\alpha h = 2$

$$pdf_{\Delta t_{pre,i}}(\Delta t) = \left(2\frac{1}{\Delta\overline{t}} \right)^2 \exp\left(-2\frac{\Delta t}{\Delta\overline{t}} \right) \Delta t \quad (0.53)$$

Appendix B Model of the PD Sequence at combined DC and AC voltage

A flow chart of the PD sequence model at combined voltage is shown in Fig. 0-2. The input for the model is the physical parameters αh, τ_s, C_b, $\widehat{\frac{dv_c}{dt}}$, as well as the applied DC voltage V_{DC}, the AC cavity voltage amplitude $K_{AC}\hat{V}_{AC}$ and the number of discharges n. The model produces the sets:

$$t_L = \left[t_{L,1}, ..., t_{L,i}, ..., t_{L,n} \right] \quad (0.54)$$

$$\theta = \left[\theta_1, \theta_2, ..., \theta_n \right] \quad (0.55)$$

$$q_a = \left[q_{a,1}, ..., q_{a,i}, ..., q_{a,n} \right] \quad (0.56)$$

$$t_R = \left[t_{R,1}, ..., t_{R,i}, ..., t_{R,n} \right] \quad (0.57)$$

The output of the model are the measurable quantities Δt_{pre}, q_a and θ. Δt_{pre} is a function of the sets, t_L and t_R.:

$$\Delta t_{pre} = \left[\left(t_{R,1} + t_{L,2} \right), ..., \left(t_{R,n-2} + t_{L,n-1} \right) \right] \quad (0.58)$$

$$\Delta t_{suc} = \left[\left(t_{R,2} + t_{L,3} \right), ..., \left(t_{R,n-1} + t_{L,n} \right) \right] \quad (0.59)$$

Although n discharges is generated in the Monte Carlo simulation, the output is $n-2$ discharges because the first and last discharge must be discarded, so:

$$q_a = \left[q_{a,2}, ..., q_{a,i}, ..., q_{a,n-1} \right] \quad (0.60)$$

$$\theta = \left[\theta_2, \theta_2, ..., \theta_{n-1} \right] \quad (0.61)$$

If a threshold is set the discharge separation time is recalculated as follows:

1) The set of time-of-occurrence before filtering, for k elements , is:

$$t = \left[\Delta t_{pre,1}, \left(\Delta t_{pre,1} + \Delta t_{pre,2} \right), ..., \sum_{j=1}^{k} \Delta t_{pre,j} \right] \quad (0.62)$$

2) The set of time-of-occurrence after filtering, t^*, is found by deleting all elements in (0.62) corresponding to $q_{a,i} < q_{a,threshold}$, resulting in m elements in t^*.
3) The filtered time to previous discharge and to successive discharge is calculated as:

$$\Delta t^*_{pre} = \left[t^*_1, \left(t^*_2 - t^*_1 \right), ..., \left(t^*_{m-1} - t^*_{m-2} \right) \right] \quad (0.63)$$

$$\Delta t_{suc}^{*} = \left[\left(t_2^{*} - t_1^{*} \right), \left(t_3^{*} - t_2^{*} \right), ..., \left(t_m^{*} - t_{m-1}^{*} \right) \right] \quad (0.64)$$

4) The corresponding filtered discharge magnitudes and phase-of-occurrences are found by

$$q_a^{*} = q_a \left(t^{*} \right) \quad (0.65)$$

$$\theta^{*} = \theta \left(t^{*} \right) \quad (0.66)$$

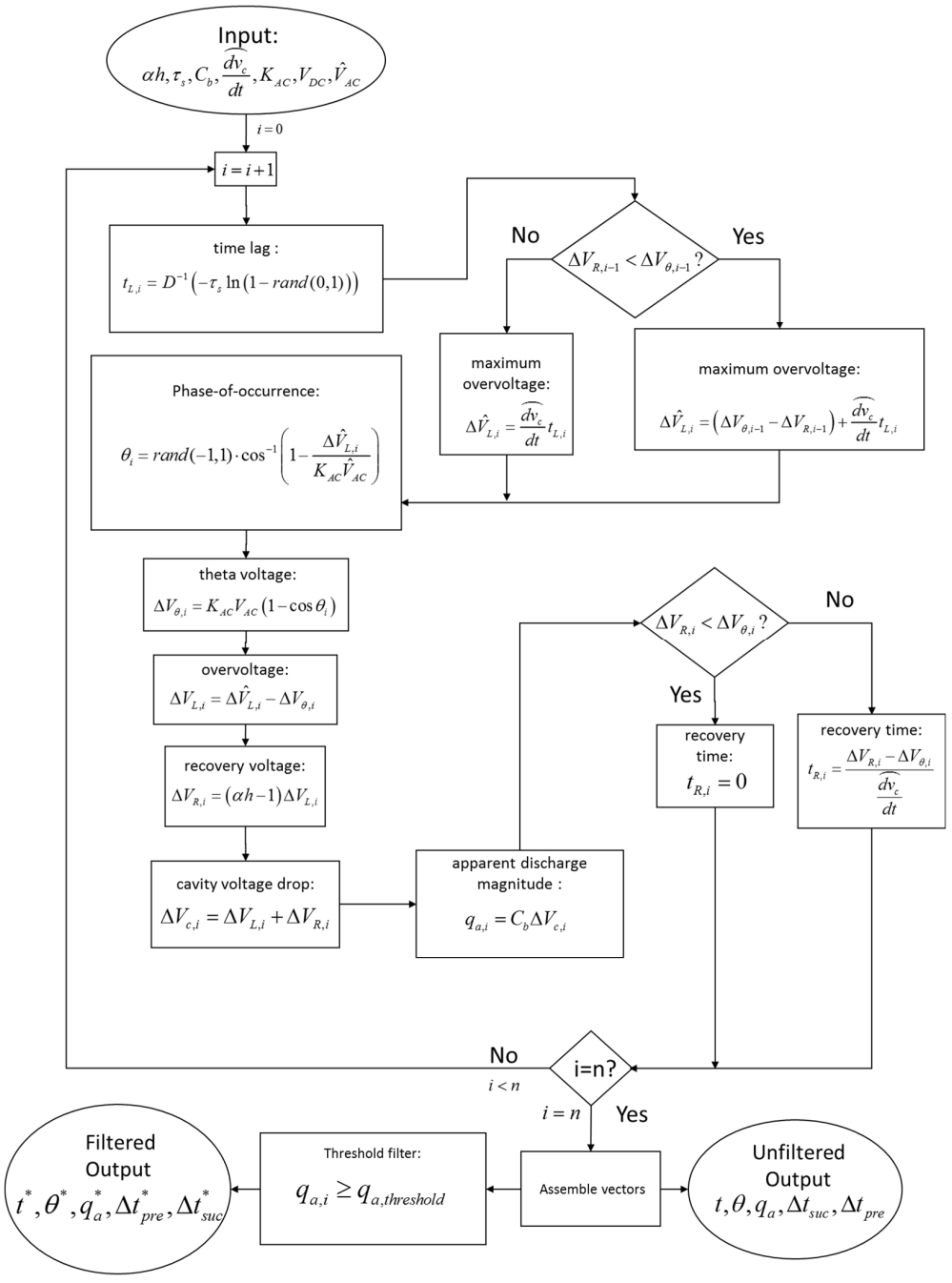

Fig. 0-2 Pulse sequence Monte Carlo model for partial discharges at DC voltage with AC ripple voltage.

B.1 Voltage over cavity after a discharge for combined voltage conditions

The voltage over the cavity after the i-th discharge is

$$v_c\left(t'\right)=v_c^{DC}\left(t'\right)+v_c^{AC}\left(t'\right) \quad (0.67)$$

Where $t'=0$ at t_{i-1} .

$$v_c^{DC}\left(t'\right)=K_{DC}V_{DC}-\left(K_{DC}V_{DC}-V_{res,offset}\right)\exp\left(-\frac{t'}{\tau}\right) \quad (0.68)$$

$$v_c^{AC}\left(t'\right)=K_{AC}\hat{V}_{AC}\cos\left(\omega t'+\theta_{i-1}\right) \quad (0.69)$$

where θ_{i-1} is the phase-of-occurrence at the previous discharge and $V_{res,offset}$ is the starting offset DC voltage. By inspection in Fig. 0-3:

$$V_{res,offset}=V_{res,i-1}+\Delta V_{\theta,i-1}-K_{AC}\hat{V}_{AC} \quad (0.70)$$

Inserting $V_{res,offset}$ in (0.70) into (0.68), then (0.68) and (0.69) into (0.67) yields:

$$v_c\left(t'\right)=V_{DC}-\left(V_{DC}+K_{AC}\hat{V}_{AC}-V_{res,i-1}-\Delta V_{\theta,i-1}\right)\exp\left(-\frac{t'}{\tau}\right)+K_{AC}\hat{V}_{AC}\cos\left(\omega t'+\theta_{i-1}\right)$$

(0.71)

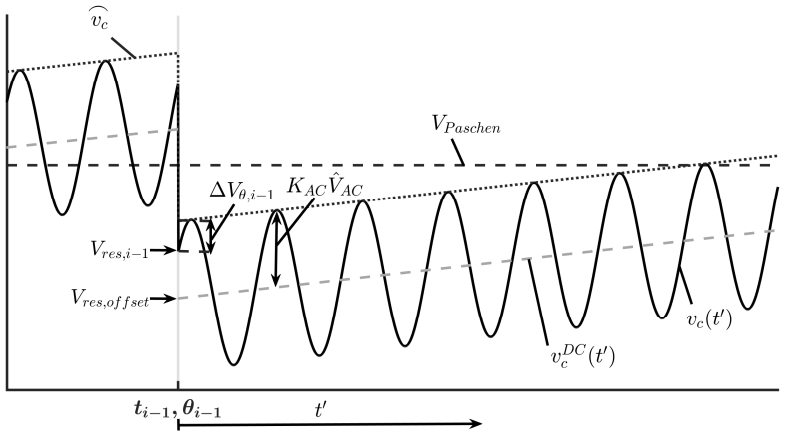

Fig. 0-3 Voltage over cavity after previous discharge.

B.2 The overvoltage

The overvoltage before the i-th discharge is

$$\Delta V_{L,i} = v_{c,i} - V_{paschen} \quad (0.72)$$

Which can be written as

$$\Delta V_{L,i} = K_{DC}V_{DC} - \left(K_{DC}V_{DC} - V_{offset}\right)\exp\left\{-\frac{t_{L,i}}{\tau}\right\} + K_{AC}\hat{V}_{AC}\cos\left(\omega t_{L,i} + \theta'\right) - V_{paschen} \quad (0.73)$$

where $t_{L,i} = 0$ when the envelope of the voltage is equal to $V_{paschen}$, θ' is the phase shift when the envelope of the voltage is equal to $V_{paschen}$. The offset voltage when $t_{L,i} = 0$, is

$$V_{offset} = V_{paschen} - K_{AC}\hat{V}_{AC} \quad (0.74)$$

θ' can be set to zero to create a reference point so that $\Delta V_{L,i} = 0$ at $t_{L,i} = 0$, the phase shift θ' can be ignored because the resulting time shift is extremely small compared to the time lag $t_{L,i}$. Setting $\omega t_{L,i} = \theta_i$ as a parameter and inserting (0.74) into (0.73) we get:

$$\Delta V_{L,i} = K_{DC}V_{DC} - \left(K_{DC}V_{DC} + K_{AC}\hat{V}_{AC} - V_{paschen}\right)\exp\left\{-\frac{t_{L,i}}{\tau}\right\} + K_{AC}\hat{V}_{AC}\cos\left(\theta_i\right) - V_{paschen} \quad (0.75)$$

Which can be reformulated as:

$$\Delta V_{L,i} = \left(K_{DC}V_{DC} + K_{AC}\hat{V}_{AC} - V_{paschen}\right)\left(1 - \exp\left(-\frac{t_{L,i}}{\tau}\right)\right) - K_{AC}\hat{V}_{AC}\left(1 - \cos\left(\theta_i\right)\right) \quad (0.76)$$

The overvoltage is a sum of a DC part depending on $t_{L,i}$ and an AC part depending on θ_i, as follows:

$$\Delta V_{L,i} = \Delta\hat{V}_{L,i} - \Delta V_{\theta,i} \quad (0.77)$$

Where

$$\Delta\hat{V}_{L,i} = \left(K_{DC}V_{DC} + K_{AC}\hat{V}_{AC} - V_{paschen}\right)\left(1 - \exp\left(-\frac{t_{L,i}}{\tau}\right)\right) \quad (0.78)$$

$$\Delta V_{\theta,i} = K_{AC}\hat{V}_{AC}\left(1 - \cos\left(\theta_i\right)\right) \quad (0.79)$$

If the the maximum overvoltage, $\Delta\hat{V}_L$, is linearised around $t_{L,i}=0$, then:

$$\Delta\hat{V}_{L,i} \approx \widehat{\frac{dv_c}{dt}} t_{L,i} \quad (0.80)$$

with

$$\widehat{\frac{dv_c}{dt}} = \frac{K_{DC}V_{DC} + K_{AC}\hat{V}_{AC} - V_{paschen}}{\tau} \quad (0.81)$$

Then the overvoltage can be expressed as:

$$\Delta V_{L,i} = \widehat{\frac{dv_c}{dt}} \cdot t_{L,i} - K_{AC}\hat{V}_{AC}\left(1-\cos\theta_i\right) \quad (0.82)$$

which is valid for $t_{L,i} \ll \tau$.

B.3 Effective start electron generation rate and the duty cycle

The combined voltage over the cavity, v_c , is shown in Fig. 0-4 for one period time of the AC voltage. The DC offset voltage, v_c^{DC} , increases during the AC period, but the increase is infitisemal when the AC period time is much shorter than the time constant of the DC offset voltage:

$$T_{AC} \ll \tau \quad (0.83)$$

The cavity voltage is above the Paschen voltage , $V_{Paschen}$, for a time interval shorter than the AC period time, marked by the grey area in Fig. 0-4. For a discharge to occur, a start electron must be available within this time interval. In contrast, if only DC voltage is applied the cavity voltage will stay above the critical voltage after a recovery time, t_R; the availability of an start electron is not restricted to a time interval. At combined voltage the start electron generation rate is equal to the mean start electron generation rate at DC voltage in the interval t_{over} and zero outside this interval. Thus, when an AC voltage is superimposed on the DC voltage, the start electron generation rate is reduced.

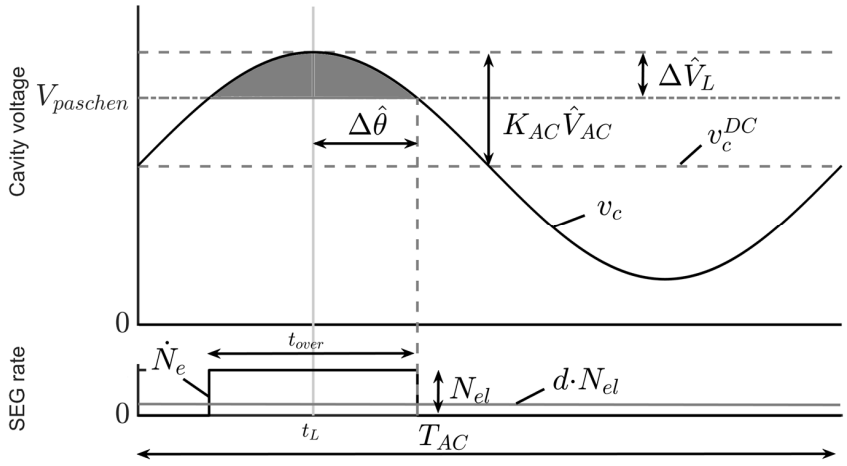

Fig. 0-4 The cavity voltage at after a time lag t_L , with start electron generation rate. The DC offset voltage is nearly constant within one time period of the AC voltage.

The effective start electron generation rate, $\dot{N}_{e,eff}$, can be given as a mean value over the an AC period time interval, after a time lag $t_L \geq 0$, see eq. (0.85). The effective start electron generation rate can be used when the AC period time is much shorter than the statistical waiting time:

$$T_{AC} \ll \tau_s \quad (0.84)$$

$$\dot{N}_{e,eff} = \frac{1}{T_{AC}} \int_{t_L}^{t_L+T_{AC}} \dot{N}_e dt = \frac{t_{over}}{T_{AC}} N_{el} \quad (0.85)$$

The ratio $\frac{t_{over}}{T_{AC}}$ is defined as the duty cycle d . In this thesis the duty cycle is defined as the fraction of one AC voltage time period in which the cavity voltage is above the critical voltage:

$$d = \frac{t_{over}}{T_{AC}} = \frac{2\Delta\hat{\theta}}{2\pi} = \frac{\Delta\hat{\theta}}{\pi} \quad (0.86)$$

where $\Delta\hat{\theta}$ is the maximum phase-of-occurrence at time lag t_L, see Fig. 0-4. The effective start electron generation rate is then

$$\dot{N}_{e,eff}\left(t_L\right) = d\left(t_L\right) \cdot N_{el} \quad (0.87)$$

An expression for d can be found as a function of $\Delta\hat{\theta}$ as follows:

1) At the maximum phase-of-occurrence the overvoltage is zero:

$$\Delta V_L\left(t_L, \Delta\hat{\theta}\right) = 0 \quad (0.88)$$

2) By the expression for the overvoltage at combined voltage given in eq. (0.77) we have:

$$\Delta\hat{V}_L\left(t_L\right) - \Delta V_\theta\left(\Delta\hat{\theta}\right) = 0 \quad (0.89)$$

3) Solving (0.89) with respect to $\Delta\hat{\theta}$, using (0.79) yields an expression for the maximum phase-of-occurence

$$\Delta\hat{\theta}\ \left(t_L\right) = \cos^{-1}\left(1 - \frac{\Delta\hat{V}_L(t_L)}{K_{AC}\hat{V}_{AC}}\right) \quad (0.90)$$

4) Inserting (0.90) into (0.86) gives the formula for the duty cycle:

$$d\left(t_L\right) = \frac{1}{\pi}\cos^{-1}\left(1 - \frac{\Delta\hat{V}_L(t_L)}{K_{AC}\hat{V}_{AC}}\right) \quad (0.91)$$

Inserting (0.80) into eq. (0.91) we obtain

$$d\left(t_L\right) = \frac{1}{\pi}\cos^{-1}\left(1 - \frac{\widehat{\frac{dv_c}{dt}}}{K_{AC}\hat{V}_{AC}}t_L\right) \quad (0.92)$$

which is valid when

$$\tau_{AC} \ll \tau_s \ll \tau \qquad (0.93)$$

Or, equivalently:

$$\frac{1}{\tau} \ll N_{el} \ll f_{AC} \qquad (0.94)$$

B.4 Time lag probability density

At combined voltage conditions the start electron generation rate is given by $\dot{N}_e = N_{el} \cdot d = \frac{1}{\tau_s} \cdot d$, where d is the duty cycle found in previous section, eq. (0.92). The function $\dot{N}_e$ is a non-negative function, it is always positive when the envelope of the cavity voltage is above the Paschen voltage and zero otherwise:

$$\dot{N}_e(t') = \begin{cases} \frac{1}{\tau_s} \cdot d, & \widehat{v_c}(t') \geq V_{paschen} \\ 0, & \widehat{v_c}(t') < V_{paschen} \end{cases} \quad (0.95)$$

The probability density for discharge happening after a time lag $t_L \geq 0$ is obtained with eq. (2.34):

$$pdf_{t_{L,i}}(t_L) = \dot{N}_e \exp\left\{-\int_0^{t_L} \dot{N}_e dt'\right\} = \frac{1}{\tau_s} d(t_L) \cdot \exp\left\{-\frac{1}{\tau_s} D(t_L)\right\} \quad (0.96)$$

where

$$D(t_L) = \int_0^{t_L} d(t') dt' \quad (0.97)$$

which has the solution

$$D(t_L) = -\frac{1}{K\pi}\left((1-Kt_L)\cos^{-1}(1-Kt_L) - \sqrt{1-(1-Kt_L)^2}\right) \quad (0.98)$$

with

$$K = \frac{\widehat{\frac{dv_c}{dt}}}{K_{AC}\hat{V}_{AC}} \quad (0.99)$$

The cumulative probability density function of a discharge happening after a time lag $t_L \geq 0$ is obtained with eq. (2.35):

$$cdf_{t_{L,i}}(t_L) = 1 - \exp\left\{-\int_0^{t_L} \dot{N}_e dt'\right\} = 1 - \exp\left\{-\frac{1}{\tau_s} D(t_L)\right\} \quad (0.100)$$

The individual time lag, $t_{L,i}$, can be found by generating a random number R between 0 and 1, set $cdf_{t_{L,i}}(t_L) = R$, and solving (3.72) numerically:

$$t_{L,i} = D^{-1}\left(-\tau_s \ln(1-R)\right) \quad (0.101)$$

B.5 Mean time lag

The mean of a random variable t_L is calculated from its probability distribution function as:

$$\overline{t_L} = \int_0^\infty t_L \cdot pdf_{t_{L,i}}(t_L) dt_L \quad (0.102)$$

Alternatively, the mean can be calculated from its cumulative distribution function [116]:

$$\overline{t_L} = \int_0^\infty (1 - cdf_{t_{L,i}}(t_L)) dt_L \quad (0.103)$$

The cumulative distribution function is

$$cdf_{t_{L,i}}(t_L) = 1 - \exp\left\{ -\int_0^{t_L} \dot{N}_e dt' \right\} \quad (0.104)$$

The simplest expression for the mean value is obtained by using the alternative definition, inserting (0.104) into (0.103) yields:

$$\overline{t_L} = \int_0^\infty \exp\left\{ -\int_0^{t_L} \dot{N}_e dt_L \right\} dt_L \quad (0.105)$$

By (0.100) we have

$$\int_0^{t_L} \dot{N}_e dt' = \frac{1}{\tau_s} D(t_L) \quad (0.106)$$

So

$$\overline{t_L} = \int_0^\infty \exp\left\{ -\frac{1}{\tau_s} D(t_L) \right\} dt_L \quad (0.107)$$

The integral in (0.107) does not have an analytic solution, but can be found numerically. The value of D depends on $\widehat{\frac{dv_c}{dt}}$ and $K_{AC}\hat{V}_{AC}$, see (0.98). The numerical integration can be represented by the function F_1 which depends on the PD sequence parameters $\widehat{\frac{dv_c}{dt}}$, $K_{AC}\hat{V}_{AC}$ and τ_s:

$$\overline{t_L} = F_1\left(\widehat{\frac{dv_c}{dt}}, K_{AC}\hat{V}_{AC}, \tau_s \right) \quad (0.108)$$

B.6 Mean cosinus of the phase-of-occurence

The mean cosinus of the phase-of-occurrence, $\overline{\cos\theta_i}$, is needed to calculate the mean discharge magnitude and separation time numerically (see B.7 and B.8). It can be obtained by the law of the unconscious statistician, see [117, p. 170]:

$$E\left[g\left(X\right)\right]=\overline{g\left(X\right)}=\int_{-\infty}^{+\infty}g\left(x\right)\cdot pdf_X\left(x\right)dx \quad (0.109)$$

If $\overline{g\left(X\right)}=\overline{\cos\theta_i}$ and $x=\theta$, then

$$\overline{\cos\theta_i}=\int_{\theta=-\pi}^{\theta=+\pi}\cos\theta\cdot pdf_{\theta_i}\left(\theta\right)d\theta \quad (0.110)$$

The probability of a discharge to occur within a certain phase interval $\left[-\Delta\hat{\theta}\,,\Delta\hat{\theta}\,\right]$ at a time lag t_L is constant, because the AC period time is much smaller than the mean statistical waiting time. The bounds of the phase interval can be approximated by setting the time lag to the mean time lag $\overline{t_L}$ in eq. (0.90):

$$\Delta\hat{\theta}\,\left(\overline{t_L}\right)=\cos^{-1}\left(1-\frac{\Delta\hat{V}_L(\overline{t_L})}{K_{AC}\hat{V}_{AC}}\right)$$

where $\overline{t_L}$ can be found by numerical integration of eq. (0.107). The probability density is constant and equal to $\frac{1}{2\Delta\hat{\theta}}$, because integrating the probability density over the interval $\left[-\Delta\hat{\theta}\,,\Delta\hat{\theta}\,\right]$ should give the value 1:

$$\int_{-\pi}^{\pi}pdf_{\theta_i}\left(\theta\right)d\theta=\int_{-\Delta\hat{\theta}}^{\Delta\hat{\theta}}pdf_{\theta_i}\left(\theta\right)d\theta=\int_{-\Delta\hat{\theta}}^{\Delta\hat{\theta}}\frac{1}{2\Delta\hat{\theta}}d\theta=\frac{2\Delta\hat{\theta}}{2\Delta\hat{\theta}}=1 \quad (0.111)$$

By approximation $pdf_{\theta_i}\left(\theta\right)=\frac{1}{2\Delta\hat{\theta}\,\left(\overline{t_L}\right)}$ and the phase interval to $\left[-\Delta\hat{\theta}\,\left(\overline{t_L}\right),\Delta\hat{\theta}\,\left(\overline{t_L}\right)\right]$ in eq. (0.110) gives

$$\overline{\cos\theta_i}=\int_{-\Delta\hat{\theta}(\overline{t_L})}^{\Delta\hat{\theta}(\overline{t_L})}\cos\theta\frac{1}{2\Delta\hat{\theta}\,\left(\overline{t_L}\right)}d\theta \quad (0.112)$$

Solving the integral yields

$$\overline{\cos\theta_i} = \frac{\sin\left(\Delta\hat{\theta}\ (\overline{t_L})\right)}{\Delta\hat{\theta}\ (\overline{t_L})} \quad (0.113)$$

This expression can be reformulated by using the identity

$$\sin^2\left(\Delta\hat{\theta}\right) + \cos^2\left(\Delta\hat{\theta}\right) = 1 \quad (0.114)$$

so

$$\sin\left(\Delta\hat{\theta}\right) = \sqrt{1-\cos^2\left(\Delta\hat{\theta}\right)} \quad (0.115)$$

Inserting (0.115) and using

$$\Delta\hat{\theta} = \cos^{-1}\left(1 - K\overline{t_L}\right) \quad (0.116)$$

yields

$$\overline{\cos\theta_i} = \frac{\sqrt{1-\left(1-K\overline{t_L}\right)^2}}{\cos^{-1}\left(1-K\overline{t_L}\right)} \quad (0.117)$$

with

$$K = \frac{\overline{\frac{\widehat{dv_c}}{dt}}}{K_{AC}\hat{V}_{AC}} \quad (0.118)$$

It is noted that the expression in (0.117) is not formally complete, but suffices as an approximation. $\overline{\cos\theta_i}$ in eq. (0.117) can be represented by the function F_2 which depends on the PD sequence parameters $\frac{\widehat{dv_c}}{dt}$, $K_{AC}\hat{V}_{AC}$ and τ_s:

$$\overline{\cos\theta_i} = F_2\left(\frac{\widehat{dv_c}}{dt}, K_{AC}\hat{V}_{AC}, \tau_s\right) \quad (0.119)$$

B.7 Analytical expression for mean discharge magnitude

In this section the mean discharge magnitude is found by numerical integration of analytic functions. The expression is obtained in the following using the formula for the i-th discharge magnitude:

$$q_{a,i} = \alpha h C_b \Delta V_{L,i} \quad (0.120)$$

With $\Delta V_{L,i}$ as defined in (0.82) we get:

$$q_{a,i} = \alpha h C_b \left(\widehat{\frac{dv_c}{dt}} \cdot t_{L,i} - K_{AC} \hat{V}_{AC} \left(1 - \cos\theta_i\right) \right) \quad (0.121)$$

The mean discharge magnitude can be obtained by the following steps:

1) Take the sum on both sides of (0.121), from $i = 1$ to $i = n$:

$$\sum_{i=1}^{n} q_{a,i} = \sum_{i=1}^{n} \alpha h C_b \left(\widehat{\frac{dv_c}{dt}} \cdot t_{L,i} - K_{AC} \hat{V}_{AC} \left(1 - \cos\theta_i\right) \right) \quad (0.122)$$

$$\sum_{i=1}^{n} q_{a,i} = \alpha h C_b \left(\widehat{\frac{dv_c}{dt}} \cdot \sum_{i=1}^{n} t_{L,i} - K_{AC} \hat{V}_{AC} \left(n - \sum_{i=1}^{n} \cos\theta_i \right) \right) \quad (0.123)$$

2) Divide by n on each side

$$\frac{1}{n} \sum_{i=1}^{n} q_{a,i} = \alpha h C_b \left(\widehat{\frac{dv_c}{dt}} \cdot \frac{1}{n} \sum_{i=1}^{n} t_{L,i} - K_{AC} \hat{V}_{AC} \left(1 - \frac{1}{n} \sum_{i=1}^{n} \cos\theta_i \right) \right) \quad (0.124)$$

3) For large number of discharges $n \to \infty$ and by the definition of the mean quantities given in C.4 , we obtain:

$$\overline{q}_a = \alpha h C_b \left(\widehat{\frac{dv_c}{dt}} \cdot \overline{t}_L - K_{AC} \hat{V}_{AC} \left(1 - \overline{\cos\theta_i}\right) \right) \quad (0.125)$$

4) The mean discharge magnitude at combined voltage is a function of the PD sequence parameters, $\overline{t}_L$ can be found by numerical integration of eq. (0.107) and $\overline{\cos\theta_i}$ can then be found by eq. (0.117).

B.8 Analytical expression for mean discharge separation time

In this section the mean discharge separation time is found by numerical integration of analytic functions. The expression is obtained in the following using the formula for the ith discharge separation time:

$$\Delta t_i = \Delta t_{pre,i} = t_{R,i-1} + t_{L,i} \quad (0.126)$$

The recovery time after the previous discharge, $t_{R,i-1}$, is found by changing the index in eq. (3.89) from i to $i-1$:

$$t_{R,i-1} = \left(\alpha h - 1\right) t_{L,i-1} - \alpha h \frac{K_{AC} \hat{V}_{AC}}{\widehat{\frac{dv_c}{dt}}} \left(1 - \cos\left(\theta_{i-1}\right)\right) \quad (0.127)$$

Inserting (0.127) into (0.126) gives the discharge separation time as a function of $t_{L,i}$, $t_{L,i-1}$ and θ_{i-1}:

$$\Delta t_{pre,i} = (\alpha h - 1) t_{L,i-1} + t_{L,i} - \alpha h \frac{K_{AC} \hat{V}_{AC}}{\widehat{\frac{dv_c}{dt}}} \left(1 - \cos(\theta_{i-1})\right) \quad (0.128)$$

The mean discharge separation time can be obtained by the following steps:

1) Take the sum on both sides of (0.128), from $i = 1$ to $i = n$:

$$\sum_{i=1}^{n} \Delta t_{pre,i} = \sum_{i=1}^{n} \left((\alpha h - 1) t_{L,i-1} + t_{L,i} - \alpha h \frac{K_{AC} \hat{V}_{AC}}{\widehat{\frac{dv_c}{dt}}} \left(1 - \cos(\theta_{i-1})\right) \right) \quad (0.129)$$

$$\sum_{i=1}^{n} \Delta t_{pre,i} = (\alpha h - 1) \sum_{i=1}^{n} t_{L,i-1} + \sum_{i=1}^{n} t_{L,i} - \alpha h \frac{K_{AC} \hat{V}_{AC}}{\widehat{\frac{dv_c}{dt}}} \left(n - \sum_{i=1}^{n} \cos(\theta_{i-1}) \right) \quad (0.130)$$

2) Divide by n on each side

$$\frac{1}{n} \sum_{i=1}^{n} \Delta t_{pre,i} = (\alpha h - 1) \frac{1}{n} \sum_{i=1}^{n} t_{L,i-1} + \frac{1}{n} \sum_{i=1}^{n} t_{L,i} - \alpha h \frac{K_{AC} \hat{V}_{AC}}{\widehat{\frac{dv_c}{dt}}} \left(1 - \frac{1}{n} \sum_{i=1}^{n} \cos(\theta_{i-1}) \right)$$

(0.131)

3) By the definition of the mean quantities given in C.4 , we obtain:

$$\overline{\Delta t} = (\alpha h - 1) \overline{t}_{L,pre} + \overline{t}_L - \alpha h \frac{K_{AC} \hat{V}_{AC}}{\widehat{\frac{dv_c}{dt}}} \left(1 - \overline{\cos\theta_{pre}}\right) \quad (0.132)$$

4) For a large number of discharges $n \to \infty$, $\overline{t}_{L,pre} = \overline{t}_L$ and $\overline{\cos\theta_{pre}} = \overline{\cos\theta_i}$, so

$$\overline{\Delta t} = \alpha h \left(\overline{t}_L - \frac{K_{AC} \hat{V}_{AC}}{\widehat{\frac{dv_c}{dt}}} \left(1 - \overline{\cos\theta_i}\right) \right) \quad (0.133)$$

5) The mean discharge separation time at combined voltage is a function of the PD sequence parameters, $\overline{t_L}$ can be found by numerical integration of eq. (0.107) and $\overline{\cos\theta_i}$ can then be found by eq. (0.117).

Appendix C Estimation of parameters

In this section three estimation methods are presented:

- The ordinary least squares method for PD at DC voltage
- The method of moments for PD at DC voltage
- The method of moments for PD at combined voltage

C.1 Estimation of PD sequence parameters by an ordinary least square method at DC voltage conditions

The mean time lag and the mean recovery time are among the physical parameters that need to be estimated at DC voltage conditions. Fromm and Morshuis [118] used PSA-plots and ordinary least squares (OLS) to estimate these parameters. The model by Fromm is based on the assumption that time lag t_L, apparent discharge magnitude q_a and recovery time are mutually related, as:

$$q_a = f_1(t_L) \quad (0.134)$$

$$t_L = f_1^{-1}(q_a) \quad (0.135)$$

$$t_R = f_2(q_a) \quad (0.136)$$

The model also assumes that the discharge magnitude q_i does not depend on the previous discharge magnitude q_{i-1}, which was experimentally verified by Fromm [74]. The following equations were deduced:

$$\Delta\bar{t}_{pre,i} = t_L(q_{a,i}) + \bar{t}_R \quad (0.137)$$

$$\Delta\bar{t}_{suc,i} = t_R(q_{a,i}) + \bar{t}_L \quad (0.138)$$

When $q_{a,i} \to 0$ both $t_L(q_{a,i}) \to 0$ and $t_R(q_{a,i}) \to 0$. The mean time lag and mean recovery time can then be estimated as:

$$\hat{\bar{t}}_R = \Delta\bar{t}_{pre,i}(q_{a,i} \to 0) \quad (0.139)$$

$$\hat{\bar{t}}_L = \Delta\bar{t}_{suc,i}(q_{a,i} \to 0) \quad (0.140)$$

Plotting the time to previous discharge and the time to succeeding discharge versus magnitude it is then possible to obtain the time lag and the recovery time using OLS regression. The estimation method uses the interval mean plots $\left(q_{a,i}, \Delta\bar{t}_{suc,i}\right)$ and

$\left(q_{a,i}, \Delta\overline{t}_{pre,i}\right)$, Fig. 0-5. The data for the least square regression are restricted to low $q_{a,i}$ because the scatter in $\Delta\overline{t}_{suc,i}$ and $\Delta\overline{t}_{pre,i}$ increases for large $q_{a,i}$. The offset value of the least square linear regression marks the estimated time lag or recovery time. At DC voltage conditions the mean time lag should be close to the mean statistical waiting time, provided that the discharge magnitude detection limit is low. I.e.. $\hat{\tau}_s = \hat{\overline{t}}_L$. The confidence interval of the estimated parameters can be given using the confidence interval for the regression coefficients [119] or by the non-parametric bootstrap method.

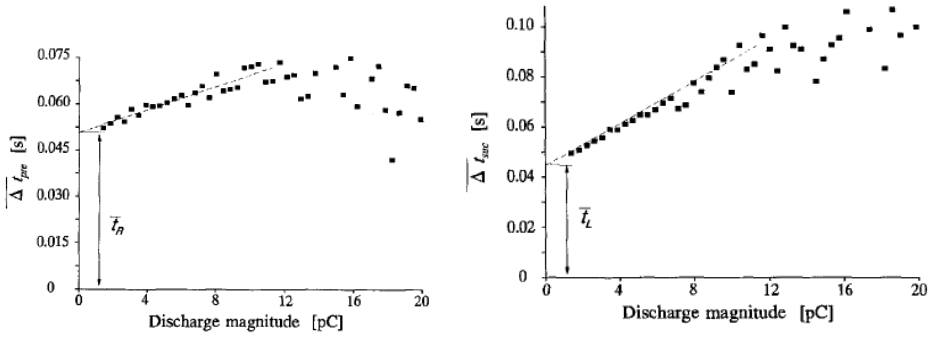

a) b)

Fig. 0-5 a) The time to the previous discharge as a function of the discharge magnitude, $\overline{t}_R$ at $q = 0$. b) time to the successive discharge as a function of the discharge magnitude, $\overline{t}_L$ at $q = 0$. From [44]**.**

In this thesis the relationship between time to previous discharge and the discharge magnitude can be written as, see 3.2.3:

$$\Delta t_{pre,i} = \frac{1}{\alpha h C_b \dfrac{dv_c}{dt}}\left((\alpha h - 1)\, q_{a,i-1} + q_{a,i}\right) \quad (0.141)$$

$\Delta t_{pre,i}$ can be expressed as a function of $q_{a,i}$ if the function $q_{a,i-1} = f\left(q_{a,i}\right)$ exist. The i-th discharge magnitude is independent of the previous discharge magnitude, because the i-th time lag is independent of the previous time lag. On average:

$$q_{a,i-1} = f\left(q_{a,i}\right) = \overline{q}_a \quad (0.142)$$

This can be confirmed by plotting $q_{a,i-1}$ versus $q_{a,i}$. Inserting (0.142) into (0.141), yields:

$$\Delta\bar{t}_{pre,i}\left(q_{a,i}\right)=\frac{1}{\alpha h C_b \dfrac{dV_c}{dt}}\left(\left(\alpha h-1\right)\bar{q}_a+q_{a,i}\right) \quad (0.143)$$

By using (0.15) it can be shown that:

$$\Delta\bar{t}_{pre,i}\left(q_{a,i}\right)=\left(\alpha h-1\right)\bar{t}_L+\frac{q_{a,i}}{\bar{q}_a}\bar{t}_L \quad (0.144)$$

Furthermore, using the relationship $\bar{t}_R=\left(\alpha h-1\right)\bar{t}_L$:

$$\Delta\bar{t}_{pre,i}\left(q_{a,i}\right)=\bar{t}_R+\frac{q_{a,i}}{\bar{q}_a}\bar{t}_L \quad (0.145)$$

Now, for the relationship between time to successive discharge and the discharge magnitude we have:

$$\Delta t_{suc,i}=\frac{1}{\alpha h C_b \dfrac{dv_c}{dt}}\left(\left(\alpha h-1\right)q_{a,i}+q_{a,i+1}\right) \quad (0.146)$$

The same argument can be applied as above and $\Delta t_{pre,i}$ can be expressed as a function of $q_{a,i}$ as:

$$\Delta\bar{t}_{suc,i}\left(q_{a,i}\right)=\bar{t}_L+\frac{q_{a,i}}{\bar{q}_a}\bar{t}_R \quad (0.147)$$

An estimator of the mean time lag and the mean recovery time can be found as:

$$\hat{\bar{t}}_R=\Delta\bar{t}_{pre,i}\left(q_{a,i}\to 0\right) \quad (0.148)$$

$$\hat{\bar{t}}_L=\Delta\bar{t}_{suc,i}\left(q_{a,i}\to 0\right) \quad (0.149)$$

Which is equivalent the offset value obtained by OLS regression on the data sets $\left(q_{a,i},\Delta\bar{t}_{pre,i}\right)$ and $\left(q_{a,i},\Delta\bar{t}_{suc,i}\right)$. At DC voltage conditions the mean time lag should be close to the mean statistical waiting time, provided that the discharge magnitude detection limit is low, i.e.. $\hat{\tau}_s=\hat{\bar{t}}_L$.

It should be noted that the relationships in (0.145) and (0.147) provides an alternative estimation of $\bar{t}_L$ and $\bar{t}_R$, by using the slope parameters:

$$\frac{d\Delta\bar{t}_{suc,i}}{dq_{a,i}} = \frac{\bar{t}_R}{\bar{q}_a} \quad (0.150)$$

$$\frac{d\Delta\bar{t}_{pre,i}}{dq_{a,i}} = \frac{\bar{t}_L}{\bar{q}_a} \quad (0.151)$$

Thus:

$$\hat{\bar{t}}_R = \bar{q}_a \frac{d\Delta\bar{t}_{suc,i}}{dq_{a,i}} \quad (0.152)$$

$$\hat{\bar{t}}_L = \bar{q}_a \frac{d\Delta\bar{t}_{pre,i}}{dq_{a,i}} \quad (0.153)$$

In this thesis the offset parameters in (0.148) and (0.149) is used, rather than the slope parameters in (0.152) and (0.153).

The estimator $\hat{\alpha}h$ is expressed in terms of the estimators $\hat{\bar{t}}_L$ and $\hat{\bar{t}}_R$ as:

$$\hat{\alpha}h = \frac{\hat{\bar{t}}_R}{\hat{\bar{t}}_L} + 1 \quad (0.154)$$

An estimator for the product $C_b \frac{dv_c}{dt}$ is found, using eq. (3.36):

$$\widehat{C_b \frac{dv_c}{dt}} = \frac{\bar{q}_a}{\Delta\bar{t}} \quad (0.155)$$

C.2 Estimation of PD sequence parameters by the method of moments at DC voltage conditions

The three unique parameters for the PD process at DC voltage conditions are αh , $C_b \frac{dV_c}{dt}$ and τ_s . The estimators $\hat{\alpha} h$ and $\widehat{C_b \frac{dv_c}{dt}}$ are found by calculation of the first moment (mean) and second moment (variance) on both sides of (0.141):

$$\frac{1}{n}\sum_{i=1}^{n}\Delta t_{pre,i} = \frac{1}{\widehat{\hat{\alpha} h C_b \frac{dv_c}{dt}}}\left(\left(\hat{\alpha} h - 1\right)\frac{1}{n}\sum_{i=1}^{n} q_{a,i-1} + \frac{1}{n}\sum_{i=1}^{n} q_{a,i} \right) \quad (0.156)$$

$$\frac{1}{n}\sum_{i=1}^{n}\left(\Delta t_{pre,i}\right)^2 = \frac{1}{\left(\widehat{\hat{\alpha} h C_b \frac{dv_c}{dt}}\right)^2}\frac{1}{n}\sum_{i=1}^{n}\left(\left(\hat{\alpha} h - 1\right) q_{a,i-1} + q_{a,i}\right)^2 \quad (0.157)$$

(0.156) and (0.157) can be written as follows:

$$\widehat{C_b \frac{dv_c}{dt}}\overline{\Delta t} = \frac{1}{\hat{\alpha} h}\left(\left(\hat{\alpha} h - 1\right)\overline{q_{a,pre}} + \overline{q_a}\right) \quad (0.158)$$

$$\left(\widehat{C_b \frac{dv_c}{dt}}\right)^2 \overline{\Delta t^2} = \frac{1}{\left(\hat{\alpha} h\right)^2}\left(\left(\left(\hat{\alpha} h\right)^2 - 2\hat{\alpha} h + 1\right)\overline{q_{a,pre}^2} + 2\left(\hat{\alpha} h - 1\right)\overline{q_{a,i}\cdot q_{a,pre}} + \overline{q_a^2}\right) \quad (0.159)$$

An quadratic equation for $\hat{\alpha} h$ is given by solving (0.158) for $\widehat{C_b \frac{dv_c}{dt}}$ and inserting into (0.159). The form of the equation is:

$$a\left(\hat{\alpha} h\right)^2 + b\hat{\alpha} h + c = 0 \quad (0.160)$$

where the coefficients are defined by the first and second moments:

$$a = \overline{q_{a,pre}^2} - \left(\overline{q_a}\right)^2 \frac{\overline{\Delta t^2}}{\left(\overline{\Delta t}\right)^2} \quad (0.161)$$

$$b = 2\left(\overline{q_a \cdot q_{a,pre}} - \overline{q_{a,pre}^2}\right) \quad (0.162)$$

$$c = \overline{q_{a,pre}^2} - 2\overline{q_a \cdot q_{a,pre}} + \overline{q_a^2} \quad (0.163)$$

$\hat{\tau}_s$ can be found by eq. (0.32) as

$$\hat{\tau}_s = \frac{\overline{\Delta t}}{\hat{\alpha} h} \quad (0.164)$$

$\widehat{C_b \frac{dv_c}{dt}}$ is defined by the first moments and $\hat{\alpha} h$

$$\widehat{C_b \frac{dv_c}{dt}} = \frac{1}{\overline{\Delta t}} \frac{1}{\hat{\alpha} h} \left((\hat{\alpha} h - 1) \overline{q_{a,pre}} + \overline{q_a} \right) \quad (0.165)$$

When n is large $\lim_{n \to \infty} \overline{q_{a,pre}} = \overline{q_a}$, so:

$$\widehat{C_b \frac{dv_c}{dt}} = \frac{\overline{q_a}}{\overline{\Delta t}} \quad (0.166)$$

C.3 Estimation of PD sequence parameters by the method of moments at combined voltage voltage conditions

At combined voltage conditions the four unique parameters which describes the PD process are αh , C_b, $\widehat{\frac{dv_c}{dt}}$ and τ_s . The parameters can be estimated using the method of moments, when $K_{AC} \hat{V}_{AC}$ is assumed known. Note that at DC conditions it was only possible to estimate the product $C_b \frac{dv_c}{dt}$, at combined voltage conditions it is possible to estimate C_b and $\widehat{\frac{dv_c}{dt}}$ explicitly. In the following a procedure for obtaining the estimators $\hat{\alpha} h$, $\hat{C}_b$ and $\widehat{\frac{dv_c}{dt}}$ at combined voltage conditions is outlined. Symbol defintions for the moments are given in C.4 .

1) Combining (0.121) and (0.128) gives a relationship between the measurable quantities as follows:

$$\widehat{\frac{dv_c}{dt}}\Delta t_{pre,i}=\frac{1}{\alpha h C_b}\left(\left(\alpha h-1\right)q_{a,i-1}+q_{a,i}\right)+K_{AC}\hat{V}_{AC}\left(\cos\theta_{i-1}-\cos\theta_i\right) \quad (0.167)$$

2) The first, second and third moment on both sides of (0.167), this gives the three equations

$$\widehat{\widehat{\frac{dv_c}{dt}}}\overline{\Delta t}=\frac{1}{\hat{\alpha}h\hat{C}_b}\left(\left(\hat{\alpha}h-1\right)\overline{q_{a,pre}}+\overline{q_a}\right)+K_{AC}\hat{V}_{AC}\left(\overline{\cos\theta_{pre}}-\overline{\cos\theta}\right) \quad (0.168)$$

$$\left(\widehat{\widehat{\frac{dv_c}{dt}}}\right)^2\overline{\Delta t^2}=\frac{1}{n}\sum\left(\frac{1}{\hat{\alpha}h\hat{C}_b}\left(\left(\hat{\alpha}h-1\right)q_{a,i-1}+q_{a,i}\right)+K_{AC}\hat{V}_{AC}\left(\cos\theta_{pre,i}-\cos\theta_i\right)\right)^2$$

(0.169)

$$\left(\widehat{\widehat{\frac{dv_c}{dt}}}\right)^3\overline{\Delta t^3}=\frac{1}{n}\sum\left(\frac{1}{\hat{\alpha}h\hat{C}_b}\left(\left(\hat{\alpha}h-1\right)q_{a,i-1}+q_{a,i}\right)+K_{AC}\hat{V}_{AC}\left(\cos\theta_{pre,i}-\cos\theta_i\right)\right)^3$$

(0.170)

3) Solve these three equations with respect to $\widehat{\widehat{\frac{dv_c}{dt}}}$, each solution is a plane defined by and $\hat{\alpha}h$ and $\hat{C}_b$.

$$\widehat{\widehat{\frac{dv_c}{dt}}}_1=\frac{1}{\overline{\Delta t}}\left(\frac{1}{\hat{\alpha}h\hat{C}_b}\left(\left(\hat{\alpha}h-1\right)\overline{q_{a,pre}}+\overline{q_a}\right)+K_{AC}\hat{V}_{AC}\left(\overline{\cos\theta_{pre}}-\overline{\cos\theta}\right)\right) \quad (0.171)$$

$$\widehat{\widehat{\frac{dv_c}{dt}}}_2=\left|\sqrt{\frac{1}{\overline{\Delta t^2}}\frac{1}{n}\sum\left(\frac{1}{\hat{\alpha}h\hat{C}_b}\left(\left(\hat{\alpha}h-1\right)q_{a,i-1}+q_{a,i}\right)+K_{AC}\hat{V}_{AC}\left(\cos\theta_{pre,i}-\cos\theta_i\right)\right)^2}\right|$$

(0.172)

$$\widehat{\widehat{\frac{dv_c}{dt}}}_3=\left|\sqrt[3]{\frac{1}{\overline{\Delta t^3}}\frac{1}{n}\sum\left(\frac{1}{\hat{\alpha}h\hat{C}_b}\left(\left(\hat{\alpha}h-1\right)q_{a,i-1}+q_{a,i}\right)+K_{AC}\hat{V}_{AC}\left(\cos\theta_{pre,i}-\cos\theta_i\right)\right)^3}\right|$$

(0.173)

4) A solution for $\hat{\alpha}h$ and $\hat{C}_b$ exist which satisfies $\frac{\widehat{dv_c}}{dt} = \frac{\widehat{dv_c}}{dt}_1 = \frac{\widehat{dv_c}}{dt}_2 = \frac{\widehat{dv_c}}{dt}_3$: Find the intersecting contour line L1 (i.e.. set of $\hat{\alpha}h$ and $\hat{C}_b$) that satisfies $\frac{\widehat{dv_c}}{dt}_1 = \frac{\widehat{dv_c}}{dt}_2$. Find the intersecting contour line L2 (i.e.. set of $\hat{\alpha}h$ and $\hat{C}_b$) that satisfies $\frac{\widehat{dv_c}}{dt}_1 = \frac{\widehat{dv_c}}{dt}_3$

5) The intersection points of the contour lines L1 and L2 give a solution for $\hat{\alpha}h$ and $\hat{C}_b$ where $\frac{\widehat{dv_c}}{dt} = \frac{\widehat{dv_c}}{dt}_1 = \frac{\widehat{dv_c}}{dt}_2 = \frac{\widehat{dv_c}}{dt}_3$.

6) $\frac{\widehat{dv_c}}{dt}$ is found by inserting the solution for $\hat{\alpha}h$ and $\hat{C}_b$ into (0.171).

So far $\hat{\alpha}h$, $\hat{C}_b$, $\frac{\widehat{dv_c}}{dt}$ have been obtained. It is possible to find the estimated mean time lag $\hat{\bar{t}}_L$ by eq. (0.133) as:

$$\hat{\bar{t}}_L = \frac{\Delta\bar{t}}{\hat{\alpha}h} + \frac{K_{AC}\hat{V}_{AC}}{\frac{\widehat{dv_c}}{dt}}\left(1 - \overline{\cos\theta_i}\right) \quad (0.174)$$

The estimated mean recovery time $\hat{\bar{t}}_R$ can be found by the first moment of the discharge separation time in (3.92):

$$\hat{\bar{t}}_R = \Delta\bar{t} - \hat{\bar{t}}_L \quad (0.175)$$

Finally it is possible to estimate the mean statistical waiting time by finding the value of $\hat{\tau}_s$ that satisfies the equation for the mean time lag developed in section B.5 :

$$\hat{\bar{t}}_L = F_1\left(\frac{\widehat{dv_c}}{dt}, K_{AC}\hat{V}_{AC}, \hat{\tau}_s\right) \quad (0.176)$$

C.4 Definition of moments

The definitions of the moments used in this thesis are given below:

$$\overline{\Delta t} = E\left[\Delta t_{pre}\right] = \frac{1}{n}\sum_{i=1}^{n}\Delta t_{pre,i} \quad (0.177)$$

$$\overline{\Delta t^2} = E^2\left[\Delta t_{pre}\right] = \frac{1}{n}\sum_{i=1}^{n}\left(\Delta t_{pre,i}\right)^2 \quad (0.178)$$

$$\overline{\Delta t^3} = E^3\left[\Delta t_{pre}\right] = \frac{1}{n}\sum_{i=1}^{n}\left(\Delta t_{pre,i}\right)^3 \quad (0.179)$$

$$\overline{q_a} = E\left[q_a\right] = \frac{1}{n}\sum_{i=1}^{n}q_{a,i} \quad (0.180)$$

$$\overline{q_a^2} = E^2\left[q_a\right] = \frac{1}{n}\sum_{i=1}^{n}\left(q_{a,i}\right)^2 \quad (0.181)$$

$$\overline{q_{a,pre}} = E\left[q_{a,pre}\right] = \frac{1}{n}\sum_{i=1}^{n}q_{a,pre,i} \quad (0.182)$$

$$\overline{q_{a,pre}^2} = E^2\left[q_{a,pre}\right] = \frac{1}{n}\sum_{i=1}^{n}\left(q_{a,pre,i}\right)^2 \quad (0.183)$$

$$\overline{q_a \cdot q_{a,pre}} = E\left[q_a \cdot q_{a,pre}\right] = \frac{1}{n}\sum_{i=1}^{n}q_{a,i} \cdot q_{a,pre,i} \quad (0.184)$$

$$\overline{\cos\theta} = E\left[\cos\theta\right] = \frac{1}{n}\sum_{i=1}^{n}\cos\theta_i \quad (0.185)$$

$$\overline{\cos\theta_{pre}} = E\left[\cos\theta_{pre}\right] = \frac{1}{n}\sum_{i=1}^{n}\cos\theta_{pre,i} \quad (0.186)$$

Appendix D Data from experiments

In this section selected data from the measurements are presented, the data points for the test series are given in D.1 and the AC ripple waveform measured at DC voltage is given in D.2.

D.1 Data points acquired for all test series

The data points per stage are shown for the test program outlined in 4.1.8:

- For the DC test series, see Fig. 0-6. The total number of discharges is 27 820.
- For the variable AC amplitude test series, see Fig. 0-7. The total number of discharges is 23 842.
- For the variable frequency test series, see Fig. 0-8. The total number of discharges is 22 565.

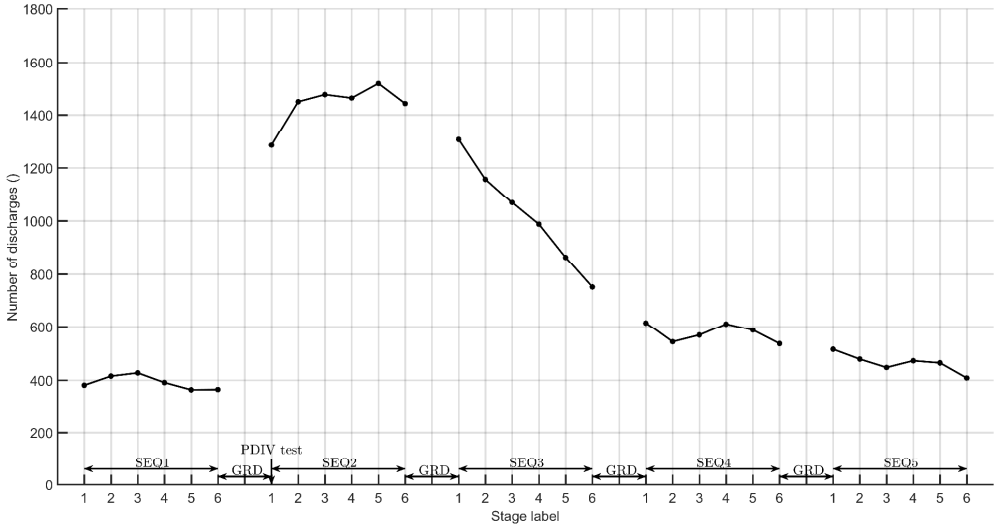

Fig. 0-6 The number of discharges in each stage for the DC test series.

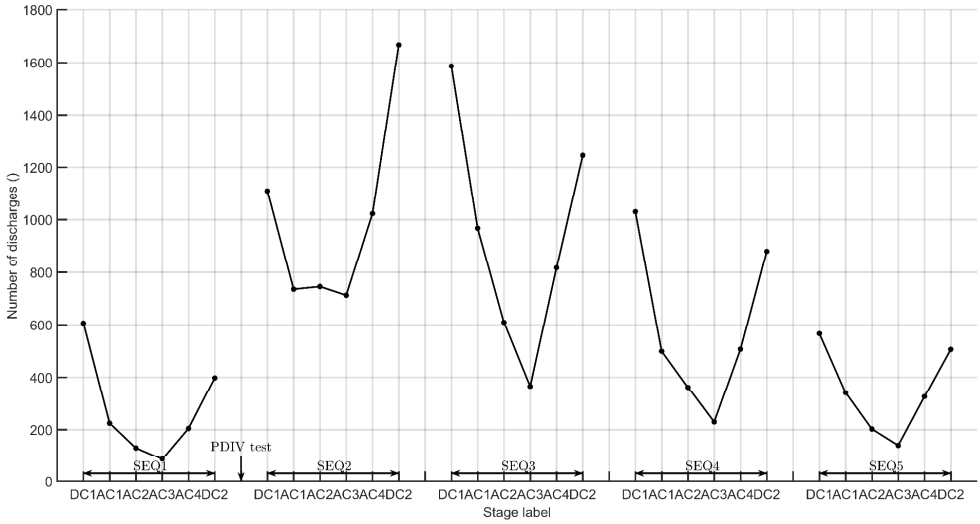

Fig. 0-7 The number of discharges in each stage for the variable AC amplitude DC test series.

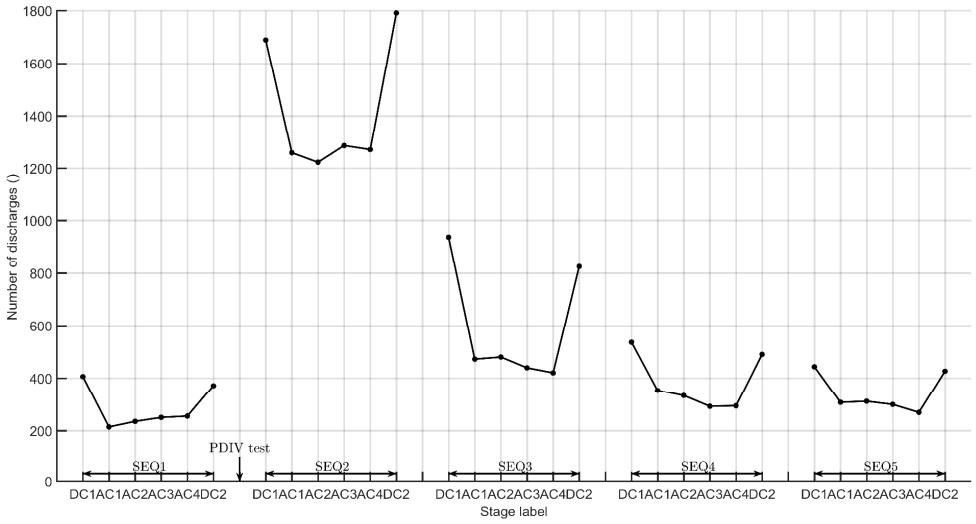

Fig. 0-8 The number of discharges in each stage for the variable AC frequency test series.

D.2 AC ripple during DC voltage test stages

The AC source introduced a small ripple during the PD tests, even if the AC voltage was set to zero. The ripple amplitude was measured to 10 V, with AC period time around 20 ms, see Fig. 0-9. The measurement was done with the AC source on and set to zero, the DC source was turned off and measuring probes connected to the terminals of the test object. The AC ripple was not detected during the PD tests because the oscilloscope trigger level was higher than the AC ripple amplitude.

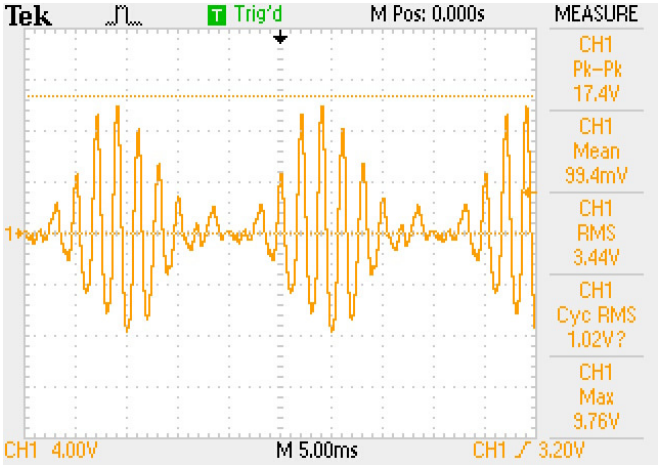

Fig. 0-9 Measured AC ripple on test object terminals, AC source on with AC voltage set to zero and DC voltage source turned off.